

Study of Nuclear Structure by Electromagnetic Excitation with Accelerated Ions

K. ALDER, A. BOHR, T. HUUS, B. MOTTELSON, AND A. WINTHER

*CERN Theoretical Study Division and Institute for Theoretical Physics,
University of Copenhagen, Copenhagen, Denmark*

TABLE OF CONTENTS

	<i>Page</i>		<i>Page</i>
Chapter I. Introduction.....	433	Chapter III. Experimental Conditions.....	487
Chapter II. Theory of Electromagnetic Excitations.....	434	A. Beam Requirements.....	487
A. Classical Theory.....	434	B. Measurements of De-Excitation γ Rays..	488
1. Electric Excitations.....	435	1. Detection Technique.....	488
2. Magnetic Excitations.....	437	2. Thick Target Yields.....	490
3. Discussion of Cross Sections.....	439	3. Background Radiation.....	491
4. Angular Distribution of De-Excitation γ Rays.....	440	C. Measurements of Conversion Electrons...	494
5. Symmetrization of Classical Cross Sections.....	443	1. Detection Technique.....	494
6. Excitation of Projectile.....	444	2. Background Effects.....	494
B. Quantum-Mechanical Theory.....	444	D. Measurements of Inelastically Scattered Projectiles.....	496
1. Derivation of Excitation Cross Sections.....	445	Chapter IV. Nuclear Data Obtained from Coulomb Excitation.....	497
2. Nonrelativistic Approximation.....	447	A. Analysis of Experimental Data.....	498
3. Reduction to Radial Matrix Elements..	449	1. Excitation Function and Relative Yields	498
4. Evaluation of the Radial Matrix Elements.....	450	2. Angular Distribution of Decay Radiation	499
5. Angular Distribution of De-Excitation γ Rays.....	454	3. Angular Distribution of Inelastically Scattered Particles.....	499
6. WKB Approximation and Classical Limit	455	4. Absolute Yields.....	499
C. Numerical Results.....	457	5. Coulomb Excitation at Higher Bombarding Energies.....	500
1. Collision Parameters.....	457	B. Compilation of Experimental Results....	502
2. Total Cross Sections.....	458	Chapter V. Collective Nuclear Excitations....	523
3. Differential Cross Sections.....	461	A. Qualitative Considerations.....	523
4. Angular Distribution of De-Excitation γ Rays.....	461	B. Rotational Excitations.....	525
5. Survey of Approximations.....	467	1. Energy Spectrum.....	525
D. Higher Order Excitation Effects.....	468	2. Excitation Cross Sections.....	530
1. Cross Sections to Second Order.....	468	3. Magnetic Dipole Decay of Rotational Excitations.....	532
2. Interference Effects.....	470	4. Coupling between Rotational and Intrinsic Motion.....	534
3. Double Excitations.....	471	C. Vibrations of Spherical Nuclei.....	535
4. Polarization Effects in Elastic Scattering	471	1. Classification of Vibrations.....	535
E. Appendices.....	472	2. Quadrupole Vibrations of Even-Even Nuclei.....	535
1. Emission of Bremsstrahlung.....	472	3. Discussion of Empirical Data.....	536
2. Born Approximation.....	473	4. Octupole Vibrations in Even-Even Nuclei	538
3. Excitation by Means of Electrons.....	475	5. Spectra of Odd- <i>A</i> Nuclei.....	538
4. Classical Orbital Integrals.....	476	D. Vibrations of Spheroidal Nuclei.....	539
5. Electric Dipole Excitations.....	477	1. Classification of Vibrations.....	539
6. Limit of $\xi=0$	482	2. Transition Probabilities.....	540
7. Limit of Large Orbital Angular Momenta	483	3. Quadrupole Vibrations.....	540
8. Some Properties of Hypergeometric Functions.....	484	4. Octupole Vibrations.....	541
		E. Regions of Closed Shells.....	541

CHAPTER I. INTRODUCTION

ALREADY in the early stages of the study of nuclear reactions, the possibility was discussed¹ of producing nuclear excitations by the long-range electric interactions with bombarding particles.² Particularly for incident energies so low that the Coulomb repulsion prevents the particles from penetrating into the nucleus, such excitation processes can be studied without interference from the more complicated nuclear interactions. Following these early theoretical suggestions, the possibility was discussed that an isomeric activity in indium, observed in charged particle bombardment, might have been produced by processes of this kind.³

In subsequent years, the theoretical description of the "Coulomb excitation" reactions was considerably developed.^{4,5} In particular, it was found that in many cases of interest a classical treatment of the trajectory of the bombarding particle is justified and leads to simple quantitative expressions for the excitation cross sections.⁵

At the same time, it was recognized that such experiments were a particularly appropriate means for investigating certain features of the nuclear structure. The nuclear states most strongly produced in the Coulomb excitation reactions are the low-lying collective excitations which are induced by the electric quadrupole field of the impinging particles. Such experiments, thus, appeared as an especially promising tool for the exploration of the nuclear rotational and vibrational spectra.^{6,7}

Nuclear gamma rays which were later identified as resulting from Coulomb excitation of tantalum were first seen as a background radiation in experiments on proton induced reactions in light nuclei, in which target backings of tantalum were employed.⁸ About a year

after these first observations, the origin of the gamma rays and the mechanism of their production were clearly established.^{9,10} It was also shown¹⁰ that the yield of this radiation as a function of the proton energy was in agreement with the theoretical expression for electric quadrupole Coulomb excitation^{5,11} and that the absolute cross sections and excitation energies could be interpreted in terms of rotational excitations.

Since these first investigations, the Coulomb excitation reaction has been extensively employed in many laboratories for the study of nuclear levels. Apart from furnishing new information on previously known nuclear states, a large number of new levels have been identified.¹²

The scope of the experiments has been extended by the utilization of alternative methods of detection. Thus, additional information has been obtained from measurements of the internal conversion electrons¹³ and of the inelastically scattered proton groups.¹⁴ While most of the experiments performed so far have employed protons, deuterons, or α particles as projectiles, the use of still heavier ions¹⁵ may in certain respects provide additional advantages. The Coulomb excitation reaction has so far been used for the study of rather low-lying states (excitation energies up to about one Mev), but with the use of higher bombarding energies it should be possible also to explore excitations of somewhat higher energy.

Extensive experimental investigations of the Coulomb excitation process itself have also been performed and have tested the adequacy of the theoretical description. Thus, the excitation cross section as a function of the energy, charge, and mass of the projectile has been found to be in good agreement with the classical theory, when the latter is appropriately modified to take into account the energy loss of the projectile.¹⁶ On the other hand, the accurately measured angular distribution of the γ radiation from Coulomb excitation revealed¹⁷ significant deviations from the theory, and stimulated the development of a complete quantum-mechanical treatment of the process.¹⁸

¹ See, e.g., the discussion in Rutherford, Chadwick, and Ellis, *Radiations from Radioactive Substances* (Cambridge University Press, Cambridge, England, 1930), p. 247 ff. and the later work by L. Landau, *Physik. Z. Sowjetunion* **1**, 88 (1932) and V. F. Weisskopf, *Phys. Rev.* **53**, 1018 (1938).

² We shall, in the present article, confine our attention mainly to electric and magnetic excitations produced by bombardment with nuclear particles. A brief review of the theory of inelastic electron scattering is given in Sec. II E.3.

³ S. W. Barnes and P. W. Aradine, *Phys. Rev.* **55**, 50 (1939); Risser, Lark-Horowitz, and Smith, *Phys. Rev.* **57**, 355 (1940).

⁴ C. J. Mullin and E. Guth, *Phys. Rev.* **82**, 141 (1951); R. Huby and H. C. Newns, *Proc. Phys. Soc. (London)* **A 64**, 619 (1951).

⁵ K. A. Ter-Martirosyan, *J. Exptl. Theoret. Phys. (U.S.S.R.)* **22**, 284 (1952).

⁶ A. Bohr and B. Mottelson, Report of the International Physics Conference, Copenhagen, June, 1952; *Kgl. Danske Videnskab. Selskab Mat. fys. Medd.* **27**, No. 16 (1953).

⁷ It has also been suggested [N. F. Ramsey, *Phys. Rev.* **83**, 659 (1951); Breit, Hull, and Gluckstern, *Phys. Rev.* **87**, 74 (1952); Malenka, Kruse, and Ramsey, *Phys. Rev.* **91**, 1165 (1953)] that the polarization of the nucleus as a whole, as well as of the projectile, could be studied in reactions where the energy of the bombarding particle was insufficient to enable it to surmount the Coulomb barrier (see Sec. II D.3).

⁸ R. B. Day and T. Huus, *Phys. Rev.* **85**, 761 (1952); C. L. McClelland, S. M. thesis, Massachusetts Institute of Technology, August, 1952.

⁹ C. L. McClelland and C. Goodman, *Phys. Rev.* **91**, 760 (1953).

¹⁰ T. Huus and Č. Zupančič, *Kgl. Danske Videnskab. Selskab. Mat. fys. Medd.* **28**, No. 1 (1953).

¹¹ K. Alder and A. Winther, *Phys. Rev.* **91**, 1578 (1953).

¹² A special reference should be made to the extensive and systematic survey performed by N. Heydenburg and G. Temmer, *Phys. Rev.* **93**, 351 and 906 (1954); **94**, 1399 (1954); **95**, 861 (1954); **96**, 426 (1954); **98**, 1308 (1955); **100**, 150 (1955).

¹³ T. Huus and J. H. Bjerregaard, *Phys. Rev.* **92**, 1579 (1953).

¹⁴ B. Elbek and C. K. Bockelman (submitted for publication).

¹⁵ Recently, Coulomb excitation studies have been made employing cyclotron accelerated nitrogen ions [Alkhozov, Andreyev, Greenberg, and Lemberg, *Nuclear Phys.* **2**, 65 (1956)].

¹⁶ K. Alder and A. Winther, *Phys. Rev.* **96**, 237 (1954).

¹⁷ F. K. McGowan and P. H. Stelson, *Phys. Rev.* **99**, 127 (1955).

¹⁸ Biedenharn, McHale, and Thaler, *Phys. Rev.* **100**, 376 (1955); K. Alder and A. Winther, *Kgl. Danske Videnskab. Selskab Mat. fys. Medd.* **29**, No. 19 (1955). Numerical results have been given by K. Alder and A. Winther, reference 11; Biedenharn, Goldstein, McHale, and Thaler, *Phys. Rev.* **101**, 662 (1956), and **102**, 1567 (1956). A WKB approximation which yields results in essential agreement with the detailed quantal treatment has been given

In the present review article, we begin in Chapter II with a discussion of the theory of Coulomb excitation, and give in tables and figures the numerical results necessary for the analysis of the experiments. Chapter III deals with the experimental techniques which have been employed in Coulomb excitation measurements, and also contains a discussion of the main background effects in these experiments. Chapter IV contains a compilation of results obtained in Coulomb excitation experiments and also a comparison with the theory of Chapter II. Finally, in Chapter V, we outline the theory of collective nuclear excitations, which makes possible an interpretation of many of the observed transitions.

We wish to acknowledge the benefit we have derived from contacts with experimental and theoretical physicists working in the field of Coulomb excitation, many of whom have kindly communicated to us the results of their investigations prior to publication. We are also indebted to the members of the Institute for Theoretical Physics, Copenhagen, as well as to Dr. N. P. Heydenburg, Dr. G. M. Temmer, and Dr. G. Breit for valuable discussions.

CHAPTER II. THEORY OF ELECTROMAGNETIC EXCITATIONS

The excitation of nuclei by impinging nuclear particles with energies well below the Coulomb barrier proceeds only through the electromagnetic interaction between the projectile and the nucleus.

The motion of the projectile in the Coulomb field of the nucleus is essentially characterized¹⁹ by the dimensionless quantity η defined by

$$\eta = Z_1 Z_2 e^2 / \hbar v, \quad (\text{II A.1})$$

where Z_1 and Z_2 are the charge numbers of the projectile and the nucleus, while v is the velocity of the incident particle. The parameter η measures the effective strength of the interaction. Thus, for $\eta \ll 1$, the Coulomb field produces only a small distortion of the incident wave, and the collision process can be treated by Born approximation. For the particle velocities involved in Coulomb excitation, however, the interaction must be strong to prevent the projectiles from entering the nucleus. Under such conditions, we always have $\eta \gg 1$, and the collision may then be approximately described by considering the particle as moving along a classical trajectory. For inelastic collisions, it is a further condition for the application of a classical description that the energy loss of the particle is small compared to the bombarding energy, so that the effect of the excitation on the particle motion can be neglected.

In such a treatment, the nuclear excitation is a result of the time dependent electromagnetic field of the

by Benedict, Daitch, and Breit, *Phys. Rev.* **101**, 171 (1956); Gluckstern, Lazarus, and Breit, *ibid.* **101**, 175 (1956); F. D. Benedict, *ibid.* **101**, 178 (1956).

¹⁹ N. Bohr, *Kgl. Danske Videnskab. Selskab Mat. fys. Medd.* **18**, No. 8 (1948).

projectile acting on the nucleus. In most cases, the effect of this field is small and may be treated by first-order quantum-mechanical perturbation theory. The excitation probability can be expressed in terms of the same nuclear matrix elements as determine the radiative transitions between the nuclear states.

In the following we shall first consider, in Sec. A, the Coulomb excitation process in terms of such a classical treatment of the projectile. We shall describe this simplified method in some detail, since it illustrates the main physical features of the process, without involving the more complex mathematical formalism of the quantum-mechanical theory.

The more rigorous treatment of the excitation process, in which the particles are described by the Coulomb wave functions, is given in Sec. B. At the end of this Section, we also consider the application of the WKB approximation, which is intermediate between the classical and the exact quantum-mechanical treatment.

In Sec. C, the final formulas for the excitation cross sections and the angular distribution of the emitted nuclear radiation are collected. These depend on the collision parameters through certain functions which have been evaluated numerically and are tabulated and given in figures.

In Sec. D, we briefly consider some of the effects associated with the higher order excitation processes, while Sec. E has the form of an appendix, which contains partly results appropriate to certain limiting cases and partly a discussion of certain processes related to Coulomb excitation, such as bremsstrahlung and nuclear excitation produced by fast electrons.

II A. Classical Theory

In the classical treatment of the Coulomb excitation process,⁵ we consider the projectile as moving along a hyperbolic orbit in the repulsive Coulomb field of the target nucleus (see Fig. II.1). The differential scattering

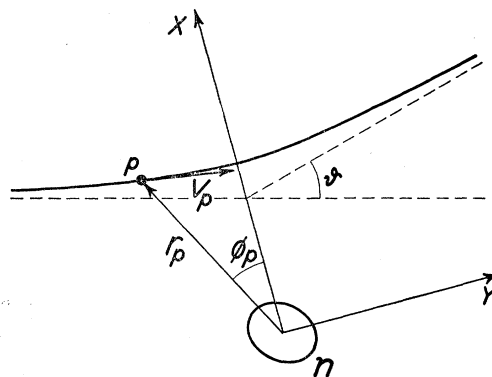


FIG. II.1. Classical picture of the projectile orbit in the Coulomb field of the nucleus. The hyperbolic orbit of the projectile, P , is shown in the frame of reference in which the nuclear mass center is at rest. The focal coordinate system employed in the evaluation of the orbital integrals (II A.24) is indicated. The position and velocity of the projectile are denoted by ϕ_p , r_p , and v_p , respectively, and the total deflection angle by θ .

cross section is given by the Rutherford law

$$d\sigma_R = \frac{1}{4}a^2 \sin^{-4}(\vartheta/2)d\Omega, \quad (\text{II A.2})$$

where ϑ is the scattering angle in the center-of-mass system, and

$$a = \frac{Z_1 Z_2 e^2}{m_0 v^2} \quad (\text{II A.3})$$

is half the distance of closest approach in a head-on collision. The reduced mass of the projectile and the nucleus is denoted by m_0 .

Since we have assumed that the orbit of the particle is not appreciably affected by the excitation, the differential excitation cross section is given by

$$d\sigma = P d\sigma_R, \quad (\text{II A.4})$$

where P is the probability that the nucleus is excited in a collision in which the particle is scattered into the solid angle $d\Omega$.

The probability P can be expressed in terms of the amplitudes b_{if} for a transition from the initial nuclear state i to the various final states f . If we ask for the probability for excitation of a given energy level, irrespective of the orientation of the initial or final nuclear state, we have

$$P = (2I_i + 1)^{-1} \sum_{M_i M_f} |b_{if}|^2, \quad (\text{II A.5})$$

where I_i is the spin of the initial nuclear state, and where M_i and M_f are the magnetic quantum numbers of the initial and final states.

Under most experimental conditions the probability for excitation in a single encounter is very small. Thus, by first-order time dependent perturbation theory,²⁰ we obtain

$$b_{if} = \frac{1}{i\hbar} \int_{-\infty}^{\infty} \langle f | \mathcal{H}(t) | i \rangle e^{i\omega t} dt, \quad (\text{II A.6})$$

where $\mathcal{H}(t)$ is the interaction energy and

$$\omega = \frac{\Delta E}{\hbar} = \frac{E_f - E_i}{\hbar} \quad (\text{II A.7})$$

is the nuclear frequency associated with the excitation energy ΔE .

II A.1. Electric Excitations

For particle velocities small compared with that of light, the main interaction is the Coulomb energy

$$\mathcal{H}_E(t) = \int \rho_n(\mathbf{r}) \varphi(\mathbf{r}, t) d\tau, \quad (\text{II A.8})$$

where

$$\varphi(\mathbf{r}, t) = \frac{Z_1 e}{|\mathbf{r} - \mathbf{r}_p(t)|} - \frac{Z_2 e}{r_p(t)} \quad (\text{II A.9})$$

and $\rho_n(\mathbf{r})$ is the nuclear charge density operator. The projectile is considered as a point charge and its position vector $\mathbf{r}_p(t)$ is measured from the nuclear center of mass. In (9)* we have subtracted the interaction between the mass centers, which is responsible for the scattering and does not contribute to the excitation.

In order to evaluate the matrix element in (6) we expand the potential (9) in multipole components, whereby one obtains

$$\mathcal{H}_E(t) = 4\pi Z_1 e \sum_{\lambda=1}^{\infty} \sum_{\mu=-\lambda}^{\lambda} \frac{1}{2\lambda+1} r_p^{-\lambda-1} \times Y_{\lambda\mu}(\theta_p, \phi_p) \mathfrak{N}^*(E\lambda, \mu), \quad (\text{II A.10})$$

which holds if the projectile remains outside the nucleus. The electric multipole moments of the nucleus are defined by

$$\mathfrak{N}(E\lambda, \mu) = \int r^\lambda Y_{\lambda\mu}(\theta, \phi) \rho_n(\mathbf{r}) d\tau. \quad (\text{II A.11})$$

The polar coordinates are referred to a coordinate system with origin in the nuclear center of mass and with a fixed direction of the polar axis. The $Y_{\lambda\mu}(\theta, \phi)$ are the normalized spherical harmonics.²¹

The multipole operators (11) are the same as those responsible for the emission of electric multipole radiation with wavelength large compared with the nuclear radius.²² If we assume that the nuclear charge density can be described in terms of point charge protons we have

$$\rho_n(\mathbf{r}) = \sum_k e_k \delta(\mathbf{r} - \mathbf{r}_k), \quad (\text{II A.12})$$

where e_k and \mathbf{r}_k are the charge and the position vector of the k th nucleon. The multipole moment can then be written in the familiar form

$$\mathfrak{N}(E\lambda, \mu) = \sum_k e_k r_k^\lambda Y_{\lambda\mu}(\theta_k, \phi_k). \quad (\text{II A.13})$$

Inserting (10) into (6) we get for the transition amplitude

$$b_{if} = \frac{4\pi Z_1 e}{i\hbar} \sum_{\lambda\mu} \frac{1}{2\lambda+1} \times \langle I_i M_i | \mathfrak{N}(E\lambda, \mu) | I_f M_f \rangle S_{E\lambda, \mu}, \quad (\text{II A.14})$$

* In each chapter we have referred to the equations in that chapter without adding the chapter or section designation. For example, this reference is to Eq. (II A.9)

²¹ We use the phases employed by E. U. Condon and G. H. Shortley, *Theory of Atomic Spectra* (Cambridge University Press, New York, 1935).

²² See, e.g., J. M. Blatt and V. F. Weisskopf, *Theoretical Nuclear Physics* (John Wiley & Sons, Inc., New York, 1952).

²⁰ P. A. M. Dirac, *The Principles of Quantum Mechanics* (Oxford University Press, New York, 1947), third edition, p. 172.

where we have introduced the notation

$$S_{E\lambda, \mu} = \int_{-\infty}^{\infty} e^{i\omega t} Y_{\lambda\mu}(\theta_p(t), \phi_p(t)) [r_p(t)]^{-\lambda-1} dt \quad (\text{II A.15})$$

for the orbital integrals, and where we have specified the nuclear states by their total angular momentum I and magnetic quantum number M .

Since the multiple moments are tensor operators, we may write²³

$$\begin{aligned} & \langle I_i M_i | \mathfrak{N}(\lambda, \mu) | I_f M_f \rangle \\ &= (-1)^{I_i - M_i} \begin{pmatrix} I_i & \lambda & I_f \\ -M_i & \mu & M_f \end{pmatrix} \langle I_i || \mathfrak{N}(\lambda) || I_f \rangle, \quad (\text{II A.16}) \end{aligned}$$

where the last factor is the reduced matrix element. We use the Wigner notation for the vector addition coefficients,²⁴ which is related to the notation employed by Condon and Shortley²¹ by

$$\begin{aligned} & \begin{pmatrix} j_1 & j_2 & j_3 \\ m_1 & m_2 & m_3 \end{pmatrix} \\ &= \frac{(-1)^{j_1 - j_2 - m_3}}{(2j_3 + 1)^{\frac{1}{2}}} \langle j_1 j_2 m_1 m_2 | j_1 j_2 j_3 - m_3 \rangle. \quad (\text{II A.17}) \end{aligned}$$

Further, we introduce

$$\begin{aligned} & B(E\lambda; I_i \rightarrow I_f) \\ &= \sum_{M_f \mu} |\langle I_i M_i | \mathfrak{N}(E\lambda, \mu) | I_f M_f \rangle|^2 \\ &= (2I_i + 1)^{-1} |\langle I_i || \mathfrak{N}(E\lambda) || I_f \rangle|^2, \quad (\text{II A.18}) \end{aligned}$$

which represents the reduced transition probability associated with a radiative transition of multipole order $E\lambda$.

By inserting into (4) Eqs. (2), (5), and (14), and using the orthogonality relation,²⁴

$$\begin{aligned} & \sum_{M_i M_f} \begin{pmatrix} I_i & \lambda & I_f \\ -M_i & \mu & M_f \end{pmatrix} \begin{pmatrix} I_i & \lambda' & I_f \\ -M_i & \mu' & M_f \end{pmatrix} \\ &= (2\lambda + 1)^{-1} \delta_{\lambda\lambda'} \delta_{\mu\mu'} \quad (\text{II A.19}) \end{aligned}$$

for the vector addition coefficients, we get for the differential excitation cross section

$$d\sigma_E = \sum_{\lambda=1}^{\infty} d\sigma_{E\lambda}, \quad (\text{II A.20})$$

²³ G. Racah, Phys. Rev. **62**, 438 (1942). In the following we assume the phases of the nuclear wave functions to be chosen in such a manner that the matrix element (II A.16) is real. In this case, one finds $\langle I_i || \mathfrak{N}(\lambda) || I_f \rangle = (-1)^{I_f - I_i} \langle I_f || \mathfrak{N}(\lambda) || I_i \rangle$.

²⁴ A. R. Edmonds, Angular Momentum in Quantum Mechanics, CERN 55-26, Geneva, 1955. The notation is also employed by A. de Shalit, Phys. Rev. **91**, 1479 (1953).

with

$$\begin{aligned} d\sigma_{E\lambda} &= \frac{4\pi^2 Z_1^2 e^2}{\hbar^2} a^2 \\ & \times \sin^{-4} \frac{\vartheta}{2} \frac{B(E\lambda)}{(2\lambda + 1)^3} \sum_{\mu} |S_{E\lambda, \mu}|^2 d\Omega. \quad (\text{II A.21}) \end{aligned}$$

The evaluation of the integrals $S_{E\lambda, \mu}$ is most easily performed if the coordinates (r_p, θ_p, ϕ_p) are given in the focal system of the hyperbolic orbit (see Fig. II.1). In this system, a convenient parametric representation is

$$\begin{aligned} x_p &= a(\cosh w + \epsilon), \\ y_p &= a(\epsilon^2 - 1)^{\frac{1}{2}} \sinh w, \\ z_p &= 0, \\ r_p &= a(\epsilon \cosh w + 1), \\ t &= \frac{a}{v} (\epsilon \sinh w + w). \end{aligned} \quad (\text{II A.22})$$

The eccentricity ϵ is related to the deflection angle ϑ by

$$\epsilon = \frac{1}{\sin(\vartheta/2)}. \quad (\text{II A.23})$$

Since $\theta_p = \pi/2$, the $S_{E\lambda, \mu}$ take the form

$$\begin{aligned} S_{E\lambda, \mu} &= Y_{\lambda\mu} \left(\frac{\pi}{2}, 0 \right) \int_{-\infty}^{\infty} \frac{(x_p + iy_p)^\mu}{r_p^{\lambda + \mu + 1}} e^{i\omega t} dt \\ &= v^{-1} a^{-\lambda} Y_{\lambda\mu} \left(\frac{\pi}{2}, 0 \right) I_{\lambda\mu}(\vartheta, \xi), \quad (\text{II A.24}) \end{aligned}$$

where²⁵

$$Y_{\lambda\mu} \left(\frac{\pi}{2}, 0 \right) = \begin{cases} \left(\frac{2\lambda + 1}{4\pi} \right)^{\frac{1}{2}} \frac{[(\lambda - \mu)! (\lambda + \mu)!]^{\frac{1}{2}}}{(\lambda - \mu)! (\lambda + \mu)!} (-1)^{(\lambda + \mu)/2} & (\lambda + \mu \text{ even}) \\ 0 & (\lambda + \mu \text{ odd}) \end{cases} \quad (\text{II A.25})$$

and where

$$\begin{aligned} I_{\lambda\mu}(\vartheta, \xi) &= \int_{-\infty}^{\infty} e^{i\xi(\epsilon \sinh w + w)} \\ & \times \frac{[\cosh w + \epsilon + i(\epsilon^2 - 1)^{\frac{1}{2}} \sinh w]^\mu}{[\epsilon \cosh w + 1]^{\lambda + \mu}} dw. \quad (\text{II A.26}) \end{aligned}$$

The dimensionless quantity ξ is defined by

$$\xi = \frac{a\Delta E}{\hbar v} = \frac{Z_1 Z_2 e^2 \Delta E}{\hbar v 2E} \quad (\text{II A.27})$$

²⁵ We have used the notation $(2n)!! = 2 \cdot 4 \cdot 6 \cdots 2n$ and $(2n+1)!! = 1 \cdot 3 \cdot 5 \cdots (2n+1)$.

with $E = \frac{1}{2}m_0v^2$. The product $\xi\epsilon$ represents the ratio between the collision time and the nuclear period, and is thus a measure of the extent to which the process is adiabatic.

The properties of the integrals $I_{\lambda\mu}$ are discussed in Secs. II E.4-7.

The differential excitation cross section (21) may thus be written

$$d\sigma_{E\lambda} = \left(\frac{Z_1e}{\hbar v}\right)^2 a^{-2\lambda+2} B(E\lambda) df_{E\lambda}(\vartheta, \xi), \quad (\text{II A.28})$$

with

$$df_{E\lambda}(\vartheta, \xi) = \frac{4\pi^2}{(2\lambda+1)^3} \sum_{\mu} \left| Y_{\lambda\mu}\left(\frac{\pi}{2}, 0\right) \right|^2 \times |I_{\lambda\mu}(\vartheta, \xi)|^2 \sin^{\frac{\vartheta}{2}} d\Omega. \quad (\text{II A.29})$$

The total excitation cross section of order $E\lambda$, obtained by integration over all scattering directions, is given by

$$\sigma_{E\lambda} = \left(\frac{Z_1e}{\hbar v}\right)^2 a^{-2\lambda+2} B(E\lambda) f_{E\lambda}(\xi), \quad (\text{II A.30})$$

where

$$f_{E\lambda}(\xi) = \int \frac{df_{E\lambda}(\vartheta, \xi)}{d\Omega} d\Omega = \frac{16\pi^3}{(2\lambda+1)^3} \sum_{\mu} \left| Y_{\lambda\mu}\left(\frac{\pi}{2}, 0\right) \right|^2 \times \int_0^{\pi} |I_{\lambda\mu}(\vartheta, \xi)|^2 \frac{\cos \frac{\vartheta}{2}}{\sin^{\frac{\vartheta}{2}}} d\vartheta. \quad (\text{II A.31})$$

The excitation processes considered so far, which are produced by the electrostatic interaction (8), are subject to the usual parity selection rule for electric multipole radiation. Thus, an excitation of order λ involves a parity change of $(-1)^\lambda$.

Excitations of opposite parity can be produced by the magnetic field from the projectile.²⁶ Such magnetic excitations usually have very small cross sections, since for bombarding energies below the Coulomb barrier the projectile velocity is small compared with that of light. Still, in cases where electric transitions are forbidden, or in the case of γ -ray angular distributions where there are interference terms between electric and magnetic excitations, it may be possible to observe the magnetic effects.

²⁶ The classical treatment of the magnetic excitations was first given by M. Jean and J. Prentki, *Compt. rend.* **238**, 2290 (1954).

II A.2. Magnetic Excitations

To lowest order in the particle velocity, the magnetic interaction is contained in the expression

$$\mathfrak{H}(t) = -\frac{1}{c} \int \mathbf{j}_n(\mathbf{r}) \cdot \mathbf{A}(\mathbf{r}, t) d\tau, \quad (\text{II A.32})$$

where $\mathbf{j}_n(\mathbf{r})$ is the nuclear current density and

$$\mathbf{A}(\mathbf{r}, t) = \frac{Z_1e}{c} \frac{\mathbf{v}_p(t)}{|\mathbf{r} - \mathbf{r}_p(t)|}, \quad (\text{II A.33})$$

is the unretarded vector potential produced by the projectile. We measure \mathbf{j}_n and \mathbf{A} in the nuclear rest system, and thus $\mathbf{v}_p(t)$ is the instantaneous relative velocity of projectile and nucleus.

In (33) we have neglected the contribution from a possible magnetic moment of the projectile. This effect, however, is usually small compared to the magnetic effect of the orbital motion, since, for $\eta \gg 1$, the main contribution to the excitation arises from collisions with large orbital angular momenta l . For $\xi \lesssim 1$, the order of magnitude of the effective l is given by $l\hbar \gtrsim m_0av = \eta\hbar \gg \hbar$.

Expanding in spherical harmonics we obtain for the vector potential (33)

$$\mathbf{A}(\mathbf{r}) = \sum_{\lambda\mu} \frac{4\pi}{2\lambda+1} \frac{Z_1e}{c} \mathbf{v}_p r_p^{-\lambda-1} \times Y_{\lambda\mu}(\theta_p, \phi_p) r^\lambda Y_{\lambda\mu}^*(\theta, \phi). \quad (\text{II A.34})$$

In this potential the terms involving r^λ contain, besides the magnetic multipole component of order λ , also electric multipole components of order $\lambda \pm 1$. These contribute a small relativistic correction to the electric excitations, and will here be disregarded.²⁷ In order to extract the magnetic part of (34) we take the component of \mathbf{A} along the direction of \mathbf{L} (see expression (II B.6) below), where

$$\mathbf{L} = -i[\mathbf{r} \times \nabla]. \quad (\text{II A.35})$$

Thus, one obtains

$$\mathbf{A}_M(\mathbf{r}) = \frac{4\pi Z_1e}{c} \sum_{\lambda} r^\lambda r_p^{-\lambda-1} \frac{\mathbf{L}(\mathbf{L} \cdot \mathbf{v}_p)}{(2\lambda+1)\lambda(\lambda+1)} \times \sum_{\mu} Y_{\lambda\mu}(\theta_p, \phi_p) Y_{\lambda\mu}^*(\theta, \phi), \quad (\text{II A.36})$$

since

$$(\mathbf{L}^2 - \lambda(\lambda+1)) Y_{\lambda\mu}(\theta, \phi) = 0. \quad (\text{II A.37})$$

The sum over μ in (36) depends only on the relative angle of the vectors \mathbf{r} and \mathbf{r}_p , and the operator \mathbf{L} acting on this sum can therefore be replaced by \mathbf{L}_p , where \mathbf{L}_p acts on the projectile coordinates.

For the magnetic multipole part of (32) we thus

²⁷ The complete relativistic interaction is derived in Sec. II B.1.

obtain

$$\mathfrak{H}_M(t) = \frac{4\pi i Z_1 e}{c} \sum_{\lambda\mu} \frac{1}{\lambda(2\lambda+1)} (\mathbf{L}_p \cdot \mathbf{v}_p) r_p^{-\lambda-1} \times Y_{\lambda\mu}(\theta_p, \phi_p) \mathfrak{N}^*(M\lambda, \mu), \quad (\text{II A.38})$$

where

$$\mathfrak{N}(M\lambda, \mu) = -\frac{i}{c(\lambda+1)} \int (\mathbf{j}_n \cdot \mathbf{L}) r^\lambda Y_{\lambda\mu}(\theta, \phi) d\tau \quad (\text{II A.39})$$

is the nuclear magnetic multipole moment, which is associated also with radiative transitions of order $M\lambda$.²²

If we describe the nuclear current in terms of a convection current of point charge protons and a magnetization current associated with point dipole moments of the nucleons, we have

$$\mathbf{j}_n(\mathbf{r}) = \sum_k e_k (\mathbf{v}_k \delta(\mathbf{r} - \mathbf{r}_k))_{\text{sym}} + \frac{e\hbar}{2M} g_{sk} \nabla \times \mathbf{s}_k \delta(\mathbf{r} - \mathbf{r}_k), \quad (\text{II A.40})$$

where \mathbf{s}_k and g_{sk} are the spin-vector and the spin-gyromagnetic ratio for the k th nucleon, while M is the proton mass. The subscript "sym" indicates a symmetrization of the factors in the parenthesis. With the expression (40) for \mathbf{j}_n we obtain the multipole moment (39) in the familiar form

$$\mathfrak{N}(M\lambda, \mu) = \frac{e\hbar}{2Mc} \sum_k \left(g_{sk} \mathbf{s}_k + \frac{2}{\lambda+1} g_{lk} \mathbf{l}_k \right) \cdot \nabla (r_k^\lambda Y_{\lambda\mu}(\theta_k, \phi_k)), \quad (\text{II A.41})$$

where g_{lk} is the orbital g factor for the k th nucleon.

Inserting (38) we get for the transition amplitude (6)

$$b_{ij} = \frac{4\pi Z_1 e}{i\hbar} \sum_{\lambda\mu} \frac{1}{2\lambda+1} \times \langle I_i M_i | \mathfrak{N}(M\lambda, \mu) | I_f M_f \rangle S_{M\lambda, \mu}, \quad (\text{II A.42})$$

where

$$S_{M\lambda, \mu} = -\frac{1}{\lambda} \frac{\hbar}{m_0 c} \mathbf{l}_p \cdot \int \nabla_p r_p^{-\lambda-1} \times Y_{\lambda\mu}(\theta_p, \phi_p) e^{i\omega t} dt. \quad (\text{II A.43})$$

We have used the relation [see (35)]

$$\mathbf{L}_p \cdot \mathbf{v}_p = \frac{i\hbar}{m_0} \mathbf{l}_p \cdot \Delta_p, \quad (\text{II A.44})$$

where $\hbar \mathbf{l}_p$ is the relative orbital angular momentum, which is a constant of the motion. This vector is perpendicular to the plane of the orbit and its magni-

tude is related to the deflection angle ϑ by

$$\hbar \mathbf{l}_p = a m_0 v \cot \frac{\vartheta}{2}. \quad (\text{II A.45})$$

It is convenient, as for the electric excitations, to evaluate the orbital integrals in the focal system (22). In this coordinate system we have

$$\mathbf{l}_p \cdot \nabla_p \Big|_{\theta_p = \pi/2} = l_p r_p^{-1} \frac{\partial}{\partial \theta_p} \Big|_{\theta_p = \pi/2} \quad (\text{II A.46})$$

and, by employing the formula

$$\frac{\partial}{\partial \theta_p} Y_{\lambda\mu}(\theta_p, \phi_p) \Big|_{\theta_p = \pi/2} = \left(\frac{2\lambda+1}{2\lambda+3} \right)^{\frac{1}{2}} [(\lambda+1)^2 - \mu^2]^{\frac{1}{2}} Y_{\lambda+1, \mu} \left(\frac{\pi}{2}, \phi_p \right), \quad (\text{II A.47})$$

we may express the orbital integrals (43) in terms of those involved in the electric excitations (15). By means of (45) and (24), one obtains

$$S_{M\lambda, \mu} = -c^{-1} a^{-\lambda} \left(\frac{2\lambda+1}{\lambda(2\lambda+3)} \right)^{\frac{1}{2}} [(\lambda+1)^2 - \mu^2]^{\frac{1}{2}} \times Y_{\lambda+1, \mu} \left(\frac{\pi}{2}, 0 \right) I_{\lambda+1, \mu}(\vartheta, \xi) \cot \frac{\vartheta}{2}. \quad (\text{II A.48})$$

In complete analogy with the derivation of the cross sections for electric excitations we thus obtain

$$d\sigma_M = \sum_{\lambda=1}^{\infty} d\sigma_{M\lambda}, \quad (\text{II A.49})$$

with

$$d\sigma_{M\lambda} = \left(\frac{Z_1 e}{\hbar c} \right)^2 a^{-2\lambda+2} B(M\lambda) df_{M\lambda}(\vartheta, \xi), \quad (\text{II A.50})$$

and

$$df_{M\lambda}(\vartheta, \xi) = \frac{4\pi^2}{(2\lambda+1)^2} \sum_{\mu} \frac{(\lambda+1)^2 - \mu^2}{\lambda^2(2\lambda+3)} \left| Y_{\lambda+1, \mu} \left(\frac{\pi}{2}, 0 \right) \right|^2 \times |I_{\lambda+1, \mu}(\vartheta, \xi)|^2 \cot^2 \frac{\vartheta}{2} \sin^{-4} \frac{\vartheta}{2} d\Omega. \quad (\text{II A.51})$$

We have here introduced

$$B(M\lambda) = \sum_{\mu M_f} |\langle I_i M_i | \mathfrak{N}(M\lambda, \mu) | I_f M_f \rangle|^2 = (2I_i+1)^{-1} |\langle I_i | \mathfrak{N}(M\lambda) | I_f \rangle|^2 \quad (\text{II A.52})$$

in analogy to (18) and have employed the relation (16).

The total excitation cross section of order $M\lambda$ is given by

$$\sigma_{M\lambda} = \left(\frac{Z_1 e}{\hbar c} \right)^2 a^{-2\lambda+2} B(M\lambda) f_{M\lambda}(\xi), \quad (\text{II A.53})$$

with

$$f_{M\lambda}(\xi) = \frac{16\pi^3}{(2\lambda+1)^2} \sum_{\mu} \frac{(\lambda+1)^2 - \mu^2}{\lambda^2(2\lambda+3)} \left| Y_{\lambda+1, \mu} \left(\frac{\pi}{2}, 0 \right) \right|^2 \times \int_0^{\pi} |I_{\lambda+1, \mu}(\vartheta, \xi)|^2 \cot^2 \frac{\vartheta}{2} \frac{\cos \frac{\vartheta}{2}}{\sin^3 \frac{\vartheta}{2}} d\vartheta. \quad (\text{II A.54})$$

II A.3. Discussion of Cross Sections

The electromagnetic excitation cross sections, derived above, are expressed in terms of the reduced nuclear transition probabilities and the functions $f(\xi)$ and $df(\vartheta, \xi)$. The orbital integrals $I_{\lambda\mu}$ entering in these functions are defined by Eq. (26) and can be expressed in terms of confluent hypergeometric functions of two variables (see Sec. II E.4). In the special cases of $\lambda=1$ or $\xi=0$, the $I_{\lambda\mu}$ reduce to simpler functions (see Secs. II E.5 and 6). The integrals have also been evaluated numerically, and the results are given, for $\lambda=2$, in Sec. II E.4. The numerically evaluated f and df functions are given in Sec. II C for $E1, E2, E3, E4, M1$, and $M2$ excitations.

An important feature of the functions $f(\xi)$ is the exponential decrease for large values of ξ (see, e.g., Fig. II.4). This is a consequence of the approximately adiabatic character of the collisions for $\xi > 1$, for which the collision time is large compared to the nuclear period [see (27)]. In the opposite limit of $\xi \rightarrow 0$, all the $f(\xi)$ approach a finite value except for the $E1$ and $M1$ excitations. The functions $f_{E1}(\xi)$ and $f_{M1}(\xi)$ increase logarithmically for small ξ (see Sec. II E.5) in analogy to the well-known logarithmic dependence of the atomic stopping power on the atomic excitation frequencies.

As already mentioned, the electromagnetic excitation involves the same nuclear matrix elements as the radiative transition of corresponding multipole order. Thus, the excitation process is subject to the usual selection rules

$$|I_i - I_f| \leq \lambda \leq I_i + I_f, \quad \pi_i \pi_f = \begin{cases} (-1)^\lambda & \text{for } E\lambda, \\ (-1)^{\lambda+1} & \text{for } M\lambda, \end{cases} \quad (\text{II A.55})$$

where π_i and π_f are the parities of the initial and final nuclear states.

There is therefore also a simple relation between the excitation cross section and the lifetime for the radiative decay of the excited state by the corresponding multipole transition. The probability per unit time for such a transition is given by²²

$$T = \frac{8\pi(\lambda+1)}{\lambda[(2\lambda+1)!!]^2} \frac{1}{\hbar} \left(\frac{\omega}{c} \right)^{2\lambda+1} B(\lambda; I_f \rightarrow I_i), \quad (\text{II A.56})$$

where the reduced transition probability $B(\lambda; I_f \rightarrow I_i)$ for the decay is related by

$$B(\lambda; I_f \rightarrow I_i) = \frac{2I_i+1}{2I_f+1} B(\lambda; I_i \rightarrow I_f) \quad (\text{II A.57})$$

to the reduced transition probability $B(\lambda; I_i \rightarrow I_f)$ entering into the expression for the excitation cross section. The relation (57) is equivalent to the fact that the magnitude of the reduced matrix elements $\langle I_i || \mathfrak{M}(\lambda) || I_f \rangle$ is symmetric with respect to interchange of initial and final state²³ (see (18)).

The electromagnetic field acting on the nucleus in a collision with a charged particle differs, however, in various respects from that involved in the emission or absorption of a photon, and this implies certain essential differences between the two processes as regards the relative contributions of the various multipole components. Thus, while in the radiative field the electric and magnetic field strengths are of equal magnitude, the magnetic field of the bombarding particle is only of order v/c as compared with the electric field. Magnetic excitations therefore are reduced, with respect to electric ones, by a factor $(v/c)^2$, apart from differences in the nuclear matrix elements. Moreover, while, in radiative processes, the relative intensities of consecutive multipole orders involve a factor $[(\omega/c)R_0]^2$, where R_0 is the nuclear radius, the corresponding factor in Coulomb excitation is $(R_0/a)^2$ [see (30) and (53)]. The latter factor is much larger than the former since, according to (27), we have $(\omega/c)a = (v/c)\xi$. Therefore, the cross section for Coulomb excitation does not decrease as rapidly with increasing multipole order as does the intensity of radiative processes.

A convenient unit in which to measure the nuclear transition probabilities $B(\lambda)$ is the "single-particle unit" defined by²²

$$B_{sp}(\lambda) = (2\lambda+1) \frac{e^2}{4\pi} \left(\frac{3}{3+\lambda} \right)^2 R_0^{2\lambda} \times \begin{cases} 1 & \text{for } E\lambda \\ 10 \left(\frac{\hbar}{McR_0} \right)^2 & \text{for } M\lambda, \end{cases} \quad (\text{II A.58})$$

where M is the proton mass. We have included, somewhat arbitrarily, a statistical factor $2\lambda+1$, since the Coulomb excitation usually, and always in even-even nuclei, involves an increase in the nuclear spin.

Figure II.1a gives the excitation cross sections for proton bombardment of a medium heavy nucleus ($Z_2=50, A_2=120$), assuming $B(\lambda)$ equal to the unit (58) with $R_0=1.2 \cdot A^{1/3} \cdot 10^{-13}$ cm.²⁸ The excitation energy is taken to be 200 kev.

²⁸ This value for the nuclear radius seems the most appropriate in connection with the interpretation of evidence regarding the nuclear charge distribution (see Chapter V).

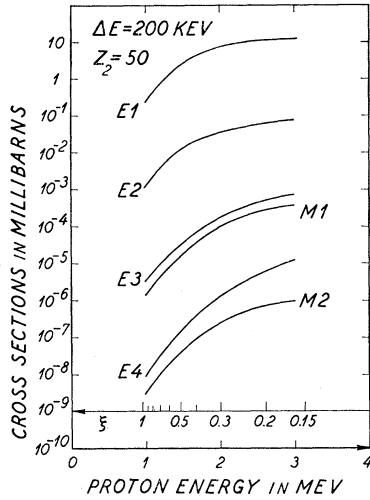


FIG. II.1a. Excitation cross sections for nuclear transitions of single particle strength. The curves give the total Coulomb excitation cross sections of various multipole orders for proton bombardment of a nucleus with $Z_2=50$ [see (II A.30) and (II A.53), and Fig. II.4]. The excitation energy is taken to be 200 kev, and the reduced nuclear transition probabilities to be given by the single particle units (II A.58) with $R_0=5.9 \cdot 10^{-13}$ cm.

The empirical values of the nuclear transition probabilities obtained from lifetime determinations of γ transitions show major departures from the single-particle unit (58).²⁹ Thus, the relatively few electric dipole transitions, which have been observed in the low-energy nuclear spectra, have in most cases transition probabilities many orders of magnitude smaller than (58). In contrast low-energy electric quadrupole transitions, which occur with great frequency, are often found to be strongly enhanced as compared with single-particle estimates. Thus, $E2$ transitions with a strength of 10–100 single-particle units occur systematically in most regions of elements (see Chapter V).

For these reasons, the electric quadrupole transitions are of special importance in the Coulomb excitation, and in fact it appears that the overwhelming majority of the excitations so far observed are of $E2$ type (see Chapter IV).

As seen from Fig. II.1a, the cross sections for magnetic excitation are very much smaller than for electric excitations; thus, even in cases where the radiative de-excitation process takes place by a mixed $M1+E2$ transition, the excitation will almost always be of rather pure $E2$ type.

II A.4. Angular Distribution of De-Excitation γ Rays

The nuclear states populated by Coulomb excitation decay by emission of γ radiation or conversion electrons. The angular distribution of this radiation can be obtained from the excitation amplitudes b_{if} given above.

²⁹ For a survey of these data, see M. Goldhaber and A. W. Sunyar, Chapter XVI of *Beta- and Gamma-Ray Spectroscopy*, edited by K. Siegbahn (North Holland Publishing Company, Amsterdam, 1955).

Denoting the nuclear state to which the de-excitation takes place by ff , the angular distribution of the emitted γ radiation is given by³⁰

$$W_{\vartheta, \varphi}(\Omega_\gamma) = \sum_{\sigma M_i M_{ff}} \left| \sum_{M_f} b_{if} \langle I_{ff} M_{ff} | H_\gamma(\Omega_\gamma, \sigma) | I_f M_f \rangle \right|^2, \quad (\text{II A.59})$$

where $H_\gamma(\Omega_\gamma, \sigma)$ is the interaction Hamiltonian for emission of a γ quantum in the direction Ω_γ , and with polarization σ . We have assumed unpolarized target nuclei and have summed over the polarizations of the γ quantum. The distribution (59) refers to a definite orbit of the projectile characterized by the polar angles ϑ, φ of the scattered particle.

We first consider the case in which the excitation takes place by a transition of pure multipole order λ which may be either electric or magnetic. Using the expressions (14) and (42), and the relation (16), we get from (59)

$$\begin{aligned} W_{\vartheta, \varphi}(\Omega_\gamma) = & \sum \begin{pmatrix} I_i & \lambda & I_f \\ -M_i & \mu & M_f \end{pmatrix} \\ & \times \begin{pmatrix} I_i & \lambda & I_f \\ -M_i & \mu' & M_f' \end{pmatrix} S_{\lambda\mu} S_{\lambda\mu'}^* \\ & \times \langle I_{ff} M_{ff} | H_\gamma(\Omega_\gamma, \sigma) | I_f M_f \rangle \\ & \times \langle I_{ff} M_{ff} | H_\gamma(\Omega_\gamma, \sigma) | I_f M_f' \rangle^*, \quad (\text{II A.60}) \end{aligned}$$

where we have left out constant factors. The summation in (60) is to be extended over $M_i, M_f, M_f', \mu, \mu', M_{ff}$, and σ .

The distribution (60) may conveniently be expressed in terms of the correlation function for a hypothetical γ - γ cascade in which the first transition is a pure 2^λ -pole radiation³¹ (see Fig. II.2). This latter correlation func-

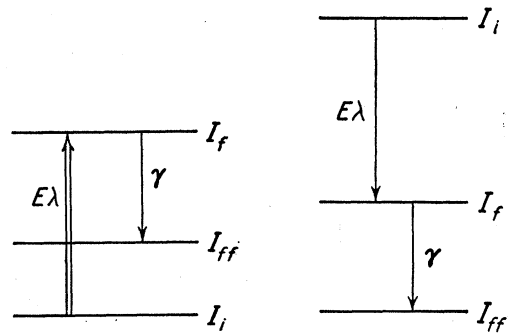


FIG. II.2. Hypothetical transitions involved in describing angular distribution of gamma rays following Coulomb excitation. The ground-state spins, the spin of the state excited by Coulomb excitation, and the spin of the final state populated by the gamma ray are denoted by I_i, I_f , and I_{ff} , respectively. The figure on the right then gives the hypothetical γ - γ cascade employed in obtaining the angular distribution of the gamma rays following Coulomb excitation.

³⁰ D. L. Falkoff and G. E. Uhlenbeck, *Phys. Rev.* **79**, 323 (1950).

³¹ L. C. Biedenharn and M. E. Rose, *Revs. Modern Phys.* **25**, 729 (1953).

tion differs from (60) only in the replacement of $S_{\lambda\mu}$ by the rotation matrix $D_{\mu\sigma'\lambda}(\mathcal{R})$, where \mathcal{R} denotes the rotation from the fixed coordinate system to a system whose z axis points in the direction $\Omega_{\gamma'}$ of the first γ quantum. The polarization index σ' refers to circular polarization.

As in the usual treatment of angular correlation, we employ the relation²⁴

$$\begin{aligned} & \sum_{M_i} \begin{pmatrix} I_i & \lambda & I_f \\ -M_i & \mu & M_f \end{pmatrix} \begin{pmatrix} I_i & \lambda' & I_f' \\ -M_i & \mu' & M_f' \end{pmatrix} \\ &= \sum_{k\kappa} (-1)^{2N'+k-I_i+\mu+M_f'} (2k+1) \begin{pmatrix} \lambda & \lambda' & k \\ \mu & -\mu' & \kappa \end{pmatrix} \\ & \quad \times \begin{pmatrix} I_f & I_f' & k \\ -M_f & M_f' & \kappa \end{pmatrix} \left\{ \begin{matrix} \lambda & \lambda' & k \\ I_f' & I_f & I_i \end{matrix} \right\}, \quad (\text{II A.61}) \end{aligned}$$

where we have introduced the well-known Wigner notation for the Racah coefficient $W(\lambda\lambda'I_f I_f | k I_i)$ through the definition

$$\begin{aligned} & \left\{ \begin{matrix} j_1 & j_2 & j_3 \\ l_1 & l_2 & l_3 \end{matrix} \right\} \\ &= (-1)^{j_1+j_2+l_2+l_1} W(j_1 j_2 l_2 | j_3 l_3). \quad (\text{II A.62}) \end{aligned}$$

In this manner, we obtain an expression for $W(\Omega_\gamma)$ which involves the $S_{\lambda\mu}$ only in the combination

$$\sum_{\mu\mu'} (-1)^\mu \begin{pmatrix} \lambda & \lambda & k \\ \mu & -\mu' & \kappa \end{pmatrix} S_{\lambda\mu} S_{\lambda\mu'}^*. \quad (\text{II A.63})$$

In the γ - γ correlation the corresponding expression reduces to

$$\begin{pmatrix} \lambda & \lambda & k \\ 1 & -1 & 0 \end{pmatrix} \left(\frac{4\pi}{2k+1} \right)^{\frac{1}{2}} Y_{k\kappa}^*(\Omega_{\gamma'}) \quad (\text{II A.64})$$

after summation over the polarization index σ' .

Thus, if we write the angular correlation in the γ - γ cascade in the usual way

$$\begin{aligned} W_{\Omega_{\gamma'}}(\Omega_\gamma) &= \sum_k A_k^{(\lambda)} P_k(\cos(\Omega_{\gamma'}, \Omega_\gamma)) \\ &= \sum_{k\kappa} A_k^{(\lambda)} \frac{4\pi}{2k+1} Y_{k\kappa}^*(\Omega_{\gamma'}) Y_{k\kappa}(\Omega_\gamma), \quad (\text{II A.65}) \end{aligned}$$

where $(\Omega_{\gamma'}, \Omega_\gamma)$ is the angle between the γ rays, it is seen that the angular distribution function (60) may be written

$$W_{\vartheta, \varphi}(\Omega_\gamma) = \sum_{k\kappa} a_{k\kappa}^{(\lambda)}(\vartheta, \varphi, \xi) A_k^{(\lambda)} Y_{k\kappa}(\Omega_\gamma). \quad (\text{II A.66})$$

The coefficients $a_{k\kappa}^{(\lambda)}$, which are independent of the nuclear states involved, and of the de-excitation process, may be expressed in the form

$$a_{k\kappa}^{(\lambda)}(\vartheta, \varphi, \xi) = b_{k\kappa}^{(\lambda)} / b_{00}^{(\lambda)}, \quad (\text{II A.67})$$

with

$$\begin{aligned} b_{k\kappa}^{(\lambda)} &= -(2k+1)^{-\frac{1}{2}} \begin{pmatrix} \lambda & \lambda & k \\ 1 & -1 & 0 \end{pmatrix}^{-1} \\ & \quad \times \sum_{\mu\mu'} (-1)^\mu \begin{pmatrix} \lambda & \lambda & k \\ \mu & -\mu' & \kappa \end{pmatrix} S_{\lambda\mu} S_{\lambda\mu'}^*. \quad (\text{II A.68}) \end{aligned}$$

The normalization of $a_{k\kappa}^{(\lambda)}$ is then such that $a_{00}^{(\lambda)} = 1$. As in the cascade, only terms with even k occur in (66). It is noted that $b_{00}^{(\lambda)}$ reduces to

$$b_{00}^{(\lambda)} = \sum_{\mu} |S_{\lambda\mu}|^2, \quad (\text{II A.69})$$

and is thus directly related to the differential excitation cross section (see (21)).

The coefficients A_k in the γ - γ correlation (65) are given by³¹

$$A_k^{(\lambda)} = F_k(\lambda, I_i I_f) \sum_{L L'} \delta_L \delta_{L'} F_k(LL' I_f I_f), \quad (\text{II A.70})$$

where δ_L^2 is the intensity of the 2^L -pole radiation in the γ transition $I_f \rightarrow I_{ff}$. With the present definition of the multipole operators, the relative values of δ_L are given by

$$\delta_L \propto i^{s(L)} \frac{q^L}{(2L+1)!!} \left(\frac{L+1}{L} \right)^{\frac{1}{2}} \langle I_{ff} | \mathfrak{M}(\pi L) | I_f \rangle, \quad (\text{II A.71})$$

with

$$s(L) = \begin{cases} L & \text{for } EL \\ L+1 & \text{for } ML. \end{cases} \quad (\text{II A.71a})$$

The product $\delta_L \delta_{L'}$ is always real since $(-1)^{s(L)} = \pi$ (the parity). The coefficients F_k are geometrical factors defined by

$$\begin{aligned} F_k(LL'I_1 I_2) &= (-1)^{I_1+I_2-1} [(2k+1)(2I_2+1)(2L+1)(2L'+1)]^{\frac{1}{2}} \\ & \quad \times \begin{pmatrix} L & L' & k \\ 1 & -1 & 0 \end{pmatrix} \left\{ \begin{matrix} L & L' & k \\ I_2 & I_2 & I_1 \end{matrix} \right\}, \quad (\text{II A.72}) \end{aligned}$$

and

$$F_k(LI_1 I_2) = F_k(LLI_1 I_2),$$

and are tabulated³² in references 31 and 33.

The orbital integrals $S_{\lambda\mu}$ in (68) are most easily evaluated in the focal system (see Fig. II.1) in which they are given by (24) and (48). One thereby obtains the angular distribution coefficients $b_{k\kappa}^{(\lambda)}$ in the focal system. It is, however, often more convenient to express

³² L. C. Biedenharn and M. E. Rose (reference 31) have given the interference terms (for $L \neq L'$) in the form $G_k(LL'I_1 I_2) = (-1)^{I_2-I_1-1} [(2I_2+1)(2L+1)(2L'+1)]^{-\frac{1}{2}} F_k(LL'I_1 I_2)$.

The coefficients A_k are tabulated in Table II.11 for some cases often encountered in Coulomb excitation.

³³ M. Ferentz and N. Rosenzweig, Argonne National Laboratory report, ANL 5324.

the angular distribution of the γ quanta in a coordinate system with the z axis in the direction of the incident beam of particles. This may be obtained by a simple transformation which, in the case of electric excitations, gives

$$b_{k\kappa}^{E\lambda}(\vartheta, \varphi, \xi) = -(2k+1)^{-\frac{1}{2}} \begin{pmatrix} \lambda & \lambda & k \\ 1 & -1 & 0 \end{pmatrix}^{-1} \\ \times \sum_{\mu\mu'\kappa'} (-1)^\mu \begin{pmatrix} \lambda & \lambda & k \\ \mu & -\mu' & \kappa' \end{pmatrix} Y_{\lambda\mu} \left(\frac{\pi}{2}, 0 \right) \\ \times Y_{\lambda\mu'} \left(\frac{\pi}{2}, 0 \right) I_{\lambda\mu}(\vartheta, \xi) I_{\lambda\mu'}(\vartheta, \xi) \\ \times D_{\kappa'\kappa}^k \left(\frac{\pi}{2} + \frac{\vartheta}{2}, \frac{\pi}{2}, \varphi \right), \quad (\text{II A.73})$$

where the Eulerian angles^{32a} $(\pi/2 + \vartheta/2, \pi/2, \varphi)$ represent the rotation from the coordinate system of the incident beam to the focal system of the orbit in question.

The distribution function (66) applies to a measurement of γ rays in coincidence with particles scattered inelastically in a definite direction. The total angular distribution of the γ 's, irrespective of the scattering angle of the projectile, is obtained by multiplying (66) by the differential excitation cross section (28) or (50), and integrating over ϑ and φ . This gives

$$W(\vartheta_\gamma) = \sum_k a_k^\lambda(\xi) A_k^{(\lambda)} P_k(\cos\vartheta_\gamma), \quad (\text{II A.74})$$

where ϑ_γ is the angle between the direction of the incident beam and the γ quantum. The coefficients $a_k^\lambda(\xi)$ are given by

$$a_k^\lambda(\xi) = b_k^\lambda/b_0^\lambda, \quad (\text{II A.75})$$

with

$$b_k^{E\lambda}(\xi) = -(2k+1)^{-\frac{1}{2}} \begin{pmatrix} \lambda & \lambda & k \\ 1 & -1 & 0 \end{pmatrix}^{-1} \sum_{\mu\mu'\kappa} (-1)^\mu \begin{pmatrix} \lambda & \lambda & k \\ \mu & -\mu' & \kappa \end{pmatrix} \\ \times Y_{\lambda\mu} \left(\frac{\pi}{2}, 0 \right) Y_{\lambda\mu'} \left(\frac{\pi}{2}, 0 \right) \int_0^\pi I_{\lambda\mu}(\vartheta, \xi) I_{\lambda\mu'}(\vartheta, \xi) Y_{k\kappa} \left(\frac{\pi}{2}, \frac{\pi}{2} + \frac{\vartheta}{2} \right) \frac{\cos \frac{\vartheta}{2}}{\sin^3 \frac{\vartheta}{2}} d\vartheta, \quad (\text{II A.76})$$

and

$$b_k^{M\lambda}(\xi) = -(2k+1)^{-\frac{1}{2}} \begin{pmatrix} \lambda & \lambda & k \\ 1 & -1 & 0 \end{pmatrix}^{-1} \sum_{\mu\mu'\kappa} (-1)^\mu \begin{pmatrix} \lambda & \lambda & k \\ \mu & -\mu' & \kappa \end{pmatrix} [(\lambda+1)^2 - \mu^2][(\lambda+1)^2 - \mu'^2]^{\frac{1}{2}} \\ \times Y_{\lambda+1, \mu} \left(\frac{\pi}{2}, 0 \right) Y_{\lambda+1, \mu'} \left(\frac{\pi}{2}, 0 \right) \int_0^\pi I_{\lambda+1, \mu}(\vartheta, \xi) I_{\lambda+1, \mu'}(\vartheta, \xi) Y_{k\kappa} \left(\frac{\pi}{2}, \frac{\pi}{2} + \frac{\vartheta}{2} \right) \cot^2 \frac{\vartheta}{2} \frac{\cos \frac{\vartheta}{2}}{\sin^3 \frac{\vartheta}{2}} d\vartheta. \quad (\text{II A.77})$$

The coefficients $a_k^{E\lambda}(\xi)$ have been evaluated numerically for $E1$ and $E2$ excitations. The results are shown in Fig. II.8, where they represent the limiting values for $\nu \rightarrow 0$ of the corresponding quantum-mechanical expressions. In the case of $M1$ excitations, where (77) only contains terms with $\mu = \mu' = \kappa = 0$ (see (25)), one obtains

$$a_2^{M1}(\xi) = 1, \quad (\text{II A.78})$$

independent of ξ .

If the polarization of the decay γ ray is measured, one may obtain the correlation functions in a similar manner as above by comparing with a γ - γ cascade in which the polarization of the second quantum is measured. Thus, the probability for emission of a γ ray at an angle ϑ_γ and with a given direction of polarization is again of the form (74) with the only difference that

the functions $P_k(\cos\vartheta_\gamma)$ are to be replaced by³¹

$$\mathcal{P}_k(LL'; \vartheta_\gamma \psi_\gamma) \\ = P_k(\cos\vartheta_\gamma) + (-1)^{p(L')} \left[\frac{(k-2)!}{(k+2)!} \right]^{\frac{1}{2}} \begin{pmatrix} L & L' & k \\ 1 & 1-2 & \end{pmatrix} \\ \times \begin{pmatrix} L & L' & k \\ 1 & -1 & 0 \end{pmatrix}^{-1} \cos 2\psi_\gamma P_k^2(\cos\vartheta_\gamma), \quad (\text{II A.78a})$$

where ψ_γ is the angle between the electric vector and the plane determined by the direction of the incident projectile and the γ ray. The phase $(-1)^{p(L')}$ is $+1$ if L' is an electric radiation, and -1 if it is magnetic. The functions P_k^2 are the associated Legendre polynomials. If the decay radiation is of mixed multipole

^{32a} We have used the same definition of the Eulerian angles as that used in reference 6 (see also reference 24).

type, each term in the coefficient $A_k^{(\lambda)}$ (see (70)) is to be multiplied by the appropriate angular function $\mathcal{O}_k(LL')$.

If the excitation is of mixed multipole type, the angular distribution of the γ rays, in contrast to the excitation cross sections, contains additional interference terms.

In order to derive the general expression for the angular distribution, we write the transition amplitude b_{if} in the following form (see (14), (16), and (42))

$$b_{if} = \frac{4\pi Z_1 e}{i\hbar} \sum_{\pi\lambda\mu} (-1)^{I_i - M_i} (2\lambda + 1)^{-1} \begin{pmatrix} I_i & \lambda & I_f \\ -M_i & \mu & M_f \end{pmatrix} \times \langle \pi_i I_i || \mathfrak{M}(\pi\lambda) || \pi_f I_f \rangle S_{\pi\lambda\mu}, \quad (\text{II A.79})$$

where π_i and π_f indicate the parity of the initial and final nuclear state, while π is the parity of the excitation process, i.e., $\pi = \pi_i \pi_f$. The $S_{\pi\lambda\mu}$ are defined by (15) and (43) for electric and magnetic excitations.

By following the same procedure as above, it is readily seen that the angular distribution (66) now takes the form

$$W_{\vartheta, \varphi}(\Omega_\gamma) = \sum_{k\kappa} \sum_{\lambda\pi\lambda'\pi'} c_{k\kappa}^{\pi\lambda, \pi'\lambda'}(\vartheta, \varphi, \xi) F_k(\lambda\lambda' I_i I_f) \times \sum_{LL'} \delta_L \delta_{L'} F_k(LL' I_f I_f) Y_{k\kappa}(\Omega_\gamma), \quad (\text{II A.80})$$

with

$$c_{k\kappa}^{\pi\lambda, \pi'\lambda'}(\vartheta, \varphi, \xi) = -[(2k+1)(2\lambda+1)^2(2\lambda'+1)^2]^{-\frac{1}{2}} \begin{pmatrix} \lambda & \lambda' & k \\ 1 & -1 & 0 \end{pmatrix}^{-1} \times \langle \pi_i I_i || \mathfrak{M}(\pi\lambda) || \pi_f I_f \rangle \langle \pi_i I_i || \mathfrak{M}(\pi'\lambda') || \pi_f I_f \rangle \times \sum_{\mu\mu'} (-1)^\mu \begin{pmatrix} \lambda & \lambda' & k \\ \mu & -\mu' & \kappa \end{pmatrix} S_{\pi\lambda\mu} S_{\pi'\lambda'\mu'}^*. \quad (\text{II A.81})$$

For $k = \kappa = 0$, the $c_{00}^{\pi\lambda, \pi'\lambda'}$ are proportional to the differential excitation cross sections. For $\lambda \neq \lambda'$, the $c_{00}^{\pi\lambda, \pi'\lambda'}$ vanish.

In order to obtain the total angular distribution of the γ quanta, we multiply (80) by the Rutherford cross section (2) and integrate over ϑ and φ . One thus obtains the angular distribution in the form

$$W(\vartheta_\gamma) = \sum_k \sum_{\lambda\lambda'} a_k^{\pi\lambda, \pi'\lambda'}(\xi) (\sigma_{\pi\lambda})^{\frac{1}{2}} (\sigma_{\pi'\lambda'})^{\frac{1}{2}} F_k(\lambda\lambda' I_i I_f) \times \sum_{LL'} \delta_L \delta_{L'} F_k(LL' I_f I_f) P_k(\cos\vartheta_\gamma), \quad (\text{II A.82})$$

where $\sigma_{\pi\lambda}$ is the total excitation cross section of multipole order $\pi\lambda$ and where the sign of the square root is the same as that of the reduced matrix element, $\langle \pi_i I_i || \mathfrak{M}(\pi\lambda) || \pi_f I_f \rangle$. These latter are the same as those occurring in the radiative decay $I_f \rightarrow I_i$ (see (71)). The a coefficients in (82) are given by

$$a_k^{\pi\lambda, \pi'\lambda'}(\xi) = b_k^{\pi\lambda, \pi'\lambda'} / (b_0^{\pi\lambda})^{\frac{1}{2}} (b_0^{\pi'\lambda'})^{\frac{1}{2}}, \quad (\text{II A.83})$$

where the $b_0^{\pi\lambda}$ are given by (76) and (77). Furthermore

$$b_k^{\pi\lambda, \pi'\lambda'} = b_k^{\pi\lambda}. \quad (\text{II A.84})$$

The most important case where interference terms appear is that of a mixed electric and magnetic excitation, for which the $b_k^{\pi\lambda, \pi'\lambda'}(\xi)$ are given by

$$b_k^{E\lambda, M\lambda'}(\xi) = (2k+1)^{-\frac{1}{2}} \begin{pmatrix} \lambda & \lambda' & k \\ 1 & -1 & 0 \end{pmatrix}^{-1} \times \sum_{\mu\mu'\kappa} (-1)^\mu \begin{pmatrix} \lambda & \lambda' & k \\ \mu & -\mu' & \kappa \end{pmatrix} [(\lambda'+1)^2 - \mu'^2]^{\frac{1}{2}} \times Y_{\lambda\mu}\left(\frac{\pi}{2}, 0\right) Y_{\lambda'+1, \mu'}\left(\frac{\pi}{2}, 0\right) \times \int_0^\pi I_{\lambda\mu}(\vartheta, \xi) I_{\lambda'+1, \mu'}(\vartheta, \xi) \times Y_{k\kappa}\left(\frac{\pi}{2}, \frac{\pi}{2}, \frac{\vartheta}{2}\right) \cot \frac{\vartheta}{2} \frac{\cos \frac{\vartheta}{2}}{\sin^3 \frac{\vartheta}{2}} d\vartheta. \quad (\text{II A.85})$$

The decay of the excited nuclear level may also take place by emission of internal conversion electrons. The angular distribution of these electrons is given by expressions similar to those applying to the γ distribution, with the only difference that the F_k factors for the decay are to be multiplied by appropriate coefficients depending on the parameters of the conversion process.³⁴

II A.5. Symmetrization of Classical Cross Sections

The classical treatment of the excitation process neglects the effect of the energy loss on the motion of the projectile. It may be expected, however, that improved expressions for the excitation cross sections may be obtained by substituting for the particle velocity v entering in these expressions, some mean value of initial and final velocity v_i and v_f , rather than the initial velocity assumed above.

While the choice of v leading to the best approximation for the cross sections cannot be decided within the scope of the classical treatment, it follows immediately from the general character of the quantum-mechanical formalism, considered in the next section, that when the probability for excitation in a single encounter is small the excitation cross section is symmetrical in v_i and v_f , except for a factor v_f/v_i . In fact, the cross section is inversely proportional to the flux of the incident par-

³⁴ See Biedenharn and Rose, reference 31, which contains tables of the coefficients (denoted in this reference by b) involved in the correlation with K -shell conversion electrons, calculated for a point charge nucleus.

ticles, and thus to v_i , while proportional to the density of final states, i.e., to v_f . In addition, the cross section involves the square of a matrix element which is symmetrical in the initial and final state [see (II B.25 and 26)].

A straightforward way of symmetrizing the classical cross sections is first to introduce symmetrized parameters a and ξ , given by

$$a = \frac{Z_1 Z_2 e^2}{m_0 v_i v_f}, \quad (\text{II A.86})$$

and

$$\xi = \frac{Z_1 Z_2 e^2}{\hbar} \left(\frac{1}{v_f} - \frac{1}{v_i} \right) \quad (\text{II A.87})$$

to replace (3) and (27), respectively. It is readily seen that the expressions (86) and (87) for a and ξ are equal to (3) and (27), respectively, to lowest order in $\Delta E/E$.³⁵ Although (87) changes sign when v_i and v_f are interchanged, the f functions are not affected, since they are even functions of ξ .

Appropriately symmetrized expressions for the excitation cross sections may thus be obtained by replacing (28) and (50) by

$$d\sigma_{E\lambda} = \left(\frac{Z_1 e}{\hbar v_i} \right)^2 a^{-2\lambda+2} B(E\lambda) df_{E\lambda}(\vartheta, \xi), \quad (\text{II A.88})$$

and

$$d\sigma_{M\lambda} = \left(\frac{Z_1 e}{\hbar c} \right)^2 \frac{v_f}{v_i} a^{-2\lambda+2} B(M\lambda) df_{M\lambda}(\vartheta, \xi), \quad (\text{II A.89})$$

and similarly for the total cross sections. In these expressions a and ξ are given by (86) and (87). Likewise, symmetrized expressions for the angular distribution of the emitted γ rays are obtained by employing, in the formulas in Sec. II A.4, the symmetrized expression (87) for ξ .

It is found, by comparison with the quantum-mechanical results (see Sec. II B.6), that the symmetrized expressions represent an essential improvement over the unsymmetrized. In fact, the symmetrized total cross sections reproduce the quantum-mechanical to within a few percent, for values of η as low as 3, and even for ξ as large as 2 (see Fig. II.6). This corresponds to a collision in which the particle loses more than half its energy, and for which the unsymmetrized cross sections would be in error by more than a factor hundred.

The angular distribution of the emitted γ radiation is found to be less accurately given by symmetrized classical formulas, except for very large values of η (see

Table II.9). Similarly, the differential excitation cross section may be expected to be fairly sensitive to quantum corrections.

II A.6. Excitation of Projectile

If the projectile is a composite particle, the collision may also lead to the excitation of the projectile. This process is entirely analogous to the excitation of the target nucleus, and corresponds merely to the interchange of the roles of nucleus and projectile. The interaction is now proportional to the nuclear charge and to the projectile transition matrix element, and the excitation cross section is thus obtained from the cross section for target excitation by simply replacing the factor Z_1^2 in (88) and (89) by Z_2^2 and the quantities ΔE , ξ , and $B(\lambda)$ by those appropriate to the projectile excitation.

The angular distribution of the emitted γ rays following projectile excitation is the same as for excitation of the target nucleus. However, the γ energies may be somewhat shifted by the Doppler effect if the stopping time for the projectile is longer than the lifetime of the excited state. To first order in the projectile velocity, the γ energy is given by

$$E_\gamma = \Delta E \left(1 + \frac{v_{1f}}{c} \cos u \right), \quad (\text{II A.90})$$

where v_{1f} is the velocity of the projectile at the time of emission (measured in the laboratory system) and u the angle between the scattered projectile and the direction of the γ ray. Even if (90) is averaged over the direction of the scattered projectile, there will remain some dependence of the average E_γ on the direction in which the γ ray is observed.

II B. Quantum-Mechanical Theory

In this Section we consider the quantum-mechanical treatment of electromagnetic excitations of nuclei. In the first part (Sec. II B.1) we give a relativistic derivation of the excitation cross section, considering the interaction as arising from the exchange of a photon between projectile and nucleus. This method is equivalent to the use of the retarded Greens functions for the interaction.³⁶ In most applications it is sufficient to include only the leading term in the projectile velocity in the expressions for the electric and magnetic excitation cross sections (Sec. II B.2).

These cross sections can be expressed as sums of terms referring to the different angular momenta of the incoming and outgoing projectile (Sec. II B.3). Each of the terms involves a radial matrix element which can be evaluated in terms of known functions, and expressed

³⁵ Arguments for the special choice (87) for ξ have been given by K. A. Ter-Martirosyan, reference 5, and by Sherr, Li, and Christy, Phys. Rev. 96, 1258 (1954).

³⁶ See M. Jean and J. Prentki, reference 26; Biedenharn, McHale, and Thaler, reference 18.

in a form convenient for numerical computation (Sec. II B.4). Similarly, in Sec. II B.5 the angular distribution of the de-excitation γ rays is expressed in terms of these radial matrix elements.

Approximate values for the radial matrix elements can be obtained by means of the WKB method (Sec. II B.6) which in most cases of interest is found to yield a high degree of accuracy. In this section we also discuss the transition of the quantum-mechanical cross sections to the symmetrized classical expressions for large values of the parameter η .

II B.1. Derivation of Excitation Cross Sections

For the system consisting of projectile, nucleus, and the quantized electromagnetic field, we take as the zero-order Hamiltonian

$$\mathcal{H}_0 = \mathcal{H}_p + \mathcal{H}_n + \mathcal{H}_{\text{rad}} + \frac{Z_1 Z_2 e^2}{r_p}, \quad (\text{II B.1})$$

where the three first terms represent the free Hamiltonians of projectile, nucleus, and radiation field, respectively. In (1) we have also included the static point charge interaction between the projectile and the nucleus. In the relativistic treatment we shall neglect the nuclear recoil, so that the nuclear center of mass may be taken as the fixed origin of the coordinate system. The recoil effects may be reintroduced in the non-relativistic part of the cross sections (see below), and thus the only essential approximation involved here is that of neglecting the effect of the recoil in the relativistic corrections.

It is convenient to divide the electromagnetic field into a transverse part described by a vector potential \mathbf{A} for which $\text{div} \mathbf{A} = 0$ and a longitudinal part. The latter contributes the instantaneous Coulomb interaction,³⁷ and the total interaction Hamiltonian is thus

$$\mathcal{H}_{\text{int}} = -\frac{1}{c} \int (\mathbf{j}_p(\mathbf{r}) + \mathbf{j}_n(\mathbf{r})) \cdot \mathbf{A}(\mathbf{r}) d\tau + \mathcal{H}_{\text{coul}} - \frac{Z_1 Z_2 e^2}{r_p}, \quad (\text{II B.2})$$

where

$$\mathcal{H}_{\text{coul}} = \int \frac{\rho_p(\mathbf{r}) \rho_n(\mathbf{r}')}{|\mathbf{r} - \mathbf{r}'|} d\tau d\tau', \quad (\text{II B.3})$$

and where ρ_p and \mathbf{j}_p are the charge and current density operators for the projectile.

The vector potential is expanded in multipole com-

ponents according to³⁸

$$\mathbf{A}(\mathbf{r}) = \sum_q \sum_{\lambda=1}^{\infty} \sum_{\mu=-\lambda}^{\lambda} \{ a(E\lambda, \mu, q) \mathbf{A}(E\lambda, \mu, q) + a(M\lambda, \mu, q) \mathbf{A}(M\lambda, \mu, q) + \text{compl. conj.} \}, \quad (\text{II B.4})$$

where the electric and magnetic multipole fields are given by

$$\mathbf{A}(E\lambda, \mu, q) = \left(\frac{8\pi c^2}{\lambda(\lambda+1)} \right)^{\frac{1}{2}} R^{-\frac{1}{2}} \nabla \times \mathbf{L}(j_\lambda(qr) Y_{\lambda\mu}(\theta, \phi)), \quad (\text{II B.5})$$

and

$$\mathbf{A}(M\lambda, \mu, q) = i \left(\frac{8\pi c^2 q^2}{\lambda(\lambda+1)} \right)^{\frac{1}{2}} R^{-\frac{1}{2}} \mathbf{L}(j_\lambda(qr) Y_{\lambda\mu}(\theta, \phi)). \quad (\text{II B.6})$$

The angular momentum operator \mathbf{L} is defined by (II A.35), and $j_\lambda(qr)$ represents the spherical Bessel function.³⁹ The multipole fields (5) and (6) are associated with photons of angular momentum λ , magnetic quantum number μ , wave number q , and parity $(-1)^\lambda$ and $(-1)^{\lambda+1}$ for the electric and magnetic multipole fields, respectively. The fields are enclosed in a large sphere of radius R .

The coefficients a in (4) and their conjugates are the photon absorption and the emission operators. With the normalization (5) and (6) the nonvanishing matrix elements of these operators are given by (see reference 37)

$$\langle n | a | n+1 \rangle = \langle n+1 | a^* | n \rangle = \left(\frac{\hbar(n+1)}{2qc} \right)^{\frac{1}{2}}, \quad (\text{II B.7})$$

where $|n\rangle$ represents a state with n photons of the type in question.

The eigenstates of the Hamiltonian (1) are represented by a wave function φ , for the projectile moving in the point Coulomb field of the nucleus multiplied by a nuclear wave function ψ , and is further specified by a number of free photons. We consider a transition from an initial state i with the nucleus in the ground state to a final state f where the projectile has transferred an energy ΔE to the nucleus. In initial and final state no photons are present. To first order in the charge of the projectile this transition receives partly a first-order contribution from the Coulomb term in (2) and partly a second-order contribution from the first term in (2) corresponding to the emission of a photon by the projectile, and its reabsorption by the nucleus (or vice versa).

To this approximation the transition matrix element

³⁸ See, e.g., W. Franz, *Z. Physik* **127**, 363 (1950); B. Stech, *Z. Naturforsch.* **7a**, 401 (1952).

³⁹ We use the same notation for the spherical cylinder functions as employed in L. I. Schiff, *Quantum Mechanics* (McGraw-Hill Book Company, Inc., New York, 1949).

³⁷ See, e.g., W. Heitler, *The Quantum Theory of Radiation* (Oxford University Press, New York, 1944), second edition, Sec. III.10.

is thus given by

$$\begin{aligned} \langle f | \mathcal{H}^{(1)} | i \rangle = \sum_{\lambda\mu q} \frac{\hbar}{2qc^3} & \left\{ \frac{\langle \varphi_f | \int \mathbf{j}_p \cdot \mathbf{A}(E\lambda, \mu, q) d\tau | \varphi_i \rangle \langle \psi_f | \int \mathbf{j}_n \cdot \mathbf{A}^*(E\lambda, \mu, q) d\tau | \psi_i \rangle}{-\Delta E - \hbar cq} \right. \\ & + \frac{\langle \psi_f | \int \mathbf{j}_n \cdot \mathbf{A}(E\lambda, \mu, q) d\tau | \psi_i \rangle \langle \varphi_f | \int \mathbf{j}_p \cdot \mathbf{A}^*(E\lambda, \mu, q) d\tau | \varphi_i \rangle}{\Delta E - \hbar cq} \\ & \left. + \text{magnetic terms} \right\} + \langle \psi_f \varphi_f | \mathcal{H}_{\text{coul}} - \frac{Z_1 Z_2 e^2}{r_p} | \psi_i \varphi_i \rangle. \quad (\text{II B.8}) \end{aligned}$$

The summation over q may be replaced by an integral

$$\sum_q \rightarrow \int_0^\infty \frac{dq}{\pi}, \quad (\text{II B.9})$$

in which the path of integration is to circumvent the pole by passing below the real axis.

The integrals over q can be evaluated by using the formulas⁴⁰

$$\int_0^\infty \frac{j_\lambda(qr) j_\lambda(qr')}{q^2 - \kappa^2} q^2 dq = \frac{i\pi\kappa}{2} j_\lambda(\kappa r_<) h_\lambda^{(1)}(\kappa r_>), \quad (\text{II B.10})$$

and

$$\int_0^\infty \frac{j_\lambda(qr) j_\lambda(qr')}{q^2 - \kappa^2} dq = \frac{i\pi}{2\kappa} j_\lambda(\kappa r_<) h_\lambda^{(1)}(\kappa r_>) - \frac{\pi r_<^\lambda r_>^{-\lambda-1}}{2\kappa^2(2\lambda+1)}, \quad (\text{II B.11})$$

where $r_>$ and $r_<$ denote the greater and smaller, respectively, of r and r' , while $h_\lambda^{(1)}$ is the spherical Hankel function of first kind. With

$$\kappa = \frac{\Delta E}{\hbar c}, \quad (\text{II B.12})$$

the integrals (10) and (11) occur in the magnetic and electric part of (8), respectively.

It is now seen that the last term in (11) leads to a contribution from the electric multipole photons to the transition matrix element (8) which just cancels the corresponding multipole contribution from the Coulomb terms. This result may be obtained by using the relation

$$\nabla \times \mathbf{L}(r^k Y_{\lambda\mu}) = i(k+1) \nabla(r^k Y_{\lambda\mu}) \quad (k=\lambda \text{ or } -\lambda-1), \quad (\text{II B.13})$$

and the continuity equation

$$\langle f | \text{div} \mathbf{j} | i \rangle = \frac{i}{\hbar} (E_f - E_i) \langle f | \rho | i \rangle. \quad (\text{II B.14})$$

Since the photon field contains no components with $\lambda=0$, the cancellation is only complete provided the last terms in (8) contain no resulting monopole component, which is the case if the projectile does not penetrate into the nucleus. While this condition is fulfilled in Coulomb excitation with projectile energies below the barrier, there may, for instance in electron scattering, be an important electric monopole interaction causing nuclear excitations.⁴¹

In the following we shall neglect the effect of penetration so that $r_p = r_>$. Specifying the nuclear states by the quantum numbers I and M , and the scattering state of the projectile by its momentum $\hbar \mathbf{k}$ at infinity, we may express the transition matrix element in the following form

$$\begin{aligned} \langle f | \mathcal{H}^{(1)} | i \rangle = \sum_{\lambda\mu} \frac{4\pi}{2\lambda+1} (-1)^\mu \{ \langle \mathbf{k}_f | \mathcal{H}(E\lambda, \mu) | \mathbf{k}_i \rangle \\ \times \langle I_f M_f | \mathcal{H}(E\lambda, -\mu) | I_i M_i \rangle \\ - \langle \mathbf{k}_f | \mathcal{H}(M\lambda, \mu) | \mathbf{k}_i \rangle \\ \times \langle I_f M_f | \mathcal{H}(M\lambda, -\mu) | I_i M_i \rangle \}, \quad (\text{II B.15}) \end{aligned}$$

with the notation

$$\mathcal{H}(E\lambda, \mu) = \frac{(2\lambda+1)!!}{\kappa^{\lambda+1} c(\lambda+1)} \int \mathbf{j}_n \cdot \nabla \times \mathbf{L}(j_\lambda(\kappa r) Y_{\lambda\mu}(\theta, \phi)) d\tau, \quad (\text{II B.16})$$

$$\mathcal{H}(M\lambda, \mu) = \frac{-i(2\lambda+1)!!}{\kappa^\lambda c(\lambda+1)} \int \mathbf{j}_n \cdot \mathbf{L}(j_\lambda(\kappa r) Y_{\lambda\mu}(\theta, \phi)) d\tau, \quad (\text{II B.17})$$

⁴⁰ G. N. Watson, *Theory of Bessel Functions* (Cambridge University Press, New York, 1944), second edition, p. 429.

⁴¹ See L. I. Schiff, *Phys. Rev.* **98**, 1281 (1955) and Sec. II E.3 following.

and

$$\mathfrak{N}(E\lambda, \mu) = \frac{i\kappa^\lambda}{c\lambda(2\lambda-1)!!} \int \mathbf{j}_p \cdot \nabla \times \mathbf{L}(h_\lambda^{(1)}(\kappa r) Y_{\lambda\mu}(\theta, \phi)) d\tau, \quad (\text{II B.18})$$

$$\mathfrak{N}(M\lambda, \mu) = \frac{\kappa^{\lambda+1}}{c\lambda(2\lambda-1)!!} \int \mathbf{j}_p \cdot \mathbf{L}(h_\lambda^{(1)}(\kappa r) Y_{\lambda\mu}(\theta, \phi)) d\tau. \quad (\text{II B.19})$$

It is often convenient to transform the electric multipole transition operators by means of the identity

$$\nabla \times \mathbf{L}(f_\lambda(\kappa r) Y_{\lambda\mu}) = i\nabla \left(\frac{\partial}{\partial r} (r f_\lambda(\kappa r)) Y_{\lambda\mu} \right) + i\kappa^2 r f_\lambda(\kappa r) Y_{\lambda\mu}, \quad (\text{II B.20})$$

where $f_\lambda(\kappa r)$ is a spherical Bessel or Hankel function. Performing a partial integration and applying the continuity equation (14) one obtains

$$\begin{aligned} \mathfrak{N}(E\lambda, \mu) &= \frac{(2\lambda+1)!!}{\kappa^\lambda(\lambda+1)} \int \rho_p \frac{\partial}{\partial r} (r j_\lambda(\kappa r)) Y_{\lambda\mu}(\theta, \phi) d\tau \\ &\quad + \frac{i(2\lambda+1)!!}{\kappa^{\lambda-1}c(\lambda+1)} \int \mathbf{j}_p \cdot r j_\lambda(\kappa r) Y_{\lambda\mu}(\theta, \phi) d\tau, \quad (\text{II B.21}) \end{aligned}$$

and

$$\begin{aligned} \mathfrak{N}(E\lambda, \mu) &= -\frac{i\kappa^{\lambda+1}}{\lambda(2\lambda-1)!!} \int \rho_p \frac{\partial}{\partial r} (r h_\lambda^{(1)}(\kappa r) Y_{\lambda\mu}(\theta, \phi)) d\tau \\ &\quad - \frac{\kappa^{\lambda+2}}{c\lambda(2\lambda-1)!!} \int \mathbf{j}_p \cdot r h_\lambda^{(1)}(\kappa r) Y_{\lambda\mu}(\theta, \phi) d\tau. \quad (\text{II B.22}) \end{aligned}$$

The nuclear transition operators (16) and (17) are precisely the same as those which determine the emission probability for electric and magnetic multipole radiation. If the radiative transition probability is written in the form (II A.56), the reduced transition probabilities $B(\lambda)$ are given in terms of the transition operators through the definition

$$B(\lambda) = \sum_{m_f} |\langle I_f M_f | \mathfrak{N}(\lambda, \mu) | I_i M_i \rangle|^2. \quad (\text{II B.23})$$

This equation is identical with the definitions (II A.18) and (II A.52), and in fact the transition operators approach the electric and magnetic multipole moments (II A.11) and (II A.39) in the limit $\kappa R_0 \ll 1$, in which one may employ the asymptotic expression

$$j_\lambda(\kappa r) \approx \frac{(\kappa r)^\lambda}{(2\lambda+1)!!}. \quad (\text{II B.24})$$

The differential cross section for excitation with unspecified orientation of the initial and final nuclear state is given by⁴²

$$d\sigma = \frac{m_f^2}{4\pi^2 \hbar^4} \frac{v_f}{v_i} (2I_i+1)^{-1} \sum_{M_i M_f} |\langle f | \mathfrak{N} | i \rangle|^2 d\Omega, \quad (\text{II B.25})$$

where m_f is the relativistic mass of the outgoing projectile. The scattering states in (15) are eigenstates in the Coulomb field $Z_1 Z_2 e^2 / r_p$, which for large distances behave as distorted plane waves plus spherical waves. While in the initial state these are outgoing, the final state should contain only incoming spherical waves.⁴³ The scattering states are normalized at infinity to one particle per unit volume. Using (15) and (23) and the relation (II A.16) the cross section may be written

$$\begin{aligned} d\sigma &= \frac{4m_f^2}{\hbar^4} \frac{v_f}{v_i} \sum_\lambda \left\{ \frac{B(E\lambda)}{(2\lambda+1)^3} \sum_\mu |\langle \mathbf{k}_f | \mathfrak{N}(E\lambda, \mu) | \mathbf{k}_i \rangle|^2 \right. \\ &\quad \left. + \frac{B(M\lambda)}{(2\lambda+1)^3} \sum_\mu |\langle \mathbf{k}_f | \mathfrak{N}(M\lambda, \mu) | \mathbf{k}_i \rangle|^2 \right\} d\Omega. \quad (\text{II B.26}) \end{aligned}$$

II B.2. Nonrelativistic Approximation

For projectile velocities small compared to that of light the product κr_p may be treated as a small quantity so that we may apply the asymptotic expansion

$$h_\lambda^{(1)}(\kappa r) \approx -i \frac{(2\lambda-1)!!}{(\kappa r)^{\lambda+1}}. \quad (\text{II B.27})$$

In fact, we have

$$\kappa r_p = \frac{v}{c} \frac{r_p}{v} \cdot \omega \lesssim \frac{v}{c},$$

since for $\omega r_p / v$ larger than unity the interaction becomes almost adiabatic.

If we furthermore consider the projectile as a point particle with charge $Z_1 e$ we get to leading order from (22) and (19)

$$\mathfrak{N}(E\lambda, \mu) = Z_1 e r_p^{-\lambda-1} Y_{\lambda\mu}(\theta_p, \phi_p), \quad (\text{II B.28})$$

$$\mathfrak{N}(M\lambda, \mu) = \frac{Z_1 e \hbar}{m c \lambda} \mathbf{1}_p \cdot \nabla_p (r_p^{-\lambda-1} Y_{\lambda\mu}(\theta_p, \phi_p)), \quad (\text{II B.29})$$

where we have used the relation (II A.44). The terms neglected in (28) and (29) are at most of the order $(v/c)^2$.

If the projectile possesses a spin with associated magnetic moment, the current density contains a contribution similar to the second term in (II A.40). The magnetic transition operator then becomes

$$\mathfrak{N}(M\lambda, \mu) = \left(\frac{1}{\lambda} \mathbf{u}_i + \mathbf{u}_s \right) \cdot \nabla_p (r_p^{-\lambda-1} Y_{\lambda\mu}(\theta_p, \phi_p)), \quad (\text{II B.30})$$

⁴² If the projectile possesses a spin the scattering states must also be specified with respect to spin indices, and the cross sections will involve appropriate averages over these indices.

⁴³ G. Breit and H. A. Bethe, Phys. Rev. 93, 888 (1954).

where \mathbf{u}_i and \mathbf{u}_s are the orbital and spin magnetic moments of the projectile. For $\eta \gg 1$, where large angular momenta are involved in the scattering, the effect of the spin moment is expected to be relatively small.^{43a}

The magnetic moment also contributes to the electric excitation through the magnetization current and its associated charge density ($c\rho_{\text{spin}} \approx (\mathbf{v}/c) \cdot \mathbf{j}_{\text{spin}}$), but the effect is again at most of the order $(v/c)^2$ as compared with the leading term (28).

As was to be expected, the interaction (15) with the nonrelativistic transition operators (28) and (29) for the projectile is identical with that assumed in the classical treatment [see (II A.10) and (II A.38)]. It is thus also evident that in the nonrelativistic approximation the nuclear recoil may be taken into account as in Sec. II A simply by replacing the projectile mass by the reduced mass m_0 of projectile and nucleus.

The excitation cross section obtained from (26), (28), and (29) may now be written

$$d\sigma = \sum_{\lambda=1}^{\infty} d\sigma_{E\lambda} + d\sigma_{M\lambda}, \quad (\text{II B.31})$$

with

$$d\sigma_{E\lambda} = \left(\frac{Z_1 e}{\hbar v_i} \right)^2 a^{-2\lambda+2} B(E\lambda) df_{E\lambda}(\vartheta, \eta_i, \xi), \quad (\text{II B.32})$$

and

$$d\sigma_{M\lambda} = \left(\frac{Z_1 e}{\hbar c} \right)^2 \frac{v_f}{v_i} a^{-2\lambda+2} B(M\lambda) df_{M\lambda}(\vartheta, \eta_i, \xi), \quad (\text{II B.33})$$

where a is given by the symmetrized expression (II A.86).

We have here introduced the dimensionless functions

$$df_{E\lambda}(\vartheta, \eta_i, \xi) = \frac{4k_i k_f}{(2\lambda+1)^3} a^{2\lambda-2} \times \sum_{\mu} |\langle \mathbf{k}_f | r_p^{-\lambda-1} Y_{\lambda\mu}(\theta_p, \phi_p) | \mathbf{k}_i \rangle|^2 d\Omega, \quad (\text{II B.34})$$

and

$$df_{M\lambda}(\vartheta, \eta_i, \xi) = \frac{4a^{2\lambda-2}}{\lambda^2(2\lambda+1)^3} \times \sum_{\mu} |\langle \mathbf{k}_f | \mathbf{l}_p \cdot \nabla_p (r_p^{-\lambda-1} Y_{\lambda\mu}(\theta_p, \phi_p)) | \mathbf{k}_i \rangle|^2 d\Omega \quad (\text{II B.35})$$

in analogy with the notation used in the classical treatment [see (II A.88) and (II A.89)]. From dimensional considerations it follows that (34) and (35) for given deflection angle ϑ may be regarded as functions only of η_i and η_f defined by (II A.1) for v equal to v_i and v_f , respectively. To stress the analogy with the classical case we consider (34) and (35) as functions of η_i and the parameter ξ

$$\xi = \eta_f - \eta_i, \quad (\text{II B.36})$$

^{43a} The expression for f_{M1} with the inclusion of spin effects has recently been given by L. C. Biedenharn and R. M. Thaler reference 62a).

which is identical with (II A.87). As may be expected, the functions $df(\vartheta, \eta_i, \xi)$ approach the classical functions $df(\vartheta, \xi)$ for $\eta_i \rightarrow \infty$ (see Sec. II B.6).

For the total excitation cross section one obtains, by integration over the direction of \mathbf{k}_f ,

$$\sigma_{E\lambda} = \left(\frac{Z_1 e}{\hbar v_i} \right)^2 a^{-2\lambda+2} B(E\lambda) f_{E\lambda}(\eta_i, \xi), \quad (\text{II B.37})$$

and

$$\sigma_{M\lambda} = \left(\frac{Z_1 e}{\hbar c} \right)^2 \frac{v_f}{v_i} a^{-2\lambda+2} B(M\lambda) f_{M\lambda}(\eta_i, \xi), \quad (\text{II B.38})$$

where

$$f(\eta_i, \xi) = \int \frac{df(\vartheta, \eta_i, \xi)}{d\Omega} d\Omega. \quad (\text{II B.39})$$

The scattering states to be used in (34) and (35) are the nonrelativistic Coulomb wave functions, which at large distances behave as distorted plane waves with appropriate in- and outgoing spherical waves. With the normalization employed, these wave functions are given by⁴⁴

$$|\mathbf{k}_i\rangle = e^{-(\pi/2)\eta_i} \Gamma(1+i\eta_i) e^{i\mathbf{k}_i \cdot \mathbf{r}} \times {}_1F_1(-i\eta_i, 1; i(k_i r - \mathbf{k}_i \cdot \mathbf{r})), \quad (\text{II B.40})$$

and

$$|\mathbf{k}_f\rangle = e^{-(\pi/2)\eta_f} \Gamma(1-i\eta_f) e^{i\mathbf{k}_f \cdot \mathbf{r}} \times {}_1F_1(i\eta_f, 1; -i(k_f r + \mathbf{k}_f \cdot \mathbf{r})), \quad (\text{II B.41})$$

where ${}_1F_1$ is the confluent hypergeometric function.

It may be observed that the approximations involved in the cross sections derived in this paragraph only involve to the neglect of relativistic effects in the motion of the projectile; thus, the nuclear matrix elements entering into the $B(\lambda)$ may be taken to be the fully relativistic expressions [see (16) and (17)] which are identical with those appearing in the radiative transitions.

The matrix elements involving the scattering states of the projectile can be evaluated explicitly in the special case of electric dipole excitations. In fact, these matrix elements are equivalent to those involved in the bremsstrahlung process (see Sec. II E.1), and can be expressed in terms of hypergeometric functions (see Sec. II E.5).

For excitations of higher multipole orders the matrix elements are of essentially more complex character. They may be evaluated,^{45,46} however, by expanding the Coulomb wave functions in partial waves; the radial matrix elements may then be expressed in terms of hypergeometric functions of two variables.

⁴⁴ See, e.g., A. Sommerfeld, *Atombau und Spektrallinien* (Friedrich Vieweg & Sohn, Braunschweig, Germany, 1939). In the following we leave out the index p for the coordinates of the projectile.

⁴⁵ Biedenharn, McHale, and Thaler, Phys. Rev. **100**, 376 (1955).
⁴⁶ K. Alder and A. Winther, Kgl. Danske Videnskab. Selskab Mat. fys. Medd. **29**, Nos. 18 and 19 (1955).

II B.3. Reduction to Radial Matrix Elements

The expansions of the Coulomb wave functions (40) and (41) in partial waves are given by⁴⁴

$$|\mathbf{k}_i\rangle = \sum_{lm} 4\pi (-1)^{m_l} e^{i\sigma_l(\eta_i)} Y_{l,-m}(\mathbf{k}_i) Y_{lm}(\theta, \phi) (k_i r)^{-1} F_l(k_i r), \quad (\text{II B.42})$$

and

$$|\mathbf{k}_f\rangle = \sum_{lm} 4\pi (-1)^{m_l} e^{-i\sigma_l(\eta_f)} Y_{l,-m}(\mathbf{k}_f) Y_{lm}(\theta, \phi) (k_f r)^{-1} F_l(k_f r), \quad (\text{II B.43})$$

where $\sigma_l(\eta) = \arg\Gamma(l+1+i\eta)$ is the Coulomb phase shift, and where $F_l(kr)$ is the regular solution to the radial wave equation for orbital angular momentum l . For large values of r , the function $F_l(kr)$ has the asymptotic form

$$F_l(kr) \sim \sin\left(kr - \frac{\pi}{2}l - \eta \ln 2kr + \sigma_l\right). \quad (\text{II B.43a})$$

The angular integrations may now be performed by means of the relation⁴⁷

$$\int Y_{l_1 m_1} Y_{l_2 m_2} Y_{l_3 m_3} d\Omega = \left(\frac{(2l_1+1)(2l_2+1)(2l_3+1)}{4\pi}\right)^{\frac{1}{2}} \begin{pmatrix} l_1 & l_2 & l_3 \\ 0 & 0 & 0 \end{pmatrix} \begin{pmatrix} l_1 & l_2 & l_3 \\ m_1 & m_2 & m_3 \end{pmatrix}, \quad (\text{II B.44})$$

and one thus obtains, for the matrix elements involved in electric excitations (34),

$$\begin{aligned} \langle \mathbf{k}_f | r^{-\lambda-1} Y_{\lambda\mu}(\theta, \phi) | \mathbf{k}_i \rangle &= (4\pi)^{\frac{3}{2}} \sum_{l_i l_f m_i m_f} i^{l_i-l_f} (-1)^{\mu} e^{i(\sigma_i+\sigma_f)} \\ &\times [(2l_i+1)(2l_f+1)(2\lambda+1)]^{\frac{1}{2}} \begin{pmatrix} l_i & l_f & \lambda \\ 0 & 0 & 0 \end{pmatrix} \begin{pmatrix} l_i & l_f & \lambda \\ m_i & -m_f & \mu \end{pmatrix} Y_{l_i, -m_i}(\mathbf{k}_i) Y_{l_f m_f}(\mathbf{k}_f) M_{l_i l_f}^{-\lambda-1}, \end{aligned} \quad (\text{II B.45})$$

where the radial matrix element M is defined by

$$M_{l_i l_f}^{-\lambda-1} = \frac{1}{k_i k_f} \int_0^\infty F_{l_f}(k_f r) r^{-\lambda-1} F_{l_i}(k_i r) dr. \quad (\text{II B.46})$$

Inserting (45) into (34) one obtains

$$\begin{aligned} df_{E\lambda}(\vartheta, \eta_i, \xi) &= \frac{16\pi}{(2\lambda+1)^2} k_i k_f a^{2\lambda-2} \sum_{l_i l_i' l_f l_f'} (2l_i+1)(2l_f+1)(2l_i'+1)(2l_f'+1) i^{l_i-l_f-l_i'+l_f'} (-1)^{\lambda+l_f+l_f'} \\ &\times \exp\{i[\sigma_{l_i}(\eta_i) + \sigma_{l_f}(\eta_f) - \sigma_{l_i'}(\eta_i) - \sigma_{l_f'}(\eta_f)]\} \begin{pmatrix} l_i & l_f & \lambda \\ 0 & 0 & 0 \end{pmatrix} \begin{pmatrix} l_i' & l_f' & \lambda \\ 0 & 0 & 0 \end{pmatrix} M_{l_i l_f}^{-\lambda-1} M_{l_i' l_f'}^{-\lambda-1} \\ &\times \sum_l (2l+1) \begin{Bmatrix} l_i & l_i' & l \\ l_f' & l_f & \lambda \end{Bmatrix} \begin{pmatrix} l_i & l_i' & l \\ 0 & 0 & 0 \end{pmatrix} \begin{pmatrix} l_f & l_f' & l \\ 0 & 0 & 0 \end{pmatrix} P_l(\cos\vartheta), \end{aligned} \quad (\text{II B.47})$$

where we have used the notation (II A.62) for the Racah coefficient.^{47a}

From (47) one obtains by integration over ϑ (see (39))

$$f_{E\lambda}(\eta_i, \xi) = \frac{64\pi^2}{(2\lambda+1)^2} k_i k_f a^{2\lambda-2} \sum_{l_i l_f} (2l_i+1)(2l_f+1) \begin{pmatrix} l_i & l_f & \lambda \\ 0 & 0 & 0 \end{pmatrix}^2 |M_{l_i l_f}^{-\lambda-1}|^2. \quad (\text{II B.48})$$

Similarly, for the magnetic excitations one obtains from (35)

$$\begin{aligned} \langle \mathbf{k}_f | \mathbf{1} \cdot \nabla (r^{-\lambda-1} Y_{\lambda\mu}(\theta, \phi)) | \mathbf{k}_i \rangle &= (4\pi)^{\frac{3}{2}} \sum_{l_i l_f m_i m_f} (-i)^{l_i-l_f} (-1)^{\mu} e^{i(\sigma_i+\sigma_f)} 2l_i(2\lambda+1)[\lambda(\lambda+1)(l_i+1)(2l_i+3)(2l_f+1)]^{\frac{1}{2}} \\ &\times \begin{pmatrix} l_i & l_f & \lambda \\ m_i & -m_f & \mu \end{pmatrix} \begin{pmatrix} l_i+1 & l_f & \lambda \\ 0 & 0 & 0 \end{pmatrix} \begin{Bmatrix} \lambda & \lambda & 1 \\ l_i & l_i+1 & l_f \end{Bmatrix} Y_{l_f m_f}(\mathbf{k}_f) Y_{l_i - m_i}(\mathbf{k}_i) M_{l_i l_f}^{-\lambda-2}, \end{aligned} \quad (\text{II B.49})$$

⁴⁷ See, e.g., reference 24 or reference 22, p. 793.

^{47a} For the numerical evaluation of df , it would be advantageous to compute (45) and insert afterwards into (34).

and

$$f_{M\lambda}(\eta_i, \xi) = \frac{64\pi^2(\lambda+1)}{\lambda(2\lambda+1)} a^{2\lambda-2} \sum_{l_i l_f} (2l_i)^2 (2l_i+1)(l_i+1)(2l_f+1) \times \begin{pmatrix} l_i+1 & l_f & \lambda \\ 0 & 0 & 0 \end{pmatrix}^2 \begin{Bmatrix} \lambda & \lambda & 1 \\ l_i & l_i+1 & l_f \end{Bmatrix}^2 |M_{l_i l_f}^{-\lambda-2}|^2. \quad (\text{II B.50})$$

The evaluation of the excitation cross sections is thus reduced to the problem of computing the radial matrix elements and performing the summation over the angular momentum components contained in the scattering states.

II B.4. Evaluation of the Radial Matrix Elements

The radial wave function in (42) and (43) can be expressed in the form⁴⁴

$$F_l(kr) = e^{-(\pi/2)\eta} \frac{|\Gamma(l+1+i\eta)|}{2\Gamma(2l+2)} (2kr)^{l+1} e^{-ikr} {}_1F_1(l+1-i\eta, 2l+2; 2ikr), \quad (\text{II B.51})$$

which may be seen from (II E.90) to be a real function.

The radial matrix element (46) and even the more general matrix element

$$M_{l_i l_f}^{-\lambda-1, q} = \frac{1}{k_i k_f} \int_0^\infty F_{l_f}(k_f r) r^{-\lambda-1} e^{-qr} F_{l_i}(k_i r) dr \quad (\text{II B.52})$$

can be evaluated explicitly⁴⁸ by employing an integral representation of ${}_1F_1$ and carrying out the integration over r first. The result is [see (II E.91) and (II E.100)]

$$M_{l_i l_f}^{-\lambda-1, q} = \frac{|\Gamma(l_i+1+i\eta_i)| |\Gamma(l_f+1+i\eta_f)|}{(2l_i+1)!(2l_f+1)!} (l_i+l_f-\lambda+1) i^{l_i+l_f-\lambda+2} x^{l_i} (-y)^{l_f} \times e^{-(\pi/2)(\eta_i+\eta_f)} (k_i - k_f + iq)^{\lambda-2} F_2(l_i+l_f-\lambda+2, l_i+1+i\eta_i, l_f+1-i\eta_f, 2l_i+2, 2l_f+2; x, y), \quad (\text{II B.53})$$

with

$$x = \frac{2\eta_f}{\xi + iq\eta_i/k_f}, \quad y = \frac{-2\eta_i}{\xi + iq\eta_i/k_f}. \quad (\text{II B.54})$$

The function F_2 is a generalized hypergeometric function of two variables, one of the so-called Appell functions, and is defined in the neighborhood of $x=y=0$ by the series expansion (II E.93). The function is multivalued and the branch which is of interest in the present context is determined from (52) in the limit $q \rightarrow 0$.

The conservation of angular momentum and parity in the excitation process implies (see (45) and (49)) that the only matrix elements occurring in the cross sections are those for which

$$l_i - l_f = -\lambda, -\lambda+2, \dots, \lambda. \quad (\text{II B.55})$$

In the special case of $\lambda=0$, the F_2 function in (53) reduces to an ordinary hypergeometric function according to the reduction relation (II E.96). One thus obtains for the monopole matrix elements⁴⁹

$$M_{l_i l_f}^{-1} = (k_i - k_f)^{-2} \left(\frac{\xi}{\eta_i + \eta_f} \right)^{i(\eta_i + \eta_f)} \frac{|\Gamma(l+1+i\eta_i)| |\Gamma(l+1+i\eta_f)|}{(2l+1)!} \times e^{-(\pi/2)\xi} (-x_0)^l F(l+1-i\eta_i, l+1-i\eta_f, 2l+2; x_0), \quad (\text{II B.56})$$

with

$$x_0 = -\frac{4\eta_i\eta_f}{\xi^2}. \quad (\text{II B.57})$$

Although these matrix elements are of no direct importance for Coulomb excitation, they are useful in expressing higher multipole matrix elements by recursion relations (see following).

The series expansion (II E.93) of the function F_2 is valid only for $|x| + |y| < 1$ and, since in our case $x+y=2$, an analytic continuation must be employed in the evaluation of (53). This analytic continuation is especially simple

⁴⁸ A. Erdélyi, *Math. Z.* **40**, 693 (1936).

⁴⁹ W. Gordon, *Ann. Physik* (5) **2**, 1031 (1929).

to perform in the case $l_i = l_f \pm \lambda$, where the F_2 function reduces to an F_1 function [see (II E.97)]. The F_1 function can again be written in terms of the Appell function F_3 [see (II E.98)] for which the analytic continuation is well known [see (II E.99)]. The application of these three formulas leads directly to the following result:

$$M_{l+\lambda, l}^{-\lambda-1} = e^{(\pi/2)\xi} \left| \frac{\Gamma(l+1+i\eta_f)}{\Gamma(l+1+\lambda+i\eta_i)} \right| \left(\frac{\eta_i}{\eta_f} \right)^l (2k_i)^{\lambda-2} \\ \times \left\{ \frac{|\Gamma(\lambda+i\xi)|^2}{(2\lambda-1)!} F_2 \left(-2\lambda+1, l+1-i\eta_f, l+1+i\eta_f, -\lambda+1-i\xi, -\lambda+1+i\xi; \frac{\xi}{2\eta_f}, \frac{\xi}{2\eta_f} \right) \right. \\ \left. + 2 \operatorname{Re} \left[\left(e^{i\pi \frac{\xi}{2\eta_f}} \right)^{\lambda+i\xi} \frac{\Gamma(l+\lambda+1-i\eta_i)\Gamma(-\lambda-i\xi)}{\Gamma(l+1-i\eta_f)} \right. \right. \\ \left. \left. \times F_2 \left(-\lambda+1+i\xi, l+\lambda+1-i\eta_i, l+1+i\eta_f, \lambda+1+i\xi, -\lambda+1+i\xi; \frac{\xi}{2\eta_f}, \frac{\xi}{2\eta_f} \right) \right] \right\}, \quad (\text{II B.58})$$

and

$$M_{l, l+\lambda}^{-\lambda-1}(\eta_i, \eta_f) = M_{l+\lambda, l}^{-\lambda-1}(\eta_f, \eta_i) = e^{-\pi\xi} M_{l+\lambda, l}^{-\lambda-1}(-\eta_f, -\eta_i). \quad (\text{II B.59})$$

In (58), the first F_2 function is a polynomial, since the first parameter is a negative integer [see (II E.93)]. Thus, for the first few λ 's, one finds

$$F_2 \left(-2\lambda+1, l+1-i\eta_f, l+1+i\eta_f, -\lambda+1-i\xi, -\lambda+1+i\xi; \frac{\xi}{2\eta_f}, \frac{\xi}{2\eta_f} \right) \\ = \begin{cases} 0, & (\lambda=1) \\ \frac{1}{2(1+\xi^2)} \frac{\eta_i(\eta_i+\eta_f)}{\eta_f^2}, & (\lambda=2) \\ \frac{1}{2(1+\xi^2)(4+\xi^2)} \frac{\eta_i(\eta_i+\eta_f)}{\eta_f^4} [5l\xi(\eta_i+\eta_f)+12\eta_f^2-8\eta_i^2]. & (\lambda=3) \end{cases} \quad (\text{II B.60})$$

If $|l_i - l_f| \neq \lambda$ the F_2 function cannot be reduced to a single F_1 function, but, as shown in Sec. II E.8, it may be written as a finite sum of such functions. The analytic continuation may thus be performed in complete analogy to the case $|l_i - l_f| = \lambda$ and the result can be expressed by two polynomials plus a finite number of F_2 functions of the arguments x^{-1} and y^{-1} . The analytic continuation can, however, be obtained more easily from (II E.99). Identifying one of the F_2 functions of this equation with that involved in (53), one obtains

$$F_2(l_i+l_f-\lambda+2, l_i+1-i\eta_i, l_f+1+i\eta_f, 2l_i+2, 2l_f+2; x, y) \\ = \frac{\Gamma(-l_i-i\eta_i)\Gamma(-l_f+i\eta_f)\Gamma(\lambda-l_i-l_f-1)}{\Gamma(\lambda+1+i\xi)\Gamma(-2l_i-1)\Gamma(-2l_f-1)} (-x)^{-l_i-1+i\eta_i} (-y)^{-l_f-1-i\eta_f} \\ \times F_3 \left(l_i+1-i\eta_i, l_f+1+i\eta_f, -l_i-i\eta_i, -l_f+i\eta_f, \lambda+1+i\xi; \frac{1}{x}, \frac{1}{y} \right) \\ + \frac{\Gamma(2l_f+1)\Gamma(-l_f+i\eta_f)\Gamma(\lambda-l_i-l_f-1)}{\Gamma(-2l_f-1)\Gamma(l_f+1+i\eta_f)\Gamma(\lambda-l_i+l_f)} (-y)^{-2l_f-1} \\ \times F_2(l_i-l_f+1-\lambda, l_i+1-i\eta_i, -l_f+i\eta_f, 2l_i+2, -2l_f; x, y) \\ + \frac{\Gamma(2l_i+1)\Gamma(-l_i-i\eta_i)\Gamma(\lambda-l_i-l_f-1)}{\Gamma(-2l_i-1)\Gamma(l_i+1-i\eta_i)\Gamma(\lambda-l_f+l_i)} (-x)^{-2l_i-1} \\ \times F_2(l_f-l_i+1-\lambda, -l_i-i\eta_i, l_f+1+i\eta_f, -2l_i, 2l_f+2; x, y) \\ + \frac{\Gamma(2l_i+1)\Gamma(2l_f+1)\Gamma(\lambda-l_i-l_f-1)\Gamma(-l_i-i\eta_i)\Gamma(-l_f+i\eta_f)}{\Gamma(-2l_i-1)\Gamma(-2l_f-1)\Gamma(l_i+l_f+\lambda+1)\Gamma(l_i+1-i\eta_i)\Gamma(l_f+1+i\eta_f)} (-x)^{-2l_i-1} (-y)^{-2l_f-1} \\ \times F_2(-l_i-l_f-\lambda, -l_i-i\eta_i, -l_f+i\eta_f, -2l_i, -2l_f; x, y). \quad (\text{II B.61})$$

This equation is, however, singular for integer values of l_i and l_f . If one first considers l_i and l_f to have noninteger values while preserving $l_i - l_f$ as an integer, the first and second F_2 functions reduce to polynomials, since the first parameter is in that case a negative integer. The third F_2 function can be eliminated by considering also the complex conjugate equation to (61) which contains the same F_2 functions, according to the transformation (II E.95). After this elimination, the limiting process l_i, l_f approaching integer values and $q \rightarrow 0$ can easily be performed and the result gives the following expression for the radial matrix element (46) or (53):

$$\begin{aligned}
M_{l_i l_f}^{-\lambda-1} = & \pi (2k_i)^{\lambda-2} \left(\frac{\eta_i}{\eta_f} \right)^{l_f} \frac{e^{(\pi/2)\xi}}{\sinh \pi \xi} \left| \frac{\Gamma(l_f+1+i\eta_f)}{\Gamma(l_i+1+i\eta_i)} \right| \frac{(2l_i)!}{(2l_f+1)!(l_i-l_f+\lambda-1)!} \left(-\frac{i\xi}{2\eta_f} \right)^{l_i-l_f-1+\lambda} \\
& \times F_2(l_f-l_i+1-\lambda, l_f+1+i\eta_f, -l_i-i\eta_i, 2l_f+2, -2l_i; y, x) \\
& + \pi (2k_f)^{\lambda-2} \left(\frac{\eta_f}{\eta_i} \right)^{l_i} \frac{e^{-(\pi/2)\xi}}{\sinh \pi \xi} \left| \frac{\Gamma(l_i+1+i\eta_i)}{\Gamma(l_f+1+i\eta_f)} \right| \frac{(2l_f)!}{(2l_i+1)!(l_f-l_i+\lambda-1)!} \left(\frac{i\xi}{2\eta_i} \right)^{l_f-l_i-1+\lambda} \\
& \times F_2(l_i-l_f+1-\lambda, l_i+1-i\eta_i, -l_f+i\eta_f, 2l_i+2, -2l_f; x, y) \\
& - \frac{\pi}{2} (k_f - k_i)^\lambda k_i^{-1} k_f^{-1} \frac{e^{-(\pi/2)|\xi|}}{\sinh \pi \xi} \left| \frac{\Gamma(l_i+1+i\eta_i)}{\Gamma(l_f+1+i\eta_f)} \right| \Re e \left\{ \left(\frac{\xi}{2} \right)^{-i\xi} \frac{\Gamma(l_f+1-i\eta_f)}{\Gamma(l_i+1-i\eta_i)\Gamma(\lambda+1-i\xi)} \right. \\
& \left. \times i^{l_f-l_i-\lambda-1} \eta_i^{i\eta_f} \eta_f^{-i\eta_i} F_3 \left(-l_i+i\eta_i, -l_f-i\eta_f, l_i+1+i\eta_i, l_f+1-i\eta_f, \lambda+1-i\xi; -\frac{1}{x}, \frac{1}{y} \right) \right\}. \quad (\text{II B.62})
\end{aligned}$$

In these equations, x and y represent the limiting values obtained from (54) by setting $q=0$. The F_2 functions in (62) are to be interpreted as the polynomials obtained in the limit of l_i and l_f approaching integer values while $l_i - l_f$ remains an integer. These polynomials are pure imaginary [see (II E.95)] and are for the lowest values of λ given explicitly by

$$F_2(l_i-l_f+1-\lambda, l_i+1-i\eta_i, -l_f+i\eta_f, 2l_i+2, -2l_f; x, y)$$

$$= \begin{cases} 0 & \lambda=1 \quad l_f=l_i+1 \\ -i \frac{\eta_i \eta_f}{\xi} \frac{1}{l_i(l_i+1)} & \lambda=2 \quad l_f=l_i \\ i \frac{\eta_i \eta_f (\eta_i + \eta_f)}{\xi^2 (l_i+1)(l_i+2)(2l_i+3)} & \lambda=2 \quad l_f=l_i+2 \\ -i \frac{2\eta_i \eta_f [l_i(l_i+1)(2l_i+1)\xi(\eta_i+\eta_f) - 6(l_i+1)^2 \eta_i^2 - 6\eta_i^2 \eta_f^2]}{\xi^3 l_i(l_i+1)^2(l_i+2)(2l_i+1)(2l_i+3)} & \lambda=3 \quad l_f=l_i+1 \\ i \frac{2\eta_i \eta_f (\eta_i + \eta_f) [5l_i \xi (\eta_i + \eta_f) + 12\eta_f^2 - 8\eta_i^2]}{\xi^4 (l_i+1)(l_i+2)(l_i+3)(2l_i+3)(2l_i+5)} & \lambda=3 \quad l_f=l_i+3. \end{cases} \quad (\text{II B.63})$$

As mentioned above, the analytic continuation of the F_2 function in (53) can be written as a finite sum of F_2 functions. This alternative form for the matrix elements may be obtained directly from (62) by expanding the F_3 function in terms of F_2 functions [see (II E.104) and (II E.97)]. The relation (II E.98) shows how (62) reduces to (58) in the special case $l_i - l_f = \pm \lambda$.

In the evaluation of the excitation cross section, it is in general necessary to extend the summation to include large values of l_i and l_f . While the main contribution in most cases arises from terms with $l \sim \eta$, the convergence for large l is rather slow, especially for small values of ξ . The numerical calculations are therefore greatly sim-

plified by the use of recursion formulas connecting matrix elements for different values of l_i, l_f , and λ .

The existence of such recursion formulas is a consequence of simple recursion properties of hypergeometric functions. Thus, five F_2 functions with parameters differing only by integer numbers are always linearly dependent. In special cases, the recursion formulas may of course contain less than five terms. One may derive these formulas either directly from the properties of the hypergeometric functions or from the differential equation for the Coulomb wave functions.^{45,46,50} The

⁵⁰ See also L. Infeld and T. E. Hull, *Revs. Modern Phys.* **23**, 21 (1951).

recursion relations obtained by the latter method are all contained in the following general formula

$$\begin{aligned}
 & x_1 \frac{|l_f+1+i\eta_f|}{\eta_f(l_f+1)} M_{l_i, l_f+1}^{-\lambda-1} + x_2 \frac{|l_i+i\eta_i|}{\eta_i l_i} M_{l_i-1, l_f}^{-\lambda-1} - x_3 \frac{|l_i+1+i\eta_i|}{\eta_i(l_i+1)} M_{l_i+1, l_f}^{-\lambda-1} \\
 & - x_4 \frac{|l_f+i\eta_f|}{\eta_f l_f} M_{l_i, l_f-1}^{-\lambda-1} - \left[\frac{x_1}{l_f+1} + \frac{x_2}{l_i} + \frac{x_3}{l_i+1} + \frac{x_4}{l_f} \right] M_{l_i, l_f}^{-\lambda-1} \\
 & = [k_i \eta_i]^{-1} [x_1(l_f-\lambda) + x_2 l_i - x_3(l_i+1) - x_4(l_f+\lambda+1)] M_{l_i, l_f}^{-\lambda-2} \\
 & + (k_i \eta_i)^{-1} (x_1 + x_2 + x_3 + x_4) \int_0^\infty F_{l_f}(k_f r) r^{-\lambda-1} \frac{d}{dr} F_{l_i}(k_i r) dr, \quad (\text{II B.64})
 \end{aligned}$$

where $x_1, x_2, x_3,$ and x_4 are arbitrary constants. Three independent recursion formulas may be obtained from (64) by giving the factors x_1 to x_4 different values satisfying

$$x_1 + x_2 + x_3 + x_4 = 0, \quad (\text{II B.65})$$

whereby the last term of (64) is suppressed.

Additional recursion relations may then be obtained by combining those derived directly from (64) and eliminating the unwanted matrix elements. In the following, we shall give some specific relations which are useful for the numerical evaluation of the radial matrix elements for low multipole orders.

For the monopole ($\lambda=0$) matrix elements (see (56)), one obtains the three term relation

$$y_1 M_{l+1, l+1}^{-1} + y_2 M_{l, l}^{-1} + y_3 M_{l-1, l-1}^{-1} = 0, \quad (\text{II B.66})$$

with

$$\begin{aligned}
 y_1 &= 2l |l+1+i\eta_i| |l+1+i\eta_f|, \\
 y_2 &= -(2l+1) \left[\frac{\eta_i^2 + \eta_f^2}{\eta_i \eta_f} l(l+1) + 2\eta_i \eta_f \right], \quad (\text{II B.67}) \\
 y_3 &= (2l+2) |l+i\eta_i| |l+i\eta_f|.
 \end{aligned}$$

This relation connects all monopole matrix elements satisfying the condition (55) with the two first ($l=0$ and 1).

For $\lambda=1$, the matrix elements are most easily obtained from the monopole matrix elements by

$$(\lambda+1) M_{l, l+1}^{-\lambda-2} = y_1 M_{l, l}^{-\lambda-1} + y_2 M_{l+1, l+1}^{-\lambda-1}, \quad (\text{II B.68})$$

with

$$\begin{aligned}
 y_1 &= k_f \frac{|l+1+i\eta_f|}{l+1}, \\
 y_2 &= -k_i \frac{|l+1+i\eta_i|}{l+1}.
 \end{aligned} \quad (\text{II B.69})$$

By means of this relation one may obtain an explicit expression for the dipole radial matrix elements in terms of usual hypergeometric functions.⁴⁹

Also in the dipole case the recursion relation which connects different values of l contains only three terms and may be written

$$y_1 M_{l-1, l-2}^{-2} + y_2 M_{l, l-1}^{-2} + y_3 M_{l+1, l}^{-2} = 0, \quad (\text{II B.70})$$

with

$$\begin{aligned}
 y_1 &= 2\eta_i \eta_f |l-1+i\eta_f| |l+i\eta_i|, \\
 y_2 &= -4\eta_i^2 \eta_f^2 - l(2l+1)\eta_i^2 - l(2l-1)\eta_f^2, \quad (\text{II B.71}) \\
 y_3 &= 2\eta_i \eta_f |l+i\eta_f| |l+1+i\eta_i|.
 \end{aligned}$$

The $\lambda=2$ matrix elements cannot be reduced to those with $\lambda=1$, since the recursion relations connecting matrix elements of multipolarity λ with those of multipole order $\lambda+1$ become singular for $\lambda=1$. There are, for $\lambda=2$, two types of matrix elements, namely those for which $l_i - l_f = \pm 2$ and those for which $l_i = l_f$. The latter are connected with the former through the relation

$$\begin{aligned}
 y M_{l, l}^{-3} &= y_1 M_{l, l+2}^{-3} + y_2 M_{l-1, l+1}^{-3} \\
 &+ y_3 M_{l+2, l}^{-3} + y_4 M_{l+1, l-1}^{-3}, \quad (\text{II B.72})
 \end{aligned}$$

with

$$\begin{aligned}
 y &= \frac{l(l+1)}{3} (\eta_f^2 - \eta_i^2), \\
 y_1 &= -\eta_i^2 |l+1+i\eta_f| |l+2+i\eta_f|, \\
 y_2 &= \eta_i \eta_f \frac{2l+3}{2l+1} |l+i\eta_i| |l+1+i\eta_f|, \quad (\text{II B.73}) \\
 y_3 &= \eta_f^2 |l+1+i\eta_i| |l+2+i\eta_i|, \\
 y_4 &= -\eta_i \eta_f \frac{2l+3}{2l+1} |l+i\eta_f| |l+1+i\eta_i|.
 \end{aligned}$$

For the matrix elements with $|l_i - l_f| = \lambda$ there exist the following four term relations

$$\begin{aligned}
 y_1 M_{l+\lambda-3, l-3}^{-\lambda-1} + y_2 M_{l+\lambda-2, l-2}^{-\lambda-1} \\
 + y_3 M_{l+\lambda-1, l-1}^{-\lambda-1} + y_4 M_{l+\lambda, l}^{-\lambda-1} = 0, \quad (\text{II B.74})
 \end{aligned}$$

with

$$\begin{aligned}
 y_1 &= 2\eta_i\eta_f |l-2+i\eta_i| |l-1+i\eta_f| |l+\lambda-2+i\eta_i|, \\
 y_2 &= -|l-1+i\eta_f| [l^2(2\eta_i^2+4\eta_f^2) \\
 &\quad + l(4(\lambda-2)(\eta_i^2+\eta_f^2)+\eta_i^2-\eta_f^2) \\
 &\quad + (\lambda-2)((2\lambda-3)\eta_i^2-3\eta_f^2)+6\eta_i^2\eta_f^2], \\
 y_3 &= \frac{\eta_f}{\eta_i} |l+\lambda-1+i\eta_i| [l^2(4\eta_i^2+2\eta_f^2) \\
 &\quad + l(4(\lambda-2)\eta_i^2+\eta_i^2-\eta_f^2) \\
 &\quad - 2(\lambda-2)\eta_i^2+6\eta_i^2\eta_f^2], \\
 y_4 &= -2\eta_f^2 |l+\lambda-1+i\eta_i| |l+\lambda+i\eta_i| |l+i\eta_f|.
 \end{aligned} \tag{II B.75}$$

For $\lambda=2$, two of these matrix elements are also connected with two monopole matrix elements by

$$\begin{aligned}
 y_1 M_{l+1, l+3}^{-3} + y_2 M_{l, l+2}^{-3} \\
 = y_3 M_{l+1, l+1}^{-1} + y_4 M_{l, l}^{-1}, \tag{II B.76}
 \end{aligned}$$

with

$$\begin{aligned}
 y_1 &= 4(l+1)\eta_i^2 |l+2+i\eta_f| |l+3+i\eta_f|, \\
 y_2 &= -4(l+1)\eta_i\eta_f |l+2+i\eta_f| |l+1+i\eta_i|, \\
 y_3 &= (k_i^2 - k_f^2) [2\eta_i^2\eta_f^2 \\
 &\quad + \eta_f^2(l+1)(2l+3) - \eta_i^2(l+1)], \\
 y_4 &= -(k_i^2 - k_f^2) 2\eta_i\eta_f |l+1+i\eta_i| |l+1+i\eta_f|.
 \end{aligned} \tag{II B.77}$$

By repeated application of this formula one obtains the recurrence relation

$$M_{l, l+2}^{-3} = f(l) \left[\frac{M_{l', l'+2}^{-3}}{f(l')} + \sum_{i=l'}^{l-1} \frac{A(j)}{f(j+1)} \right], \tag{II B.78}$$

with $l' < l$ and

$$f(l) = \left(\frac{\eta_f}{\eta_i} \right)^l \left| \frac{\Gamma(l+1+i\eta_i)}{\Gamma(l+3+i\eta_f)} \right|, \tag{II B.79}$$

$$\begin{aligned}
 A(l) &= \frac{k_i^2 - k_f^2}{4(l+1) |l+2+i\eta_f| |l+3+i\eta_f| \eta_i^2} \\
 &\quad \times \{ [2\eta_i^2\eta_f^2 + \eta_f^2(l+1)(2l+3) - \eta_i^2(l+1)] \\
 &\quad \times M_{l+1, l+1}^{-1} - 2\eta_i\eta_f |l+1+i\eta_i| \\
 &\quad \times |l+1+i\eta_f| M_{l, l}^{-1} \}. \tag{II B.80}
 \end{aligned}$$

$$b_k^{E\lambda}(\eta_i, \xi) = \begin{pmatrix} \lambda & \lambda & k \\ 1 & -1 & 0 \end{pmatrix}^{-1} \sum_{i, i', l'} (-1)^{l'+1} (2l_i+1)(2l_i'+1)(2l_f+1) i^{l'-l'} \exp i(\sigma_{l_i}(\eta_i) - \sigma_{l_i'}(\eta_i))$$

$$\times \begin{Bmatrix} \lambda & \lambda & k \\ l_i & l_i' & l_f \end{Bmatrix} \begin{pmatrix} \lambda & l_i & l_f \\ 0 & 0 & 0 \end{pmatrix} \begin{pmatrix} \lambda & l_i' & l_f \\ 0 & 0 & 0 \end{pmatrix} \begin{pmatrix} l_i & l_i' & k \\ 0 & 0 & 0 \end{pmatrix} M_{l_i, l_f}^{-\lambda-1} M_{l_i', l_f}^{-\lambda-1}. \tag{II B.85}$$

In the $\lambda=2$ case, one thus needs to calculate directly from (58) either the six matrix elements $M_{02}, M_{13}, M_{24}, M_{20}, M_{31}$, and M_{42} , from which the remaining ones may be obtained from (72) and (74), or one may use the relations (78) and (72) and thereby obtain all matrix elements from M_{02}, M_{20} , and the monopole matrix elements (see (56) and (66)).

For $\lambda=3$ the matrix elements with $l_i-l_f=\pm 1$ may be obtained from the quadrupole matrix elements by means of Eq. (68). The matrix elements with $l_i-l_f=\pm 3$ can again be reduced to the six first by means of (74).

II B.5. Angular Distribution of De-Excitation γ Rays

The angular distribution of the γ quanta following an electromagnetic excitation is given by

$$\begin{aligned}
 W_{\mathbf{k}_i, \mathbf{k}_f}(\Omega_\gamma) &= \sum_{M_i, M_{f\sigma}} |\sum_{M_f} \langle I_{f\sigma} M_{f\sigma} | H_\gamma(\Omega_\gamma, \sigma) | I_f M_f \rangle \\
 &\quad \times \langle f | \mathcal{H}^{(\lambda)} | i \rangle|^2, \tag{II B.81}
 \end{aligned}$$

in analogy to the expression (II A.59). The transition matrix element $\langle f | \mathcal{H}^{(\lambda)} | i \rangle$ is given by (15) and is of just the same form as the classical transition amplitude b_{if} [see (II A.79)].

The quantum-mechanical angular distribution (81) can thus be directly obtained from the formulas in Sec. II A.4 by the substitution

$$S_{\pi\lambda\mu} \rightarrow \langle \mathbf{k}_f | \mathcal{H}(\pi\lambda, \mu) | \mathbf{k}_i \rangle. \tag{II B.82}$$

While the classical integrals S aside from constant factors depend only on the scattering angles and the parameter ξ [see (II A.24) and (II A.48)] the quantum-mechanical matrix elements depend also on the parameter η_i . Thus, the a and b coefficients involved in the quantum-mechanical angular distributions will also depend on η_i .

In order to obtain the total γ distribution irrespective of scattering angle one simply integrates (81) over the direction of \mathbf{k}_f , since the Rutherford cross section is already contained in $|\langle f | \mathcal{H}^{(\lambda)} | i \rangle|^2$. In the most important case of excitations of pure $E\lambda$ type one thus obtains [see (II A.74)]^{61,46}

$$W(\vartheta_\gamma) = \sum_k a_k^{E\lambda}(\eta_i, \xi) A_k^{(\lambda)} P_k(\cos\vartheta_\gamma), \tag{II B.83}$$

with

$$a_k^{E\lambda}(\eta_i, \xi) = b_k^{E\lambda}/b_0^{E\lambda}, \tag{II B.84}$$

and, according to (II A.68), (II B.28), and (II B.45),

⁶¹L. C. Biedenharn and M. E. Rose, ORNL report 1789 (1954). See also Breit, Ebel, and Russell, Phys. Rev. **101**, 1504 (1956).

We have here employed the relation²⁴

$$\sum_{\mu_1, \mu_2, \mu_3} (-1)^{l_1+l_2+l_3+\mu_1+\mu_2+\mu_3} \begin{pmatrix} j_1 & l_2 & l_3 \\ m_1 & \mu_2 & -\mu_3 \end{pmatrix} \begin{pmatrix} l_1 & j_2 & l_3 \\ -\mu_1 & m_2 & \mu_3 \end{pmatrix} \begin{pmatrix} l_1 & l_2 & j_3 \\ \mu_1 & -\mu_2 & m_3 \end{pmatrix} = \begin{pmatrix} j_1 & j_2 & j_3 \\ m_1 & m_2 & m_3 \end{pmatrix} \begin{Bmatrix} j_1 & j_2 & j_3 \\ l_1 & l_2 & l_3 \end{Bmatrix}, \quad (\text{II B.86})$$

and have inserted

$$Y_{l_i m_i}(\mathbf{k}_i) = \left(\frac{2l_i+1}{4\pi} \right)^{\frac{1}{2}} \delta_{m_i 0}, \quad (\text{II B.87})$$

corresponding to the fact that the emission angle ϑ_γ of the γ quantum is measured from the direction of the incident beam.

The coefficient $b_0^{E\lambda}(\eta_i, \xi)$ is related to the total excitation function $f_{E\lambda}(\eta_i, \xi)$ (see (48)) by the equation

$$f_{E\lambda}(\eta_i, \xi) = \frac{64\pi^2}{(2\lambda+1)^2} k_i k_f a^{2\lambda-2} b_0^{E\lambda}(\eta_i, \xi). \quad (\text{II B.88})$$

II B.6. WKB Approximation and Classical Limit

For $\eta > 1$, a rather accurate approximation to the Coulomb excitation cross sections may be obtained by replacing the radial matrix elements by those derived from the WKB approximation.⁵² This treatment is also convenient for the discussion of the transition of the quantum-mechanical expressions to the classical formulas in the limit $\eta \gg 1$.^{16, 53}

The WKB approximation for the radial wave function is given by

$$F_l(kr) = [f(r)/k^2]^{-\frac{1}{2}} \sin \varphi, \quad (\text{II B.89})$$

where

$$\varphi = \frac{\pi}{4} + \int_{r_0}^r [f(r)]^{\frac{1}{2}} dr, \quad (\text{II B.90})$$

and

$$f(r) = k^2 - \frac{2k\eta}{r} - \frac{l(l+1)}{r^2}. \quad (\text{II B.91})$$

The expression (89) holds outside the classical turning point r_0 defined by $f(r_0) = 0$. The contribution to the radial matrix element from the region $r < r_0$ is of lower order in η and is neglected in the present approximation.

Inserting (89), one finds that the radial matrix element (46) involves two terms, the first containing the sum of the phases φ_i and φ_f of initial and final wave function and the second containing the difference $\varphi_i - \varphi_f$. The first term may be neglected due to the rapid oscillation of the integrand. In the second term, the

phase difference may be expanded as follows

$$\varphi_i - \varphi_f \simeq (k_i - k_f) \int_{r_0}^r [f(r)]^{-\frac{1}{2}} k dr - [l_i(l_i+1) - l_f(l_f+1)] \int_{r_0}^r [f(r)]^{-\frac{3}{2}} \frac{dr}{2r^2}, \quad (\text{II B.92})$$

since $k_i \eta_i = k_f \eta_f$.

In the integrals in (92) the parameters k , η , and l refer to average values for initial and final state. The differences between the turning points for the initial and final state have been neglected, since these contributions are of higher order in ξ/η .

Evaluating the integrals in (92) and introducing the substitution

$$kr = (\eta^2 + l(l+1))^{\frac{1}{2}} \cosh w + \eta, \quad (\text{II B.93})$$

one obtains

$$\varphi_i - \varphi_f \simeq \xi (\epsilon \sinh w + w) + \mu \cos^{-1} \frac{\epsilon + \cosh w}{1 + \epsilon \cosh w}, \quad (\text{II B.94})$$

where

$$\xi = \eta_f - \eta_i, \quad (\text{II B.95})$$

while

$$\epsilon = \frac{(\eta^2 + l(l+1))^{\frac{1}{2}}}{\eta} = \left\{ 1 + \frac{(l_i + \mu/2)(l_i + 1 + \mu/2)}{\eta^2} \right\}^{\frac{1}{2}}, \quad (\text{II B.96})$$

and

$$\mu = l_f - l_i. \quad (\text{II B.97})$$

For the radial matrix element (46) we thus obtain

$$M_{l_i, l_i + \mu}^{-\lambda-1} = \frac{k^{\lambda-2}}{4\eta^\lambda} \int_{-\infty}^{\infty} e^{i\xi(\epsilon \sinh w + w)} \times \frac{[\cosh w + \epsilon + i(\epsilon^2 - 1)^{\frac{1}{2}} \sinh w]^\mu}{(\epsilon \cosh w + 1)^{\lambda + \mu}} dw. \quad (\text{II B.98})$$

It is seen that this integral is identical with the orbital integral (II A.26) involved in the classical treatment. The quantity ϵ given by (96) just corresponds to the eccentricity of the orbit [see (II A.23 and 45)] and μ represents the transfer of angular momentum in the direction perpendicular to the plane of the orbit. By introducing the deflection angle of this corresponding

⁵² Benedict, Daitch, and Breit, Phys. Rev. **101**, 171 (1956); K. Alder and A. Winther, CERN report T/KA-AW-4 (1955).

⁵³ K. Alder and A. Winther, Phys. Rev. **96**, 237 (1954); G. Breit and P. B. Daitch, Phys. Rev. **96**, 1447 (1954).

TABLE II.1. Comparison between WKB approximation and exact values for the radial matrix elements. The radial matrix elements, M_{l_i, l_f}^{-3} , occurring in $E2$ Coulomb excitation are given for various values of η_i , ξ , l_i , and l_f . The table compares the values obtained from the exact calculation (Sec. II B.4) and from the WKB approximation (II B.100).

		M_{l_i+2, l_i}^{-3}		M_{l_i+1, l_i+1}^{-3}		M_{l_i, l_i+2}^{-3}	
		Quantal	WKB	Quantal	WKB	Quantal	WKB
$\xi=0.2$ $\eta_i=1.0$	0	0.06548	0.06615	0.05993	0.05393	0.02402	0.02338
	3	0.01544	0.01528	0.00932	0.00922	0.00171	0.00172
	6	0.00589	0.00583	0.00258	0.00264	0.00032	0.00033
$\xi=0.2$ $\eta_i=4.0$	0	0.008463	0.008577	0.007777	0.007616	0.006137	0.006184
	2	0.006717	0.006750	0.005740	0.005669	0.003318	0.003316
	5	0.004052	0.004052	0.003947	0.003918	0.001266	0.001266
$\xi=0.2$ $\eta_i=8.0$	0	0.002219	0.002228	0.002085	0.002073	0.001877	0.001883
	1	0.002212	0.002220	0.002007	0.001996	0.001678	0.001681
	3	0.002048	0.002053	0.001901	0.001892	0.001468	0.001470
$\xi=1.0$ $\eta_i=4.0$	0	0.001690	0.001714	0.001155	0.001155	0.000729	0.000727
	2	0.001659	0.001681	0.000799	0.000782	0.000273	0.000274
	5	0.001024	0.001032	0.000340	0.000338	0.000061	0.000061
$\xi=1.0$ $\eta_i=8.0$	0	0.0004295	0.0004308	0.0003492	0.0003452	0.0002712	0.0002712
	1	0.0004655	0.0004672	0.0003316	0.0003281	0.0002184	0.0002183
	3	0.0004932	0.0004953	0.0002802	0.0002779	0.0001335	0.0001334

classical orbit

$$\vartheta = 2 \sin^{-1} \frac{1}{\epsilon}, \quad (\text{II B.99})$$

where ϵ is given by (96), the matrix element (98) may also be written

$$M_{l_i, l_i+\mu}^{-\lambda-1} = \frac{\hbar^{\lambda-2}}{4\eta^\lambda} I_{\lambda\mu}(\vartheta, \xi). \quad (\text{II B.100})$$

Since the WKB approximation for the radial wave function is valid not only when $\eta \gg 1$, but also when $l \gg 1$, the limiting formula (100) holds also for large l irrespective of the magnitude of η .

The formula (100) has also been derived⁴⁵ by expressing the exact radial integral (46) in a suitable form and going to the limit $|l+i\eta| \rightarrow \infty$ for fixed ξ . In this way one obtains an expansion of the matrix element with (98) as the leading term.

The WKB formula (100) gives very accurate values for the radial matrix elements even for moderate values of η and l ; indeed the accuracy is much greater than might have been expected in view of the inaccuracy of the wave function (89) in the neighborhood of the turning point.⁵⁴

An illustration of the accuracy of (100) is given in Table II.1, where exact values of quadrupole matrix elements computed from the formulas in Sec. II B.4 are compared with the WKB values. From this table it is also seen that for not too large values of l_i the particular choice of l in (96) is essential for the close agreement.

If one employs the WKB formula (100) for the radial matrix elements in expressions such as (47), (48), or (85), one obtains cross sections which are valid even for

⁵⁴ The reasons for the high accuracy of the WKB approximation have been discussed especially by G. Breit and P. B. Daicht, Proc. Natl. Acad. Sci. 41, 653 (1955); J. P. Lazarus and S. Sack, Phys. Rev. 100, 370 (1955).

moderate values of η and which represent a major improvement over the classical expressions (see Fig. II.3).

In order to exhibit the transition of the total cross sections to the classical limit one may take advantage of the fact that for large η 's the main contribution arises from the large values of l . One may thus use the asymptotic formula

$$\begin{pmatrix} l_1 & l_2 & \lambda \\ m_1 & m_2 & \mu \end{pmatrix} = \frac{(-1)^{l_2-\lambda-m_1}}{(2l_1+1)^{\frac{1}{2}}} D_{\mu, l_1-l_2}^{\lambda}(\theta, \theta, 0), \quad (\text{II B.101})$$

with

$$\cos \theta = \frac{m_2}{[l_2(l_2+1)]^{\frac{1}{2}}},$$

for the vector addition coefficient in the limit of large l_1

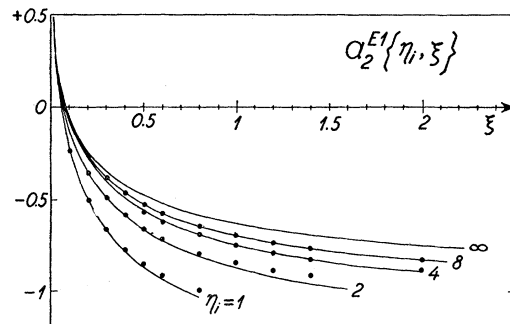


FIG. II.3. Comparison of WKB approximation and exact calculation for the angular distribution of the gamma rays. The coefficient $\alpha_2^{E1}(\eta_i, \xi)$ which describes the angular distribution of the gamma rays following $E1$ Coulomb excitation (II C.26), or bremsstrahlung (II E.17), is plotted as a function of ξ for different values of η_i . The full-drawn curve corresponds to the exact calculation,⁶¹ while the black points have been obtained by the WKB approximation.⁶⁰

and l_2 , for fixed λ . This formula may be derived from the explicit expressions for the Clebsch-Gordon coefficient and the rotation matrix D .^{24,55}

If in (48) one further inserts [see (96) and (99)],

$$l = \eta \cot \frac{\vartheta}{2}, \quad (\text{II B.102})$$

and replaces the sum over l_i by an integral over ϑ , i.e.,

$$\sum_{l_i} \rightarrow \frac{\eta}{2} \sum_{\mu} \int_0^{\pi} d\vartheta \left(\frac{\vartheta}{2} \right)^{-2}, \quad (\text{II B.103})$$

one obtains immediately the classical expression (II A.31).

In the case of the magnetic cross section one must in addition employ the asymptotic expression

$$\begin{aligned} & \left\{ \begin{matrix} \lambda_1 & \lambda_2 & \lambda_3 \\ l_1 & l_2 & l_3 \end{matrix} \right\} \\ &= \frac{(-1)^{2l_1-2\lambda_1}}{(2l_1+1)^{\frac{1}{2}}} \begin{pmatrix} \lambda_1 & \lambda_2 & \lambda_3 \\ l_3-l_2 & l_1-l_3 & l_2-l_1 \end{pmatrix}, \quad (\text{II B.104}) \end{aligned}$$

for the Racah coefficient in the limit of large l_1 , l_2 , and l_3 with fixed λ 's. The expression (50) then reduces to (II A.54).

In a similar way the classical limit (II A.29) for the differential cross-section function is obtained from (47) by employing the further relation

$$\begin{aligned} & \left\{ \begin{matrix} l_1 & l_2 & l_3 \\ l_4 & l_5 & \lambda \end{matrix} \right\} \\ &= \frac{(-1)^{l_1+l_2+l_3}}{[(2l_1+1)(2l_2+1)]^{\frac{1}{2}}} D_{l_4-l_2, l_1-l_5}^{\lambda}(0, \theta, 0), \quad (\text{II B.105}) \end{aligned}$$

with

$$\cos \theta = \frac{l_3(l_3+1) - l_1(l_1+1) - l_2(l_2+1)}{2[l_1(l_1+1)l_2(l_2+1)]^{\frac{1}{2}}},$$

holding for l_1 , l_2 , l_3 , l_4 , and l_5 large. The formulas (104) and (105) may be derived from the explicit formulas for the Racah coefficients.²⁴

II C. Numerical Results

In this Section we shall give the results of the numerical computations of excitation cross sections and γ distributions based on the formulas derived in the preceding two Sections. A survey of the approximations involved in these formulas is contained in Sec. II C.5.

II C.1. Collision Parameters

For the application of the theoretical expressions it is convenient to write all parameters involved as func-

⁵⁵ E. P. Wigner, *Gruppentheorie* (Friedrich Vieweg & Sohn, Braunschweig, Germany, 1931).

tions of the energy of the incident projectile

$$E = \frac{1}{2} m_1 v_i^2, \quad (\text{II C.1})$$

and the energy independent quantities such as the charge and mass numbers and the excitation energy.

Thus, while the initial projectile velocity is given by

$$v_i = \left(\frac{2E}{A_1 M} \right)^{\frac{1}{2}}, \quad (\text{II C.2})$$

where A_1 is the projectile mass in units of the proton mass M , the final relative velocity v_f is obtained from the equation

$$\frac{1}{2} m_1 v_f^2 = E - \Delta E', \quad (\text{II C.3})$$

with

$$\Delta E' = (1 + A_1/A_2) \Delta E. \quad (\text{II C.4})$$

The nuclear mass number is denoted by A_2 , and ΔE represents the excitation energy. Introducing the parameter

$$\zeta = \Delta E'/E, \quad (\text{II C.5})$$

we may also write

$$v_f = \left(\frac{2E}{A_1 M} \right)^{\frac{1}{2}} (1 - \zeta)^{\frac{1}{2}}. \quad (\text{II C.6})$$

For the symmetrized parameter a defined by (II A.86) we thus obtain

$$\begin{aligned} a &= \frac{1}{2} (1 + A_1/A_2) \frac{Z_1 Z_2 e^2}{E} (1 - \zeta)^{-\frac{1}{2}} \\ &= 0.07199 (1 + A_1/A_2) \frac{Z_1 Z_2 (1 - \zeta)^{-\frac{1}{2}}}{E_{\text{Mev}}} \cdot 10^{-12} \text{ cm}, \quad (\text{II C.7}) \end{aligned}$$

where E_{Mev} is the initial energy (1) expressed in Mev.

Furthermore, the parameter η (see (II A.1)), for the initial and final states may be written

$$\eta_i = \frac{Z_1 Z_2}{2} \left(\frac{A_1}{10.008 \cdot E_{\text{Mev}}} \right)^{\frac{1}{2}}, \quad (\text{II C.8})$$

and

$$\eta_f = \eta_i (1 - \zeta)^{-\frac{1}{2}}. \quad (\text{II C.9})$$

The quantum-mechanical excitation and angular distribution functions are expressed as functions of η_i and $\xi = \eta_f - \eta_i$. Since both these parameters depend on the bombarding energy it is sometimes convenient instead of η_i to use the energy independent parameter ν defined by

$$\begin{aligned} \nu &= 2(\eta_i^{-2} - \eta_f^{-2})^{\frac{1}{2}} \\ &= \frac{4}{Z_1 Z_2} \left(\frac{10.008 \Delta E'_{\text{Mev}}}{A_1} \right)^{\frac{1}{2}}, \quad (\text{II C.10}) \end{aligned}$$

where the effective energy loss $\Delta E'$ defined by (4) is

TABLE II.2. List of numerically evaluated functions.

Results for	Method	Given in	
Total cross section			
$E1, E2, E3, E4,$ $M1, M2$	Classical	Tables II.3, 4	Figs. II.4, 5
$E1, E2$	Quantal	Table II.5	Fig. II.6
Differential cross section			
$E1, E2$	Classical	Tables II.7, 8	Fig. II.7
$E3, E4, M1, M2$	Classical		Fig. II.7
Angular distribution of γ rays			
$E1$	Quantal		Fig. II.8
$E2$	Quantal	Tables II.9, 10	Fig. II.8
$M1$		Text	

measured in Mev. The parameter ν is related to η_i by

$$\eta_i = 2\xi^{1/2}/\nu, \quad (\text{II C.11})$$

and for ξ one finds

$$\xi = -\frac{2}{\nu} \xi^{1/2} [(1-\xi)^{-1/2} - 1]. \quad (\text{II C.12})$$

The dependence of $\xi\nu$ on ζ is given graphically in Fig. III.10. A convenient expansion of ξ in powers of the energy loss is given by

$$\xi = \frac{Z_1 Z_2 A_1^{1/2} \Delta E'_{\text{Mev}}}{12.65 (E_{\text{Mev}} - \frac{1}{2} \Delta E'_{\text{Mev}})^{3/2}} \times \left(1 + \frac{5}{32} \left(\frac{\Delta E'}{E} \right)^2 + \dots \right). \quad (\text{II C.13})$$

The numerically evaluated excitation functions and angular distribution functions^{11,56-61} are given in the series of tables and figures listed in Table II.2.

II C.2. Total Cross Sections

The total cross section for excitation of a given level may be written

$$\sigma = \sum_{\lambda=1}^{\infty} (\sigma_{E\lambda} + \sigma_{M\lambda}), \quad (\text{II C.14})$$

where the partial cross sections are given by (II B.37) and (II B.38). Inserting (2) and (7) one obtains, for the electric excitation,

$$\sigma_{E\lambda} = c_{E\lambda} E_{\text{Mev}}^{\lambda-2} (E_{\text{Mev}} - \Delta E'_{\text{Mev}})^{\lambda-1} \times B(E\lambda) f_{E\lambda}(\eta_i, \xi), \quad (\text{II C.15})$$

⁵⁶ K. Alder and A. Winther, CERN report T/KA-AW-1 (1954); see also reference 88.

⁵⁷ L. C. Biedenharn and C. M. Class, Phys. Rev. **98**, 691 (1955) and **100**, 1790 (1955).

⁵⁸ K. Alder and A. Winther, Kgl. Danske Videnskab. Selskab Mat. fys. Medd. **29**, No. 19 (1955).

⁵⁹ K. Alder and A. Winther, reference 52.

⁶⁰ Biedenharn, Goldstein, McHale, and Thaler, Phys. Rev. **101**, 662 (1956).

⁶¹ Thaler, Goldstein, McHale, and Biedenharn, Phys. Rev. **102**, 1567 (1956).

with

$$c_{E\lambda} = \frac{Z_1^2 A_1}{40.03} [0.07199(1 + A_1/A_2) Z_1 Z_2]^{-2\lambda+2} \text{ barns} \quad (\text{II C.16})$$

i.e.,

$$c_{E\lambda} = \begin{cases} 2.498 \cdot 10^{-2} Z_1^2 A_1 \text{ barns} & (\lambda=1) \\ 4.819 \cdot (1 + A_1/A_2)^{-2} \frac{A_1}{Z_2^2} \text{ barns} & (\lambda=2) \\ 9.298 \cdot 10^2 (1 + A_1/A_2)^{-4} \frac{A_1}{Z_1^2 Z_2^4} \text{ barns} & (\lambda=3) \\ 1.794 \cdot 10^5 (1 + A_1/A_2)^{-6} \frac{A_1}{Z_1^4 Z_2^6} \text{ barns} & (\lambda=4). \end{cases} \quad (\text{II C.17})$$

The reduced nuclear transition probability, $B(E\lambda)$ defined by (II B.21 and 23) [see also (II A.13)] is measured in units of $e^2 \cdot (10^{-24} \text{ cm}^2)^\lambda$.

Similarly, for the magnetic excitations, one obtains

$$\sigma_{M\lambda} = c_{M\lambda} E_{\text{Mev}}^{\lambda-3/2} (E_{\text{Mev}} - \Delta E'_{\text{Mev}})^{\lambda-3/2} \times B(M\lambda) f_{M\lambda}(\eta_i, \xi), \quad (\text{II C.18})$$

with

$$c_{M\lambda} = 5.888 \cdot 10^{-9} Z_1^2 \times [0.07199(1 + A_1/A_2) Z_1 Z_2]^{-2\lambda+2} \text{ barns} \quad (\text{II C.19})$$

$$= \begin{cases} 5.888 \cdot 10^{-9} Z_1^2 \text{ barns} & (\lambda=1) \\ 1.136 \cdot 10^{-6} (1 + A_1/A_2)^{-2} \frac{1}{Z_2^2} \text{ barns} & (\lambda=2). \end{cases} \quad (\text{II C.20})$$

The reduced transition probabilities $B(M\lambda)$ defined by (II B.17) and (II B.23) [see also (II A.41)] are measured in units of $(e\hbar/2Mc)^2 \cdot (10^{-24} \text{ cm}^2)^{\lambda-1}$.

TABLE II.3. Classical f functions for $E1$, $E2$, and $M1$ excitations. The entry is given by a number and the power of ten (in parenthesis) by which it should be multiplied. The data are taken from reference 56.

ξ	$f_{E1}(\xi)$	$f_{E2}(\xi)$	$f_{M1}(\xi)$
0.0	∞	0.895 (0)	∞
0.1	0.580 (2)	0.859 (0)	2.230 (1)
0.2	2.721 (1)	0.729 (0)	0.828 (1)
0.3	1.349 (1)	0.561 (0)	3.719 (0)
0.4	0.693 (1)	4.046 (-1)	1.809 (0)
0.5	3.591 (0)	2.781 (-1)	0.905 (0)
0.6	1.872 (0)	1.844 (-1)	4.603 (-1)
0.7	0.980 (0)	1.189 (-1)	2.368 (-1)
0.8	0.514 (0)	0.751 (-1)	1.229 (-1)
0.9	2.707 (-1)	4.663 (-2)	0.642 (-1)
1.0	1.428 (-1)	2.855 (-2)	3.377 (-2)
1.2	3.992 (-2)	1.035 (-2)	0.944 (-2)
1.4	1.121 (-2)	3.628 (-3)	2.664 (-3)
1.6	3.154 (-3)	1.238 (-3)	0.757 (-3)
1.8	0.889 (-3)	4.143 (-4)	2.160 (-4)
2.0	2.511 (-4)	1.363 (-4)	0.618 (-4)
4.0	0.839 (-9)	1.247 (-9)	2.404 (-10)

The classical treatment of the excitation process given in Sec. II A leads, after symmetrization of the cross sections, to expressions of the same form as (15) and (18) [see (II A.88) and (II A.89)]. The entire difference between the classical and quantal cross sections is contained in the f functions, which in the classical case depend only on ξ , and correspond to the limiting values of the quantum-mechanical functions $f(\eta_i, \xi)$ for $\eta_i \rightarrow \infty$.

In most practical cases the quantal f functions differ only slightly from the classical limit. It is thus convenient to write

$$f_\lambda(\eta_i, \xi) = f_\lambda(\xi) \cdot R_\lambda(\eta_i, \xi), \quad (\text{II C.21})$$

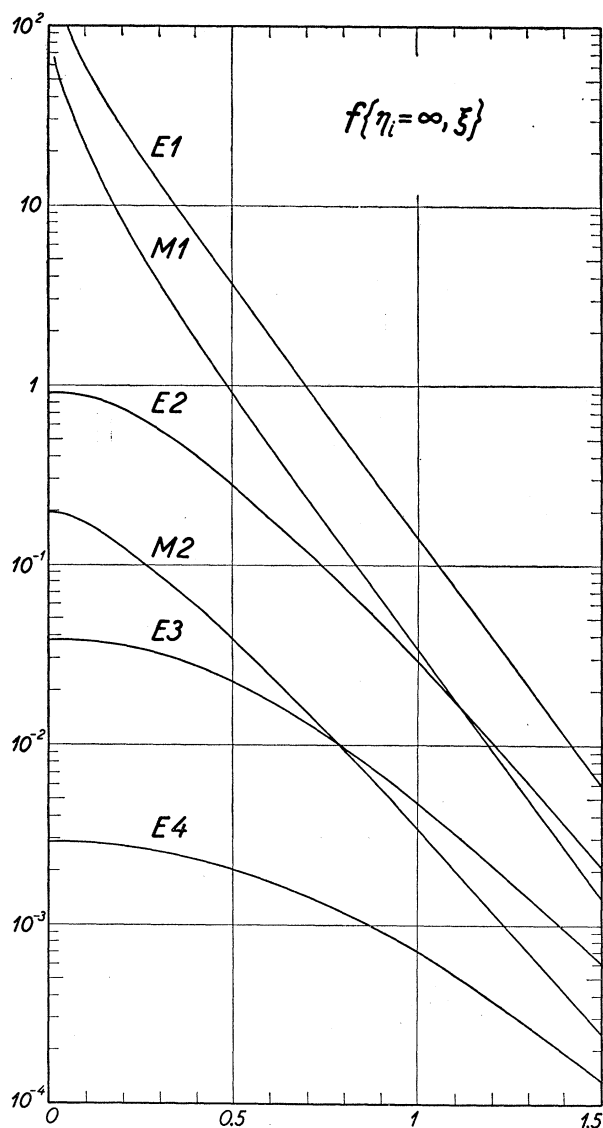


FIG. II.4. The total excitation cross section functions $f_\lambda(\xi)$ in the classical approximation. In the limit of large values for η_i , the f functions approach those obtained from a classical description (see Secs. II A.1 and II A.2). The classical f functions for the lowest electric and magnetic multipole orders are plotted against the parameter ξ . The data are taken from reference 56.

TABLE II.4. Classical f functions for $E3$, $E4$, and $M2$ excitations. The entry is given by a number and the power of ten (in parenthesis) by which it should be multiplied. The data are taken from reference 56.

ξ	$f_{E3}(\xi)$	$f_{E4}(\xi)$	$f_{M2}(\xi)$
0.0	3.797 (-2)	2.862 (-3)	1.936 (-1)
0.2	3.532 (-2)	2.729 (-3)	1.233 (-1)
0.4	2.723 (-2)	2.330 (-3)	0.577 (-1)
0.6	1.736 (-2)	1.760 (-3)	2.391 (-2)
0.8	0.956 (-2)	1.176 (-3)	0.920 (-2)
1.0	4.722 (-3)	0.705 (-3)	3.378 (-3)
1.5	0.593 (-3)	1.370 (-4)	2.433 (-4)
2.0	0.565 (-4)	1.870 (-5)	1.562 (-5)
4.0	1.398 (-9)	1.204 (-9)	1.560 (-10)

where $f_\lambda(\xi)$ is the classical f function and where the quantum effects are contained in the correction factor R_λ .

The classical f functions have been calculated^{11,56} for excitations of order $E1$, $E2$, $E3$, $E4$, $M1$, and $M2$ and the results are presented in Tables II.3 and II.4 and Figs. II.4 and II.5.

The functions were obtained from (II A.31) and (II A.54) with the orbital integrals $I_{\lambda\mu}(\vartheta, \xi)$ given by (II A.26). For the evaluation of these integrals, see Secs. II E.4-6.

The quantal f functions have been computed in the case of $E1$ ⁶¹ and $E2$ ^{57-60,62} excitations.^{62a} The function $f_{E2}(\eta_i, \xi)$ is given in Table II.5 and the correction factors $R_{E\lambda}(\eta_i, \xi)$ for $\lambda=1$ and 2 are illustrated in Fig. II.6.

The f_{E1} and f_{E2} functions have been obtained from (II B.48) which for $\lambda=1$ reduces to

$$f_{E1}(\eta_i, \xi) = \frac{64\pi^2}{9} k_i k_f b_0^{E1}, \quad (\text{II C.22})$$

with

$$b_0^{E1} = \sum_{l=0}^{\infty} \{ l |M_{l-1, l^{-2}}|^2 + (l+1) |M_{l+1, l^{-2}}|^2 \}. \quad (\text{II C.23})$$

For $\lambda=2$ one obtains

$$f_{E2}(\eta_i, \xi) = \frac{64\pi^2}{25} \eta_i \eta_f b_0^{E2}, \quad (\text{II C.24})$$

with

$$b_0^{E2} = \sum_{l=0}^{\infty} \left\{ \frac{3l(l-1)}{2(2l-1)} |M_{l-2, l^{-3}}|^2 + \frac{3(l+1)(l+2)}{2(2l+3)} |M_{l+2, l^{-3}}|^2 + \frac{l(l+1)(2l+1)}{(2l-1)(2l+3)} |M_{l, l^{-3}}|^2 \right\}. \quad (\text{II C.25})$$

⁶² The quantum-mechanical calculation of the electric quadrupole cross section was first performed for $\xi=0$ and for a particular value of η_i by direct numerical integration of the radial matrix elements by Daitch, Lazarus, Hull, Benedict, and Breit, Phys. Rev. **96**, 1449 (1954).

^{62a} Note added in proof.—Recently, the quantal f function for $M1$ excitation has been given by L. C. Biedenharn and R. M. Thaler (to be published in Phys. Rev.). This reference also contains the coefficient a_2 describing the angular distribution of the γ rays from an $M1$ or mixed $M1+E2$ excitation process.

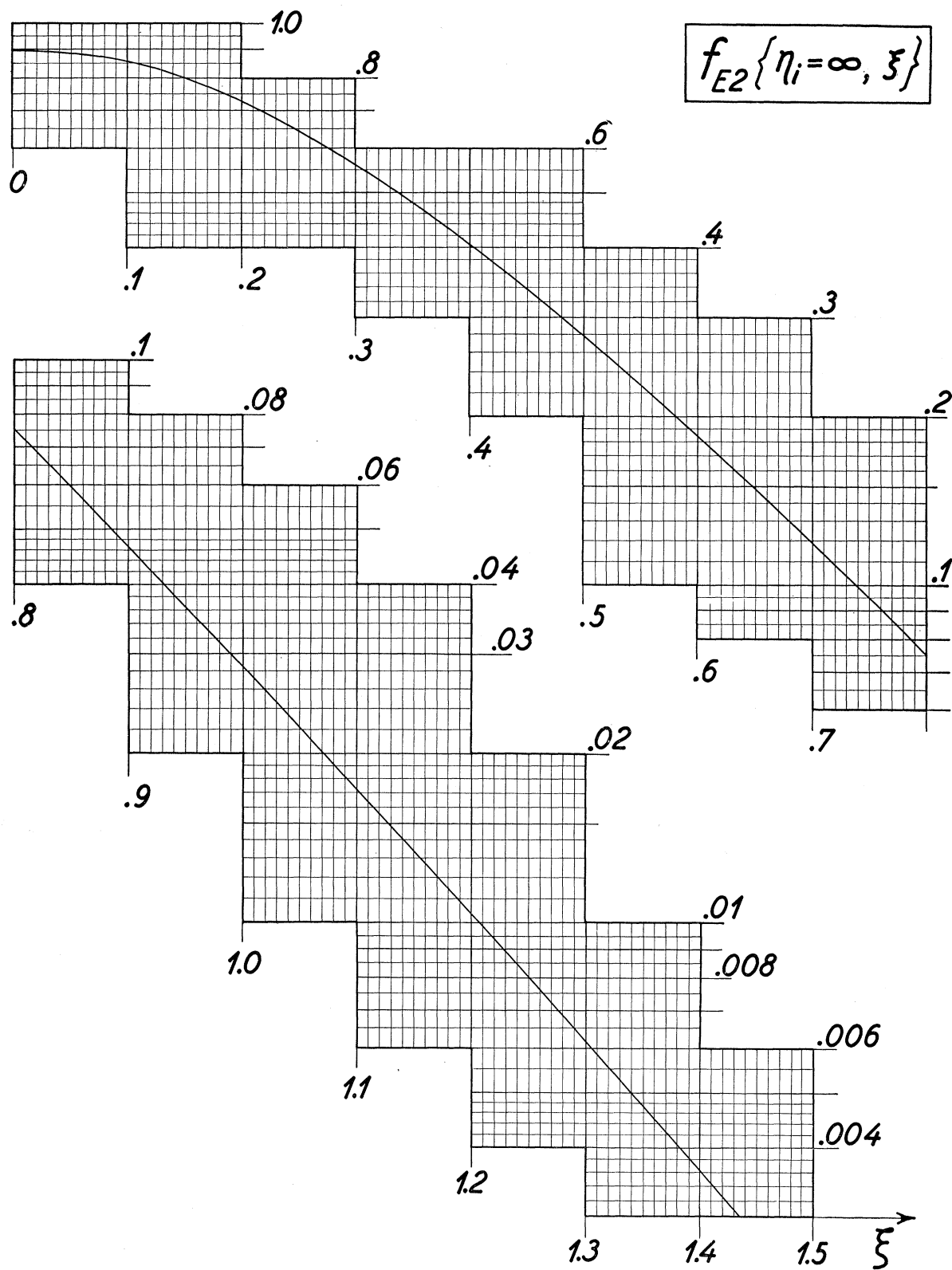


FIG. II.5. The total excitation cross-section function $f_{E2}(\xi)$ in the classical approximation. The data are taken from reference 56.

TABLE II.5. Total f function for $E2$ Coulomb excitation. The total f function for $E2$ excitation, as obtained from the complete quantum-mechanical calculation,^{59,60} is listed as a function of η_i and ξ .

ξ η_i	0	0.1	0.2	0.3	0.4	0.5	0.6
0.5	0.321	0.344	0.307	0.243			
1	0.620	0.614	0.528	0.409	0.295	0.203	0.1350
1.5	0.754	0.732	0.624	0.480	0.346	0.237	0.1570
2	0.812	0.784	0.666	0.512	0.368	0.253	0.1672
2.5	0.842	0.810	0.688	0.529	0.380	0.261	0.1726
3	0.858	0.825	0.700	0.538	0.387	0.266	0.1759
3.5	0.869	0.834	0.708	0.545	0.392	0.269	0.1779
4	0.875	0.840	0.713	0.548	0.395	0.271	0.1793
5	0.881	0.847	0.719	0.553	0.398	0.273	0.1810
6	0.886	0.851	0.722	0.556	0.400	0.275	0.1819
7	0.888	0.854	0.724	0.558	0.401	0.276	0.1825
8	0.890	0.855	0.726	0.559	0.402	0.276	0.1829
∞	0.895	0.859	0.729	0.561	0.405	0.278	0.1844

ξ η_i	0.8	1.0	1.2	1.4	1.6	2.0
1	0.0553					
1.5	0.0640	0.0244	0.00887	0.00312		
2	0.0680	0.0259	0.00939	0.00330	0.001130	
2.5	0.0702	0.0267	0.00968	0.00340	0.001162	0.0001287
3	0.0715	0.0272	0.00986	0.00345	0.001181	0.0001306
3.5	0.0724	0.0275	0.00996	0.00349	0.001194	0.0001319
4	0.0730	0.0277	0.01005	0.00352	0.001203	0.0001328
5	0.0737	0.0280	0.01015	0.00356	0.001214	0.0001339
6	0.0741	0.0282	0.01021	0.00358	0.001221	0.0001345
7	0.0743	0.0283	0.01024	0.00359	0.001225	0.0001350
8	0.0745	0.0283	0.01027	0.00360	0.001228	0.0001353
∞	0.0751	0.0286	0.01035	0.00363	0.001238	0.0001363

The radial matrix elements in (23) and (25) have been evaluated by the methods described in Sec. II B.4. The sum over l must be extended to $l \sim 300$ for large η_i and small ξ , while the convergence for large ξ is much more rapid.

II C.3. Differential Cross Sections

The differential excitation cross sections are obtained from (15) and (18) by replacing $f(\eta_i, \xi)$ by $df(\vartheta, \eta_i, \xi)$, where ϑ is the deflection angle in the center-of-mass system [see (II B.32) and (II B.33)]. These functions have so far only been evaluated⁶⁶ in the classical limit $\eta_i \rightarrow \infty$ in which they are equal to the $df(\vartheta, \xi)$ given by (II A.29) and (II A.51). The results for excitations of

TABLE II.6. Normalization for the angular distributions given in Fig. II.7. The absolute values of the classical differential f functions may be obtained from the relative values given in Fig. II.7 by employing the absolute normalization given in the present table. For electric excitations, the table gives $df/d\Omega$ at $\vartheta = 180^\circ$, while for magnetic excitation the value given is for $\vartheta = 90^\circ$. The entry is given by a number and the power of ten by which it should be multiplied.

	$\xi=0.0$	$\xi=0.2$	$\xi=0.4$	$\xi=0.6$	$\xi=1.0$	$\xi=2.0$	$\xi=4.0$
$df_{E1}(180^\circ, \xi)/d\Omega$	1.40 (0)	5.62 (-1)	1.95 (-1)	6.40 (-2)	6.39 (-3)	1.66 (-5)	8.41 (-11)
$df_{E2}(180^\circ, \xi)/d\Omega$	5.58 (-2)	3.89 (-2)	1.96 (-2)	8.60 (-3)	1.32 (-3)	6.76 (-6)	7.37 (-11)
$df_{E3}(180^\circ, \xi)/d\Omega$	4.56 (-3)	3.76 (-3)	2.36 (-3)	1.26 (-3)	2.71 (-4)	2.51 (-6)	5.58 (-11)
$df_{E4}(180^\circ, \xi)/d\Omega$	5.16 (-4)	4.47 (-4)	3.20 (-4)	1.97 (-4)	5.46 (-5)	8.39 (-7)	3.57 (-11)
$df_{M1}(90^\circ, \xi)/d\Omega$	2.58 (-1)	1.63 (-1)	7.23 (-2)	2.76 (-2)	3.25 (-3)	8.97 (-6)	3.16 (-11)
$df_{M2}(90^\circ, \xi)/d\Omega$	6.94 (-3)	5.64 (-3)	3.45 (-3)	1.77 (-3)	3.44 (-4)	2.30 (-6)	2.36 (-11)

⁶⁸ A WKB calculation was given in reference 59.

order $E1, E2, E3, E4, M1,$ and $M2,$ are given in Fig. II.7, and for $E1$ and $E2$ excitations also in the Tables II.7 and II.8.

The quantum corrections to the differential cross sections are expected to be greater than for the total cross sections. An indication of the effect of these corrections is provided by a comparison with the results of the Born-approximation treatment which corresponds to the limit $\eta_i = \xi = 0,$ and which for $E2$ excitations leads to an isotropic distribution of the inelastically scattered particles⁴ (see Sec. II E.2).

II. C.4. Angular Distribution of De-Excitation γ Rays

The angular distribution of the γ rays following electromagnetic excitation is given by (II B.83).

For $E1$ excitations the distribution can be written

$$W(\vartheta_\gamma) = 1 + a_2^{E1}(\eta_i, \xi) A_2^{(1)} P_2(\cos \vartheta_\gamma), \quad (\text{II C.26})$$

where the $A_2^{(1)}$ coefficients refer to the hypothetical γ - γ correlation of Fig. II.2 and may be obtained from (II A.70). The coefficients a_2^{E1} are given by (II B.84) and (II B.85) which for $\lambda=1$ reduce to

$$a_2^{E1}(\eta_i, \xi) = (b_0^{E1})^{-1} \sum_l \left\{ -\frac{(l-1)l}{2l+1} |M_{l-1, l}^{-2}|^2 - \frac{(l+1)(l+2)}{2l+1} |M_{l+1, l}^{-2}|^2 + \frac{6l(l+1)}{2l+1} M_{l+1, l}^{-2} M_{l-1, l}^{-2} \right\} \times \cos(\sigma_{l+1}(\eta_i) - \sigma_{l-1}(\eta_i)), \quad (\text{II C.27})$$

where b_0^{E1} is given by (23). The numerical results^{61, 63} for a_2^{E1} are shown in Fig. II.8.

In the classical limit $\eta_i \rightarrow \infty$ or $\nu \rightarrow 0$ the value of $a_2^{E1}(\eta_i, \xi)$ is equal to $a_2^{E1}(\xi)$ which is given by [see

TABLE II.7. Classical differential cross section function for $E1$ excitation. The table lists $df_{E1}/d\Omega$ as a function of ϑ (in degrees) and ξ .⁵⁶ The entry is given by a number and the power of ten by which it should be multiplied.

$\vartheta \backslash \xi$	0.0	0.1	0.2	0.3	0.4	0.5	0.6	0.7
0	∞	0.000	0.000	0.000	0.000	0.000	0.000	0.000
10	1.838 (2)	0.595 (2)	0.783 (1)	0.827 (0)	0.791 (-1)	0.714 (-2)	0.620 (-3)	0.525 (-4)
20	4.630 (1)	2.792 (1)	1.052 (1)	3.342 (0)	0.976 (0)	2.709 (-1)	0.727 (-1)	1.904 (-2)
30	2.084 (1)	1.420 (1)	0.724 (1)	3.236 (0)	1.346 (0)	0.535 (0)	2.066 (-1)	0.779 (-1)
40	1.194 (1)	0.839 (1)	4.843 (0)	2.520 (0)	1.234 (0)	0.581 (0)	2.664 (-1)	1.196 (-1)
50	0.782 (1)	0.551 (1)	3.373 (0)	1.898 (0)	1.015 (0)	0.524 (0)	2.645 (-1)	1.309 (-1)
60	0.558 (1)	3.920 (0)	2.462 (0)	1.446 (0)	0.813 (0)	4.438 (-1)	2.370 (-1)	1.245 (-1)
70	4.244 (0)	2.954 (0)	1.877 (0)	1.127 (0)	0.653 (0)	3.682 (-1)	2.037 (-1)	1.111 (-1)
80	3.379 (0)	2.331 (0)	1.485 (0)	0.902 (0)	0.531 (0)	3.053 (-1)	1.727 (-1)	0.964 (-1)
90	2.792 (0)	1.909 (0)	1.213 (0)	0.740 (0)	4.391 (-1)	2.554 (-1)	1.463 (-1)	0.828 (-1)
100	2.379 (0)	1.613 (0)	1.021 (0)	0.622 (0)	3.703 (-1)	2.165 (-1)	1.248 (-1)	0.712 (-1)
110	2.081 (0)	1.401 (0)	0.881 (0)	0.536 (0)	3.185 (-1)	1.864 (-1)	1.078 (-1)	0.617 (-1)
120	1.862 (0)	1.245 (0)	0.779 (0)	4.714 (-1)	2.795 (-1)	1.634 (-1)	0.944 (-1)	0.541 (-1)
130	1.700 (0)	1.131 (0)	0.703 (0)	4.236 (-1)	2.503 (-1)	1.459 (-1)	0.841 (-1)	4.814 (-2)
140	1.581 (0)	1.047 (0)	0.648 (0)	3.885 (-1)	2.286 (-1)	1.328 (-1)	0.764 (-1)	4.360 (-2)
150	1.496 (0)	0.988 (0)	0.608 (0)	3.634 (-1)	2.131 (-1)	1.234 (-1)	0.707 (-1)	4.026 (-2)
160	1.440 (0)	0.948 (0)	0.582 (0)	3.466 (-1)	2.026 (-1)	1.170 (-1)	0.669 (-1)	3.799 (-2)
170	1.407 (0)	0.925 (0)	0.567 (0)	3.369 (-1)	1.966 (-1)	1.133 (-1)	0.647 (-1)	3.667 (-2)
180	1.396 (0)	0.918 (0)	0.562 (0)	3.338 (-1)	1.946 (-1)	1.121 (-1)	0.640 (-1)	3.623 (-2)

$\vartheta \backslash \xi$	0.8	0.9	1.0	1.2	1.4	1.6	1.8	2.0	4.0
0	0.000	0.000	0.000	0.000	0.000	0.000	0.000	0.000	0.000
10	4.365 (-6)	3.573 (-7)	2.890 (-8)	1.840 (-10)	1.140 (-12)	0.693 (-14)	4.144 (-17)	2.449 (-19)	0.894 (-41)
20	4.898 (-3)	1.243 (-3)	3.117 (-4)	1.911 (-5)	1.142 (-6)	0.669 (-7)	3.863 (-9)	2.204 (-10)	0.569 (-22)
30	2.893 (-2)	1.059 (-2)	3.839 (-3)	4.919 (-4)	0.615 (-4)	0.754 (-5)	0.911 (-6)	1.089 (-7)	4.613 (-17)
40	0.529 (-1)	2.311 (-2)	0.999 (-2)	1.826 (-3)	3.256 (-4)	0.571 (-4)	0.986 (-5)	1.685 (-6)	2.566 (-14)
50	0.639 (-1)	3.084 (-2)	1.474 (-2)	3.296 (-3)	0.720 (-3)	1.547 (-4)	3.279 (-5)	0.688 (-5)	0.818 (-12)
60	0.645 (-1)	3.311 (-2)	1.684 (-2)	4.266 (-3)	1.058 (-3)	2.581 (-4)	0.622 (-4)	1.482 (-5)	0.642 (-11)
70	0.598 (-1)	3.192 (-2)	1.690 (-2)	4.643 (-3)	1.251 (-3)	3.317 (-4)	0.869 (-4)	2.255 (-5)	2.301 (-11)
80	0.532 (-1)	2.912 (-2)	1.582 (-2)	4.587 (-3)	1.305 (-3)	3.662 (-4)	1.015 (-4)	2.790 (-5)	0.511 (-10)
90	4.643 (-2)	2.582 (-2)	1.427 (-2)	4.286 (-3)	1.265 (-3)	3.685 (-4)	1.062 (-4)	3.033 (-5)	0.832 (-10)
100	4.030 (-2)	2.263 (-2)	1.264 (-2)	3.880 (-3)	1.173 (-3)	3.502 (-4)	1.035 (-4)	3.034 (-5)	1.097 (-10)
110	3.507 (-2)	1.980 (-2)	1.112 (-2)	3.458 (-3)	1.060 (-3)	3.213 (-4)	0.965 (-4)	2.877 (-5)	1.251 (-10)
120	3.078 (-2)	1.741 (-2)	0.980 (-2)	3.066 (-3)	0.947 (-3)	2.893 (-4)	0.877 (-4)	2.639 (-5)	1.288 (-10)
130	2.737 (-2)	1.547 (-2)	0.871 (-2)	2.727 (-3)	0.844 (-3)	2.588 (-4)	0.787 (-4)	2.380 (-5)	1.236 (-10)
140	2.473 (-2)	1.396 (-2)	0.784 (-2)	2.452 (-3)	0.758 (-3)	2.322 (-4)	0.707 (-4)	2.137 (-5)	1.136 (-10)
150	2.278 (-2)	1.283 (-2)	0.719 (-2)	2.240 (-3)	0.690 (-3)	2.110 (-4)	0.641 (-4)	1.934 (-5)	1.024 (-10)
160	2.145 (-2)	1.205 (-2)	0.674 (-2)	2.092 (-3)	0.642 (-3)	1.957 (-4)	0.592 (-4)	1.784 (-5)	0.927 (-10)
170	2.067 (-2)	1.159 (-2)	0.648 (-2)	2.004 (-3)	0.614 (-3)	1.865 (-4)	0.563 (-4)	1.692 (-5)	0.863 (-10)
180	2.041 (-2)	1.144 (-2)	0.639 (-2)	1.975 (-3)	0.604 (-3)	1.834 (-4)	0.553 (-4)	1.661 (-5)	0.841 (-10)

(II A.75)]

$$a_2^{E1}(\xi) = -\frac{1}{2} + \int_0^\pi 3I_{1,1}I_{1,-1} \cos\vartheta \frac{\cos\frac{\vartheta}{2}}{\sin^2\frac{\vartheta}{2}} d\vartheta$$

$$\times \left\{ \int_0^\pi [|I_{1,1}|^2 + |I_{1,-1}|^2] \frac{\cos\frac{\vartheta}{2}}{\sin^3\frac{\vartheta}{2}} d\vartheta \right\}^{-1}. \quad (\text{II C.28})$$

For $E2$ excitations the angular distribution of the γ rays is given by

$$W(\vartheta_\gamma) = 1 + a_2^{E2}(\eta_i, \xi) A_2^{(2)} P_2(\cos\vartheta_\gamma) + a_4^{E2}(\eta_i, \xi) A_4^{(2)} P_4(\cos\vartheta_\gamma), \quad (\text{II C.29})$$

where the $A_k^{(2)}$ coefficients may be obtained from

(II A.70). For some of the most frequently occurring transitions these coefficients are given in Table II.11. The a coefficients of (29) are tabulated as functions of

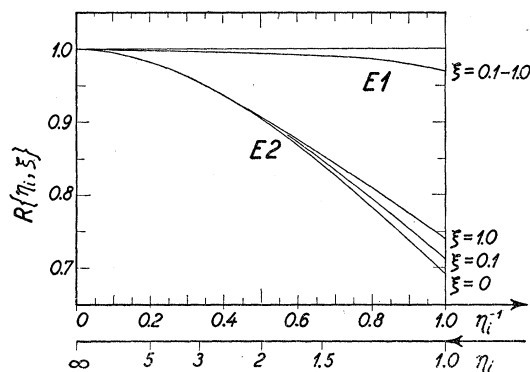


FIG. II.6. Quantum-mechanical corrections to the classical total f functions. The ratio $R_{E\lambda}(\eta_i, \xi)$ between the quantal and the classical total f function for $\lambda=1$ and 2 [see (II C.21)] is plotted as a function of η_i^{-1} for different values of ξ . The data are taken from references 59, 60, and 61.

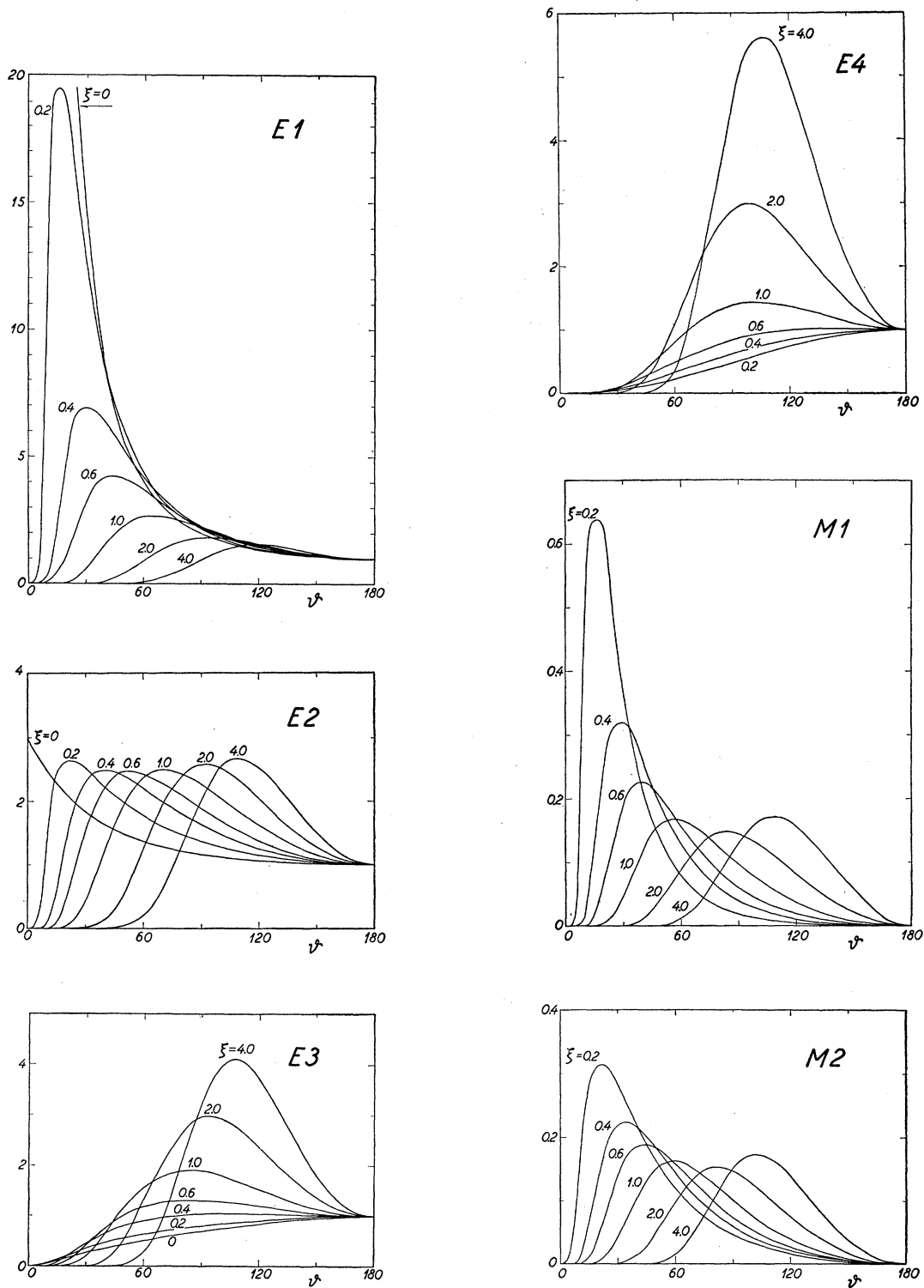


FIG. II.7. Angular distribution of the inelastically scattered particles in classical approximation. The classical differential excitation cross section functions $d f_{\lambda}(\vartheta, \xi) / d \Omega$ are plotted as a function of ϑ for fixed values of ξ . The electric multipole cross sections are normalized to unity at 180° , while the magnetic are normalized to give a total cross section of unity. The absolute values can be obtained by means of Table II.6. The data are taken from reference 56.

TABLE II.8. Classical differential cross section function for $E2$ excitation. The table lists $df_{E2}/d\Omega$ as a function of ϑ (in degrees) and ξ .⁵⁶ The entry is given by a number and the power of ten by which it should be multiplied.

$\vartheta \backslash \xi$	0.0	0.1	0.2	0.3	0.4	0.5	0.6	0.7
0	1.676 (-1)	0.000	0.000	0.000	0.000	0.000	0.000	0.000
10	1.385 (-1)	1.403 (-1)	0.521 (-1)	1.110 (-2)	1.788 (-3)	2.443 (-4)	2.996 (-5)	3.403 (-6)
20	1.178 (-1)	1.286 (-1)	1.016 (-1)	0.578 (-1)	2.678 (-2)	1.085 (-2)	4.005 (-3)	1.382 (-3)
30	1.027 (-1)	1.087 (-1)	0.981 (-1)	0.716 (-1)	4.474 (-2)	2.508 (-2)	1.300 (-2)	0.635 (-2)
40	0.916 (-1)	0.943 (-1)	0.873 (-1)	0.694 (-1)	4.895 (-2)	3.154 (-2)	1.899 (-2)	1.085 (-2)
50	0.832 (-1)	0.837 (-1)	0.772 (-1)	0.634 (-1)	4.715 (-2)	3.251 (-2)	2.113 (-2)	1.311 (-2)
60	0.768 (-1)	0.758 (-1)	0.690 (-1)	0.570 (-1)	4.341 (-2)	3.095 (-2)	2.095 (-2)	1.361 (-2)
70	0.719 (-1)	0.697 (-1)	0.624 (-1)	0.513 (-1)	3.932 (-2)	2.846 (-2)	1.967 (-2)	1.311 (-2)
80	0.680 (-1)	0.649 (-1)	0.570 (-1)	4.643 (-2)	3.549 (-2)	2.579 (-2)	1.798 (-2)	1.213 (-2)
90	0.650 (-1)	0.612 (-1)	0.527 (-1)	4.234 (-2)	3.210 (-2)	2.326 (-2)	1.624 (-2)	1.100 (-2)
100	0.627 (-1)	0.583 (-1)	4.930 (-2)	3.895 (-2)	2.920 (-2)	2.100 (-2)	1.460 (-2)	0.988 (-2)
110	0.608 (-1)	0.559 (-1)	4.651 (-2)	3.617 (-2)	2.676 (-2)	1.905 (-2)	1.314 (-2)	0.884 (-2)
120	0.593 (-1)	0.541 (-1)	4.428 (-2)	3.391 (-2)	2.475 (-2)	1.741 (-2)	1.190 (-2)	0.794 (-2)
130	0.582 (-1)	0.526 (-1)	4.252 (-2)	3.210 (-2)	2.311 (-2)	1.606 (-2)	1.086 (-2)	0.718 (-2)
140	0.573 (-1)	0.515 (-1)	4.115 (-2)	3.068 (-2)	2.182 (-2)	1.499 (-2)	1.003 (-2)	0.657 (-2)
150	0.566 (-1)	0.507 (-1)	4.013 (-2)	2.961 (-2)	2.085 (-2)	1.418 (-2)	0.939 (-2)	0.609 (-2)
160	0.562 (-1)	0.501 (-1)	3.942 (-2)	2.887 (-2)	2.017 (-2)	1.361 (-2)	0.895 (-2)	0.576 (-2)
170	0.559 (-1)	4.980 (-2)	3.900 (-2)	2.844 (-2)	1.977 (-2)	1.328 (-2)	0.869 (-2)	0.557 (-2)
180	0.558 (-1)	4.969 (-2)	3.887 (-2)	2.829 (-2)	1.963 (-2)	1.316 (-2)	0.860 (-2)	0.550 (-2)

$\vartheta \backslash \xi$	0.8	0.9	1.0	1.2	1.4	1.6	1.8	2.0	4.0
0	0.000	0.000	0.000	0.000	0.000	0.000	0.000	0.000	0.000
10	3.652 (-7)	3.750 (-8)	3.719 (-9)	3.374 (-11)	2.824 (-13)	2.227 (-15)	1.679 (-17)	1.220 (-19)	1.750 (-41)
20	4.531 (-4)	1.427 (-4)	4.351 (-5)	3.752 (-6)	2.998 (-7)	2.265 (-8)	1.638 (-9)	1.144 (-10)	1.134 (-22)
30	2.960 (-3)	1.331 (-3)	0.581 (-3)	1.032 (-4)	1.708 (-5)	2.680 (-6)	4.032 (-7)	0.587 (-7)	0.929 (-16)
40	0.595 (-2)	3.159 (-3)	1.631 (-3)	4.076 (-4)	0.953 (-4)	2.118 (-5)	4.523 (-6)	0.936 (-6)	0.518 (-13)
50	0.784 (-2)	4.553 (-3)	2.577 (-3)	0.777 (-3)	2.203 (-4)	0.595 (-4)	1.549 (-5)	3.913 (-6)	1.643 (-12)
60	0.855 (-2)	0.523 (-2)	3.123 (-3)	1.054 (-3)	3.356 (-4)	1.022 (-4)	3.001 (-5)	0.857 (-5)	1.269 (-11)
70	0.847 (-2)	0.534 (-2)	3.294 (-3)	1.191 (-3)	4.079 (-4)	1.339 (-4)	4.249 (-5)	1.312 (-5)	4.434 (-11)
80	0.796 (-2)	0.510 (-2)	3.211 (-3)	1.211 (-3)	4.338 (-4)	1.494 (-4)	4.985 (-5)	1.621 (-5)	0.950 (-10)
90	0.727 (-2)	4.700 (-3)	2.986 (-3)	1.153 (-3)	4.245 (-4)	1.506 (-4)	0.519 (-4)	1.743 (-5)	1.477 (-10)
100	0.653 (-2)	4.232 (-3)	2.699 (-3)	1.054 (-3)	3.936 (-4)	1.420 (-4)	4.983 (-5)	1.708 (-5)	1.842 (-10)
110	0.582 (-2)	3.769 (-3)	2.402 (-3)	0.939 (-3)	3.526 (-4)	1.282 (-4)	4.538 (-5)	1.572 (-5)	1.964 (-10)
120	0.520 (-2)	3.345 (-3)	2.123 (-3)	0.826 (-3)	3.094 (-4)	1.125 (-4)	3.990 (-5)	1.387 (-5)	1.869 (-10)
130	4.660 (-3)	2.979 (-3)	1.879 (-3)	0.724 (-3)	2.691 (-4)	0.973 (-4)	3.439 (-5)	1.193 (-5)	1.640 (-10)
140	4.224 (-3)	2.678 (-3)	1.677 (-3)	0.637 (-3)	2.344 (-4)	0.840 (-4)	2.947 (-5)	1.016 (-5)	1.364 (-10)
150	3.888 (-3)	2.445 (-3)	1.519 (-3)	0.569 (-3)	2.069 (-4)	0.733 (-4)	2.546 (-5)	0.870 (-5)	1.106 (-10)
160	3.650 (-3)	2.280 (-3)	1.407 (-3)	0.521 (-3)	1.870 (-4)	0.656 (-4)	2.254 (-5)	0.763 (-5)	0.904 (-10)
170	3.509 (-3)	2.181 (-3)	1.340 (-3)	4.918 (-4)	1.751 (-4)	0.609 (-4)	2.078 (-5)	0.698 (-5)	0.779 (-10)
180	3.462 (-3)	2.148 (-3)	1.318 (-3)	4.822 (-4)	1.712 (-4)	0.593 (-4)	2.019 (-5)	0.676 (-5)	0.737 (-10)

η_i and ξ in Tables II.9 and II.10 and are illustrated as functions of ξ and ν [see (10)] in Fig. II.8.^{57-60,64,65} These coefficients have been computed from the expressions

$$a_k^{E2}(\eta_i, \xi) = b_k^{E2}/b_0^{E2}, \quad (\text{II C.30})$$

where b_0^{E2} is given by (25), while

$$b_2^{E2} = \sum_l \left\{ \frac{3l(l-1)(l-2)}{(2l-1)^2} |M_{l-2, l^{-3}}|^2 + \frac{3(l+1)(l+2)(l+3)}{(2l+3)^2} |M_{l+2, l^{-3}}|^2 \right. \\ \left. - \frac{l(l+1)(2l-3)(2l+1)(2l+5)}{(2l-1)^2(2l+3)^2} |M_{l^{-3}}|^2 - \frac{6(l-1)l(l+1)}{(2l-1)^2} M_{l-2, l^{-3}} M_{l^{-3}} \cos(\sigma_l(\eta_i) - \sigma_{l-2}(\eta_i)) \right. \\ \left. - \frac{6l(l+1)(l+2)}{(2l+3)^2} M_{l+2, l^{-3}} M_{l^{-3}} \cos(\sigma_l(\eta_i) - \sigma_{l+2}(\eta_i)) \right\}, \quad (\text{II C.31})$$

⁶⁴ The coefficients a_2^{E2} , given in references 58 and 59, contain a numerical error responsible for the somewhat irregular behavior. We are indebted to Dr. L. C. Biedenharn for discussions concerning this point.

⁶⁵ A WKB calculation for special values of η_i and ξ has been given by F. D. Benedict, Phys. Rev. **101**, 178 (1956).

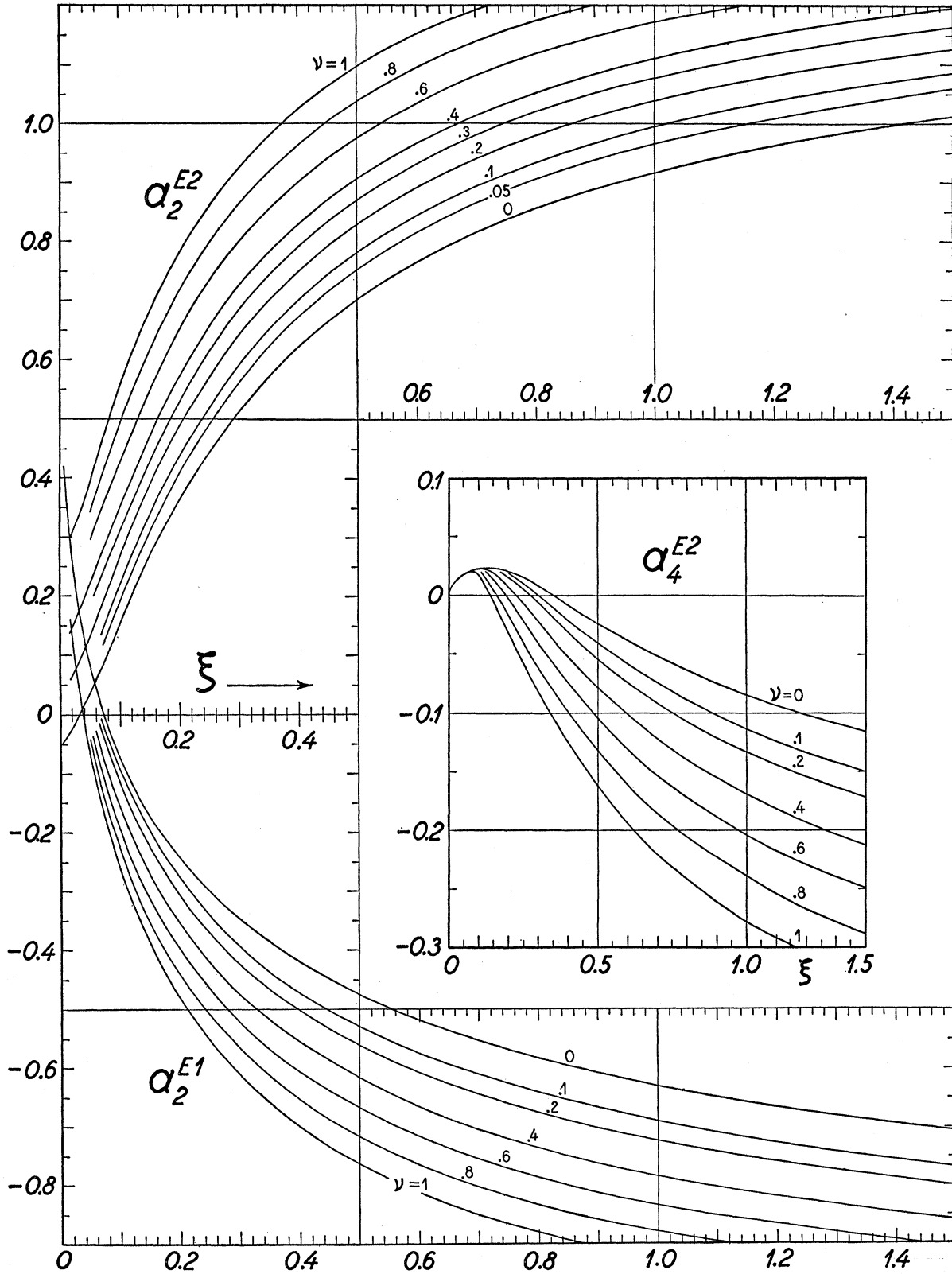


FIG. II.8. Gamma-ray angular distributions following Coulomb excitation. The coefficients $a_k^{E\lambda}(\nu, \xi)$ which describe the angular distribution of the gamma rays following Coulomb excitation (II C.26) and (II C.29) are plotted as a function of ξ for different values of the parameter ν . The classical limit corresponds to $\nu=0$. The data are taken from references 59, 60, and 61.

TABLE II.9. Gamma-ray angular distribution coefficients $a_2^{E2}(\eta_i, \xi)$. The coefficient a_2^{E2} which describes the angular distribution of the gamma rays following $E2$ Coulomb excitation [see (II C.29)] is given as a function of η_i and ξ . The data are taken from references 59 and 60.

$\xi \backslash \eta_i$	0.0	0.1	0.2	0.3	0.4	0.5	0.6	0.8	1.0	1.2	1.4	1.6	2.0
0.0	0.50	2.000	2.000	2.000	2.000	2.000	2.000	2.000	2.000	2.000	2.000	2.000	2.000
0.5	0.20	0.800	1.142	1.325									
1.0	0.07	0.501	0.809	1.002	1.130	1.223	1.285						
1.5	-0.00	0.372	0.660	0.843	0.970	1.065	1.132	1.228	1.290	1.334	1.360		
2.0	-0.02	0.307	0.577	0.758	0.884	0.971	1.046	1.144	1.210	1.256	1.290		
2.5	-0.03	0.270	0.526	0.707	0.831	0.922	0.993	1.089	1.158	1.206	1.242	1.270	
3.0	-0.04	0.247	0.497	0.673	0.793	0.882	0.956	1.053	1.122	1.171	1.208	1.237	1.279
4.0	-0.04	0.220	0.462	0.633	0.752	0.841	0.909	1.008	1.075	1.125	1.163	1.192	1.235
5.0	-0.04	0.204	0.440	0.606	0.724	0.813	0.878	0.979	1.046	1.095	1.131	1.162	1.207
6.0	-0.05	0.194	0.426	0.589	0.705	0.794	0.859	0.959	1.026	1.075	1.110	1.142	1.185
8.0	-0.05	0.178	0.408	0.569	0.685	0.769	0.838	0.934	1.000	1.048	1.086	1.116	1.159
10.0	-0.05	0.173	0.399	0.557	0.672	0.758	0.823	0.919	0.984	1.030	1.069	1.099	1.143
12.0	-0.05	0.170	0.393	0.549	0.661	0.748	0.813	0.908	0.973	1.019	1.057	1.087	1.130
16.0	-0.05	0.165	0.387	0.540	0.651	0.735	0.803	0.894	0.959	1.005	1.043	1.072	1.115
∞	-0.05	0.150	0.361	0.510	0.619	0.700	0.763	0.853	0.915	0.961	0.996	1.023	1.064

and

$$\begin{aligned}
 b_4^{E2} = \sum_l \left\{ & -\frac{9l(l-1)(l-2)(l-3)}{16(2l-1)^2(2l+1)} |M_{l-2, l^{-3}}|^2 - \frac{9(l+1)(l+2)(l+3)(l+4)}{16(2l+1)(2l+3)^2} |M_{l+2, l^{-3}}|^2 \right. \\
 & - \frac{9(l-1)l(l+1)(l+2)(2l+1)}{4(2l-1)^2(2l+3)^2} |M_{ll^{-3}}|^2 + \frac{15(l-2)(l-1)l(l+1)}{4(2l-1)^2(2l+3)} M_{l-2, l^{-3}} M_{ll^{-3}} \cos(\sigma_l(\eta_i) - \sigma_{l-2}(\eta_i)) \\
 & + \frac{15l(l+1)(l+2)(l+3)}{4(2l-1)(2l+3)^2} M_{l+2, l^{-3}} M_{ll^{-3}} \cos(\sigma_l(\eta_i) - \sigma_{l+2}(\eta_i)) \\
 & \left. - \frac{105(l-1)l(l+1)(l+2)}{8(2l-1)(2l+1)(2l+3)} M_{l+2, l^{-3}} M_{l-2, l^{-3}} \cos(\sigma_{l+2}(\eta_i) - \sigma_{l-2}(\eta_i)) \right\}. \quad (\text{II C.32})
 \end{aligned}$$

The classical limit ($\eta_i \rightarrow \infty$ or $\nu = 0$) is obtained from the formula (II A.76) which in the case $\lambda = 2$ reduces to^{11, 56, 66}

$$b_0^{E2}(\xi) = \int_0^\pi \left(\frac{3}{2} |I_{22}|^2 + |I_{20}|^2 + \frac{3}{2} |I_{2,-2}|^2 \right) \frac{\cos \frac{\vartheta}{2}}{\sin^3 \frac{\vartheta}{2}} d\vartheta, \quad (\text{II C.33})$$

$$b_2^{E2}(\xi) = \int_0^\pi \left(\frac{3}{2} |I_{22}|^2 - |I_{20}|^2 + \frac{3}{2} |I_{2,-2}|^2 - 3I_{20}(I_{22} + I_{2,-2}) \cos \vartheta \right) \frac{\cos \frac{\vartheta}{2}}{\sin^3 \frac{\vartheta}{2}} d\vartheta, \quad (\text{II C.34})$$

$$b_4^{E2}(\xi) = \int_0^\pi \left(-\frac{9}{64} |I_{22}|^2 - \frac{9}{16} |I_{20}|^2 - \frac{9}{64} |I_{2,-2}|^2 + \frac{9}{16} I_{20}(I_{22} + I_{2,-2}) \cos \vartheta - \frac{105}{32} I_{22} I_{2,-2} \cos 2\vartheta \right) \frac{\cos \frac{\vartheta}{2}}{\sin^3 \frac{\vartheta}{2}} d\vartheta. \quad (\text{II C.35})$$

⁶⁶ The γ -ray angular distribution coefficients of references 11 and 56 contain errors of sign as pointed out by Breit, Ebel, and Benedict (Phys. Rev. **100**, 429 (1955)), who have re-evaluated the distributions for certain values of ξ (see also F. D. Benedict and G. Tice, Phys. Rev. **100**, 1545 (1955)).

TABLE II.10. Gamma-ray angular distribution coefficient $a_4^{E2}(\eta_i, \xi)$. The coefficient a_4^{E2} which describes the angular distribution of the gamma rays following $E2$ Coulomb excitation [see (II C.29)] is given as a function of η_i and ξ . The data are taken from references 59 and 60.

ξ / η_i	0.0	0.1	0.2	0.3	0.4	0.5	0.6	0.8	1.0	1.2	1.4	1.6	2.0
0	+0.0625	-1.500	-1.500	-1.500	-1.500	-1.500	-1.500						
0.5	+0.016	-0.007	-0.179	-0.338	-0.463								
1.0	+0.002	+0.020	-0.040	-0.114	-0.183	-0.241	-0.291	-0.368					
1.5	0.000	+0.026	-0.006	-0.054	-0.101	-0.144	-0.182	-0.242	-0.289	-0.324	-0.352		
2.0	0.000	+0.027	+0.006	-0.031	-0.069	-0.104	-0.136	-0.188	-0.229	-0.262	-0.288	-0.309	
2.5	0.000	+0.027	+0.011	-0.020	-0.053	-0.084	-0.112	-0.159	-0.197	-0.227	-0.251	-0.272	-0.303
3.0	0.000	+0.027	+0.014	-0.013	-0.043	-0.071	-0.097	-0.141	-0.176	-0.205	-0.228	-0.247	-0.278
4.0	0.000	+0.026	+0.017	-0.006	-0.033	-0.058	-0.080	-0.120	-0.151	-0.178	-0.199	-0.218	-0.246
5.0	0.000	+0.025	+0.018	-0.003	-0.027	-0.050	-0.071	-0.108	-0.137	-0.162	-0.182	-0.200	-0.221
6.0	-0.001	+0.025	+0.018	-0.001	-0.023	-0.045	-0.065	-0.100	-0.128	-0.151	-0.171	-0.188	-0.217
8.0	-0.001	+0.024	+0.019	+0.001	-0.019	-0.039	-0.058	-0.090	-0.117	-0.139	-0.157	-0.173	-0.199
10.0	-0.001	+0.024	+0.019	+0.003	-0.016	-0.036	-0.053	-0.084	-0.109	-0.130	-0.147	-0.162	-0.185
12.0	-0.001	+0.023	+0.019	+0.004	-0.013	-0.034	-0.051	-0.081	-0.105	-0.124	-0.142	-0.157	-0.177
16.0	-0.001	+0.023	+0.020	+0.005	-0.010	-0.031	-0.048	-0.076	-0.100	-0.118	-0.135	-0.149	-0.174
∞	-0.001	+0.022	+0.020	+0.007	-0.009	-0.024	-0.039	-0.064	-0.085	-0.101	-0.116	-0.128	-0.146

It is seen from the figures and tables of the a coefficients that the deviations from the classical limit are considerable even for rather large values of η_i .

In the limit of $\xi \rightarrow 0$, the curves for $\nu \neq 0$ would exhibit rapid variation and would approach the Born approximation values which are appreciably different from those of the classical approximation (see Sec. II E.2). Since the region of rapid variation corresponds to $\eta \ll 1$ it is outside the domain of Coulomb excitation experiments.

For $M1$ excitations the angular distribution of the γ rays in the classical approximation is given by (see II A.74)

$$W(\vartheta_\gamma) = 1 + A_2^{(1)} P_2(\cos \vartheta_\gamma), \quad (\text{II C.36})$$

where the $A_2^{(1)}$ may be obtained from (II A.70). It is noted that for mixed multipole excitations, the γ -ray angular distribution contains additional interference terms.^{66a}

The angular distribution of the γ 's following other multipole excitations, as well as the angular distribution for specified direction of the inelastically scattered projectile, may be obtained in the classical approximation from the formulas of Sec. II A.4 using the tabulated values of the orbital integrals (see Table II.12 and reference 88).

The polarization of the decay γ rays is obtained by replacing $A_k^{(\lambda)} P_k(\cos \vartheta_\gamma)$ in (26), (29), and (36) by the appropriate expressions which depend also on the polarization angle ψ_γ , and which are given in Sec. II A [see (II A.70) and (II A.78a)].

II C.5. Survey of Approximations

We here summarize the various effects which have been neglected in the formulas considered in the earlier parts of this Section.

^{66a} See reference 62a, where it is also shown that Eq. (36) remains valid in the quantum-mechanical treatment, provided spin effects are neglected.

a. Relativity effects.—The relativistic treatment of the excitation process (see Sec. II B.1) involves a modification of the excitation functions, but the correction terms are at most of order v^2/c^2 , where v is the projectile velocity. The effect of the projectile spin, which is not included in (15) and (18), again implies corrections to the electric excitation cross section of order v^2/c^2 or less, while the corrections to the magnetic excitations are of relatively greater significance and may be obtained from (II B.30).^{66a}

It is noted that the treatment of the nuclear structure is fully relativistic, provided the expressions (II B.16 and 17) for the multipole operators are employed.

b. Screening by the atomic electrons.—The screening of the nuclear Coulomb field by the atomic electrons gives rise to a minor modification of the projectile orbit. The effect is, however, very small, since the distance of closest approach, $2a$, even in heavy atoms and for proton energies as low as one Mev, is an order of magnitude smaller than the radius of the atomic K shell. The attraction from the electrons implies a small acceleration of the projectiles during their passage to the center of the atom, which results in a small increase in the effective energy in the Coulomb excitation process. This energy increase amounts to about 10 kev in a heavy atom ($Z_2 \sim 80$). An effect of similar magnitude but opposite sign results from the vacuum polarization which implies a small increase of the order of one-half of a percent in the repulsion between the nucleus and the projectile at distances of a few times the nuclear radius.⁶⁷

There are also various processes by which the projectile may lose small amounts of energy in traversing the atom (e.g., ionization of K, L, \dots shells, or bremsstrahlung (see Sec. III B.3)). These effects are connected with the influence of straggling on the Coulomb excitation yield, and are of minor importance.

c. Attenuation effects in angular distributions.—The atomic electric and magnetic fields may cause a pre-

⁶⁷ L. L. Foldy and E. Eriksen, Phys. Rev. **95**, 1048 (1954).

TABLE II.11. Some γ - γ angular correlation coefficients. The table gives the γ - γ angular correlation coefficients,⁶¹ $A_k(2)$, for values of the spins I_i , I_f , and I_{ff} which may occur especially often in Coulomb excitation experiments. The excitation process is assumed to be pure $E2$ and the de-excitation is assumed to proceed by mixed $M1$ and $E2$ radiation; δ^2 is the ratio between the intensities of $E2$ and $M1$ gamma radiation, and the sign of δ is defined as in Eq. (II A.70).

I_i	I_f	I_{ff}	$A_2(2)$	$A_4(2)$
0	2	0	0.3571	1.143
1/2	3/2	1/2	$\frac{-0.250+0.8660\delta+0.250\delta^2}{1+\delta^2}$	0
1/2	5/2	1/2	0.2857	0.3810
1/2	5/2	3/2	$\frac{-0.2000+1.014\delta+0.1020\delta^2}{1+\delta^2}$	-0.4354 $1+\delta^2$
3/2	5/2	3/2	$\frac{-0.07143+0.3622\delta+0.03644\delta^2}{1+\delta^2}$	0.4976 $1+\delta^2$
3/2	7/2	3/2	0.2186	0.1282
3/2	7/2	5/2	$\frac{-0.1530+0.884\delta+0.0364\delta^2}{1+\delta^2}$	-0.2280 $1+\delta^2$
5/2	7/2	5/2	$\frac{-0.0255+0.1472\delta+0.00607\delta^2}{1+\delta^2}$	0.4054 $1+\delta^2$
5/2	9/2	5/2	0.1870	0.07204
5/2	9/2	7/2	$\frac{-0.1310+0.809\delta+0.00852\delta^2}{1+\delta^2}$	-0.1572 $1+\delta^2$
7/2	9/2	7/2	$\frac{-0.00597+0.0368\delta+0.000389\delta^2}{1+\delta^2}$	0.3430 $1+\delta^2$
7/2	11/2	7/2	0.1688	0.0500
7/2	11/2	9/2	$\frac{-0.1182+0.762\delta-0.00649\delta^2}{1+\delta^2}$	-0.1231 $1+\delta^2$
9/2	11/2	9/2	$\frac{0.00454-0.0293\delta+0.00025\delta^2}{1+\delta^2}$	0.3030 $1+\delta^2$
9/2	13/2	9/2	0.1570	0.03881

cession of the angular momentum vector of the excited nucleus, giving rise to an attenuation of the angular anisotropy of the emitted radiation.⁶⁸ In most cases one expects the largest effect to arise from the quadrupole coupling to the electric field. This coupling may be especially strong at the interstitial positions reached by the recoiling nucleus. The conditions are somewhat similar to those encountered in the α decay of the very heavy elements, where the α - γ correlations are observed to be appreciably attenuated⁶⁹ even for lifetimes as

⁶⁸ H. Frauenfelder, Chapter XIX of *Beta- and Gamma-Ray Spectroscopy* (edited by K. Siegbahn) (North Holland Publishing Company, Amsterdam, 1955).

⁶⁹ See e.g., J. O. Newton, *Progress in Nuclear Physics* (edited by O. R. Frisch) (Pergamon Press, London, 1954), Volume 4, p. 256.

short as $5 \cdot 10^{-10}$ second.⁷⁰ The excited states involved in these α - γ correlations are expected to have especially large quadrupole moments (see Sec. V B.2). It may thus be concluded that a lower limit to the lifetimes for which the attenuation effects may be of significance in Coulomb excitations is of the order 10^{-10} second.

d. Higher order interaction effects.—In Secs. II A and B, the probability for exciting the nucleus is treated in first-order perturbation theory. Under most experimental conditions so far studied, the probability for excitation in a single encounter is very small, and such a treatment therefore well justified. The influence of higher order effects giving rise to multiple excitations is considered in Sec. II D. Such effects become of special importance in the case of high projectile charge and large bombarding energies.

II D. Higher Order Excitation Effects

In the theory of Coulomb excitation presented in the preceding sections, the probability for excitation of the nucleus was calculated in lowest order perturbation theory. In most of the experiments which have so far been performed, this approximation is well justified since the excitation probability in a single encounter is very small compared to unity. Thus, for an $E2$ excitation with $\xi=0$ the excitation probability, in a backward scattering, is given by [see (II A.2) and (II A.28) and Table II.8]

$$P = d\sigma_{E2}/d\sigma_R = 207 \frac{A_1}{Z_1^2 Z_2^4} E_{\text{Mev}}^3 B(E2), \quad (\text{II D.1})$$

where $B(E2)$ is measured in units of $e^2 \cdot (10^{-24} \text{ cm}^2)^2$.

As an example, one finds for 6-Mev α particles on a target with $Z_2=70$ a value for P of about 0.01 for $B(E2) \approx 5$ corresponding to the largest transition probabilities encountered (see Table IV.2).

It is seen, however, that the probability, P , may become appreciable for large bombarding energies, which may especially be employed with highly charged projectiles.⁷¹ Moreover, even when the probability is small, higher order effects may be observed if the direct transition to the final state is weak.

We shall in this section consider the treatment of higher order effects based on the classical description of the projectile orbit, and briefly discuss a few applications.

II D.1. Cross Sections to Second Order

To second order in the charge of the projectile, the amplitude for a transition from the initial nuclear state

⁷⁰ While none of these lifetimes has been directly measured, they are expected to be similar to those for the first excited states in Th^{232} and U^{238} inferred from the Coulomb excitation cross sections (Table IV.2).

⁷¹ See G. Breit and J. P. Lazarus, *Phys. Rev.* **100**, 942 (1955).

i to the final state f is given by

$$b_{if}^{(2)} = b_{if}(\omega) + \sum_z b_{izf}, \quad (\text{II D.2})$$

where b_{if} is the first-order amplitude (II A.6) and where²⁰

$$b_{izf} = \frac{1}{(i\hbar)^2} \int_{-\infty}^{\infty} dt \langle f | \mathcal{H}(t) | z \rangle \times e^{i\omega_2 t} \int_{-\infty}^t dt' \langle z | \mathcal{H}(t') | i \rangle e^{i\omega_1 t'}. \quad (\text{II D.3})$$

The summation in (2) is to be performed over all intermediate states z , including the initial and final state. The frequencies ω_1 , ω_2 , and ω , are given by

$$\begin{aligned} \omega_1 &= (E_z - E_i)/\hbar, \\ \omega_2 &= (E_f - E_z)/\hbar, \\ \omega &= \omega_1 + \omega_2 = (E_f - E_i)/\hbar, \end{aligned} \quad (\text{II D.4})$$

where the energies of the initial, intermediate, and final states are denoted by E_i , E_z , and E_f , respectively.

In the evaluation of the double integral (3), it is convenient to introduce the unit step function

$$\epsilon(t-t') = -\lim_{\delta \rightarrow 0^+} \frac{1}{2\pi i} \int_{-\infty}^{\infty} \frac{e^{-i(t-t')q}}{q+i\delta} dq = \begin{cases} 1 & t > t' \\ 0 & t < t'. \end{cases} \quad (\text{II D.5})$$

We then get

$$b_{izf} = -\lim_{\delta \rightarrow 0^+} \frac{1}{2\pi i} \int_{-\infty}^{\infty} \frac{dq}{q+i\delta} b_{iz}(\omega_1+q) b_{zf}(\omega_2-q) = \frac{1}{2} b_{iz}(\omega_1) b_{zf}(\omega_2) + \frac{i}{2\pi} \mathcal{P} \int_{-\infty}^{\infty} \frac{b_{iz}(\omega_1+q) b_{zf}(\omega_2-q)}{q} dq, \quad (\text{II D.6})$$

where \mathcal{P} stands for the principal part of the integral.

In the focal system the b_{if} are pure imaginary and for electric excitation are given by [see (II A.14), (II A.16), and (II A.24)]

$$b_{if}(\omega) = -i \frac{4\pi Z_1 e}{\hbar v} \sum_{\lambda \mu} \frac{(-1)^{I_i - M_i}}{2\lambda + 1} \begin{pmatrix} I_i & \lambda & I_f \\ -M_i & \mu & M_f \end{pmatrix} \langle I_i || \mathfrak{H}(E\lambda) || I_f \rangle a^{-\lambda} Y_{\lambda \mu} \left(\frac{\pi}{2}, 0 \right) I_{\lambda \mu}(\vartheta, \xi). \quad (\text{II D.7})$$

Thus, the last form of (6) represents a decomposition of b_{izf} into real and imaginary parts.

Inserting (7) into (6) one obtains the following expression for the amplitude to second order:

$$b_{if}^{(2)} = -i \frac{4\pi Z_1 e}{\hbar} \sum_{k \kappa} \frac{(-1)^{I_i - M_i}}{2k + 1} \begin{pmatrix} I_i & k & I_f \\ -M_i & \kappa & M_f \end{pmatrix} [\langle I_i || \mathfrak{H}(Ek) || I_f \rangle S_{Ek, \kappa} + T_{k\kappa}], \quad (\text{II D.8})$$

where

$$T_{k\kappa} = \frac{2\pi Z_1 e}{\hbar v^2} \sum_{z \lambda_1 \lambda_2} \frac{(-1)^{\lambda_1 + \lambda_2 + I_i + I_f + k + \kappa}}{a^{\lambda_1 + \lambda_2}} \frac{(2k + 1)^2}{(2\lambda_1 + 1)(2\lambda_2 + 1)} \langle I_i || \mathfrak{H}(E\lambda_1) || I_z \rangle \times \langle I_z || \mathfrak{H}(E\lambda_2) || I_f \rangle \begin{Bmatrix} \lambda_1 & \lambda_2 & k \\ I_f & I_i & I_z \end{Bmatrix} [\beta_{k, -\kappa}(\lambda_1 \lambda_2 \xi_1 \xi_2 \vartheta) - i\alpha_{k, -\kappa}(\lambda_1 \lambda_2 \xi_1 \xi_2 \vartheta)]. \quad (\text{II D.8a})$$

We have here employed the relation (II A.6) and have introduced the real functions $\alpha_{k\kappa}$ and $\beta_{k\kappa}$ through the definitions

$$\alpha_{k\kappa}(\lambda_1 \lambda_2 \xi_1 \xi_2 \vartheta) = \sum_{\mu_1 \mu_2} \begin{pmatrix} \lambda_1 & \lambda_2 & k \\ \mu_1 & \mu_2 & \kappa \end{pmatrix} Y_{\lambda_1 \mu_1} \left(\frac{\pi}{2}, 0 \right) Y_{\lambda_2 \mu_2} \left(\frac{\pi}{2}, 0 \right) I_{\lambda_1 \mu_1}(\vartheta, \xi_1) I_{\lambda_2 \mu_2}(\vartheta, \xi_2), \quad (\text{II D.9})$$

and

$$\beta_{k\kappa}(\lambda_1 \lambda_2 \xi_1 \xi_2 \vartheta) = \sum_{\mu_1 \mu_2} \begin{pmatrix} \lambda_1 & \lambda_2 & k \\ \mu_1 & \mu_2 & \kappa \end{pmatrix} Y_{\lambda_1 \mu_1} \left(\frac{\pi}{2}, 0 \right) Y_{\lambda_2 \mu_2} \left(\frac{\pi}{2}, 0 \right) \frac{1}{\pi} \mathcal{P} \int_{-\infty}^{\infty} \frac{d\xi'}{\xi'} I_{\lambda_1 \mu_1}(\vartheta, \xi_1 + \xi') I_{\lambda_2 \mu_2}(\vartheta, \xi_2 - \xi'). \quad (\text{II D.10})$$

The two indices refer to the two transitions in the double excitation; thus $\xi_1 = \omega_1 a/v$, $\xi_2 = \omega_2 a/v$, and $\xi = \xi_1 + \xi_2$.

The differential cross section to second order is obtained by inserting (8) into (II A.5 and 4) and may be written in the form

$$d\sigma = d\sigma^{(1)} + d\sigma^{(1,2)} + d\sigma^{(2)}. \quad (\text{II D.11})$$

The first term is the first-order excitation cross section (II A.28). The second term represents the interference between first-order and second-order transitions and receives a contribution only from the imaginary part of (6) (the real part of (8a)). Additional terms of the same order of magnitude as the third term in (9) (proportional to Z_1^4) may arise from cross terms between first- and third-order terms in the transition amplitude.

Performing the summation over the magnetic quantum numbers, the two last terms in (11) take the form

$$d\sigma^{(1,2)} = (-1)^{I_i+I_f} 16\pi^3 \left(\frac{Z_1 e}{\hbar v}\right)^3 a^2 \sin^{-4} \frac{\vartheta}{2} d\Omega$$

$$\times \sum_{z, \lambda, \lambda_1, \lambda_2} (-1)^{\lambda+\lambda_1+\lambda_2} \left\{ \begin{matrix} \lambda & \lambda_1 & \lambda_2 \\ I_z & I_f & I_i \end{matrix} \right\} \frac{\langle I_i || \mathfrak{M}(E\lambda) || I_f \rangle \langle I_i || \mathfrak{M}(E\lambda_1) || I_z \rangle \langle I_z || \mathfrak{M}(E\lambda_2) || I_f \rangle}{a^{\lambda+\lambda_1+\lambda_2} (2\lambda+1)(2\lambda_1+1)(2\lambda_2+1)(2I_i+1)}$$

$$\times \sum_{\mu} (-1)^{\mu} Y_{\lambda\mu} \left(\frac{\pi}{2}, 0\right) I_{\lambda\mu}(\vartheta, \xi_1 + \xi_2) \beta_{\lambda, -\mu}(\lambda_1 \lambda_2 \xi_1 \xi_2, \vartheta), \quad (\text{II D.12})$$

and

$$d\sigma^{(2)} = 16\pi^4 \left(\frac{Z_1 e}{\hbar v}\right)^4 a^2 \sin^{-4} \frac{\vartheta}{2} d\Omega$$

$$\cdot \sum_{z, z', \lambda_1 \lambda_1' \lambda_2 \lambda_2'} (-1)^{\lambda_1+\lambda_1'+\lambda_2+\lambda_2'} \frac{\langle I_i || \mathfrak{M}(E\lambda_1) || I_z \rangle \langle I_z || \mathfrak{M}(E\lambda_2) || I_f \rangle \langle I_i || \mathfrak{M}(E\lambda_1') || I_{z'} \rangle \langle I_{z'} || \mathfrak{M}(E\lambda_2') || I_f \rangle}{a^{\lambda_1+\lambda_1'+\lambda_2+\lambda_2'} (2\lambda_1+1)(2\lambda_2+1)(2\lambda_1'+1)(2\lambda_2'+1)(2I_i+1)}$$

$$\times \sum_{kk} (2k+1) \left\{ \begin{matrix} k & \lambda_1 & \lambda_2 \\ I_z & I_f & I_i \end{matrix} \right\} \left\{ \begin{matrix} k & \lambda_1' & \lambda_2' \\ I_{z'} & I_f & I_i \end{matrix} \right\} [\alpha_{kk}(\lambda_1 \lambda_2 \xi_1 \xi_2, \vartheta) \alpha_{kk}(\lambda_1' \lambda_2' \xi_1' \xi_2', \vartheta)$$

$$+ \beta_{kk}(\lambda_1 \lambda_2 \xi_1 \xi_2, \vartheta) \beta_{kk}(\lambda_1' \lambda_2' \xi_1' \xi_2', \vartheta)]. \quad (\text{II D.13})$$

Since the summations over the magnetic quantum numbers have been performed, the summation index z (or z') in (12) and (13) refers only to summation over different energy levels.

Also intermediate levels with energy well above that of the final state may give a significant contribution, since β_{kk} for large ξ_1 ($\approx -\xi_2$) behaves approximately as ξ_1^{-1} in contrast to the strong exponential dependence on ξ_1 , which is characteristic of $I_{\lambda\mu}(\xi_1)$ and thus also of α_{kk} . Even for an intermediate energy transfer ($E_z - E_i$) comparable with, or larger than, the projectile energy, the above results remain valid provided only that $E_f - E_i$ is small compared to the projectile energy. In fact, as may be seen in more detail from a quantum-mechanical treatment, the effective energy loss of the projectile in the intermediate state is that associated with those values of $\xi_1 + \xi_2'$ which contribute the main part of the integral in (10), and which are of the order $\xi/2$.

In the summation over the multipole orders in (12) and (13) the main contribution will usually arise from the lowest value of λ compatible with the spin and parity selection rules for the nuclear matrix elements.

The coefficients α_{kk} and β_{kk} needed for the evaluation of the cross sections (12) and (13) may be calculated from the classical integrals $I_{\lambda\mu}$. For $\lambda=2$ and positive ξ , these are given in Table II.12.⁷² The $I_{\lambda\mu}$ for negative arguments are obtained by means of (II E.54).

The angular distribution of the γ quanta following Coulomb excitation will also be subject to second-order corrections.⁷³ Since the second-order amplitude (8) has the same dependence on the magnetic quantum num-

bers as the first-order amplitude (7), the angular distribution to second order is obtained from (II A.80-81) by the substitution

$$\langle I_i || \mathfrak{M}(E\lambda) || I_f \rangle S_{\lambda\mu} \rightarrow \langle I_i || \mathfrak{M}(E\lambda) || I_f \rangle S_{\lambda\mu} + T_{\lambda\mu}. \quad (\text{II D.13a})$$

II D.2. Interference Effects

An interesting case where interference between the first- and the second-order terms in (2) may become significant is that in which the intermediate state z is one of the magnetic substates of the final nuclear level.⁷¹ The transition $z \rightarrow f$ then occurs through the interaction of the projectile with the quadrupole moment of the final state.

From (6) and (7) one obtains for the order of magnitude of b_{izf} [see (II C.7) and (II C.8)] in the case $\lambda=2$

$$\frac{b_{izf}}{b_{if}} \approx 5 \frac{A_1^{\frac{1}{2}}}{Z_1 Z_2^2} E_{\text{MeV}}^3 Q_f, \quad (\text{II D.14})$$

where the quadrupole moment Q_f , which is measured in units of 10^{-24} cm², is related to the reduced matrix element through [see (II A.18) and (V.32a)]

$$\left(\frac{5}{16\pi}\right)^{\frac{1}{2}} Q_e = \langle I || \mathfrak{M}(E2) || I \rangle$$

$$\times \left(\frac{I(2I-1)}{(2I+1)(I+1)(2I+3)} \right)^{\frac{1}{2}}. \quad (\text{II D.15})$$

If the initial state (ground state) also possesses a quadrupole moment ($I_i \geq 1$), a corresponding effect

⁷² For $\lambda=1, 3$, and 4 , the $I_{\lambda\mu}$ are tabulated in reference 88.

⁷³ Breit, Gluckstern, and Russell, Phys. Rev. (submitted for publication).

arises from intermediate transitions to the substates of this level.

A more detailed calculation has been made for the particular case $I_i=0$, $I_f=2$, and $\xi_1=\xi=0.4$. For the differential excitation cross section at 90° one obtains from (12)

$$d\sigma_{90^\circ} = d\sigma_{90^\circ}^{(1)} [1 + 1.55 Z_1^{-1} Z_2^{-2} A_1^{\frac{1}{2}} E_{\text{Mev}}^{\frac{3}{2}} Q_f]. \quad (\text{II D.16})$$

Effects of similar order of magnitude are expected in the angular distribution of the de-excitation γ rays.^{71,73}

It is of interest that the interference effects considered are linear in Q and thus provide a means of determining not only the magnitude, but also the sign of the quadrupole moment of the excited state. The present estimates indicate, however, that the effects become of significance only for high bombarding energies and thus especially for heavy ions.

II D.3. Double Excitations

Another important second-order effect is that of a double $E2$ excitation leading to a final state which cannot be reached directly from the ground state by an $E2$ excitation. The order of magnitude of the cross section for such a double excitation may be obtained from (6) and, provided $E_z \lesssim E_f$, is given approximately by [see (II A.2) and (II A.4)]

$$\sigma_{E2, E2} \approx \frac{1}{4} \alpha^{-2} \sigma_{E2}(I_i \rightarrow I_z) \sigma_{E2}(I_z \rightarrow I_f). \quad (\text{II D.17})$$

A direct numerical evaluation of (11) for the specific case $I_i=0$, $I_z=2$, and $I_f=4$, and for $\xi_1=\xi_2=\xi=0$ gives

$$d\sigma_{90^\circ} = d\sigma_{90^\circ}^{(1)} \left[1 + 0.17 \left(\frac{Z_1^2 A_1 B(E2, 0 \rightarrow 2) B(E2, 2 \rightarrow 4)}{E_{\text{Mev}} e^2 B(E4, 0 \rightarrow 4)} \right)^{\frac{1}{2}} + 0.4 \frac{Z_1^2 A_1 B(E2, 0 \rightarrow 2) B(E2, 2 \rightarrow 4)}{E_{\text{Mev}} e^2 B(E4, 0 \rightarrow 4)} \right]. \quad (\text{II D.20})$$

The square root of the reduced transition probabilities $B(E\lambda)$ is to be taken with the sign of the reduced matrix elements.

II D.4. Polarization Effects in Elastic Scattering

The virtual excitations also give rise to a modification of the elastic scattering cross section.⁷⁴⁻⁷⁶ Such polarization effects are especially simple to estimate if the frequencies of the virtual excitations are large compared to the inverse collision time ($\xi_1 = -\xi_2 \gg 1$). Under these conditions, one may for each position of the projectile consider the static polarization of the nucleus and derive the resulting potential which reacts on the projectile.

Expanding the interaction (II A.8) and (II A.9) in multipoles [see (II A.10)] one obtains by a perturbation

⁷⁴ P. Debye and W. Hardmeier, *Physik. Z.* **27**, 196 (1926).

⁷⁵ N. F. Ramsey, *Phys. Rev.* **83**, 659 (1951), and Malenka, Kruse, and Ramsey, reference 7.

⁷⁶ Breit, Hull, and Gluckstern, *Phys. Rev.* **87**, 74 (1952).

$$\sigma_{E2, E2} = 0.240 \left(\frac{Z_1 e}{\hbar v} \right)^4 \alpha^{-6} \times B(E2, 0 \rightarrow 2) B(E2, 2 \rightarrow 4), \quad (\text{II D.18})$$

which corresponds rather closely to (17).

On account of the large values of $B(E2)$ in collective excitations, the cross section (18) may become appreciable for large bombarding energies (see numerical estimates in Sec. V B.2). Also excitations of higher order than the second may become feasible. The corresponding cross sections can be estimated in analogy to (17).

The excitation of the $I=4$ state may also take place by a direct $E4$ transition with the cross section (II A.30). For $\xi_1=\xi_2=\xi=0$, the ratio of the two cross sections is found to be

$$\frac{\sigma_{E2, E2}}{\sigma_{E4}} = 2.1 \frac{A_1 Z_1^2 B(E2, 0 \rightarrow 2) B(E2, 2 \rightarrow 4)}{E_{\text{Mev}} e^2 B(E4, 0 \rightarrow 4)}. \quad (\text{II D.19})$$

If one would employ the single particle estimate (II A.58) for the $B(E\lambda)$ one would obtain a value of about 1/3 for the ratio (19) in the case of 20-Mev α particles. However, if the $E2$ transitions are of collective type, the ratio (19) may be several orders of magnitude larger.

The cross section for the excitation of the $I=4$ state also contains an interference term between the direct $E4$ transition and the double $E2$ transition. As an example the differential cross section at 90° has been evaluated from (12) and (13) for the case $\xi_1=0.2$, $\xi_2=0.4$, with the result

calculation

$$V_{\text{pol}}(r_p) = 4\pi Z_1^2 e^2 \sum_{\lambda=1}^{\infty} (2\lambda+1)^{-2} r_p^{-2\lambda-2} \times \sum_{z \neq i} \frac{B(E\lambda, i \rightarrow z)}{E_i - E_z} \quad (\text{II D.21})$$

for the potential energy of the projectile, arising from the nuclear polarization. In obtaining (21) we have averaged over initial orientations M_i of the target nucleus and summed over M_z ; thus, the sum over z only refers to summation over different energy levels.

A similar term in the potential energy may arise from the polarization of the projectile if this is a composite nucleus.

The effect on the elastic scattering cross section may now be obtained by inserting V_{pol} as a perturbing potential into the Schroedinger equation for the scattering process.⁷⁶ If the scattering can be treated classically ($\eta \gg 1$), the polarizing effect may also be obtained by inserting (21) into the classical equations of motion.

If the target nucleus possesses a spin, additional effects on the elastic scattering cross section may arise from the interaction of the projectile with the static electric moments of the nucleus. For aligned target nuclei this interaction gives rise to changes in the cross section linear in the nuclear moments. This linear term, however, vanishes when averaged over the orientations M_i , but there remains a second-order term which may be comparable with the effect of (21).

In most cases, it is to be expected that the principal polarization effect arises from the quadrupole interaction, on account of the high excitation frequencies associated with the main part of the dipole oscillator strength. For many nuclei the most important quadrupole excitations have rather low frequencies (see Chapter V), and it may then not be possible to consider the nucleus simply in terms of its static polarizability. In such cases $\xi_1 = -\xi_2 \lesssim 1$, and it becomes necessary to treat in more detail the coupled motion of projectile and nucleus.

II E. Appendices

II E.1. Emission of Bremsstrahlung

The emission of bremsstrahlung in the collision between the projectile and the nucleus, which constitutes an important background effect in the Coulomb excitation experiments (see Sec. III B.3), may be treated in close analogy to the nuclear excitation process. The first theoretical treatments of the bremsstrahlung process were based on a classical description of the particle orbit.⁷⁷ The quantum-mechanical theory of the electric dipole bremsstrahlung was given by Sommerfeld.⁷⁸

The cross section for scattering of the projectile into the solid angle $d\Omega$ with emission of a photon with wave number between q and $q+dq$ is given by [see (II B.2), (II B.9), and (II B.25)]

$$d\sigma = \frac{m_f^2 c}{4\pi^2 \hbar^4} \frac{v_f}{v_i} \frac{R}{\pi} \times \sum_{\lambda\mu\pi} \left| \left\langle 1_{\pi\lambda\mu} \mathbf{k}_f \left| \frac{1}{c} \int \mathbf{j}_p \cdot \mathbf{A} d\tau \right| 0 \mathbf{k}_i \right\rangle \right|^2 dq d\Omega. \quad (\text{II E.1})$$

We have here assumed the nucleus to be infinitely heavy and have neglected the spin of the projectile. The matrix element represents a transition from an initial state with no photons present to a final state with one photon of multipole order λ , μ , and parity π . Using the multipole expansion (II B.4), we obtain from (1) by means

of (II B.7)

$$d\sigma = \frac{m_f^2 c}{\pi^2 \hbar^3} \frac{v_f}{v_i} \sum_{\lambda\mu} \frac{(\lambda+1)q^{2\lambda+1}}{\lambda[(2\lambda+1)!!]^2} \times \{ |\langle \mathbf{k}_f | \mathfrak{M}_p(E\lambda, \mu) | \mathbf{k}_i \rangle|^2 + |\langle \mathbf{k}_f | \mathfrak{M}_p(M\lambda, \mu) | \mathbf{k}_i \rangle|^2 \} dq d\Omega, \quad (\text{II E.2})$$

where the multipole moments $\mathfrak{M}_p(\lambda, \mu)$ are defined by (II B.16) and (II B.17) by replacing \mathbf{j}_n by \mathbf{j}_p .

In the nonrelativistic case, the multipole moments are given by (II A.13) and (II A.39). For the electric part of the bremsstrahlung cross section, which is the most important, one thus obtains

$$d\sigma_E = \frac{1}{\pi^2} \left(\frac{m_1 c}{\hbar} \right)^2 \frac{Z_1^2 e^2}{\hbar c} \frac{v_f}{v_i} \sum_{\lambda} \frac{q^{2\lambda+1} (\lambda+1)}{\lambda[(2\lambda+1)!!]^2} \times |\langle \mathbf{k}_f | r^\lambda Y_{\lambda\mu}(\theta, \phi) | \mathbf{k}_i \rangle|^2 d\Omega dq. \quad (\text{II E.3})$$

The effect of the nuclear recoil may be taken into account by replacing m_1 with the reduced mass m_0 and the multipole moment in (3), which refers to the center of the nucleus, by the combined moment of projectile and nucleus with respect to the center of mass. The latter replacement simply corresponds to the substitution

$$Z_1 \rightarrow (A_1 + A_2)^{-\lambda} [Z_1 A_2^\lambda + (-1)^\lambda Z_2 A_1^\lambda]. \quad (\text{II E.4})$$

The reduction of the matrix element in (3) to radial matrix elements can be made in complete analogy to the case of Coulomb excitation [see (II B.45)], and the resultant cross sections can be derived directly from (II B.47) and (II B.48). For the total electric cross section for emission of a photon in the wave-number interval dq , one obtains

$$d\sigma_E = \sum_{\lambda=1}^{\infty} d\sigma_{E\lambda}, \quad (\text{II E.5})$$

with

$$d\sigma_{E\lambda} = \frac{e^2}{\hbar c} (A_1 + A_2)^{-2\lambda} [Z_1 A_2^\lambda + (-1)^\lambda Z_2 A_1^\lambda]^2 \left(\frac{c}{v_i} \right)^2 \times a^2 (qa)^{2\lambda+2} f_{E\lambda}^b(\eta_i, \xi) \frac{dq}{q}, \quad (\text{II E.6})$$

and

$$f_{E\lambda}^b(\eta_i, \xi) = \frac{16(\lambda+1)k_i k_f}{\lambda[(2\lambda-1)!!]^2 (2\lambda+1)} a^{-2\lambda-4} \times \sum_{l_i l_f} (2l_i+1)(2l_f+1) \begin{pmatrix} l_i & l_f & \lambda \\ 0 & 0 & 0 \end{pmatrix}^2 |M_{l_i l_f}^\lambda|^2. \quad (\text{II E.7})$$

In these expressions, a is the symmetrized distance of closest approach defined by (II A.86).

The radial matrix elements are defined by (II B.46) and can be expressed in terms of hypergeometric func-

⁷⁷ H. A. Kramers, *Phil. Mag.* **46**, 836 (1923); G. Wentzel, *Z. Physik* **27**, 257 (1924); see also L. Landau and E. Lifshitz, *The Classical Theory of Fields* (Addison-Wesley Press, Cambridge, 1951), pp. 197 ff.

⁷⁸ A. Sommerfeld, reference 44, pp. 495 ff.

tions, as is shown in Sec. II B.4. The bremsstrahlung matrix elements, however, are more elementary than the Coulomb excitation matrix elements, since they can all be expressed, from the monopole matrix elements (II B.56), through recursion formulas (see, e.g., II B.68).

We shall here especially consider the electric dipole bremsstrahlung, in which case the matrix elements can be directly related to the $E1$ Coulomb excitation matrix elements.⁷⁹ The connection⁴⁹ is given through the equation of motion

$$m_0 \frac{d^2 \mathbf{r}}{dt^2} = -\frac{Z_1 Z_2 e^2}{r^3} \mathbf{r}, \quad (\text{II E.8})$$

which leads to

$$\langle \mathbf{k}_f | r Y_{1\mu} | \mathbf{k}_i \rangle = -\frac{Z_1 Z_2 e^2}{m_0 \omega^2} \langle \mathbf{k}_f | r^{-2} Y_{1\mu} | \mathbf{k}_i \rangle \quad (\text{II E.9})$$

or

$$M_{l, l \pm 1}^{+1} = -\frac{Z_1 Z_2 e^2}{m_0 \omega^2} M_{l, l \pm 1}^{-2} \\ = -\frac{4\eta_i \eta_f}{(\eta_f^2 - \eta_i^2)^2} a^3 M_{l, l \pm 1}^{-2}. \quad (\text{II E.10})$$

By inserting (9) into (3) and comparing the result with the Coulomb excitation f function (II B.34), one obtains⁸⁰

$$f_{E1}^b(\eta_i, \xi) = \frac{24}{\pi^2 \xi^4} \left[\frac{\eta_i \eta_f}{(\eta_i + \eta_f)^2} \right]^2 f_{E1}(\eta_i, \xi). \quad (\text{II E.11})$$

The dipole bremsstrahlung cross section thus takes the form

$$d\sigma_{E1} = \frac{3}{2\pi^2} \frac{e^2}{\hbar c} \left(\frac{Z_1}{A_1} - \frac{Z_2}{A_2} \right)^2 \\ \times \left(\frac{\hbar}{Mc} \right)^2 \eta_i^2 f_{E1}(\eta_i, \xi) \frac{dq}{q}, \quad (\text{II E.12})$$

where M is the proton mass. Introducing numerical values for the constants involved, one obtains [see (II C.8)]

$$d\sigma_{E1} = 1.225 \cdot 10^{-8} Z_1^2 Z_2^2 \left(\frac{Z_1}{A_1} - \frac{Z_2}{A_2} \right)^2 \\ \times A_1 E_{\text{MeV}}^{-1} f_{E1}(\eta_i, \xi) \frac{dE_x}{E_x} \text{ barns} \quad (\text{II E.13})$$

where E_x is the photon energy. If one inserts for $f_{E1}(\eta_i, \xi)$ in (12) the exact expression (II E.64), one gets the bremsstrahlung formula of Sommerfeld. Numerical values for the f_{E1} function are given in Sec. II C.2.⁸¹

⁷⁹ C. J. Mullin and E. Guth, reference 4.
⁸⁰ See also L. C. Biedenharn, Phys. Rev. **102**, 262 (1956); K. Alder and A. Winther, CERN report T/KA-AW-4 (1955).

⁸¹ S. Drell and K. Huang, Phys. Rev. **99**, 686 (1955) have evaluated the Sommerfeld expression for the bremsstrahlung in a specific case by expanding in powers of ξ [see (II E.66)].

The relative intensity of consecutive multipole contributions to the bremsstrahlung is at most of the order $(qa)^2 \approx [\xi(v/c)]^2$. The magnetic multipole contributions are reduced with respect to the electric ones by a factor $(v/c)^2$. Thus, in most cases, the electric dipole bremsstrahlung strongly dominates. However, due to the factor $Z_1/A_1 - Z_2/A_2$, the $E1$ cross section may vanish for α -particle bombardment on light nuclei. In such instances, the bremsstrahlung is mainly of electric quadrupole and magnetic dipole type.

The angular distribution of the bremsstrahlung γ quanta may also be evaluated in a similar way as the angular distribution of de-excitation γ quanta in Coulomb excitation (see Sec. II A.4 and Sec. II B.5). For pure electric λ -pole bremsstrahlung, one has the following angular distribution function

$$W_{\mathbf{k}_i, \mathbf{k}_f}(\Omega_\gamma) \\ = \sum_{\sigma} \left| \sum_{\mu} \langle \mathbf{k}_f | r^\lambda Y_{\lambda\mu}(\theta, \phi) | \mathbf{k}_i \rangle D_{\mu\sigma}^\lambda(\mathcal{R}) \right|^2, \quad (\text{II E.14})$$

where the rotation matrix $D(\mathcal{R})$ represents the transition amplitude for emission of a 2^λ -pole photon in the direction Ω_γ and with polarization σ . By the usual technique of γ - γ correlation, one obtains from (14)

$$W_{\mathbf{k}_i, \mathbf{k}_f}(\Omega_\gamma) = \sum_{\mu\mu'k\kappa} \langle \mathbf{k}_f | r^2 Y_{\lambda\mu} | \mathbf{k}_i \rangle \langle \mathbf{k}_f | r^\lambda Y_{\lambda\mu'} | \mathbf{k}_i \rangle^* \\ \times \begin{pmatrix} \lambda & \lambda & k \\ 1 & -1 & 0 \end{pmatrix} \begin{pmatrix} \lambda & \lambda & k \\ -\mu & \mu' & \kappa \end{pmatrix} \\ \times (2k+1)^{1/2} Y_{k\kappa}(\Omega_\gamma). \quad (\text{II E.15})$$

For $\lambda=1$, the matrix elements are proportional to the dipole Coulomb excitation matrix elements, and in this case one has by comparing with (II A.68) and (II B.82)

$$W_{\mathbf{k}_i, \mathbf{k}_f}(\Omega_\gamma) = 1 + \sum_{\kappa} \frac{1}{2} a_{2\kappa}^{E1}(\vartheta, \varphi, \eta_i, \xi) Y_{k\kappa}(\Omega_\gamma), \quad (\text{II E.16})$$

where the a coefficients are those occurring in (II A.66). If one integrates over all proton directions, one obtains in the electric dipole case^{82, 80}

$$W(\vartheta_\gamma) = 1 + \frac{1}{2} a_2^{E1}(\eta_i, \xi) P_2(\cos \vartheta_\gamma), \quad (\text{II E.17})$$

where ϑ_γ is the direction of the γ quantum with respect to the incoming beam of projectiles. The coefficient a_2^{E1} is defined by (II B.84) and (II B.85) and is given numerically in Sec. II C.4.

II E.2. Born Approximation

Under experimental conditions where the Coulomb repulsion is sufficiently strong to prevent the projectile from entering into the nucleus, the parameter η is large (see introduction to Chapter II). Although the Born approximation cannot be applied in such cases, it

⁸² The angular distribution in the classical treatment has been considered by G. Wentzel (reference 77).

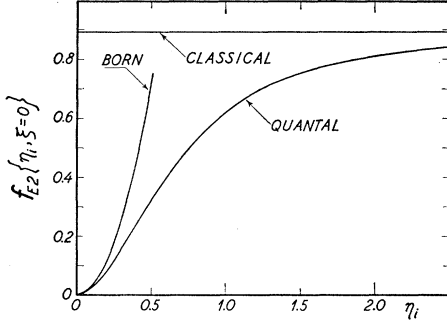


FIG. II.9. Comparison of quantal, classical, and Born approximation for $E2$ Coulomb excitation. The total f functions for $E2$ Coulomb excitation as given by the quantum-mechanical, classical, and Born approximation calculations are plotted as functions of η_i for the case of vanishing energy loss ($\xi=0$).

nevertheless provides an interesting limit of the general theory presented above. Moreover, for high energy projectiles with $\eta \ll 1$, some of the Born approximation results may find application, although under these circumstances the effects of the penetration of the projectile into the nucleus must also be taken into account.

In the Born approximation, the initial and final scattering states are considered as plane waves and the matrix element in (II B.34) thus takes the form

$$\langle \mathbf{k}_f | r^{-\lambda-1} Y_{\lambda\mu}(\theta, \phi) | \mathbf{k}_i \rangle = 4\pi i^\lambda \int_0^\infty j_\lambda(Kr) r^{-\lambda+1} dr \cdot Y_{\lambda\mu}(\mathbf{K}), \quad (\text{II E.18})$$

where we have used the expansion

$$e^{i(\mathbf{k}_i - \mathbf{k}_f) \cdot \mathbf{r}} = e^{i\mathbf{K} \cdot \mathbf{r}} = \sum_{lm} 4\pi i^l j_l(Kr) Y_{lm}(\mathbf{K}) Y_{lm}^*(\theta, \phi) \quad (\text{II E.19})$$

and denoted the difference between the wave numbers for the initial and final state by \mathbf{K} . The integration over r in (18) leads to

$$\langle \mathbf{k}_f | r^{-\lambda-1} Y_{\lambda\mu}(\theta, \phi) | \mathbf{k}_i \rangle = \frac{4\pi i^\lambda}{(2\lambda-1)!!} K^{\lambda-2} Y_{\lambda\mu}(\mathbf{K}), \quad (\text{II E.20})$$

and the differential cross section function [see (II B.34)] is thus given by^{79,83}

$$df_{E\lambda} = \frac{16\pi}{[(2\lambda+1)!!]^2} a^{2\lambda-2} k_i k_f |\mathbf{k}_i - \mathbf{k}_f|^{2\lambda-4} d\Omega. \quad (\text{II E.21})$$

The total cross section function is easily obtained by integration over the angles. Since

$$|\mathbf{k}_i - \mathbf{k}_f|^2 = k_i^2 + k_f^2 - 2k_i k_f \cos\vartheta, \quad (\text{II E.22})$$

⁸³ R. Huby and H. C. Newns, reference 4.

one finds, for $\lambda \neq 1$,

$$f_{E\lambda} = \frac{16\pi^2}{(\lambda-1)[(2\lambda+1)!!]^2} \times \{(\eta_i + \eta_f)^{2(\lambda-1)} - (\eta_f - \eta_i)^{2(\lambda-1)}\}, \quad (\text{II E.23})$$

and for $\lambda=1$

$$f_{E1} = \frac{32\pi^2}{9} \ln \frac{\eta_i + \eta_f}{\eta_f - \eta_i}. \quad (\text{II E.24})$$

These expressions are expected to coincide with the exact quantum-mechanical expressions for $\eta_i < \eta_f \ll 1$. A comparison for the case $\lambda=2$ and $\xi=0$ is shown in Fig. II.9. It is seen that the Born approximation results deviate appreciably from the exact ones already for rather small values of η .

As regards the differential cross section given by (21), it is of interest that the angular distribution is isotropic in the especially important case of $\lambda=2$.

For large values of η , the Born approximation greatly overestimates the excitation cross section. This is associated with the neglect of the Coulomb repulsion which implies that the small distances give too large a contribution. Thus, the expressions (23) and (24) also do not show the adiabatic behavior for large values of ξ . One may improve the approximation by introducing a cutoff in the radial integral (18) for small distances.⁸³ If one chooses this cutoff at the distance of closest approach, $2a$, one obtains values for the total cross section in rather good agreement with the exact theory for small values of ξ . However, the differential cross section remains essentially incorrect for $\eta > 1$.

The angular distribution of the de-excitation γ quanta can also be easily evaluated in the Born approximation. According to (II A.68) and (II B.82), one obtains by means of (20)

$$b_k^{E\lambda} = \begin{pmatrix} \lambda & \lambda & k \\ 1 & -1 & 0 \end{pmatrix}^{-1} \sum_{\mu} \begin{pmatrix} \lambda & \lambda & k \\ \mu & -\mu & 0 \end{pmatrix} (-1)^\mu \times \int |Y_{\lambda\mu}(\mathbf{K})|^2 K^{2\lambda-4} d\Omega, \quad (\text{II E.25})$$

where the integration is over all directions of \mathbf{k}_f . In the case $\xi=0$, the polar angle for \mathbf{K} is equal to $\pi/2 + \vartheta/2$, where ϑ is the deflection angle, and the integral is thus proportional to [see (22)]

$$\int_0^\pi \left| Y_{\lambda\mu} \left(\frac{\pi}{2} + \frac{\vartheta}{2}, 0 \right) \right|^2 (1 - \cos\vartheta)^{2\lambda-4} \sin\vartheta d\vartheta. \quad (\text{II E.26})$$

The sum over μ can then be evaluated explicitly with

the result⁸⁴

$$a_k^{E\lambda} = \frac{2\lambda(\lambda+1)\Gamma(2\lambda-5/2)\Gamma(2\lambda-2)}{[2\lambda(\lambda+1)-k(k+1)]\Gamma(2\lambda-k/2-5/2)\Gamma(2\lambda+k/2-2)} \quad (\text{II E.27})$$

For $\lambda=1$ one obtains

$$a_2^{E1} = 1, \quad (\text{II E.28})$$

while for $\lambda=2$

$$a_2^{E2} = \frac{1}{2} \quad \text{and} \quad a_4^{E2} = \frac{1}{16}. \quad (\text{II E.29})$$

It is also of interest to consider the radial matrix elements in the Born approximation. The radial wave

functions are in this case spherical Bessel functions and the matrix element takes the form

$$M_{iif}^{-\lambda-1} = \int_0^\infty j_{lf}(kr)r^{-\lambda+1}j_{li}(kr)dr, \quad (\text{II E.30})$$

the evaluation of which leads to⁸⁵

$$M_{iif}^{-\lambda-1} = \frac{\pi}{2^{\lambda+1}} k_i^{\lambda-2} \left(\frac{k_f}{k_i}\right)^{l_f} \frac{\Gamma\left(\frac{l_i+l_f-\lambda+2}{2}\right)}{\Gamma(l_f+\frac{3}{2})\Gamma\left(\frac{l_i-l_f+\lambda+1}{2}\right)} F\left(\frac{l_i+l_f-\lambda+2}{2}, \frac{l_f-l_i-\lambda+1}{2}, l_f+\frac{3}{2}; \frac{k_f^2}{k_i^2}\right), \quad (\text{II E.31})$$

where F is the ordinary hypergeometric function (II E.84) which, in this case, may be expressed by elementary functions. A special discussion of the radial matrix elements in the limit of large l is given in Sec. II E.7.

II E.3. Excitation by Means of Electrons

Although the present article is concerned with electromagnetic excitations produced by heavy projectiles, we shall in this paragraph briefly consider the nuclear excitations by fast electrons.⁸⁶ This process has been treated in the Born approximation⁸⁷ which is expected to be valid for light target nuclei. We shall give here an equivalent treatment which leads to cross sections in a form analogous to those derived for Coulomb excitation.

The general expressions (II B.8) and (II B.25) for the transition matrix element and the cross section are equally valid for electron excitations. In the Born approximation, the wave functions for the scattering states are plane waves

$$| \mathbf{k} \rangle = | u \rangle e^{i\mathbf{k}\cdot\mathbf{r}}, \quad (\text{II E.32})$$

where $| u \rangle$ is the spinor and \mathbf{k} the wave number of the electron. It is in this case convenient to perform the integration over the coordinate \mathbf{r} already in the expression (II B.8) and afterwards to perform the integration over the wave number q of the photon. This leads to the following result for the transition matrix element

$$\begin{aligned} \langle f | \mathcal{H}^{(1)} | i \rangle = & \frac{16\pi^2}{\lambda(2\lambda+1)!!} K^\lambda e^{i\lambda+1} \sum_{\lambda\mu} (-1)^\mu \left\{ \langle I_f M_f | \mathfrak{H}(E\lambda, -\mu, K) | I_i M_i \rangle \frac{\langle u_f | \alpha | u_i \rangle \mathbf{K}}{K^2 - \kappa^2} \cdot \frac{\mathbf{K}}{K} \times \mathbf{L}_K Y_{\lambda\mu}(\mathbf{K}) \right. \\ & - \langle I_f M_f | \mathfrak{H}(M\lambda, -\mu, K) | I_i M_i \rangle \frac{\langle u_f | \alpha | u_i \rangle}{K^2 - \kappa^2} \cdot \mathbf{L}_K Y_{\lambda\mu}(\mathbf{K}) \\ & \left. + i \langle I_f M_f | \mathfrak{H}(C\lambda, -\mu, K) | I_i M_i \rangle \lambda \frac{\langle u_f | u_i \rangle}{K^2} Y_{\lambda\mu}(\mathbf{K}) \right\}. \quad (\text{II E.33}) \end{aligned}$$

The wave numbers \mathbf{K} and κ represent the momentum and energy transfer in the collision and are given by

$$\mathbf{K} = \mathbf{k}_i - \mathbf{k}_f, \quad (\text{II E.34})$$

and

$$\kappa = \frac{\Delta E}{\hbar c}. \quad (\text{II E.35})$$

The operator \mathbf{L}_K is defined by (II A.35) and operates on \mathbf{K} . In the derivation of (33), we have used the identities

$$\begin{aligned} \int e^{i\mathbf{K}\cdot\mathbf{r}} \mathbf{L}(j_\lambda(qr)Y_{\lambda\mu}(\theta,\phi))d^3\tau \\ = 2\pi^2 i^\lambda q^{-2} \delta(q-K) \mathbf{L}_K Y_{\lambda\mu}(\mathbf{K}), \quad (\text{II E.36}) \end{aligned}$$

⁸⁴ A. Erdélyi et al., *Higher Transcendental Functions* (McGraw-Hill Book Company, Inc., New York, 1953), Vol. I, p. 171.

⁸⁵ P. 401 of reference 40.

⁸⁶ For recent experimental results obtained in high energy electron scattering, see J. H. Fregeau and R. Hofstadter, *Phys. Rev.* **99**, 1503 (1955).

⁸⁷ L. I. Schiff, *Phys. Rev.* **96**, 765 (1954), which also contains references to earlier work.

and

$$\int e^{i\mathbf{K}\cdot\mathbf{r}} \nabla \times \mathbf{L}(j_\lambda(qr)Y_{\lambda\mu}(\theta, \phi)) d^3\tau \\ = 2\pi^2 i^{\lambda-1} q^{-2} \delta(q-K) \mathbf{K} \times \mathbf{L}_K Y_{\lambda\mu}(\mathbf{K}). \quad (\text{II E.37})$$

The nuclear transition operators $\mathfrak{N}(E\lambda, \mu, K)$ and $\mathfrak{N}(M\lambda, \mu, K)$ are defined by (II B.16) and (II B.17), where κ is to be replaced by K . Whereas in the Coulomb excitation the wave number dependence of the multipole moments is usually unimportant, since $(\kappa R_0 \ll 1)$, the K dependence of the nuclear moments in (33) is essential. The last term in (33) arises from the multipole expansion of the instantaneous Coulomb interaction, and the transition operator involved is defined by

$$\mathfrak{N}(C\lambda, \mu, K) = (2\lambda+1)!! K^{-\lambda} \\ \times \int \rho_n j_\lambda(Kr) Y_{\lambda\mu}(\theta, \phi) d\tau. \quad (\text{II E.38})$$

In the limit $K \rightarrow 0$, this operator approaches the moment (II A.11).

While the multipole moments $\mathfrak{N}(E\lambda)$ and $\mathfrak{N}(M\lambda)$ vanish for $\lambda=0$, the moment (38) also gives rise to electric monopole transitions.⁴¹

The differential cross section (II B.25) is now easily obtained by performing the summation over the electron spin indices and the nuclear magnetic quantum numbers. Using the identity

$$\sum_{\mu} (\mathbf{k}_i \cdot \mathbf{K} \times \mathbf{L}_K Y_{\lambda\mu}(\mathbf{K})) (\mathbf{k}_f \cdot \mathbf{K} \times \mathbf{L}_K Y_{\lambda\mu}(\mathbf{K}))^* \\ = \frac{\lambda(\lambda+1)(2\lambda+1)}{8\pi} [K^2 \mathbf{k}_i \cdot \mathbf{k}_f - (\mathbf{k}_i \cdot \mathbf{K})(\mathbf{k}_f \cdot \mathbf{K})], \quad (\text{II E.39})$$

$$V_L(\vartheta) = \frac{4 \frac{m^2 c^2}{\hbar^2 k_i k_f} + \frac{k_i}{k_f} + \frac{k_f}{k_i} - \frac{\kappa^2}{k_i k_f} + 2 \cos \vartheta}{\left(\frac{k_i}{k_f} + \frac{k_f}{k_i} - 2 \cos \vartheta \right)^2}, \quad (\text{II E.45})$$

$$V_T(\vartheta) = \frac{\left(\frac{k_i}{k_f} \right)^2 + \left(\frac{k_f}{k_i} \right)^2 + 4 - \frac{\kappa^2}{k_i k_f} \left(\frac{k_i}{k_f} + \frac{k_f}{k_i} \right) - 2 \left(2 \frac{k_i}{k_f} + 2 \frac{k_f}{k_i} - \frac{\kappa^2}{k_i k_f} \right) \cos \vartheta + 2 \cos^2 \vartheta}{\left(\frac{k_i}{k_f} + \frac{k_f}{k_i} - 2 \cos \vartheta \right) \left[\frac{k_i}{k_f} + \frac{k_f}{k_i} - \frac{\kappa^2}{k_i k_f} - 2 \cos \vartheta \right]^2}. \quad (\text{II E.46})$$

It is noted that the angular dependence of the cross sections is contained not only in the functions V_L and V_T and in the factor $K^{2\lambda}$, but also in the nuclear transition probabilities.

II E.4. Classical Orbital Integrals

The orbital integrals $I_{\lambda\mu}(\vartheta, \xi)$ [defined by (II A.26)] are the basic functions in the classical theory of Coulomb excitation. In addition they provide an approximation, valid for η or l large compared with unity, for

and similar relations, one obtains

$$d\sigma = \sum_{\lambda=0}^{\infty} d\sigma_{E\lambda} + \sum_{\lambda=1}^{\infty} d\sigma_{M\lambda}, \quad (\text{II E.40})$$

where

$$d\sigma_{E\lambda} = \left(\frac{e}{\hbar c} \right)^2 \frac{4\pi(\lambda+1)}{\lambda[(2\lambda+1)!!]^2} \frac{K^{2\lambda}}{k_i^2} \left\{ \frac{\lambda}{\lambda+1} B(C\lambda, K) V_L(\vartheta) \right. \\ \left. + B(E\lambda, K) V_T(\vartheta) \right\} d\Omega, \quad (\text{II E.41})$$

and

$$d\sigma_{M\lambda} = \left(\frac{e}{\hbar c} \right)^2 \frac{4\pi(\lambda+1)}{\lambda[(2\lambda+1)!!]^2} \frac{K^{2\lambda}}{k_i^2} \\ \times B(M\lambda, K) V_T(\vartheta) d\Omega. \quad (\text{II E.42})$$

The reduced nuclear transition probabilities $B(\lambda, K)$ are given by (II B.23) in terms of the multipole matrix elements involved in (33). The dimensionless functions $V_L(\vartheta)$ and $V_T(\vartheta)$ are given by

$$V_L = k_i k_f \frac{2k_i^2 + 2k_f^2 + 4m^2 c^2 / \hbar^2 - \kappa^2 - K^2}{K^4}, \quad (\text{II E.43})$$

$$V_T = k_i k_f \frac{(k_i^2 + k_f^2 - \kappa^2) K^2 - 2(\mathbf{k}_i \cdot \mathbf{K})(\mathbf{k}_f \cdot \mathbf{K})}{K^2 (K^2 - \kappa^2)^2}, \quad (\text{II E.44})$$

and may also be expressed in terms of k_i , k_f , and ϑ as

the radial matrix elements in the quantum-mechanical treatment [see (II B.100) and Table II.1].

In this paragraph, we shall discuss some properties of these functions, which are given by the integral

$$I_{\lambda\mu}(\vartheta, \xi) = \int_{-\infty}^{\infty} e^{i\xi(\epsilon \sinh w + w)} \\ \times \frac{[\cosh w + \epsilon + i(\epsilon^2 - 1)^{\frac{1}{2}} \sinh w]^\mu}{(\epsilon \cosh w + 1)^{\lambda+\mu}} dw, \quad (\text{II E.47})$$

with

$$\epsilon = \frac{1}{\sin(\vartheta/2)}. \quad (\text{II E.48})$$

$$I_{\lambda\mu}(\vartheta, \xi) = e^{-(\pi/2)\xi} \int_{-\infty}^{\infty} e^{-\xi\epsilon \cosh w} e^{i\xi w} \frac{[i \sinh w + \epsilon - (\epsilon^2 - 1)^{1/2} \cosh w]^\mu}{(i\epsilon \sinh w + 1)^{\lambda+\mu}} dw. \quad (\text{II E.49})$$

Numerical values of $I_{\lambda\mu}(\vartheta, \xi)$ calculated in this way are given in Table II.12 for $\lambda=2$ and for $\lambda=1, 3$, and 4 in reference 88.

A series representation of the classical integrals can

$$I_{\lambda, -\lambda}(\vartheta, \xi) = 2^\lambda \sin^\lambda \frac{\vartheta}{2} \exp \left[-\xi \left(\frac{\vartheta}{2} - \frac{\pi}{2} + \cot \frac{\vartheta}{2} \right) \right] \left\{ \frac{|\Gamma(\lambda + i\xi)|^2}{(2\lambda - 1)!} \Psi_2(-2\lambda + 1, -\lambda + 1 - i\xi, -\lambda + 1 + i\xi; z, z^*) \right. \\ \left. + 2 \operatorname{Re} [e^{-\pi\xi} \Gamma(-\lambda - i\xi) z^{\lambda+i\xi} \Psi_2(-\lambda + 1 + i\xi, \lambda + 1 + i\xi, -\lambda + 1 + i\xi; z, z^*)] \right\}, \quad (\text{II E.50})$$

with

$$z = \frac{\xi}{2} \left(\cot \frac{\vartheta}{2} - i \right) = e^{-i(\vartheta/2)} \frac{\xi}{2 \sin \frac{\vartheta}{2}}. \quad (\text{II E.51})$$

We have here used the relation (II B.100) between the radial matrix elements and the classical integrals, and the limiting formula (II B.102). The confluent Appell function Ψ_2 is defined in (II E.105). The integral with $\mu = \lambda$ is given by (II B.59) which leads to the relation

$$I_{\lambda, \lambda}(\vartheta, \xi) = (-1)^\lambda e^{-\pi\xi} I_{\lambda, -\lambda}(-\vartheta, \xi). \quad (\text{II E.52})$$

The integrals with $|\mu| \neq \lambda$ can be obtained from the expression (II B.62) by inserting the expansion of the function F_3 in terms of F_2 functions (II E.104) and (II E.97) and then performing the confluence. In this way, one obtains, however, a nonterminating series of Ψ_2 functions (see reference 45). A more convenient form is obtained by means of the recursion formulas for the orbital integrals. These may be derived from the recursion relations for the radial matrix elements (see Sec. II B.4) by performing the limit $\eta \rightarrow \infty$. From (II B.72) one thus obtains the following relation

$$\frac{2\xi}{3} I_{20}(\vartheta, \xi) = 2 \tan^2 \frac{\vartheta}{2} \left(\frac{\partial I_{22}}{\partial \vartheta} - \frac{\partial I_{2,-2}}{\partial \vartheta} \right) + \xi (I_{22} + I_{2,-2}) \\ + \left(\tan^3 \frac{\vartheta}{2} - \tan \frac{\vartheta}{2} \right) (I_{22} - I_{2,-2}). \quad (\text{II E.53})$$

As a function of the parameter ξ the classical integrals

Values of $I_{\lambda\mu}$ may be obtained directly by a numerical integration of (47). However, due to the oscillations of the integrand, which are especially pronounced for large ξ , it is convenient to translate the path of integration by an amount of $i(\pi/2)$, whereby one obtains

be obtained by performing the limiting process $\eta \rightarrow \infty$ in the radial matrix elements. For the integrals with $\mu = -\lambda$ one gets directly from (II B.58) by a simple confluence [see (II E.105)]

possess the symmetry property

$$I_{\lambda\mu}(\vartheta, -\xi) = I_{\lambda, -\mu}(\vartheta, \xi), \quad (\text{II E.54})$$

which follows directly from (47).

For $\xi=0$, the integrals may be evaluated in terms of elementary functions (see Sec. II E.6).

In the limit of $\xi \gg 1$, the integrals decrease exponentially, reflecting the adiabatic character of the excitation process, and the resultant f functions contain the factor $e^{-2\pi\xi}$.⁸⁹ More detailed expressions appropriate to this limit have been obtained by the method of steepest descent.⁵

As a function of ϑ or ϵ the classical integrals have symmetry properties of the type (52). For $\vartheta = \pi$ (or $\epsilon = 1$), the orbital integrals are independent of μ . For $\vartheta \ll 1$ ($\epsilon \gg 1$), the $I_{\lambda\mu}$ are simply related to the integrals for straight line orbits, as is discussed in Sec. II E.7.

II E.5. Electric Dipole Excitations

For $\lambda=1$, the classical integrals can be expressed in terms of Hankel functions.^{90,5} By a partial integration, one may write (49) in the form

$$I_{1, \pm 1}(\vartheta, \xi) = -\frac{\xi e^{-(\pi/2)\xi}}{(\epsilon^2 - 1)^{1/2}} \int_{-\infty}^{\infty} e^{-\xi\epsilon \cosh w + i\xi w} \\ \times (i \sinh w + \epsilon \mp (\epsilon^2 - 1)^{1/2} \cosh w) dw, \quad (\text{II E.55})$$

which, by means of the integral representation

$$K_\nu(z) = \int_0^\infty e^{-z \cosh t + \nu t} dt \quad (\text{II E.56})$$

for the Hankel function of imaginary argument,⁹¹ can

⁸⁸ K. Alder and A. Winther, Kgl. Danske Videnskab. Selskab Mat. fys. Medd. 31, No. 1 (1956).

⁸⁹ L. Landau, reference 1.

⁹⁰ G. Wentzel, Z. Physik 27, 257 (1924).

⁹¹ See Vol. II, p. 82 of reference 84.

TABLE II.12. The classical orbital integrals for $E2$ Coulomb excitation. The table lists the values of the classical orbital integrals $I_{2\mu}(\vartheta, \xi)$. The first column gives the deflection angle ϑ in degrees. The second column gives the values of λ and μ ($\lambda=2$ for all the integrals listed). The subsequent columns give the values of $I_{2\mu}$ for the ξ value indicated; these entries are given in the form of a number followed by the power of ten by which it should be multiplied. The data are taken from reference 88.

ϑ	$\lambda \cdot \mu$	$\xi=0.0$	$\xi=0.1$	$\xi=0.2$	$\xi=0.3$	$\xi=0.4$	$\xi=0.5$
10°	2.2	5.064 (-3)	8.675 (-4)	1.895 (-4)	4.425 (-5)	1.069 (-5)	2.637 (-6)
	2.0	1.332 (-2)	6.505 (-3)	2.280 (-3)	7.311 (-4)	2.245 (-4)	6.716 (-5)
	2.-2	5.064 (-3)	1.195 (-2)	7.765 (-3)	3.637 (-3)	1.468 (-3)	5.442 (-4)
20°	2.2	2.010 (-2)	7.251 (-3)	2.957 (-3)	1.257 (-3)	5.467 (-4)	2.413 (-4)
	2.0	4.687 (-2)	3.417 (-2)	2.040 (-2)	1.137 (-2)	6.111 (-3)	3.211 (-3)
	2.-2	2.010 (-2)	4.063 (-2)	4.092 (-2)	3.206 (-2)	2.217 (-2)	1.423 (-2)
30°	2.2	4.466 (-2)	2.117 (-2)	1.080 (-2)	5.658 (-3)	3.013 (-3)	1.621 (-3)
	2.0	9.323 (-2)	7.628 (-2)	5.381 (-2)	3.582 (-2)	2.309 (-2)	1.457 (-2)
	2.-2	4.466 (-2)	7.763 (-2)	8.538 (-2)	7.699 (-2)	6.242 (-2)	4.737 (-2)
40°	2.2	7.799 (-2)	4.290 (-2)	2.466 (-2)	1.443 (-2)	8.538 (-3)	5.089 (-3)
	2.0	1.471 (-1)	1.268 (-1)	9.683 (-2)	7.022 (-2)	4.942 (-2)	3.410 (-2)
	2.-2	7.799 (-2)	1.217 (-1)	1.359 (-1)	1.291 (-1)	1.119 (-1)	9.142 (-2)
50°	2.2	1.191 (-1)	7.214 (-2)	4.482 (-2)	2.815 (-2)	1.779 (-2)	1.130 (-2)
	2.0	2.048 (-1)	1.817 (-1)	1.451 (-1)	1.106 (-1)	8.192 (-2)	5.955 (-2)
	2.-2	1.191 (-1)	1.716 (-1)	1.904 (-1)	1.843 (-1)	1.647 (-1)	1.397 (-1)
60°	2.2	1.667 (-1)	1.083 (-1)	7.117 (-2)	4.700 (-2)	3.113 (-2)	2.067 (-2)
	2.0	2.636 (-1)	2.380 (-1)	1.957 (-1)	1.539 (-1)	1.178 (-1)	8.858 (-2)
	2.-2	1.667 (-1)	2.258 (-1)	2.468 (-1)	2.401 (-1)	2.176 (-1)	1.881 (-1)
70°	2.2	2.193 (-1)	1.505 (-1)	1.033 (-1)	7.093 (-2)	4.870 (-2)	3.344 (-2)
	2.0	3.215 (-1)	2.938 (-1)	2.463 (-1)	1.980 (-1)	1.551 (-1)	1.193 (-1)
	2.-2	2.193 (-1)	2.826 (-1)	3.035 (-1)	2.944 (-1)	2.682 (-1)	2.340 (-1)
80°	2.2	2.755 (-1)	1.977 (-1)	1.406 (-1)	9.966 (-2)	7.043 (-2)	4.969 (-2)
	2.0	3.770 (-1)	3.475 (-1)	2.955 (-1)	2.413 (-1)	1.920 (-1)	1.502 (-1)
	2.-2	2.755 (-1)	3.402 (-1)	3.586 (-1)	3.456 (-1)	3.147 (-1)	2.755 (-1)
90°	2.2	3.333 (-1)	2.485 (-1)	1.823 (-1)	1.327 (-1)	9.609 (-2)	6.934 (-2)
	2.0	4.292 (-1)	3.980 (-1)	3.420 (-1)	2.825 (-1)	2.275 (-1)	1.801 (-1)
	2.-2	3.333 (-1)	3.968 (-1)	4.106 (-1)	3.922 (-1)	3.558 (-1)	3.114 (-1)
100°	2.2	3.912 (-1)	3.016 (-1)	2.274 (-1)	1.694 (-1)	1.253 (-1)	9.219 (-2)
	2.0	4.772 (-1)	4.446 (-1)	3.850 (-1)	3.208 (-1)	2.608 (-1)	2.083 (-1)
	2.-2	3.912 (-1)	4.507 (-1)	4.580 (-1)	4.329 (-1)	3.904 (-1)	3.406 (-1)
110°	2.2	4.473 (-1)	3.555 (-1)	2.746 (-1)	2.089 (-1)	1.575 (-1)	1.179 (-1)
	2.0	5.205 (-1)	4.866 (-1)	4.239 (-1)	3.556 (-1)	2.911 (-1)	2.342 (-1)
	2.-2	4.473 (-1)	5.002 (-1)	4.992 (-1)	4.665 (-1)	4.176 (-1)	3.627 (-1)
120°	2.2	5.000 (-1)	4.086 (-1)	3.227 (-1)	2.504 (-1)	1.920 (-1)	1.460 (-1)
	2.0	5.586 (-1)	5.236 (-1)	4.583 (-1)	3.864 (-1)	3.180 (-1)	2.572 (-1)
	2.-2	5.000 (-1)	5.439 (-1)	5.333 (-1)	4.925 (-1)	4.372 (-1)	3.773 (-1)
130°	2.2	5.476 (-1)	4.594 (-1)	3.705 (-1)	2.926 (-1)	2.279 (-1)	1.758 (-1)
	2.0	5.913 (-1)	5.554 (-1)	4.878 (-1)	4.130 (-1)	3.412 (-1)	2.771 (-1)
	2.-2	5.476 (-1)	5.805 (-1)	5.593 (-1)	5.101 (-1)	4.487 (-1)	3.845 (-1)
140°	2.2	5.887 (-1)	5.063 (-1)	4.165 (-1)	3.345 (-1)	2.645 (-1)	2.067 (-1)
	2.0	6.182 (-1)	5.817 (-1)	5.122 (-1)	4.349 (-1)	3.605 (-1)	2.937 (-1)
	2.-2	5.887 (-1)	6.088 (-1)	5.766 (-1)	5.192 (-1)	4.522 (-1)	3.845 (-1)
150°	2.2	6.220 (-1)	5.479 (-1)	4.593 (-1)	3.748 (-1)	3.005 (-1)	2.379 (-1)
	2.0	6.393 (-1)	6.022 (-1)	5.314 (-1)	4.522 (-1)	3.756 (-1)	3.067 (-1)
	2.-2	6.220 (-1)	6.282 (-1)	5.849 (-1)	5.199 (-1)	4.480 (-1)	3.777 (-1)
160°	2.2	6.466 (-1)	5.828 (-1)	4.976 (-1)	4.124 (-1)	3.351 (-1)	2.684 (-1)
	2.0	6.545 (-1)	6.170 (-1)	5.451 (-1)	4.646 (-1)	3.865 (-1)	3.161 (-1)
	2.-2	6.466 (-1)	6.381 (-1)	5.840 (-1)	5.122 (-1)	4.367 (-1)	3.647 (-1)
170°	2.2	6.616 (-1)	6.101 (-1)	5.303 (-1)	4.460 (-1)	3.670 (-1)	2.973 (-1)
	2.0	6.636 (-1)	6.258 (-1)	5.534 (-1)	4.720 (-1)	3.931 (-1)	3.218 (-1)
	2.-2	6.616 (-1)	6.383 (-1)	5.743 (-1)	4.969 (-1)	4.188 (-1)	3.465 (-1)
180°	2.2	6.667 (-1)	6.288 (-1)	5.561 (-1)	4.745 (-1)	3.953 (-1)	3.237 (-1)
	2.0	6.667 (-1)	6.288 (-1)	5.561 (-1)	4.745 (-1)	3.953 (-1)	3.237 (-1)
	2.-2	6.667 (-1)	6.288 (-1)	5.561 (-1)	4.745 (-1)	3.953 (-1)	3.237 (-1)

TABLE II.12.—Continued.

ϑ	$\lambda \cdot \mu$	$\xi=0.6$	$\xi=0.7$	$\xi=0.8$	$\xi=0.9$	$\xi=1.0$	$\xi=1.2$
10°	2.2	6.598 (-7)	1.668 (-7)	4.250 (-8)	1.090 (-8)	2.807 (-9)	1.886 (-10)
	2.0	1.975 (-5)	5.739 (-6)	1.652 (-6)	4.724 (-7)	1.343 (-7)	1.071 (-8)
	2.-2	1.908 (-4)	6.438 (-5)	2.110 (-5)	6.765 (-6)	2.131 (-6)	2.031 (-7)
20°	2.2	1.077 (-4)	4.841 (-5)	2.190 (-5)	9.959 (-6)	4.546 (-6)	9.567 (-7)
	2.0	1.661 (-3)	8.496 (-4)	4.309 (-4)	2.171 (-4)	1.088 (-4)	2.696 (-5)
	2.-2	8.685 (-3)	5.117 (-3)	2.936 (-3)	1.650 (-3)	9.119 (-4)	2.681 (-4)
30°	2.2	8.795 (-4)	4.799 (-4)	2.631 (-4)	1.448 (-4)	7.997 (-5)	2.457 (-5)
	2.0	9.064 (-3)	5.578 (-3)	3.404 (-3)	2.064 (-3)	1.245 (-3)	4.473 (-4)
	2.-2	3.438 (-2)	2.415 (-2)	1.655 (-2)	1.113 (-2)	7.368 (-3)	3.114 (-3)
40°	2.2	3.050 (-3)	1.836 (-3)	1.109 (-3)	6.717 (-4)	4.079 (-4)	1.514 (-4)
	2.0	2.321 (-2)	1.563 (-2)	1.044 (-2)	6.932 (-3)	4.577 (-3)	1.971 (-3)
	2.-2	7.174 (-2)	5.464 (-2)	4.068 (-2)	2.975 (-2)	2.144 (-2)	1.076 (-2)
50°	2.2	7.203 (-3)	4.604 (-3)	2.953 (-3)	1.894 (-3)	1.219 (-3)	5.063 (-4)
	2.0	4.270 (-2)	3.031 (-2)	2.134 (-2)	1.493 (-2)	1.039 (-2)	4.972 (-3)
	2.-2	1.142 (-1)	9.080 (-2)	7.069 (-2)	5.412 (-2)	4.088 (-2)	2.257 (-2)
60°	2.2	1.375 (-2)	9.164 (-3)	6.114 (-3)	4.084 (-3)	2.731 (-3)	1.224 (-3)
	2.0	6.570 (-2)	4.824 (-2)	3.514 (-2)	2.543 (-2)	1.831 (-2)	9.368 (-3)
	2.-2	1.572 (-1)	1.281 (-1)	1.024 (-1)	8.054 (-2)	6.254 (-2)	3.658 (-2)
70°	2.2	2.298 (-2)	1.579 (-2)	1.085 (-2)	7.464 (-3)	5.134 (-3)	2.432 (-3)
	2.0	9.053 (-2)	6.803 (-2)	5.072 (-2)	3.757 (-2)	2.768 (-2)	1.483 (-2)
	2.-2	1.980 (-1)	1.636 (-1)	1.328 (-1)	1.061 (-1)	8.384 (-2)	5.083 (-2)
80°	2.2	3.502 (-2)	2.466 (-2)	1.735 (-2)	1.221 (-2)	8.583 (-3)	4.242 (-3)
	2.0	1.159 (-1)	8.853 (-2)	6.710 (-2)	5.053 (-2)	3.785 (-2)	2.096 (-2)
	2.-2	2.345 (-1)	1.952 (-1)	1.598 (-1)	1.290 (-1)	1.030 (-1)	6.383 (-2)
90°	2.2	4.991 (-2)	3.586 (-2)	2.572 (-2)	1.843 (-2)	1.319 (-2)	6.748 (-3)
	2.0	1.407 (-1)	1.088 (-1)	8.350 (-2)	6.364 (-2)	4.825 (-2)	2.737 (-2)
	2.-2	2.654 (-1)	2.217 (-1)	1.823 (-1)	1.480 (-1)	1.188 (-1)	7.464 (-2)
100°	2.2	6.757 (-2)	4.938 (-2)	3.601 (-2)	2.621 (-2)	1.905 (-2)	1.002 (-2)
	2.0	1.643 (-1)	1.282 (-1)	9.928 (-2)	7.637 (-2)	5.842 (-2)	3.373 (-2)
	2.-2	2.901 (-1)	2.424 (-1)	1.996 (-1)	1.623 (-1)	1.307 (-1)	8.270 (-2)
110°	2.2	8.781 (-2)	6.515 (-2)	4.818 (-2)	3.555 (-2)	2.617 (-2)	1.411 (-2)
	2.0	1.859 (-1)	1.462 (-1)	1.140 (-1)	8.827 (-2)	6.799 (-2)	3.979 (-2)
	2.-2	3.079 (-1)	2.569 (-1)	2.114 (-1)	1.719 (-1)	1.385 (-1)	8.786 (-2)
120°	2.2	1.103 (-1)	8.294 (-2)	6.213 (-2)	4.639 (-2)	3.454 (-2)	1.903 (-2)
	2.0	2.054 (-1)	1.623 (-1)	1.272 (-1)	9.905 (-2)	7.669 (-2)	4.534 (-2)
	2.-2	3.189 (-1)	2.652 (-1)	2.176 (-1)	1.767 (-1)	1.422 (-1)	9.014 (-2)
130°	2.2	1.346 (-1)	1.025 (-1)	7.765 (-2)	5.861 (-2)	4.410 (-2)	2.477 (-2)
	2.0	2.222 (-1)	1.763 (-1)	1.388 (-1)	1.085 (-1)	8.431 (-2)	5.024 (-2)
	2.-2	3.232 (-1)	2.675 (-1)	2.188 (-1)	1.771 (-1)	1.422 (-1)	8.980 (-2)
140°	2.2	1.602 (-1)	1.234 (-1)	9.447 (-2)	7.202 (-2)	5.470 (-2)	3.126 (-2)
	2.0	2.362 (-1)	1.880 (-1)	1.484 (-1)	1.164 (-1)	9.071 (-2)	5.437 (-2)
	2.-2	3.210 (-1)	2.643 (-1)	2.151 (-1)	1.735 (-1)	1.388 (-1)	8.717 (-2)
150°	2.2	1.865 (-1)	1.451 (-1)	1.122 (-1)	8.632 (-2)	6.613 (-2)	3.840 (-2)
	2.0	2.472 (-1)	1.972 (-1)	1.560 (-1)	1.226 (-1)	9.578 (-2)	5.765 (-2)
	2.-2	3.131 (-1)	2.561 (-1)	2.074 (-1)	1.664 (-1)	1.326 (-1)	8.264 (-2)
160°	2.2	2.127 (-1)	1.671 (-1)	1.304 (-1)	1.012 (-1)	7.813 (-2)	4.605 (-2)
	2.0	2.552 (-1)	2.039 (-1)	1.615 (-1)	1.271 (-1)	9.945 (-2)	6.002 (-2)
	2.-2	3.000 (-1)	2.437 (-1)	1.961 (-1)	1.565 (-1)	1.240 (-1)	7.665 (-2)
170°	2.2	2.380 (-1)	1.887 (-1)	1.485 (-1)	1.162 (-1)	9.036 (-2)	5.398 (-2)
	2.0	2.600 (-1)	2.079 (-1)	1.649 (-1)	1.298 (-1)	1.017 (-1)	6.146 (-2)
	2.-2	2.825 (-1)	2.278 (-1)	1.821 (-1)	1.444 (-1)	1.138 (-1)	6.962 (-2)
180°	2.2	2.616 (-1)	2.092 (-1)	1.660 (-1)	1.308 (-1)	1.024 (-1)	6.194 (-2)
	2.0	2.616 (-1)	2.092 (-1)	1.660 (-1)	1.308 (-1)	1.024 (-1)	6.194 (-2)
	2.-2	2.616 (-1)	2.092 (-1)	1.660 (-1)	1.308 (-1)	1.024 (-1)	6.194 (-2)

TABLE II.12.—Continued.

ϑ	$\lambda \cdot \mu$	$\xi=1.4$	$\xi=1.6$	$\xi=1.8$	$\xi=2.0$	$\xi=4.0$
10°	2.2	1.282 (-11)	8.788 (-13)	6.068 (-14)	4.213 (-15)	1.294 (-26)
	2.0	8.426 (-10)	6.566 (-11)	5.078 (-12)	3.904 (-13)	2.362 (-24)
	2.-2	1.858 (-8)	1.651 (-9)	1.433 (-10)	1.222 (-11)	1.464 (-22)
20°	2.2	2.034 (-7)	4.355 (-8)	9.385 (-9)	2.032 (-9)	5.342 (-16)
	2.0	6.595 (-6)	1.598 (-6)	3.844 (-7)	9.193 (-8)	4.709 (-14)
	2.-2	7.587 (-5)	2.086 (-5)	5.612 (-6)	1.484 (-6)	1.479 (-12)
30°	2.2	7.613 (-6)	2.374 (-6)	7.440 (-7)	2.342 (-7)	2.546 (-12)
	2.0	1.587 (-4)	5.574 (-5)	1.944 (-5)	6.737 (-6)	1.411 (-10)
	2.-2	1.269 (-3)	5.031 (-4)	1.953 (-4)	7.455 (-5)	2.972 (-9)
40°	2.2	5.652 (-5)	2.122 (-5)	7.996 (-6)	3.024 (-6)	2.025 (-10)
	2.0	8.377 (-4)	3.527 (-4)	1.473 (-4)	6.119 (-5)	7.780 (-9)
	2.-2	5.215 (-3)	2.463 (-3)	1.140 (-3)	5.189 (-4)	1.225 (-7)
50°	2.2	2.113 (-4)	8.856 (-5)	3.723 (-5)	1.569 (-5)	3.034 (-9)
	2.0	2.348 (-3)	1.098 (-3)	5.093 (-4)	2.349 (-4)	8.468 (-8)
	2.-2	1.206 (-2)	6.284 (-3)	3.212 (-3)	1.616 (-3)	1.052 (-6)
60°	2.2	5.505 (-4)	2.481 (-4)	1.121 (-4)	5.071 (-5)	1.947 (-8)
	2.0	4.732 (-3)	2.366 (-3)	1.174 (-3)	5.787 (-4)	4.049 (-7)
	2.-2	2.073 (-2)	1.148 (-2)	6.235 (-3)	3.337 (-3)	4.089 (-6)
70°	2.2	1.154 (-3)	5.478 (-4)	2.604 (-4)	1.239 (-4)	7.655 (-8)
	2.0	7.842 (-3)	4.105 (-3)	2.131 (-3)	1.099 (-3)	1.203 (-6)
	2.-2	2.991 (-2)	1.720 (-2)	9.721 (-3)	5.415 (-3)	1.004 (-5)
80°	2.2	2.096 (-3)	1.035 (-3)	5.112 (-4)	2.525 (-4)	2.209 (-7)
	2.0	1.145 (-2)	6.189 (-3)	3.319 (-3)	1.768 (-3)	2.647 (-6)
	2.-2	3.847 (-2)	2.269 (-2)	1.315 (-2)	7.521 (-3)	1.842 (-5)
90°	2.2	3.443 (-3)	1.755 (-3)	8.932 (-4)	4.543 (-4)	5.177 (-7)
	2.0	1.531 (-2)	8.473 (-3)	4.651 (-3)	2.535 (-3)	4.757 (-6)
	2.-2	4.565 (-2)	2.735 (-2)	1.612 (-2)	9.379 (-3)	2.772 (-5)
100°	2.2	5.254 (-3)	2.746 (-3)	1.433 (-3)	7.462 (-4)	1.048 (-6)
	2.0	1.920 (-2)	1.082 (-2)	6.041 (-3)	3.350 (-3)	7.413 (-6)
	2.-2	5.102 (-2)	3.086 (-2)	1.838 (-2)	1.081 (-2)	3.617 (-5)
110°	2.2	7.569 (-3)	4.044 (-3)	2.153 (-3)	1.144 (-3)	1.904 (-6)
	2.0	2.296 (-2)	1.310 (-2)	7.412 (-3)	4.163 (-3)	1.040 (-5)
	2.-2	5.440 (-2)	3.307 (-2)	1.981 (-2)	1.172 (-2)	4.243 (-5)
120°	2.2	1.042 (-2)	5.670 (-3)	3.074 (-3)	1.661 (-3)	3.188 (-6)
	2.0	2.643 (-2)	1.523 (-2)	8.700 (-3)	4.933 (-3)	1.349 (-5)
	2.-2	5.585 (-2)	3.400 (-2)	2.041 (-2)	1.211 (-2)	4.582 (-5)
130°	2.2	1.380 (-2)	7.637 (-3)	4.206 (-3)	2.306 (-3)	5.000 (-6)
	2.0	2.950 (-2)	1.713 (-2)	9.856 (-3)	5.628 (-3)	1.645 (-5)
	2.-2	5.551 (-2)	3.375 (-2)	2.025 (-2)	1.202 (-2)	4.629 (-5)
140°	2.2	1.770 (-2)	9.942 (-3)	5.552 (-3)	3.085 (-3)	7.437 (-6)
	2.0	3.211 (-2)	1.874 (-2)	1.084 (-2)	6.224 (-3)	1.909 (-5)
	2.-2	5.365 (-2)	3.251 (-2)	1.945 (-2)	1.152 (-2)	4.426 (-5)
150°	2.2	2.206 (-2)	1.256 (-2)	7.104 (-3)	3.994 (-3)	1.057 (-5)
	2.0	3.418 (-2)	2.003 (-2)	1.163 (-2)	6.703 (-3)	2.126 (-5)
	2.-2	5.056 (-2)	3.048 (-2)	1.816 (-2)	1.071 (-2)	4.036 (-5)
160°	2.2	2.680 (-2)	1.545 (-2)	8.838 (-3)	5.023 (-3)	1.444 (-5)
	2.0	3.569 (-2)	2.097 (-2)	1.221 (-2)	7.053 (-3)	2.288 (-5)
	2.-2	4.654 (-2)	2.787 (-2)	1.651 (-2)	9.689 (-3)	3.532 (-5)
170°	2.2	3.181 (-2)	1.854 (-2)	1.072 (-2)	6.149 (-3)	1.903 (-5)
	2.0	3.660 (-2)	2.154 (-2)	1.256 (-2)	7.265 (-3)	2.388 (-5)
	2.-2	4.190 (-2)	2.489 (-2)	1.464 (-2)	8.538 (-3)	2.976 (-5)
180°	2.2	3.691 (-2)	2.173 (-2)	1.268 (-2)	7.337 (-3)	2.421 (-5)
	2.0	3.691 (-2)	2.173 (-2)	1.268 (-2)	7.337 (-3)	2.421 (-5)
	2.-2	3.691 (-2)	2.173 (-2)	1.268 (-2)	7.337 (-3)	2.421 (-5)

be expressed by

$$I_{1,\pm 1}(\vartheta, \xi) = -2\xi e^{-(\pi/2)\xi} \times \left[K_{i\xi}'(\xi\epsilon) \pm \frac{(\epsilon^2-1)^{1/2}}{\epsilon} K_{i\xi}(\xi\epsilon) \right]. \quad (\text{II E.57})$$

The K' represents the derivative of the function (56) with respect to the argument.

The integral over the square of $I_{1,\pm 1}$, which is needed for the total cross-section function [see (II A.31)], can also be expressed in terms of Hankel functions by means of the Lommel integral formulas.⁹² This leads to

$$f_{E1}(\xi) = -\frac{32\pi^2}{9} \cdot e^{-\pi\xi} \xi K_{i\xi}(\xi) K_{i\xi}'(\xi). \quad (\text{II E.58})$$

In the limit of $\xi \rightarrow 0$, this expression diverges with the following asymptotic behavior

$$f_{E1}(\xi) = \frac{32\pi^2}{9} \ln \frac{2}{\gamma\xi} (1 - \pi\xi + \dots). \quad (\text{II E.59})$$

The number γ is given by

$$\gamma = e^C = 1.781 \dots, \quad (\text{II E.60})$$

where C is the Euler constant.

In the limit $\xi \gg 1$, one obtains from (58) the following asymptotic formula

$$f_{E1}(\xi) = \frac{32\pi^3}{9\sqrt{3}} e^{-2\pi\xi} (1 + 0.218\xi^{-3} + \dots). \quad (\text{II E.61})$$

Also the quantum-mechanical formulas for the electric dipole excitation cross sections can be expressed in an especially simple form. The matrix element between the scattering states in (II B.34) is equivalent to that involved in the bremsstrahlung cross section (see Sec. II E.1) and may be evaluated by expressing the Coulomb wave functions in parabolic coordinates.⁷⁸

The resulting expression for the differential f function may be written^{79, 83, 5}

$$df_{E1}(\vartheta, \eta_i, \xi) = \frac{32\pi^3 \eta_i \eta_f}{9\xi^2} \frac{e^{2\pi\eta_i}}{(e^{2\pi\eta_i} - 1)(e^{2\pi\eta_f} - 1)} \times \frac{d}{dx} \left\{ -x \frac{d}{dx} |F(-i\eta_i, -i\eta_f, 1; x)|^2 \right\} d\Omega, \quad (\text{II E.62})$$

where F is the hypergeometric function (II E.84) of the variable

$$x = -\frac{4\eta_i \eta_f}{\xi^2} \sin^2 \frac{\vartheta}{2}. \quad (\text{II E.63})$$

For the total f function (II B.39) one obtains^{79, 83, 5}

$$f_{E1}(\eta_i, \xi) = -\frac{32\pi^4}{9} \frac{e^{2\pi\eta_i}}{(e^{2\pi\eta_i} - 1)(e^{2\pi\eta_f} - 1)} (-x_0) \times \frac{d}{dx_0} |F(-i\eta_i, -i\eta_f, 1; x_0)|^2, \quad (\text{II E.64})$$

with

$$x_0 = -\frac{4\eta_i \eta_f}{\xi^2}. \quad (\text{II E.65})$$

Since the variable x_0 is always larger than unity, it is necessary for the numerical evaluation of (64) to use the analytic continuation (II E.87) of the hypergeometric function. After differentiation one obtains in this manner

$$f_{E1}(\eta_i, \xi) = -\frac{32\pi^3}{9} \frac{\eta_i \eta_f}{\xi} \frac{1}{e^{2\pi\xi} - 1} \times \vartheta m \left\{ \frac{1}{\eta_i} F\left(i\eta_i, i\eta_i, 1 - i\xi; \frac{1}{x_0}\right) \times \left[F\left(1 - i\eta_i, -i\eta_i, 1 + i\xi; \frac{1}{x_0}\right) + e^{i\varphi} F\left(1 - i\eta_f, -i\eta_f, 1 - i\xi; \frac{1}{x_0}\right) \right] + \eta_i \rightleftharpoons \eta_f \right\}, \quad (\text{II E.66})$$

where $\eta_i \rightleftharpoons \eta_f$ implies the addition of terms with η_i and η_f interchanged, and where

$$\varphi = 2 \arg \{ \Gamma(i\xi) \Gamma(i\eta_i) / \Gamma(i\eta_f) \} + \xi \ln |x_0|. \quad (\text{II E.66a})$$

In the limit of $\xi \ll 1$, the expression (66) reduces to

$$f_{E1}(\eta_i, \xi) = \frac{32\pi^2}{9} \left(\ln \frac{2\eta}{\xi} + \psi(1) - \text{Re} \{ \psi(i\eta) \} \right), \quad (\text{II E.66b})$$

where ψ is the logarithmic derivative of the Γ function.

The classical limit ($\eta_i \rightarrow \infty$) of $f_{E1}(\eta_i, \xi)$ may be obtained by performing a confluence in the hypergeometric functions in (64). This leads to the expression (58).

The $E1$ Coulomb excitation process is closely related to the problem of the excitation and ionization of atoms by fast charged particles. The atomic stopping power may thus be written in the form

$$\frac{1}{N} \frac{dE}{dx} = \sum_f \sigma_{E1}(i \rightarrow f) (E_f - E_i), \quad (\text{II E.67})$$

where N is the number of atoms per unit volume and dE/dx the energy loss of the particle per unit path length.

⁹² See p. 133 ff of reference 40.

In order to compare (67) with the usual form for the stopping power, it is convenient to introduce the atomic oscillator strength for the transition $i \rightarrow f$ defined by

$$s_{if} = \frac{8\pi}{9} \frac{m}{e^2 \hbar^2} B(E1; i \rightarrow f)(E_f - E_i), \quad (\text{II E.67a})$$

where m is the electronic mass and where s_{if} is normalized in such a manner that the total oscillator strength equals the number of electrons in the atom. The expression (67) may then be written in the form [see (II B.37)]

$$\frac{1}{N} \frac{dE}{dx} = 4\pi \frac{Z_1^2 e^4}{m v_i^2} \sum_f s_{if} \frac{9}{32\pi^2} f_{E1}(\eta_i, \xi_{if}), \quad (\text{II E.67b})$$

where η and ξ refer to the collision between the incident particle and an atomic electron; the influence of the nuclear field on the motion of the particle is of minor importance. In the case of collisions with fast particles, the values of ξ_{if} for the important transitions are small compared to unity, so that we may use the asymptotic form of f_{E1} for $\xi \ll 1$.

When the collision can be treated by classical mechanics ($\eta \gg 1$), it is thus seen from (59) that (67b) gives the classical stopping formula.^{98a} In the opposite limit of $\eta \ll 1$, where (24) applies, one obtains the stopping formula derived in Born approximation.^{98b} The more general quantum-mechanical expression for the stopping power,^{98c} valid for all η , is obtained from (67b) by inserting (66b).

II E.6. Limit of $\xi = 0$

In the limiting case of $\xi = 0$, several expressions from the general theory of Coulomb excitation reduce appreciably. In the classical theory, the exponential factor in the orbital integrals (47) disappears and the resulting integrals can be performed explicitly in terms of elementary functions.⁵ Thus, one obtains

$$\begin{aligned} I_{\lambda\mu}(\vartheta, 0) &= (\epsilon^2 - 1)^{-\lambda + \frac{1}{2}} \int_{-\phi_0}^{\phi_0} e^{i\mu\phi} (\epsilon \cos\phi - 1)^{\lambda-1} d\phi \\ &= (2\pi)^{\frac{1}{2}} (\lambda - 1)! \epsilon^{-\frac{1}{2}} (\epsilon^2 - 1)^{-(\lambda/2) + 1/4} \\ &\quad \times P_{\mu - \frac{1}{2}}^{-\lambda + \frac{1}{2}} \left(\frac{1}{\epsilon} \right). \quad (\text{II E.68}) \end{aligned}$$

We have here introduced the azimuthal angle ϕ of the projectile given by [see (II A.22)]

$$\tan\phi = \frac{(\epsilon^2 - 1)^{\frac{1}{2}} \sinh w}{\epsilon + \cosh w}, \quad (\text{II E.69})$$

and the limits ϕ_0 are

$$\phi_0 = \tan^{-1}(\epsilon^2 - 1)^{\frac{1}{2}} = \frac{\pi}{2} - \frac{\vartheta}{2}. \quad (\text{II E.70})$$

In the last expression in (68) the integral has been expressed in terms of Legendre functions of half-integer order.⁹⁴

For the lowest multipole orders, one obtains the following explicit expressions

$$\begin{aligned} I_{1,\pm 1}(\vartheta, 0) &= 2 \frac{\vartheta}{2}, \\ I_{2,\pm 2}(\vartheta, 0) &= \frac{2}{3} \frac{\vartheta}{2} \sin^2 \frac{\vartheta}{2}, \\ I_{20}(\vartheta, 0) &= 2 \tan^2 \frac{\vartheta}{2} \left[1 - \frac{\pi - \vartheta}{2} \tan \frac{\vartheta}{2} \right], \\ I_{3,\pm 3}(\vartheta, 0) &= \frac{4}{15} \frac{\vartheta}{2} \sin^3 \frac{\vartheta}{2}, \\ I_{3,\pm 1}(\vartheta, 0) &= 2 \frac{\sin^3 \frac{\vartheta}{2}}{\cos^4 \frac{\vartheta}{2}} \left[\frac{2 + \sin^2 \frac{\vartheta}{2}}{3} - \frac{\pi - \vartheta}{2} \tan \frac{\vartheta}{2} \right], \quad (\text{II E.71}) \\ I_{4,\pm 4}(\vartheta, 0) &= \frac{4}{35} \frac{\vartheta}{2} \sin^4 \frac{\vartheta}{2}, \\ I_{4,\pm 2}(\vartheta, 0) &= 2 \frac{\sin^4 \frac{\vartheta}{2}}{\cos^6 \frac{\vartheta}{2}} \left[\frac{8 + 9 \sin^2 \frac{\vartheta}{2} - 2 \sin^4 \frac{\vartheta}{2}}{20} - \frac{3\pi - \vartheta}{4} \tan \frac{\vartheta}{2} \right], \\ I_{40}(\vartheta, 0) &= 2 \tan^6 \frac{\vartheta}{2} \left[\frac{2}{3 \sin^2 \frac{\vartheta}{2}} + \frac{11}{6} - \frac{\pi - \vartheta}{2} - \frac{3 + 5 \tan^2 \frac{\vartheta}{2}}{2} \right]. \end{aligned}$$

The differential f functions are given directly in terms of these integrals by means of (II A.29) and (II A.51) and the results are illustrated in Fig. II.7.

The total f function is obtained from df by an integration over the deflection angle ϑ . This integration can also be simply performed, and one obtains

$$\begin{aligned} f_{E2}(0) &= \frac{8\pi^2}{25} \left(\frac{\pi^2}{16} - \frac{1}{3} \right) = 0.8954, \\ f_{E3}(0) &= \frac{8\pi^2}{49} \left(\frac{8}{45} - \frac{\pi^2}{64} \right) = 0.03797, \quad (\text{II E.72}) \\ f_{M2}(0) &= \frac{8\pi^2}{25} \left(\frac{\pi^2}{16} - \frac{5}{9} \right) = 0.1936. \end{aligned}$$

⁹⁸ (a) N. Bohr, Phil. Mag. 25, 10 (1913); see also reference 19. (b) H. A. Bethe, Ann. Physik (5) 5, 325 (1930). (c) F. Bloch, Ann. Physik (5) 16, 285 (1933).

For $\lambda = 1$, the f functions diverge in the limit $\xi \rightarrow 0$.

⁹⁴ See p. 159 of reference 84.

The a coefficients in the angular distribution of the de-excitation γ rays (II A.75) also involve integrals over ϑ of the orbital integrals. From (II A.75), (II A.76), and (II A.77) one obtains

$$\begin{aligned} a_2^{E1}(0) &= 1, \\ a_2^{E2}(0) &= \frac{21\pi^2 - 208}{3\pi^2 - 16} = -0.05425, \\ a_4^{E2}(0) &= -\frac{441\pi^2 - 4352}{48(3\pi^2 - 16)} = -0.0007587, \\ a_2^{M1}(0) &= 1. \end{aligned} \quad (\text{II E.73})$$

$$\begin{aligned} M_{l, l+1}^{-2} &= M_{l+1, l}^{-2} = \frac{1}{2k} \frac{1}{|l+1+i\eta|}, \\ M_{l, l+2}^{-3} &= M_{l+2, l}^{-3} = \frac{1}{6} \frac{1}{|l+1+i\eta| |l+2+i\eta|}, \\ M_{l, l}^{-3} &= \frac{1}{2l(l+1)} [2l+1 - \pi\eta + 2\eta \operatorname{Im}\psi(l+1+i\eta)], \\ M_{l, l+3}^{-4} &= M_{l+3, l}^{-4} = \frac{k}{15} \frac{1}{|l+1+i\eta| |l+2+i\eta| |l+3+i\eta|}, \\ M_{l, l+1}^{-4} &= M_{l+1, l}^{-4} = \frac{k}{3l(l+1)(l+2)(2l+1)(2l+3) |l+1+i\eta|} \\ &\quad \times \{3 |l+1+i\eta|^2 [2l+1 - \pi\eta + 2\eta \operatorname{Im}\psi(l+1+i\eta)] - l(l+1)(2l+1)\}. \end{aligned} \quad (\text{II E.75})$$

The imaginary part of the logarithmic derivative ψ of the Γ function can be expressed by elementary functions through the relation

$$\operatorname{Im}\psi(l+1+i\eta) = \pi \coth\pi\eta + \eta^{-1} - 2\eta \sum_{n=0}^{\infty} \frac{1}{n^2 + \eta^2}. \quad (\text{II E.76})$$

In the classical limit ($\eta \rightarrow \infty$), the matrix elements (75) are related to the above calculated orbital integrals (71) by means of (II B.100).

To obtain the differential and the total f function as well as the γ -ray angular distribution functions, a summation over the angular momentum has to be performed [see (II B.48), (II B.50), and (II B.85)]. For large l , the terms in these sums decrease as $l^{-2\lambda+1}$. For $\lambda=1$, the total f function as well as the b coefficients diverge, and one obtains

$$a_2^{E1}(\eta, 0) = 1. \quad (\text{II E.77})$$

For $\lambda > 1$, the convergence is rather slow and may be

Also in the quantum-mechanical treatment, the case $\xi=0$ is especially simple. For the matrix elements with $l_i - l_f = \pm\lambda$ the last term of (II B.58) vanishes (for $\lambda > 1$) and the first F_2 function is unity. For $\xi=0$, one thus obtains for these matrix elements

$$\begin{aligned} M_{l, l+\lambda}^{-\lambda-1}(\xi=0) &= M_{l+\lambda, l}^{-\lambda-1}(\xi=0) \\ &= (2k)^{\lambda-2} \frac{[(\lambda-1)!]^2}{(2\lambda-1)!} \left| \frac{\Gamma(l+1+i\eta)}{\Gamma(l+\lambda+1+i\eta)} \right|, \end{aligned} \quad (\text{II E.74})$$

where $\eta = \eta_i = \eta_f$. This formula may also be seen to hold for $\lambda=1$. The matrix elements with $|l_i - l_f| < \lambda$ may most easily be obtained by means of the recursion formulas (II B.72) and (II B.68). For the lowest multipole orders, one obtains the following expressions⁹⁵

improved by employing the Euler sum formula. It should be pointed out that the convergence for $\xi \neq 0$ is more rapid due to the adiabatic cutoff for high l 's; the sum then becomes a geometric series.

II E.7. Limit of Large Orbital Angular Momenta

An interesting limit of the Coulomb excitation matrix elements is that of $l \gg 1$.⁹⁶ As pointed out in Sec. II B.6, the radial matrix elements in this limit can be expressed by means of (II B.100). This result can be obtained by employing the WKB approximation or by performing a confluence in the explicit expressions for the radial matrix elements, and holds for $l \gg 1$ irrespective of the value of η .

If $l \gg \eta$, the deflection angle of the associated classical orbit is small ($\vartheta \approx 2\eta/l$) and the orbits approach straight lines. It is thus of interest to compare the $I_{\lambda\mu}$ with the corresponding integrals for straight line orbits given by

⁹⁵ For $\lambda=2$ these results have been given by L. C. Biedenharn and C. M. Class, Phys. Rev. **98**, 691 (1955).

⁹⁶ This limit has been studied by Gluckstern, Lazarus, and Breit, reference 18.

[see (II A.24)]

$$I_{\lambda\mu}^{st}(\vartheta, \xi) = a^\lambda \cdot v \int_{-\infty}^{\infty} \frac{e^{i\omega t} [p + ivt]^\mu}{[p^2 + (vt)^2]^{\frac{1}{2}(\lambda + \mu + 1)}} dt$$

$$= \epsilon^{-\lambda} \int_{-\infty}^{\infty} \frac{e^{i\xi \epsilon \sinh w} [1 + i \sinh w]^\mu}{(\cosh w)^{\lambda + \mu}} dw, \quad (\text{II E.78})$$

where p is the impact parameter. We have introduced the parameters $\vartheta = 2a/p$ and $\epsilon = p/a$ which, for $p \gg a$, correspond to the deflection angle and eccentricity of the hyperbolic orbit with the impact parameter p .

The integral (78) is the same as the limit of (47) for $\epsilon \gg 1$ except for the phase factor $e^{i\xi w}$. The effect of this factor may be seen by transforming (47) according to (49). In the latter form the phase factor $e^{i\xi w}$ can be neglected for large ϵ and we thus have the relation

$$I_{\lambda\mu}(\vartheta, \xi) \approx e^{-(\pi/2)\xi} I_{\lambda\mu}^{st}(\vartheta, \xi), \quad (\text{II E.79})$$

holding for $\vartheta \ll 1$.

The large difference between the orbital integrals for straight line and hyperbolic orbits in the case of $\xi \gtrsim 1$ is associated with the fact that for such values of ξ the integral is very sensitive to the impact parameter. Thus, an increase of p by the amount a , which represents the order of magnitude of the displacement during the collision, implies a reduction of $I_{\lambda\mu}$ by a factor of the order of that involved in (79).

Since the $I_{\lambda\mu}^{st}$ corresponds to the neglect of the Coulomb force on the motion of the projectile, these integrals are for large l related to the Born approximation radial matrix elements by an equation analogous to (II B.100). From (79) we thus obtain

$$M_{l_i l_f}^{-\lambda-1} \approx e^{-(\pi/2)\xi} M_{l_i l_f}^{-\lambda-1} \text{ (Born appr.)}, \quad (\text{II E.80})$$

holding for $l_i, l_f \gg 1$. This relation shows that the Coulomb phase in the wave functions, for large l , gives rise to a simple factor, independent of l .⁹⁷

The integral (78) can be expressed by means of the Whittaker function⁹⁸ in the form

$$I_{\lambda\mu}^{st}(\vartheta, \xi) = (-1)^{(\lambda + \mu)/2} \epsilon^{-1} \left(\frac{\xi}{2\epsilon} \right)^{(\lambda - 1)/2}$$

$$\times \Gamma \left(\frac{-\lambda + \mu + 1}{2} \right) W_{-\mu/2, -\lambda/2}(2\xi\epsilon). \quad (\text{II E.81})$$

$$F(\alpha, \beta, \gamma; z) = \frac{\Gamma(\gamma)\Gamma(\beta - \alpha)}{\Gamma(\beta)\Gamma(\gamma - \alpha)} (-z)^{-\alpha} F(\alpha, 1 - \gamma + \alpha, 1 - \beta + \alpha; 1/z)$$

For large values of $\epsilon \xi$ one obtains by employing the asymptotic expansion of the Whittaker function^{99,5}

$$I_{\lambda\mu}^{st}(\vartheta, \xi) \approx \frac{2\pi}{\Gamma \left(\frac{\lambda + 1 - \mu}{2} \right)}$$

$$\times e^{-\xi \epsilon} \xi^{(\lambda - \mu - 1)/2} (2\epsilon)^{-(\lambda + \mu + 1)/2}. \quad (\text{II E.82})$$

For the radial matrix elements in the limit $l \gg 1$, one thus obtains the result

$$M_{l_i l_f}^{-\lambda-1} \approx \frac{k^{\lambda-2}}{4\eta^\lambda} \frac{2\pi}{\Gamma \left(\frac{\lambda + 1 - \mu}{2} \right)} e^{-(l/\eta + \pi/2)\xi}$$

$$\times \xi^{(\lambda - \mu - 1)/2} (2l/\eta)^{-(\lambda + \mu + 1)/2}. \quad (\text{II E.83})$$

A more accurate result may be obtained by an expansion of the Born approximation radial matrix elements (31) employing (86).

II E.8. Some Properties of Hypergeometric Functions

In this paragraph, we shall collect some formulas for hypergeometric functions which are of interest in the theory of Coulomb excitation.¹⁰⁰

The ordinary hypergeometric function of one variable is defined by the series expansion

$$F(\alpha, \beta, \gamma; z) = \sum_m \frac{\alpha_m \beta_m}{\gamma_m m!} z^m, \quad (\text{II E.84})$$

where

$$a_m = \frac{\Gamma(a+m)}{\Gamma(a)} = a(a+1) \cdots (a+m-1). \quad (\text{II E.85})$$

This series is only convergent for $|z| < 1$. However, the analytic continuation can again be expressed by hypergeometric functions. We note especially the Kummer transformation

$$F(\alpha, \beta, \gamma; z) = (1-z)^{-\alpha} F \left(\alpha, \gamma - \beta, \gamma; \frac{z}{z-1} \right) \quad (\text{II E.86})$$

and the relation in terms of the reciprocal argument

$$+ \frac{\Gamma(\gamma)\Gamma(\alpha - \beta)}{\Gamma(\alpha)\Gamma(\gamma - \beta)} (-z)^{-\beta} F(\beta, 1 - \gamma + \beta, 1 - \alpha + \beta; 1/z). \quad (\text{II E.87})$$

⁹⁷ In the applications of the relations (79) and (80) in reference 96 the exponential factor has been omitted.

⁹⁸ See p. 274 of reference 84.

⁹⁹ See p. 278, reference 84.

¹⁰⁰ Most of these formulas may be found in reference 84 or in the treatise by P. Appell and J. Kampé de Fériet, *Fonctions Hypergéométriques etc.* (Gauthiers Villars, Paris, 1926).

The analytic continuation is also given by the integral representation

$$F(\alpha, \beta, \gamma; z) = \frac{\Gamma(\gamma)}{\Gamma(\beta)\Gamma(\gamma-\beta)} \int_0^1 u^{-\beta-1}(1-u)^{\gamma-\beta-1}(1-uz)^{-\alpha} du, \tag{II E.88}$$

valid for $\text{Re}\beta > 0$ and $\text{Re}(\gamma-\beta) > 0$.

When one of the parameters α or β tends to infinity while z becomes small, the function (84) approaches the confluent hypergeometric function

$${}_1F_1(\alpha, \gamma; z) = \lim_{\beta \rightarrow \infty} F(\alpha, \beta, \gamma; z/\beta) = \sum_m \frac{\alpha_m}{\gamma_m m!} z^m, \tag{II E.89}$$

which is convergent for all z .

From the formula (86) one obtains the Kummer transformation for the confluent function

$${}_1F_1(a, \gamma; z) = e^z {}_1F_1(\gamma - a, \gamma; -z). \tag{II E.90}$$

An integral representation of the function ${}_1F_1$ is given by

$${}_1F_1(\alpha, \gamma; z) = \frac{\Gamma(\gamma)}{\Gamma(\alpha)\Gamma(\gamma-\alpha)} \int_0^1 e^{zt} t^{\alpha-1} (1-t)^{\gamma-\alpha-1} dt, \tag{II E.91}$$

valid for $\text{Re}\alpha > 0$ and $\text{Re}(\gamma-\alpha) > 0$.

Among the hypergeometric functions of more than one variable, the simplest are the so-called Appell functions. We shall here be concerned with the functions $F_1, F_2,$ and F_3 defined by the series

$$F_1(\alpha, \beta, \beta', \gamma; x, y) = \sum_{mn} \frac{\alpha_m \beta_m \beta'_n}{\gamma_{m+n} m! n!} x^m y^n \quad \begin{matrix} |x| < 1 \\ |y| < 1 \end{matrix}, \tag{II E.92}$$

$$F_2(\alpha, \beta, \beta', \gamma, \gamma'; x, y) = \sum_{mn} \frac{\alpha_m \beta_m \beta'_n}{\gamma_m \gamma'_n m! n!} x^m y^n \quad |x| + |y| < 1, \tag{II E.93}$$

$$F_3(\alpha, \alpha', \beta, \beta', \gamma; x, y) = \sum_{mn} \frac{\alpha_m \alpha'_n \beta_m \beta'_n}{\gamma_{m+n} m! n!} x^m y^n \quad \begin{matrix} |x| < 1 \\ |y| < 1 \end{matrix}, \tag{II E.94}$$

whose regions of convergence are indicated.

These functions have properties similar to those of the hypergeometric functions of one variable. Thus, for the function F_2 there exist transformations of the Kummer type

$$\begin{aligned} F_2(\alpha, \beta, \beta', \gamma, \gamma'; x, y) &= (1-y)^{-\alpha} F_2\left(\alpha, \beta, \gamma' - \beta', \gamma, \gamma'; \frac{x}{1-y}, \frac{y}{y-1}\right) \\ &= (1-x-y)^{-\alpha} F_2\left(\alpha, \gamma - \beta, \gamma' - \beta', \gamma, \gamma'; \frac{x}{x+y-1}, \frac{y}{x+y-1}\right). \end{aligned} \tag{II E.95}$$

For special values of the parameters, the Appell functions reduce according to the following relations

$$F_2(\alpha, \beta, \beta', \alpha, \alpha; x, y) = (1-x)^{-\beta} (1-y)^{-\beta'} F\left(\beta, \beta', \alpha; \frac{xy}{(1-x)(1-y)}\right), \tag{II E.96}$$

$$F_2(\alpha, \beta, \beta', \gamma, \alpha; x, y) = (1-y)^{-\beta'} F_1\left(\beta, \alpha - \beta', \beta', \gamma; x, \frac{x}{1-y}\right), \tag{II E.97}$$

$$F_1(\alpha, \beta, \beta', \gamma; x, y) = (1-y)^{-\beta'} F_3\left(\alpha, \gamma - \alpha, \beta, \beta', \gamma; x, -\frac{y}{1-y}\right). \tag{II E.98}$$

The analytic continuation of the function F_3 can be expressed by four F_2 functions of the arguments x^{-1}, y^{-1} as follows:

$$\begin{aligned}
 &F_3(\alpha, \alpha', \beta, \beta', \gamma; x, y) \\
 &= \frac{\Gamma(\gamma)\Gamma(\beta-\alpha)\Gamma(\beta'-\alpha')}{\Gamma(\beta)\Gamma(\beta')\Gamma(\gamma-\alpha-\alpha')} (-x)^{-\alpha} (-y)^{-\alpha'} F_2\left(\alpha+\alpha'+1-\gamma, \alpha, \alpha', \alpha+1-\beta, \alpha'+1-\beta'; \frac{1}{x}, \frac{1}{y}\right) \\
 &\quad + \frac{\Gamma(\gamma)\Gamma(\beta-\alpha)\Gamma(\alpha'-\beta')}{\Gamma(\beta)\Gamma(\alpha')\Gamma(\gamma-\alpha-\beta')} (-x)^{-\alpha} (-y)^{-\beta'} F_2\left(\alpha+\beta'+1-\gamma, \alpha, \beta', \alpha+1-\beta, \beta'+1-\alpha'; \frac{1}{x}, \frac{1}{y}\right) \\
 &\quad + \frac{\Gamma(\gamma)\Gamma(\alpha-\beta)\Gamma(\beta'-\alpha')}{\Gamma(\alpha)\Gamma(\beta')\Gamma(\gamma-\beta-\alpha')} (-x)^{-\beta} (-y)^{-\alpha'} F_2\left(\beta+\alpha'+1-\gamma, \beta, \alpha', \beta+1-\alpha, \alpha'+1-\beta'; \frac{1}{x}, \frac{1}{y}\right) \\
 &\quad + \frac{\Gamma(\gamma)\Gamma(\alpha-\beta)\Gamma(\alpha'-\beta')}{\Gamma(\alpha)\Gamma(\alpha')\Gamma(\gamma-\beta-\beta')} (-x)^{-\beta} (-y)^{-\beta'} F_2\left(\beta+\beta'+1-\gamma, \beta, \beta', \beta+1-\alpha, \beta'+1-\alpha'; \frac{1}{x}, \frac{1}{y}\right). \quad (\text{II E.99})
 \end{aligned}$$

The analytic continuation of the function F_2 can, in the general case, not be expressed in terms of Appell functions, but may be given by the integral representation

$$F_2(\alpha, \beta, \beta', \gamma, \gamma'; x, y) = \frac{\Gamma(\gamma)\Gamma(\gamma')}{\Gamma(\beta)\Gamma(\beta')\Gamma(\gamma-\beta)\Gamma(\gamma'-\beta')} \int_0^1 \int_0^1 du dv u^{\beta-1} v^{\beta'-1} (1-u)^{\gamma-\beta-1} (1-v)^{\gamma'-\beta'-1} (1-ux-vy)^{-\alpha}, \quad (\text{II E.100})$$

valid for $\text{Re}\beta > 0$, $\text{Re}\beta' > 0$, $\text{Re}(\gamma-\beta) > 0$, and $\text{Re}(\gamma'-\beta') > 0$. One of the integrations can be performed according to (88) yielding the result

$$F_2(\alpha, \beta, \beta', \gamma, \gamma'; x, y) = \frac{\Gamma(\gamma')}{\Gamma(\beta)\Gamma(\gamma'-\beta')} \int_0^1 dv v^{\beta'-1} (1-v)^{\gamma'-\beta'-1} (1-vy)^{-\alpha} F\left(\alpha, \beta, \gamma; \frac{x}{1-vy}\right). \quad (\text{II E.101})$$

A similar integral representation of F_1 is given by

$$F_1(\alpha, \beta, \beta', \gamma; x, y) = \frac{\Gamma(\gamma)}{\Gamma(\alpha)\Gamma(\gamma-\alpha)} \int_0^1 du u^{\alpha-1} (1-u)^{\gamma-\alpha-1} (1-ux)^{-\beta} (1-uy)^{-\beta'}, \quad (\text{II E.102})$$

valid for $\text{Re}\alpha > 0$ and $\text{Re}(\gamma-\alpha) > 0$.

There exist a large number of relations by which one may expand one Appell function in terms of other hypergeometric functions. An expansion of F_2 is obtained from (101) by transforming the F function according to (87) and (86). By the integral representation (102), this leads to

$$\begin{aligned}
 F_2(\alpha, \beta, \beta', \gamma, \gamma'; x, y) &= \frac{\Gamma(\beta)\Gamma(\gamma')\Gamma(\gamma-\beta)\Gamma(\beta'-\alpha)}{\Gamma(\gamma)\Gamma(\beta')\Gamma(\gamma'-\alpha)} (-y)^{-\alpha} \left(\frac{y}{y-1}\right)^{\alpha-\gamma'+1} \\
 &\quad \times \sum_m \frac{(1-\beta')_m (1-\gamma'+\alpha)_m}{(1-\beta'+\alpha)_m m!} (y-1)^{-m} F_1\left(\beta, -m, \alpha-\gamma'+1+m, \gamma; x, \frac{x}{1-y}\right) \\
 &\quad + \frac{\Gamma(\beta)\Gamma(\gamma')\Gamma(\gamma-\beta)\Gamma(\alpha-\beta')}{\Gamma(\gamma)\Gamma(\alpha)\Gamma(\gamma'-\beta')} (-y)^{-\beta'} \left(\frac{y}{y-1}\right)^{\alpha-\beta'+1} \\
 &\quad \times \sum_m \frac{(1-\alpha)_m (1-\gamma'+\beta')_m}{(1+\beta'-\alpha)_m m!} (y-1)^{-m} F_1\left(\beta, \alpha-\beta'-m, \beta'-\gamma'+1+m, \gamma; x, \frac{x}{1-y}\right). \quad (\text{II E.103})
 \end{aligned}$$

A similar relation for F_3 is given by

$$F_3(\alpha, \alpha', \beta, \beta', \gamma; x, y) = (1-x)^{-\alpha} \sum_m \frac{(\gamma-\beta-\beta')_m \alpha_m'}{\gamma_m m!} (-y)^m F_1\left(\gamma-\beta+m, \alpha, \alpha'+m, \gamma+m; \frac{x}{x-1}, y\right). \quad (\text{II E.104})$$

For large parameters, the Appell functions reduce to confluent functions. Thus, for the F_2 function with β, β' large, one obtains

$$\Psi_2(\alpha, \gamma, \gamma'; x, y) = \lim_{\beta, \beta' \rightarrow \infty} F_2\left(\alpha, \beta, \beta', \gamma, \gamma'; \frac{x}{\beta}, \frac{y}{\beta'}\right) = \sum_{m, n} \frac{\alpha_{m+n}}{\gamma_m \gamma_n' m! n!} x^m y^n, \quad (\text{II E.105})$$

which is convergent for all x and y .

CHAPTER III. EXPERIMENTAL CONDITIONS

In the present chapter, we consider the conditions for the experimental investigations of the Coulomb excitation process. Section III A deals with the requirements on the ion beam, and the following sections treat the problems connected with the observation of the nuclear excitations. These can be detected by observing either the γ rays (III B) or the internal conversion electrons (III C) which are emitted in the decay of the excited states. It is also possible to detect directly the inelastically scattered projectiles (III D).

III A. Beam Requirements

The range of projectile energies which can be employed in the excitation of a given nuclear level is limited on the low-energy side by the condition that the collision time must not be longer than the nuclear period, since otherwise the collision becomes adiabatic and the excitation cross section small. On the other hand, for too high bombarding energies, the projectiles may penetrate into the nucleus, and the interpretation of the observed excitations then becomes more difficult due to the onset of proper nuclear reactions.

For the Coulomb barrier we may write

$$E_B = \frac{Z_1 Z_2 e^2}{R}, \quad (\text{III.1})$$

where R is the effective radius of interaction which may be represented by

$$R = r_0 A_2^{1/3} + \rho. \quad (\text{III.2})$$

The radius of the projectile is denoted by ρ and is taken to be zero in the case of protons. If one neglects ρ and assumes $r_0 = 1.5 \times 10^{-13}$ cm, one obtains the approximate estimate

$$E_B \approx Z_1 Z_2 A_2^{-1/3} \text{ Mev}. \quad (\text{III.3})$$

Even for bombarding energies somewhat smaller than (1), there may be a significant quantum-mechanical penetration of the barrier. This effect is less important when heavier projectiles or target nuclei are involved (see Fig. III.1). Furthermore, even if the cross section for compound nucleus formation exceeds that for Coulomb excitation, it may still be possible to observe the latter effect, since the compound nucleus usually decays predominantly into other channels than that corresponding to the inelastic scattering (see Sec. IV A.5).

The low-energy limit to the bombarding energy may be expressed by the condition $\xi \lesssim 1$ [see (II A.27)]. According to (II C.13), this condition may also be written

$$E_{\text{Mev}} \gtrsim 0.2 Z_1 (A_1/Z_1)^{1/3} (Z_2 \Delta E_{\text{Mev}})^{1/3}, \quad (\text{III.4})$$

where E_{Mev} and ΔE_{Mev} are the bombarding energy and the excitation energy in Mev. In (4) we have neglected the center-of-mass corrections and the relative energy loss $\Delta E/E$.

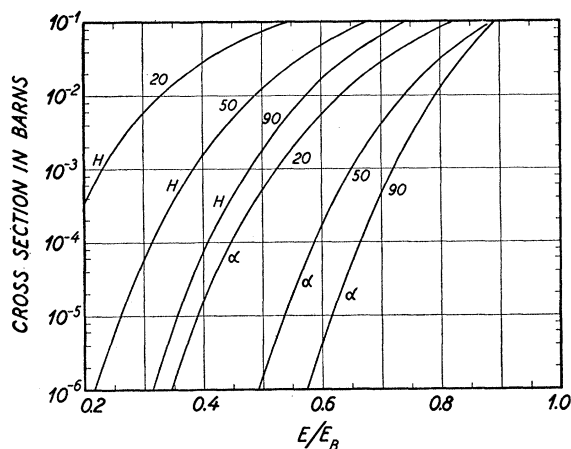


FIG. III.1. Cross sections for compound nucleus formation. The figure gives theoretical estimates of the cross sections as a function of the ratio E/E_B , where E is the kinetic energy in the center-of-mass system, and where E_B is the height of the Coulomb barrier. The curves are labeled H for protons and α for α particles, whereas the numbers indicate the charge number Z_2 of the target element. The cross sections are taken from the tables given by J. M. Blatt and V. F. Weisskopf [*Theoretical Nuclear Physics* (John Wiley and Sons, Inc., New York, 1952)], and correspond to an effective interaction radius given by (III.2) with $r_0 = 1.5 \cdot 10^{-13}$ cm. The value of ρ is taken to be zero for protons, and $1.2 \cdot 10^{-13}$ cm for α particles.

If the conditions (4) and $E < E_B$ are expressed in terms of ξ , one obtains, employing the estimate (3)

$$\left(\frac{A_1 A_2}{Z_1 Z_2} \right)^{1/2} \cdot \frac{\Delta E_{\text{Mev}}}{13} \lesssim \xi \lesssim 1 \quad (\text{III.5})$$

for the usable range of ξ values.

From (5) it follows that the various types of accelerated ions can be used in approximately the same range of ξ values. Moreover, it is seen that, by employing sufficiently high bombarding energies, it may be possible to excite levels with ΔE as high as 5 Mev. Since, however, ΔE must be small compared to E , it is necessary in the Coulomb excitation of such high-lying levels to employ high energies, and thus rather heavy projectiles, especially in the case of light target nuclei.

For a given value of ξ , the cross section for an excitation of multipole order $E\lambda$ is proportional to $Z_1^2 (A_1/Z_1)^{2\lambda/3}$ [see (II C.13), (II C.15), and (II C.16)]; thus, the largest cross sections are obtained with the heavier projectiles. The advantage of the heavier projectiles is even greater in the case of higher order excitations (see Sec. II D).

In order to obtain the same ξ value for the different projectiles, it is necessary that they be accelerated to energies which are proportional to $Z_1 (A_1/Z_1)^{1/3}$. For a given acceleration voltage this may be approximately achieved, provided the ions can be completely stripped of electrons. However, if this is not the case, the relative magnitude of the excitation cross sections obtainable with different projectiles depends essentially on the available voltage.

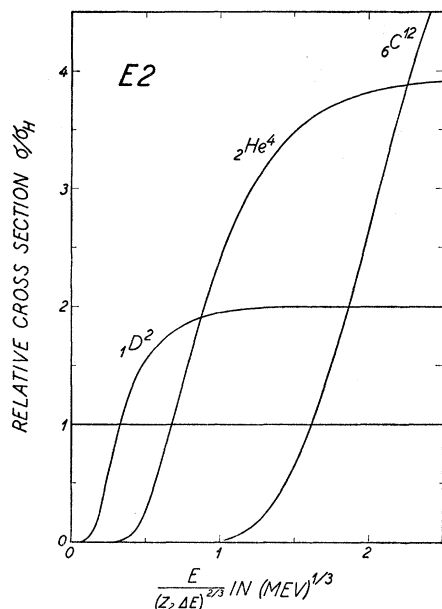


FIG. III.2. Relative excitation cross sections for different projectiles. The curves show the ratio of the theoretical $E2$ cross sections for Coulomb excitation with deuterons, α particles, and carbon ions, to those for protons of the same energy. The ratios also depend on the excitation energy ΔE and the atomic number Z_2 of the target nuclei, but can be expressed approximately as a function of the single parameter $E/(Z_2 \Delta E)^2$.

For projectiles having the same energy, the cross sections for $E2$ excitations are compared in Fig. III.2. The cross sections are proportional to the mass of the projectiles when the excitation energy is so low that the ξ values are much smaller than unity. In such cases, the excitations are best produced by bombardments with the heavier particles, in contrast to the higher lying levels which are more easily excited by means of protons. In the case of thick target experiments the yield for protons is always larger than for heavier projectiles of the same energy, due to the larger range of the protons. On the other hand, the background radiations produced by α -particle bombardments are in general considerably smaller than those produced by protons (see later discussion), and this may, therefore, often be a compensating consideration.

Apart from the question of which type of projectile provides the optimum conditions for Coulomb excitation under given experimental circumstances, it is often a great advantage to be able to compare the yields for different projectiles. Not only does such a comparison constitute a very direct test of the Coulomb excitation character of the process, but it may also yield additional information about the multipole order and the excitation energy (see Sec. IV A.1).

The absolute values of the excitation cross sections depend on the reduced transition probabilities $B(\lambda)$. The largest cross sections are associated with the collective excitations of low energy, which are produced by $E2$ transitions (see Chapter V). As an example,

cross sections of the order of millibarns are observed for the excitation of rotational levels in heavy elements with 2-Mev protons. Because of the nonresonant character of the process, such cross sections imply thick target yields of the order of 10^{-7} excitation per proton. Thus, the demands on the current as well as on the energy homogeneity of the beam are often rather modest.

So far most Coulomb excitation experiments have been performed by means of protons, deuterons, and α particles, accelerated in electrostatic generators. It has also been shown that it is feasible to make such experiments with external ion beams from cyclotrons.¹⁰¹

III B. Measurements of De-Excitation Gamma Rays

III B.1. Detection Technique

The great sensitivity and simplicity of the scintillation spectrometers employed in γ -ray measurements

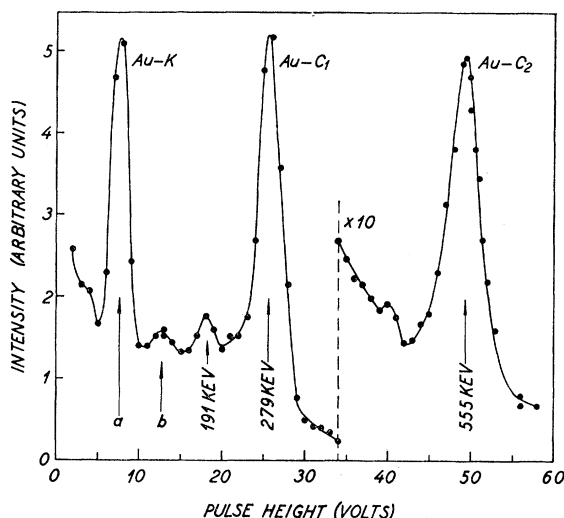


FIG. III.3. Gamma rays from the Coulomb excitation of gold. The figure shows the pulse-height spectrum observed with a crystal scintillation spectrometer [Cook, Class, and Eisinger, Phys. Rev. **96**, 658 (1954)]. The excitation was produced by bombardment of a thick Au target with 3-Mev protons. The peaks C_1 and C_2 correspond to the transitions from the first two strongly excited levels to the ground state, whereas the peak a is due to the characteristic x-rays which follow the ionization of the K shell. The 191-kev peak corresponds to a weaker excitation of a level at 268 kev (see Table IV.2), and b is an escape peak (Compton peak) belonging to the C_1 line.

have rendered these instruments the most widely used detectors in experiments on Coulomb excitation. Typical examples of the pulse-height spectra which have been obtained in this way are given in Figs. III.3, 4, and 5.

The comparatively poor energy resolution of the scintillation spectrometers is often a disadvantage, espe-

¹⁰¹ Such experiments have been carried out in Zürich with 7-Mev protons (private communication from P. Marmier) and in Leningrad with 15 Mev $(N^{14})^{+++}$ ions (Alkhasov *et al.*, see reference 15).

cially for low-energy radiation, where the background of x-rays is large (see Sec. III B.3). Some improvements can be obtained by using the spectrometer in combination with various absorbers. The absorption coefficients are strongly energy dependent in this region and the effect of the absorbers is therefore dependent on the energy distribution of the radiation. This is illustrated in Fig. III.6, where the background peak is seen to be suppressed relative to the peak due to Coulomb excitation, when the absorber thickness is increased. In cases where a peak is composite, this may be revealed by a change in the shape of the peak when the absorbers are introduced. The measurement of the absorption coefficient can also sometimes be useful in providing an independent energy determination which makes it possible to avoid misinterpretations of the experimental spectra, e.g., due to coincidences or to the so-called escape peaks.

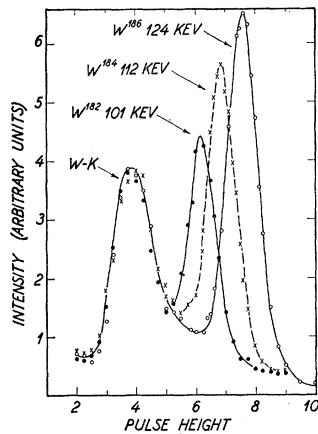


FIG. III.4. Gamma rays from the excitation of separated isotopes of tungsten. The γ rays are observed with a crystal spectrometer and result from bombardments of thick WO_3 targets of the separated isotopes with 2.5-Mev protons. The pulse-height spectrum is taken from McClelland, Mark, and Goodman [Phys. Rev. 93, 904 (1953)]. The three γ rays represent the first excited states in the even- A isotopes.

The large yields for the Coulomb excitation processes, which are encountered for low excitation energies, also make feasible the use of proportional counters for the detection. The comparatively high resolution of this type of counter may in such cases be of greater importance than the correspondingly lower efficiency. The Coulomb excitation of some of the heaviest elements has recently been studied in this manner (see Fig. III.7).^{101a}

Besides the efficiency and simplicity of the scintillation detector, the observation of the γ radiation has several other intrinsic advantages associated with the relatively small scattering or absorption in the target. This facilitates the measurements of angular distribu-

^{101a} Note added in proof.—The very high resolution of the bent crystal spectrometer has recently been employed in an experiment performed with the high current (~ 100 mA) from a linear accelerator (private communication from H. Mark).

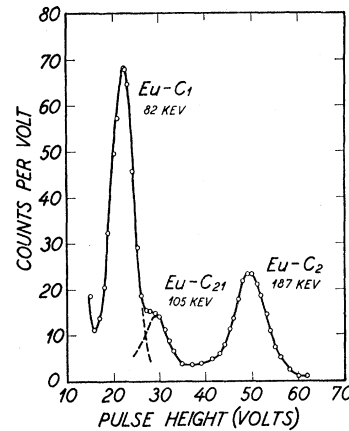


FIG. III.5. Gamma rays from the excitation of europium. The γ rays resulting from a bombardment of a thick Eu_2O_3 target with 6-Mev α particles are observed with a crystal spectrometer. The pulse-height spectrum is taken from N. P. Heydenburg and G. M. Temmer [Phys. Rev. 100, 150 (1955)]. All three lines are assigned to the isotope Eu^{153} ; the C_1 and C_2 lines correspond to the ground-state transitions from the first two rotational excitations, respectively, whereas the C_{21} line represents the cascade transition from the second to the first level.

tions, since the correction for the target thickness is usually small. An example of the measured γ -ray angular distributions is shown in Fig. III.8.

If one wishes to determine directly the total γ -ray yield, one may either employ a 2π -geometry,¹⁰² or one

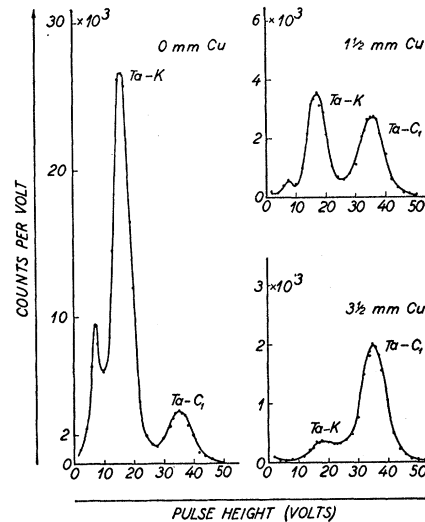


FIG. III.6. Effect of absorbers in γ -ray measurements. The figure illustrates the effect of Cu absorbers inserted between the crystal and the target when Ta is bombarded by 1.75-Mev protons. The pulse-height spectra, obtained with a thick target, are taken from T. Huus and Č. Zupančič [Kgl. Danske Videnskab. Selskab Mat.-fys. Medd. 28, No. 1 (1953)]. With a 3.5-mm copper absorber the characteristic x-rays from the K shell are strongly reduced, while the 137-kev C_1 line from the decay of the first excited nuclear state is much less affected. The spectra also show an escape peak associated with the x-rays.

¹⁰² N. P. Heydenburg and G. M. Temmer, Phys. Rev. 100, 150 (1955).

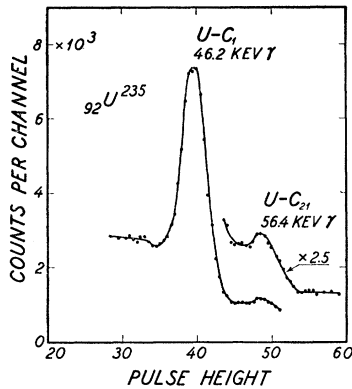


FIG. III.7. Gamma rays from U^{235} observed with a proportional counter. The pulse-height spectrum is obtained with a xenon-filled proportional counter when a target of U^{235} is bombarded by 3-Mev α particles. The figure is reproduced from data communicated to us by J. O. Newton (unpublished). The lines correspond to the ground-state transition from the first rotational state and the cascade transition from the second rotational state.

may make the observations at an angle of 55 or 125 degrees with respect to the beam.¹⁰³ For these angles, the P_2 function in (II C.26) and (II C.29) vanishes, and since the coefficient of P_4 in (II C.29) is almost always very small, one observes a yield approximately proportional to the cross section averaged over all angles.

III B.2. Thick Target Yields

The small scattering and absorption of the γ rays in the target make it possible to employ thick targets in the measurements of the excitation cross sections and of the angular distributions. The determination of the cross section from the observed yield then involves either a differentiation of the yield as a function of the bombarding energy, or an integration of the theoretical excitation function along the trajectory of the projectile in the target.

It is convenient to express the result of the latter calculation in terms of an effective target thickness δE_λ which is related to the true thick target yield by

$$Y = \sigma(E_0) \frac{E_0 N}{(dE/ds)_0} \frac{\delta E_\lambda}{E_0}, \quad (\text{III.6})$$

where Y is the fraction of the incoming particles which produce the nuclear excitation and N the density of the investigated atoms in the target. The stopping power of the target material is denoted by dE/ds and is evaluated at the bombarding energy E_0 . Thus, the fraction $\delta E_\lambda/E_0$ represents the ratio of the observed yield to that which would result if the excitation cross section σ and the stopping power were independent of the energy of the projectile and had the values corresponding to the energy E_0 .

The calculation of δE_λ has been performed assuming $dE/ds \sim E^{-0.55}$. This energy dependence represents

¹⁰³ P. H. Stelson and F. K. McGowan, Phys. Rev. **99**, 112 (1955).

rather well the stopping power of protons and α particles in almost the entire range from the lowest energies employed in Coulomb excitation experiments and up to energies equal to the Coulomb barrier.¹⁰⁴

By means of the theoretical excitation cross section (II C.15) one then obtains

$$\frac{\delta E_\lambda}{E_0} = \frac{1}{u_\lambda(\nu, \xi_0)} \int_{\xi_0}^1 u_\lambda(\nu, \xi) \frac{d\xi}{\xi}, \quad (\text{III.7})$$

where the functions u_λ are defined by

$$u_\lambda(\nu, \xi) = \xi^{1.45-2\lambda} (1-\xi)^{\lambda-1} f_{E\lambda}(\nu, \xi). \quad (\text{III.8})$$

The relations between the parameters (ν, ξ) and (η_i, ξ) are given by Eqs. (II C.11) and (II C.12), and the subscript zero indicates that the values correspond to the bombarding energy E_0 . The values of δE_λ computed from these formulas are given in Fig. III.9 as a function of ξ_0 , for the case $\nu \rightarrow 0$, which corresponds to the classical limit. The results are rather insensitive to the assumed energy dependence for the stopping power, due to the rapid variation of σ with the energy of the projectile for all but the smallest ξ values. Even in the extreme case of $\xi_0 = 0$, the value of δE_2 will be changed by only 8% of its magnitude if, instead of $E^{-0.55}$, one employs the rather different energy dependences $E^{-0.3}$

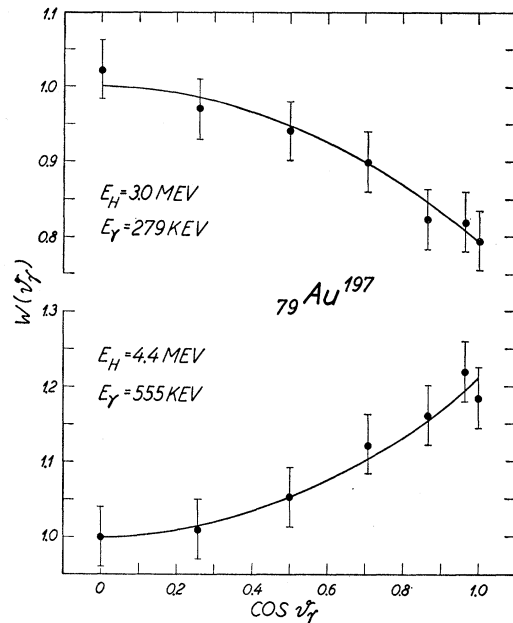


FIG. III.8. Angular distribution of γ rays from gold. The figure shows the angular distribution of the two intense γ rays resulting from the Coulomb excitation of Au^{197} (see Fig. III.3). The data is taken from Cook, Class, and Eisinger [Phys. Rev. **96**, 658 (1954)]. The curves represent a least-square fit to the experimental data. For the 555-kev γ ray the distribution corresponds to the sequence $3/2(E2)7/2(E2)3/2$ of spins and multiplicities (see Table IV.2). For the 279-kev γ ray the angular distribution indicates the sequence $3/2(E2)5/2(M1+E2)3/2$ with an $E2$ intensity of approximately 40% in the decay radiation.

¹⁰⁴ Cf. J. Lindhard and M. Scharff, Kgl. Danske Videnskab. Selskab Mat. fys. Medd. **27**, No. 15 (1953).

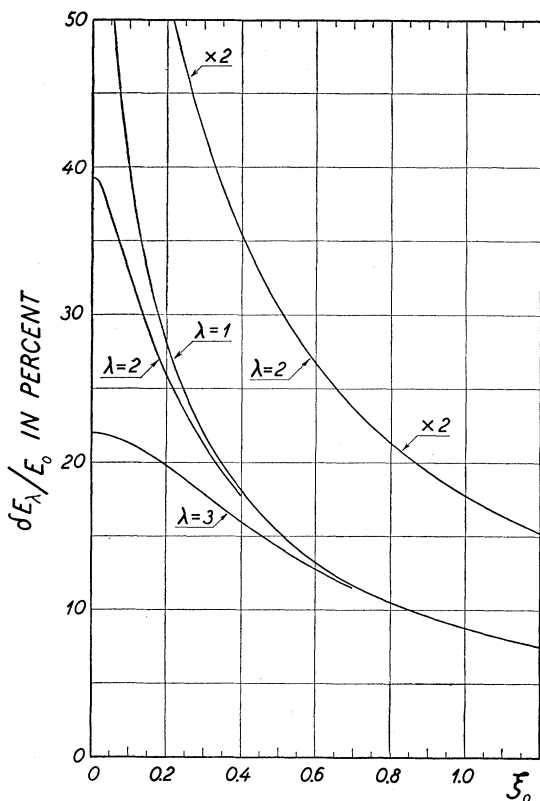


FIG. III.9. Effective target thickness. The curves give the ratio $\delta E_\lambda/E_0$ which enters into the determination of the theoretical thick target yields [see (III.6)]. The ratio has been computed from (III.7) by means of the classical f functions ($\nu=0$) for electric excitation of multipole order $\lambda=1, 2$, and 3 ; the stopping power has been assumed to depend on the energy of the projectile as $E^{-0.55}$. The abscissa gives the ξ value corresponding to the bombarding energy E_0 .

or $E^{-0.7}$ for the stopping power. The curves in Fig. III.9 should thus be applicable to all target materials, including compounds, and the uncertainties are expected in most cases to be less than 2%. Also the effect of the energy straggling, which is neglected in (8), is smaller than this amount.

For finite values of the parameter ν , slightly different curves are obtained, but, to an accuracy of better than a few percent, they can be found from the curves for $\nu=0$ by multiplying with a correction factor which is a function of the product $\nu\xi_0$ or ζ_0 , only. This correction factor C is given in Fig. III.10 together with a curve for the determination of the ξ value [see (II C.12)].

For the angular distribution coefficients $\bar{a}_k^{E\lambda}$ appropriate to thick target measurements, one obtains in a similar way the expressions

$$\bar{a}_k^{E\lambda}(\nu, \zeta_0) = \frac{\int_{\zeta_0}^1 a_k^{E\lambda}(\nu, \zeta) u_\lambda(\nu, \zeta) \frac{d\zeta}{\zeta}}{\int_{\zeta_0}^1 u_\lambda(\nu, \zeta) \frac{d\zeta}{\zeta}}, \quad (\text{III.9})$$

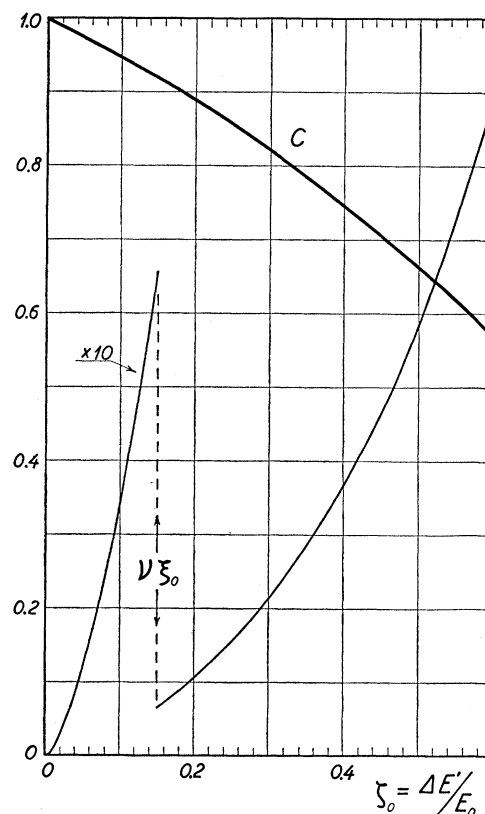


FIG. III.10. Correction factor to the effective target thickness. The quantity C gives the factor by which the value read from Fig. III.9 should be multiplied in order to take into account the finite value of ν [see (II C.10)]. This correction factor may be represented approximately as a function of the single parameter ζ_0 [see (II C.4) and (II C.5)]. The ξ value (II C.12), to be employed in the reading of Fig. III.9, can be obtained from the $\nu\xi_0$ curve, which is shown in the present figure.

where $a_k^{E\lambda}$ are the thin target coefficients [see (II B.83), Fig. II.8]. The values for the thick target coefficients are to a good approximation the same as those for the thin target coefficients, if the latter are evaluated for a bombarding energy which is smaller than the actual one by the factor $(1 + \delta E_\lambda/E_0)$. The estimated errors are less than three percent under the condition that the coefficients can be considered to depend linearly on ζ within energy intervals of the order of δE_λ .

The multiple scattering of the projectiles in the target gives rise to an angular spread of at most a few degrees for a target thickness of δE_λ .¹⁰⁵ The effect on the angular distribution of the γ rays is thus of minor importance.

III B.3. Background Radiation

When one studies the radiations following Coulomb excitation, it is of course not only important that the absolute yield is sufficient to give a reasonable counting rate, but also that the yield relative to the existing back-

¹⁰⁵ See, for example, reference 19 and also T. Huus, Kgl. Danske Videnskab. Selskab Mat. fys. Medd. 26, No. 4 (1951).

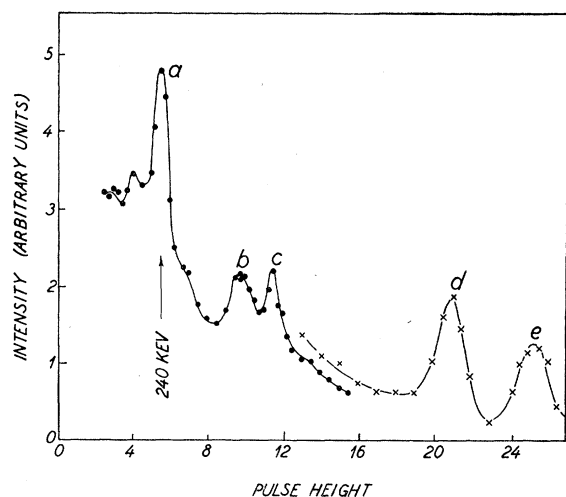


FIG. III.11. Effect of impurities in γ -ray measurements. The pulse-height spectrum, obtained with a crystal, has been observed in the bombardment of a thick Lu_2O_3 target with 2.6-Mev protons [McClelland, Mark, and Goodman, *Phys. Rev.* **97**, 1191 (1955)]. In addition to the peak *a* which corresponds to a 240-kev γ ray from the cross-over transition from the second excited state in Lu^{175} , other peaks are observed, arising from the presence of light elements in the target. The peak *b* at 439 kev is assigned to sodium impurities, and the peak *c* at 490 kev to the $\text{O}^{16}(\beta, \gamma)$ process. The peaks *d* and *e* at 0.843 Mev and 1.017 Mev, respectively, are ascribed to inelastic scattering in aluminum, contained in the target material as an impurity; nominal purity of the sample was given as 99.9%.

ground radiations is high enough to be detectable in the actual experiments.

The background arises partly from external sources, such as the radiations from the accelerator, or from reactions with impurities in the target and with substances chemically bound to the element under investigation. Thus, oxide targets emit a strong γ radiation in the region of a few hundred kev when bombarded with protons (see Fig. III.11), and a line at 342 kev when bombarded with α particles.¹⁰² In addition to this type of background, there is the background radiation due to processes taking place in the atoms of the investigated element itself. The production of the latter kind of background radiation can of course not be avoided. However, it can be discriminated against, if coincidence measurements can be performed,¹⁰⁶ or if the nuclear decay involves a sufficient delay.¹⁰⁷ When such possibilities do not exist, the best that can be done is to choose the experimental conditions so as to give the smallest possible ratio of background to nuclear radiation. It is therefore important to know how the atomic processes depend on the various parameters of the bombardment.

In the region of low γ -ray energies, the most important background process is the emission of the characteristic x-rays which follow the ionizations produced by the projectiles (see Figs. III.3, III.4, III.6, and III.13).

¹⁰² See, for example, reference 103, and G. M. Temmer and N. P. Heydenburg, *Bull. Am. Phys. Soc. Ser. II* **1**, 43 (1956).

¹⁰⁷ T. Huus and A. Lundén, *Phil. Mag.* **45**, 966 (1954).

The theoretical cross sections for the ionization of the *K* shell have been computed in Born approximation for nonrelativistic electron wave functions.¹⁰⁸ The result may be written in the form

$$\sigma_K \approx Z_1^2 (E_{\text{Mev}}/A_1)^4 (36/Z_2)^{12} 10^{-24} \text{ cm}^2, \quad (\text{III.10})$$

provided the *K* shell binding energy exceeds the maximum energy which a free electron can acquire in a collision with the projectile. Even for bombarding energies close to the Coulomb barrier, this condition is fulfilled for $Z_2 > 40$.

The experimental cross sections¹⁰⁹ are found to be somewhat larger than given by (10) for protons in the energy range employed in Coulomb excitation; thus, in the case of 4-Mev protons on tantalum, the observed cross sections are about five times larger than the estimate (10). The discrepancy has been ascribed partly to the inadequacy of the Born approximation, partly to relativistic effects in the electron motion.¹¹⁰ However, the dependence of the cross section on the various parameters is approximately represented by the formula (10). If these x-rays constitute the dominating background, it is of no advantage to employ bombarding energies much higher than those for which the cross section for Coulomb excitation increases approximately as E^4 , because then the signal to noise ratio will begin to decrease. For *E2* excitations, this condition corresponds to $\xi \approx 0.5$, as can be seen from Fig. III.12. From Eqs. (10) and (II C.13), (II C.15), and (II C.17) it also

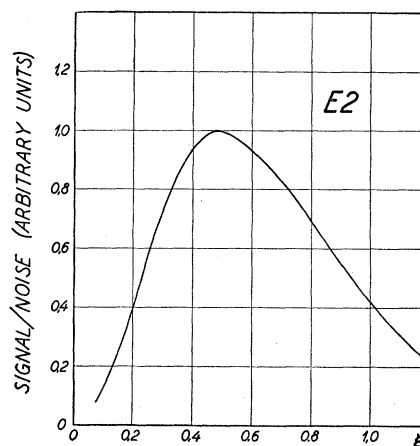


FIG. III.12. Ratio of Coulomb excitation to production of characteristic x-rays. The curve gives the ratio between the theoretical cross sections for *E2* Coulomb excitation and ionization of the *K* shell, as a function of ξ . It is seen that an optimum is obtained for a bombarding energy corresponding to $\xi = 0.5$. For this ξ value the signal to noise is proportional to $(A_1/Z_1)^4$. The same ξ dependence of the signal to noise ratio applies to the background of δ rays in the electron measurements.

¹⁰⁸ W. Henneberg, *Z. Physik* **86**, 592 (1933).

¹⁰⁹ Lewis, Simmons, and Merzbacher, *Phys. Rev.* **91**, 943 (1953); T. Huus and Č. Zupančič, reference 10 (on p. 17 of this reference, read "larger" instead of "smaller").

¹¹⁰ Lewis *et al.* (see reference 109), and D. Jamnik and Č. Zupančič, *Kgl. Danske Videnskab. Selskab Mat. fys. Medd.* **31**, No. 2 (1956).

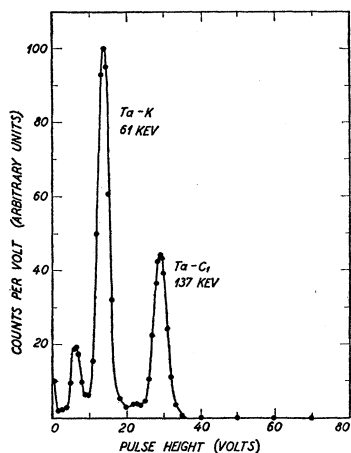


FIG. III.13. X-rays from internal conversion of the nuclear excitation. The pulse-height spectrum, obtained with a crystal, shows the relative strength of the K x-rays and the 137-kev γ ray from tantalum bombarded with 3-Mev α particles [G. M. Temmer and N. P. Heydenburg, Phys. Rev. **93**, 351 (1954)]. No absorbers were employed. The K conversion coefficient for the nuclear radiation is about 1.7, and the major part of the K peak is therefore accounted for by the internal conversion of the γ ray. In the case of proton bombardment the main part of the K x-rays arises from the direct ionization of the K shell (see Fig. III.6).

follows that at the optimum the signal to noise ratio will be proportional to $(A_1/Z_1)^4$, which is 16 times larger for α particles than for protons. Thus, in the α -particle experiments, the observed K x-ray peak is usually small and can sometimes be accounted for nearly exclusively by the effect of the internal conversion of the nuclear radiation (see Fig. III.13).

At γ -ray energies well above the K shell binding energy, one observes in the case of proton bombardment a background radiation which can be ascribed to bremsstrahlung associated with the deflection of the protons in the nuclear field¹¹¹ (see Fig. III.14). The cross section for this process is given in Sec. II E.1, where it is shown that the variation with the bombarding energy and the angle of observation is the same as for the $E1$ Coulomb excitation. If from Eq. (II E.13) one computes the corresponding thick target yield by means of Eq. (7) for the effective target thickness (see Fig. III.9), one finds that the total yield for all angles, multiplied by $E \cdot Z_2^{-5/2}$, to a good approximation is a function of the parameter ξ_0 only. This is confirmed by the measured yields¹⁰³ which furthermore show a ξ dependence in conformity with the theory. Also the predicted absolute intensity seems to be in agreement with the experimental evidence¹¹² within the rather large uncertainties of the available data. However, the possibility exists that there may be additional sources of background radiation,

¹¹¹ Č. Zupančič and T. Huus, Phys. Rev. **94**, 205 (1954).

¹¹² Mark, McClelland, and Goodman, as quoted in reference 81. Also the measurements in reference 111 agree within the experimental error if the correct expression (II E.59) is used rather than the expression (II E.24), which was employed in this reference.

such as, e.g., bremsstrahlung associated with the ionization of the inner atomic shells.

The $E1$ excitation cross sections, and thus also the bremsstrahlung, increase with the bombarding energy in very nearly the same way as do the $E2$ excitation cross sections, except for the very high bombarding energies, where the latter become relatively greater, as illustrated by Fig. III.15. In the region of the spectra where the bremsstrahlung is the important background, one thus obtains a nearly constant signal to noise ratio in the case of an $E2$ excitation decaying to the ground state ($E_x = \Delta E$). The signal equals the noise for a partial $B(E2)$ value (see Sec. IV B) given by

$$\epsilon B(E2) \approx \left(\frac{Z_1}{A_1}\right)^{2/3} \cdot \left(\frac{Z_1 - Z_2}{A_1} \frac{Z_2}{A_2}\right)^2 \left(\frac{Z_2}{85}\right)^{8/3} \\ \times \left(\frac{100}{E_x}\right)^{4/3} \frac{dE_x}{E_x} e^{210^{-48}} \text{ cm}^4, \quad (\text{III.11})$$

where E_x is measured in kev and where dE_x is the resolution of the spectrometer. For a cascade γ ray, the signal-to-noise ratio is usually considerably smaller than for the ground-state decay, and increases with the bombarding energy.

In the case of α -particle bombardment, the bremsstrahlung is very weak due to the fact that the projectiles have nearly the same charge to mass ratio as the target nuclei [see (II E.13)]. The continuous background is indeed also found to be very low in the α -particle measurements, as illustrated by Fig. III.5.

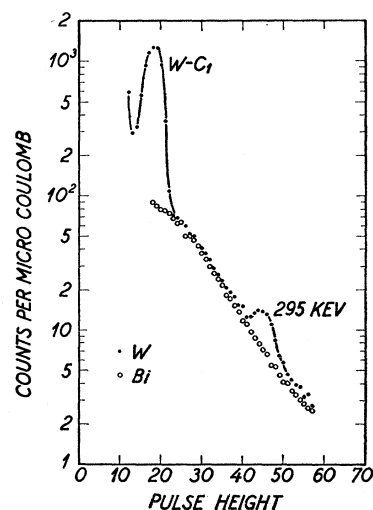


FIG. III.14. Proton bremsstrahlung. The figure shows the pulse-height spectra obtained by bombarding thick targets of natural W and Bi with 4-Mev protons [P. H. Stelson and F. K. McGowan, Phys. Rev. **99**, 112 (1955)]. The C_1 peak is a composite peak corresponding to the first rotational states in the even- A isotopes (see Fig. III.4), whereas the 295-kev peak is assigned to the odd isotope W^{183} . The radiation in the region between the two peaks can be ascribed to proton bremsstrahlung and has practically the same yield for W as for Bi, which give no nuclear radiation.

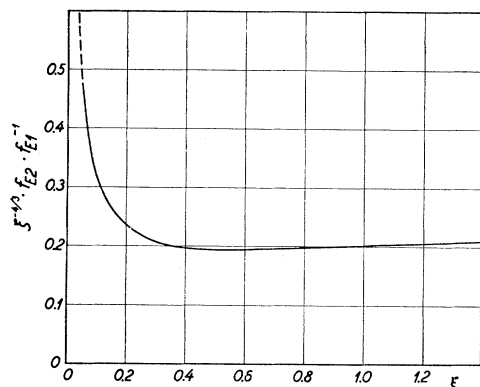


FIG. III.15. Comparison of theoretical cross sections for $E2$ and $E1$ Coulomb excitation. The ordinate is proportional to the ratio of the two cross sections, for the same value of ξ . It is seen that the $E1$ and $E2$ excitation functions are nearly identical over a wide range of ξ values. The excitation function for the dipole bremsstrahlung is the same as for the $E1$ Coulomb excitation (see Sec. II E.1), and the curve therefore also represents the signal-to-noise ratio for $E2$ excitation compared with bremsstrahlung. Thus, high bombarding energies, corresponding to small ξ values, are the most advantageous as far as this type of background radiation is concerned.

III C. Measurements of Conversion Electrons

III C.1. Detection Technique

The study of the internal conversion electrons emitted in the decay of the excited states is to some extent complementary to the γ -ray measurements. For heavy elements and low-energy transitions, an appreciable or even major fraction of the excitations will decay by the emission of such electrons, which may therefore be rather easily detected. Moreover, the derived excitation cross sections may be less sensitive to the value of the conversion coefficients.

Figures III.16–III.20 show some spectra of conversion electrons produced by Coulomb excitation. They have been measured by double-focusing magnetic spectrometers of the wedge-gap type,¹¹³ which are convenient for the purpose. Such spectrometers readily allow the target to be “viewed” from the same side as that turned against the bombarding particles, so that the electrons do not have to penetrate a target support. The comparatively high resolving power is often of particular advantage, because of the great similarity of many of the nuclear spectra (see Figs. III.4 and III.17), and because of the relatively small energy difference between the successive transitions in rotational cascade decays (see Figs. III.5 and III.16).

The fact that conversion electrons from more than one of the atomic shells can be observed makes it possible to obtain additional information by this method. From the measured energy difference between the K and L conversion lines one can unambiguously assign the element in which the excitation has taken

¹¹³ Kofoid-Hansen, Lindhard, and Nielsen, Kgl. Danske Videnskab. Selskab Mat. fys. Medd. 25, No. 16 (1950).

place, and from the intensity ratio between the K and L peaks one obtains information about the multipolarity of the radiation (see Figs. III.16 and III.17). With a somewhat higher resolution it should also be possible to determine the multiplicities from a comparison between the lines of the various L subshells. The theoretical angular distribution coefficients have only been partially evaluated. For $M1$ conversion in the K shell, the estimated anisotropies are rather small (see reference 31).

The strong interaction between the electrons and the target atoms implies that in general thin targets have to be employed in the experiments, if one wants to preserve the high resolution. It is important that the target be homogeneous and that the beam remains focused on the same spot, in particular since the conversion lines often appear on top of a strong continuous background. Thick targets can be used when the electrons have a relatively high energy, so that they can penetrate with sufficient ease the layer corresponding to the effective target thickness for the projectiles.

III C.2. Background Effects

If special precautions are not taken, there may be a considerable background due to the large number of scattered beam particles in the spectrometer, but it is rather easy to trap these by means of an appropriate set of stops. Also the background effects resulting from the presence of light atoms in the target are relatively harmless, since these elements have small conversion coefficients and give negligible contributions to the stopping electrons (see later discussion). This is an advantage when, for practical reasons, one employs

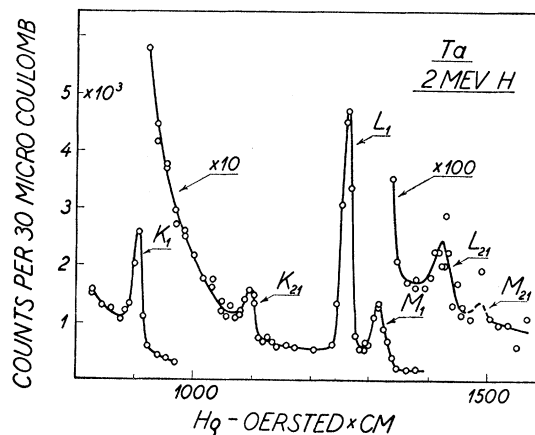


FIG. III.16. Internal conversion electrons from the excitation of tantalum with protons. The figure shows the spectrum of electrons from a 0.3 mg/cm^2 thin Ta target bombarded with 2-Mev protons [T. Huus and J. H. Bjerregaard, Phys. Rev. 92, 1579 (1953)]. The measurements are made with a magnetic spectrometer of the wedge-gap type. The K , L , and M conversion lines with the indices 1 and 21 are assigned to the ground-state transition from the first rotational state of Ta^{181} , and to the cascade transition from the second to the first rotational state, respectively. The large K/L ratios indicate predominantly $M1$ transitions.

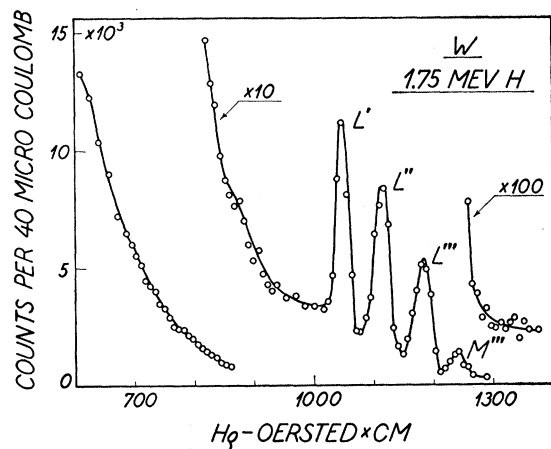


FIG. III.17. Conversion electrons from the excitation of tungsten. The spectrum shows the conversion lines observed in the bombardment of thin targets of natural W by 1.75-Mev protons [T. Huus and J. H. Bjerregaard, Phys. Rev. **92**, 1579 (1953)]. The peaks labeled L' , L'' , and L''' are predominantly due to the L conversion of the ground-state transitions from the first rotational levels in the even- A isotopes W^{182} , W^{184} , and W^{186} . The strong continuous background at the lower momenta is due to the production of stopping electrons. These conceal the presence of the K lines, but the fact that these lines are not clearly visible implies that the K/L ratios are small, in accordance with the $E2$ character of the transitions.

chemical compounds, such as oxides, for the target preparation. Similarly, the target support gives rise to no difficulties if it is made of light materials.

As in the case of the γ -ray measurements, however, atomic processes in the target element under investigation give rise to background effects which cannot be avoided. The maximum energy which a free electron can acquire in a collision with the projectile is less than 20 kev, even for bombarding energies close to the barrier. Collisions with the outer atomic electrons therefore do not give rise to any significant background. The tightly bound electrons, however, may be ejected with much higher energies, and such δ rays constitute the main background radiation in the electron experiments. The observed yield per energy interval can be represented approximately by the semiempirical expression¹¹¹

$$d\sigma \simeq 2Z_1^2 (E_{\text{MeV}}/A_1)^4 Z_2^4 E_\delta^{-7} dE_\delta 10^{-24} \text{ cm}^2, \quad (\text{III.12})$$

where E_δ is the kinetic energy of the ejected electrons measured in kev. The cross section increases very strongly with decreasing E_δ , as is illustrated by Figs. III.16–III.19. The yield of the δ rays increases with Z_2 in contrast to the total ionization cross sections [see (10)]. It is therefore difficult to measure the conversion electrons from the decay of the first excited state of the very heavy elements, and for this reason the method has been applied mostly to the study of somewhat lighter nuclei.

The cross section (12) depends on the bombarding energy and the type of projectile in the same way as the cross section (10), and thus the largest signal to

noise ratio for $E2$ excitations is again obtained for $\xi \simeq 0.5$ (see Fig. III.12). For bombarding conditions corresponding to this ξ value, the signal equals the noise, as represented by (12), for a partial $B(E2)$ value (see Sec. IV B) given by

$$\epsilon B(E2) \simeq \left(\frac{Z_1}{A_1}\right)^4 \left(\frac{Z_2}{85}\right)^8 \left(\frac{100}{\Delta E}\right)^4 \times \frac{dE_\delta}{E_\delta} \left(\frac{\Delta E}{E_\delta}\right)^6 e^2 10^{-48} \text{ cm}^4, \quad (\text{III.13})$$

where the excitation energy ΔE is measured in kev, and where E_δ equals the energy of the observed conversion electrons, also measured in kev. It is evident from (13) that the B values corresponding to the noise are the smallest for the heavier projectiles. Consequently, it sometimes proves to be an advantage to use deuterons rather than protons for the excitation of the lowest states (see Fig. III.19), even though the background of penetrating radiation, which is always generated in deuteron bombardments, gives rise to some difficulties. If a sufficiently high acceleration voltage is available, the best results are obtained with α particles (see Figs. III.18 and III.20).

In estimating thick target yields of ejected electrons by means of Eq. (12), it must be taken into account that they come only from a rather thin surface layer. For heavier elements, the effective thickness of this layer is approximately given by¹¹⁴

$$t_\infty \simeq (E_\delta/50)^2 \text{ mg/cm}^2, \quad (\text{III.14})$$

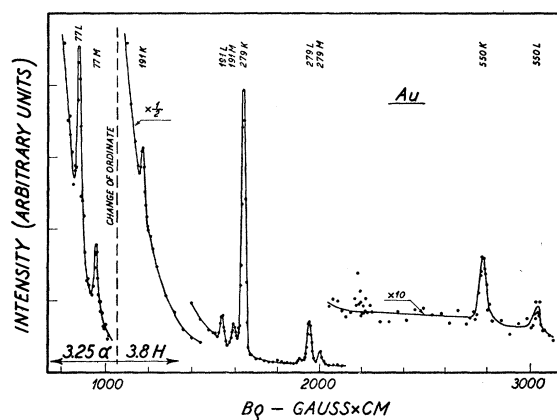


FIG. III.18. Conversion electrons from the excitation of gold. For the assignment of the observed transitions, confer the level scheme in Table IV.2. For the low electron energies the best results are obtained with α particles, and this part of the curve is reproduced from E. M. Bernstein and H. W. Lewis [Phys. Rev. **100**, 1345 (1955)]. For the high energies, the spectrum has been obtained by bombardment with protons. This part of the spectrum represents results obtained by M. S. Moore and C. M. Class (private communication).

¹¹⁴ See Huus, Bjerregaard, and Elbek, Kgl. Danske Videnskab. Selskab Mat. fys. Medd. **30**, No. 17 (1956).

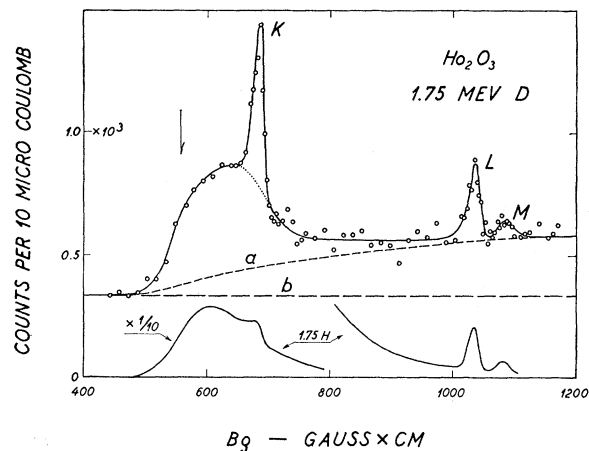


FIG. III.19. Conversion electrons from the excitation of holmium. The observed K , L , and M lines [Huus, Bjerregaard, and Elbek, Kgl. Danske Videnskab. Selskab Mat. fys. Medd. **30**, No. 17 (1956)], are associated with the first rotational state in Ho^{165} . The excitations were produced by the bombardment with 1.75-Mev deuterons which give a relatively small background of stopping electrons (dotted line), as is evident from the comparison with the curve for protons of the same energy, which is also shown in the figure. The arrow marks the cutoff due to the counter window. The dashed line a indicates the background contributions from the generation of β activities and the production of neutrons. The contribution from the latter effect alone is indicated by the dashed line b .

where E_s represents the energy, in kev, with which the electrons emerge from the surface.

In principle, the ejected electrons can be used for calibration of the target thickness, since the rate of their production depends in a smooth way on the atomic number of the target material. However, if the target thickness is not considerably smaller than t_∞ , the calibration will be dependent on the homogeneity of the targets. The calibrations may therefore usually be performed more reliably by means of the intensity of the elastically scattered projectiles which are not so easily influenced by the structure of the target.

III D. Measurements of Inelastically Scattered Projectiles

Perhaps the most straightforward method of detection in the Coulomb excitation experiments is to measure directly the inelastically scattered projectiles. This method has the special advantage that each particle group corresponds to the excitation of a definite level, and that the yield is a direct measure of the cross section for the excitation, irrespective of the mode of decay. An example of a spectrum of inelastically scattered protons in a heavy element is shown in Fig. III.21. The measurements have been performed by means of a magnetic spectrometer of high resolving power. Because of the correspondingly small transmission, the particles were detected by means of a photographic plate.

A high resolution can only be obtained with thin targets, and a thickness determination must therefore

be included in the measurements. The elastic scattering offers a convenient means for yield calibrations, and in the present case it is even not necessary to know the transmission of the spectrometer, since the solid angle is practically the same for two lines which are close to each other. However, a comparison cannot be made in a single exposure due to the widely different intensities and will, consequently, be dependent on the calibration of a beam integrator. The uncertainties introduced in this way are not of any great significance, in particular if approximately the same currents are employed in the two exposures. One thus directly compares the cross sections for Coulomb excitation with the Rutherford cross section, and the reduced nuclear transition probabilities $B(\lambda)$ derived from such a procedure should therefore be very reliable. At present, the accuracy of the analysis is limited to some extent by the fact that the differential excitation cross sections have only been calculated theoretically in the classical approximation (see Sec. II C.3).

The large cross sections for elastic scattering imply that even extremely small contaminations in the targets give rise to peaks in the spectra (see Fig. III.21), but these lines can be identified by the way in which they move with respect to the main Rutherford line, when the bombarding energy or the angle of observation is changed. Elastic scattering from the target nuclei will, however, give rise to a continuous background if the beam employed for the bombardment is not completely free of energy degraded particles. Even if the beam is passed through a magnetic analyzer before it strikes the target, there may still be a significant background due to scattering from stop edges etc. For this reason, it is in general preferable to observe in the backward directions, where the elastic scattering relative to the Coulomb excitations is the smallest. The ratio of the cross sections for $E2$ Coulomb excitation

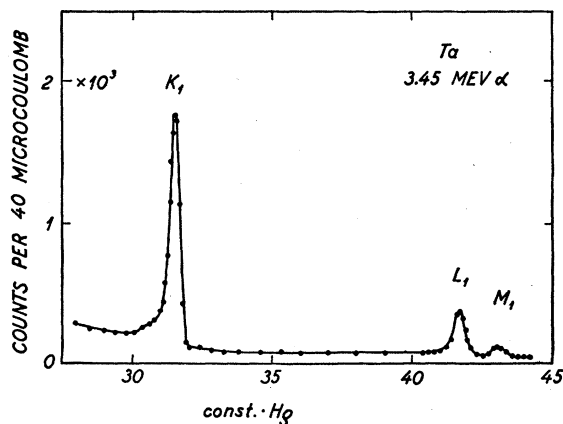


FIG. III.20. Conversion electrons from the excitation of tantalum with α particles. The spectrum shows the conversion lines from the decay of the first rotational excitation of Ta^{181} [E. M. Bernstein and H. W. Lewis, Phys. Rev. **100**, 1345 (1955)]. The background of stopping electrons is seen to be much smaller than in the case of proton bombardments (see Fig. III.16).

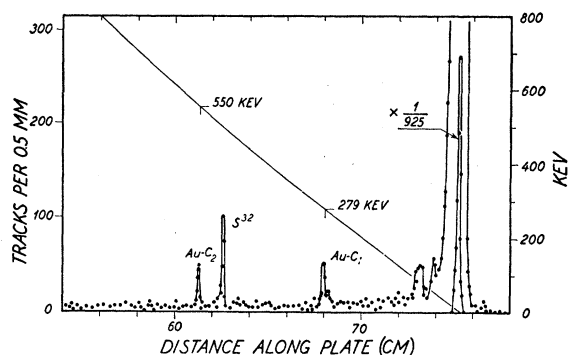


FIG. III.21. Spectrum of protons scattered from gold. The figure shows the energy spectrum of protons scattered from a 0.1 mg/cm^2 thin Au target (B. Elbek, and C. K. Bockelman, to appear in Phys. Rev.). The measurements were made with a magnetic spectrometer of high resolving power, and the particles were detected by means of a photographic plate. The exposure corresponded to approximately 4 millicoulomb. The angle of observation was 130° and the bombarding energy 6 Mev. The energy intervals between the inelastic groups and the strong peak from elastic scattering can be obtained from the calibration curve shown in the figure. The two strongly excited states in Au^{197} correspond to the peaks C_1 and C_2 , and there is also an indication of the more weakly excited 268-kev level (see Table IV.2). The peak labeled S^{32} is due to elastic scattering from a contamination of sulfur.

and elastic scattering is proportional to $A_1 Z_1^{-2} E^3$, and it is therefore advantageous to employ high bombarding energies. For energies of the order of the Coulomb barrier, the signal to noise increases as $A_1 Z_1$.

The energy region over which the inelastic groups can be observed extends from the elastic peak down to the continuous background from the target support. This free region is related to the recoil energy; the extension increases with the mass and energy of the projectile and with the scattering angle, and decreases with increasing mass of the nuclei in the target support. Light elements in the target support may, on the other hand, give rise to nuclear reactions with the emission of charged particles. Aluminum has been used as a support in experiments with protons, at energies about 6 Mev.¹¹⁵

Because of the great strength of the elastic scattering, it is desirable that the spectrometer gives a very sharp image, but even then the elastic peak will always have a significant low-energy tail due to the energy straggling in the target. In the study of the low excitation energies, it is therefore necessary to employ very thin targets, even when the observations are made on particles which have penetrated the target and, thus, on the average have lost the same energy.

In addition to the above-mentioned contributions to the background radiation there will, just as for the γ rays and the conversion electrons, be contributions from atomic processes in the target. Thus, the considerations made earlier with regard to the effect of the bremsstrahlung also apply here, with the supplementary remark that the backward angles of observation favor the

¹¹⁵ B. Elbek (to be published).

$E2$ Coulomb excitations as compared to the $E1$ bremsstrahlung, for which the angular distribution is given by the functions $df_{E1}(\vartheta)$ (see Fig. II.7). The processes leading to the ionization of the inner atomic shells, which give rise to an important background in the measurements on the decay radiations (see foregoing), are of less importance in the detection of the inelastically scattered projectiles, since the angular distribution of the particles responsible for the ionization is expected to be rather strongly peaked in the forward direction.

CHAPTER IV. NUCLEAR DATA OBTAINED FROM COULOMB EXCITATION

In this chapter, we discuss the analysis of the experimental results on Coulomb excitation in terms of the theory given in Chapter II. This analysis confirms the accuracy of the theoretical description of the excitation process and leads to the determination of the nuclear parameters involved in the theory. The chapter also contains a compilation of the experimental results that have been obtained from Coulomb excitation investigations.

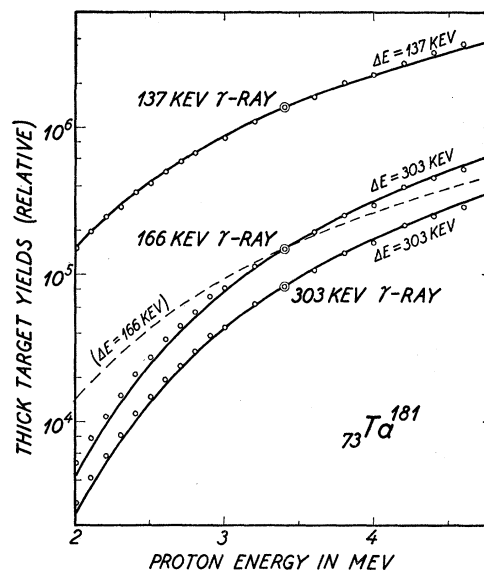


FIG. IV.1. Excitation functions for levels in Ta^{181} . The figure gives the thick target yield of the three γ rays observed in proton bombardment of Ta^{181} . The experimental data are taken from P. H. Stelson and F. K. McGowan, Phys. Rev. **99**, 112 (1955). The full drawn curves give the theoretical energy dependence of the yield, assuming $E2$ Coulomb excitation [see (II C.15) and (III.6) and Figs. II.5 and 6 and III.9 and 10]. The stopping power has been assumed to vary as $E^{-0.55}$, and the curves are normalized to the experimental value at 3.4 Mev, as indicated by the large circles. The theoretical curves are rather sensitive to the excitation energy ΔE . It is seen that the 137 kev and 303 kev γ rays have excitation functions with $\Delta E = E_\gamma$ and thus represent ground-state transitions, while the 166-kev γ ray has an excitation function with $\Delta E = 303$ kev and is thus associated with a cascade decay of a level at this energy (see Fig. V.7). For comparison, the excitation function corresponding to $\Delta E = 166$ kev is drawn with a broken curve. The contribution to the 137-kev radiation resulting from the 303-kev excitation decaying by cascade has not been subtracted from the experimental yield. The correction amounts to about 10% at the highest bombarding energies employed.

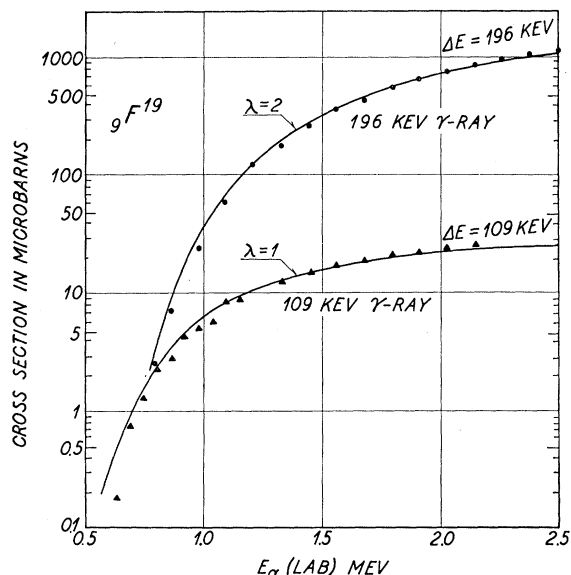


FIG. IV.2. Excitation function for levels in F^{19} . The figure shows the measured excitation cross sections for the 109-kev and 196-kev γ rays observed in α bombardment of a thin target of CaF_2 [Sherr, Li, and Christy, *Phys. Rev.* **96**, 1258 (1954)]. The theoretical excitation functions given by the full drawn curves are obtained from (II C.15) and Figs. II.4, 5, and 6, by assuming $E1$ excitation with $\Delta E=109$ kev for the 109-kev γ ray, and $E2$ excitation with $\Delta E=196$ kev for the 196-kev γ ray. The excitation functions are not sensitive to the multipole order, but the assumed values of λ are those indicated by other experimental evidence (see the references in Table IV.2). The theoretical curves are normalized to the experimental cross sections at $E_\alpha=1.55$ Mev.

IV A. Analysis of Experimental Data

IV A.1. Excitation Function and Relative Yields

The theoretical expressions for the Coulomb excitation yields as a function of the bombarding energy are independent of the nuclear structure. It is thus possible with considerable certainty to identify an observed radiation as resulting from Coulomb excitation by a measurement of its yield function. Examples of well-measured yield functions are given in Figs. IV.1 and IV.2. It is seen that the theoretical expressions reproduce the observed relative yields over a range in which the cross sections vary by several orders of magnitude.

The yield function depends on the multipole order λ and the excitation energy ΔE , and may thus be used to determine these two quantities. The sensitivity of the yield curve to the excitation energy, ΔE , may often be exploited to decide whether an observed radiation represents a ground-state decay or a cascade radiation from a higher lying state. As an example, Fig. IV.1 clearly shows that the observed 166-kev gamma ray in Ta^{181} originates from an excited state with an energy of about 303 kev. This fact is also directly confirmed by the observation of coincidences between the 166-kev and 137-kev γ rays (see Table IV.2). Similarly, the yield of the 110-kev radiation from Tm^{169} has been shown to indicate that this transition results from the excitation

of a 119-kev level decaying to a 9-kev state (see Table IV.2).

The possibility of determining the multipole order of the excitation process on the basis of the yield curve is illustrated in Fig. IV.3. While it would be rather easy to recognize higher multipole orders ($\lambda=3$ or 4), it is usually difficult to distinguish $E2$ from $E1$ on the basis of the excitation function.^{115a} These two multipole transitions have very nearly parallel yield functions, except for small ξ values corresponding to high bombarding energies or low excitation energies (see Fig. III.15).

An alternative method for determining the multipole order of the excitation is provided by a comparison of the yield for two different bombarding particles. If, for instance, one chooses bombarding energies corresponding to the same value of ξ , the cross section for an excitation of order $E\lambda$ is, to a first approximation, proportional to $Z_1^2(A_1/Z_1)^{2\lambda/3}$ [see (II C.13), (II C.15), and (II C.16)]. Thus, the ratio of the cross sections for proton and alpha-particle bombardments would differ for $E1$ and $E2$ excitation by about a factor of 1.6. This method for determining λ has been used, for example, to establish the $E2$ character of the 446-kev transition in Na^{23} (see Fig. IV.7) and of the 100-kev transition in W^{182} (see Table IV.2).

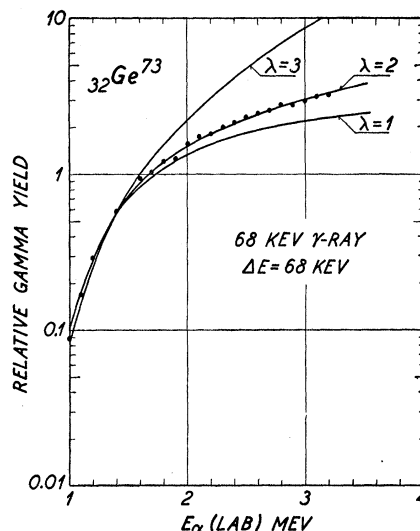


FIG. IV.3. Dependence of excitation function on multipole order. The figure shows the thin target yield of the 68 kev γ ray observed in α bombardment of Ge^{73} [G. M. Temmer and N. P. Heydenburg, *Phys. Rev.* **96**, 426 (1954)]. The full drawn curves give the theoretical excitation functions for $E1$, $E2$, and $E3$ Coulomb excitation, assuming $\Delta E=68$ kev [see (II C.15) and Fig. II.4]. The curves are normalized to the experimental value at 1.4 Mev. The possibility of distinguishing in the present case between $E1$ and $E2$ excitation on the basis of the yield function is associated with the rather small ξ values for the excitation ($\xi=0.14$ for $E_\alpha=3$ Mev).

^{115a} Note added in proof.—Recently, an $E3$ excitation process, leading to the 40 kev isomeric level in Rh^{103} , has been identified as of $E3$ type on the basis of the measured excitation function (G. A. Jones and W. R. Phillips, presented at the Amsterdam Conference on Nuclear Reactions, July, 1956).

IV A.2. Angular Distribution of Decay Radiation

The angular distribution of the radiation following Coulomb excitation provides information on the spins and parities of the states involved as well as on the multipole order of the excitation mode and the decay.

Extensive angular distribution measurements have been made¹⁷ of the γ rays from even-even nuclei which should follow the unique $0(E2)2(E2)0$ correlation which is given by [see (II C.29) and Table II.11]

$$W(\vartheta) = 1 + 0.357a_2E^2P_2(\cos\vartheta) + 1.143a_4E^2P_4(\cos\vartheta), \quad (\text{IV.1})$$

where the coefficients a_2 and a_4 are characteristic of the Coulomb excitation process. The observed distributions have been analyzed to yield experimental values of these coefficients which are seen in Figs. IV.4 and IV.5 to be in approximate agreement with the theoretical values given in Fig. II.8. It seems that the small differences between the experimental and theoretical values are not outside the experimental uncertainties.

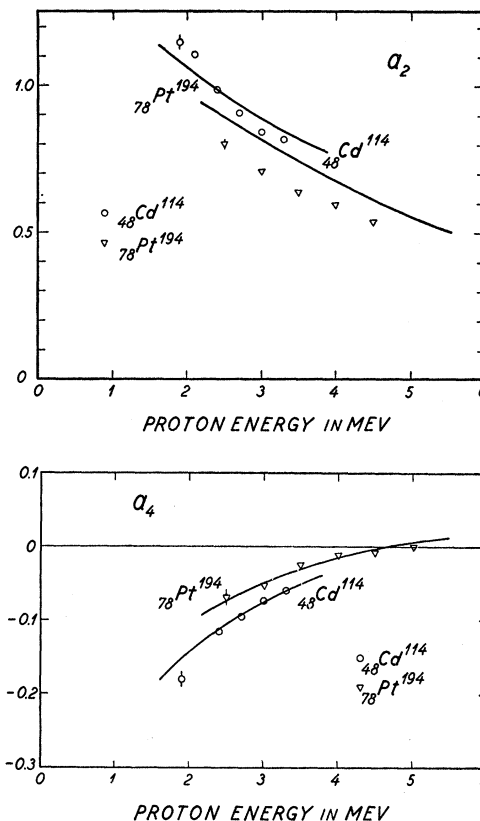
As discussed in Sec. II C.5, there may be in certain cases important effects on the angular distribution resulting from the precession of the nuclear spin in the excited state. In the present cases, however, these effects are expected to be very small due to the short lifetimes of the states involved [$\tau_{\frac{3}{2}} \approx 1 \cdot 10^{-11}$ sec for Cd^{114} and $\tau_{\frac{3}{2}} \approx 4 \cdot 10^{-11}$ sec for Pt^{194} , as determined from the absolute yield of the Coulomb excitation of these levels (see Sec. IV A.4 and Table IV.2)]. Moreover, for the excited states involved, the static quadrupole moments are expected to be small, even though the transition moments are rather large (see Sec. V C.2). Also the higher order effects in the excitation process are expected to be small in the present circumstances (see Sec. II D.2).¹¹⁶

Besides these investigations of the even-even nuclei, a number of measurements of the angular distribution of the γ rays from odd- A nuclei have also been made (see, e.g., Fig. III.8). The analysis of these experiments by means of the theoretical expressions in Sec. II C.4 has yielded the spin determinations and multipole assignments listed in Table IV.2.

In the frequently occurring case of an $E2$ excitation followed by a mixed $M1+E2$ decay, there may often be an ambiguity in the mixing ratio δ as determined from the angular distribution of the γ rays. This ambiguity may be removed by a measurement of the polarization of the γ quantum¹¹⁷ [see (II A.78a)].

¹¹⁶ It has been suggested (reference 17) that the multiple scattering of the projectile in the target may give rise to an important correction to the measured angular distribution of the γ rays. However, this effect appears to be very small under most experimental conditions (see the comments in Sec. III B.2).

¹¹⁷ P. H. Stelson and F. K. McGowan, Bull. Am. Phys. Soc. Ser. II, I, 164 (1956).



FIGS. IV.4 and IV.5. Angular distribution coefficients a_2 and a_4 . The angular distribution of the γ rays following $E2$ Coulomb excitation depends on the excitation process only through the coefficients a_2 and a_4 [see (II C.29)]. The figures plot the experimentally determined a_2 and a_4 coefficients as a function of the proton bombarding energy; the data is taken from the thick target measurements by F. K. McGowan and P. H. Stelson [Phys. Rev. **99**, 127 (1955) and unpublished data, quoted in Goldstein *et al.* (Phys. Rev. **100**, 436 (1955))]. The full drawn curves give the theoretical thick target values for a_2 and a_4 obtained from Fig. II.8 by employing the thick target correction described in Sec. III B.2; the values of δE_2 involved in this correction are taken from Fig. III.9.

IV A.3. Angular Distribution of Inelastically Scattered Particles

The angular distribution of inelastically scattered particles depends only on the multipole order of the excitation, but not on the spins of the states involved. The measured angular distributions of the inelastically scattered protons from Au^{197} are compared in Fig. IV.6 with the theoretical distributions for $\lambda=1$ and 2, obtained in the classical approximation (see Sec. II C.3). The exact quantum-mechanical angular distributions have not so far been evaluated.

IV A.4. Absolute Yields

From the measured absolute cross sections one may derive the reduced transition probability $B(E\lambda)$ by means of the theoretical expressions in Sec. II C.2, and the values obtained in this manner are listed in Table

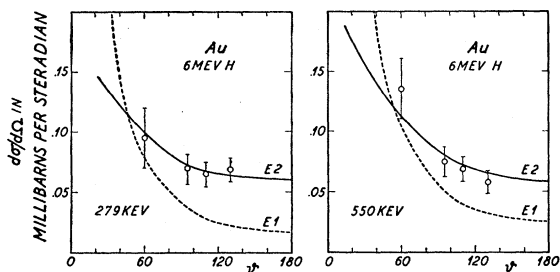


FIG. IV.6. Angular distribution of inelastically scattered protons from Au^{197} . The figure shows the differential cross sections in millibarns per steradian for excitation of the 279-kev and 550-kev levels in Au^{197} with protons of 6 Mev (B. Elbek and C. K. Bockelmann, to appear in Phys. Rev.) The full drawn curves give the theoretical cross sections obtained from (II C.15) and Fig. II.7, assuming $E2$ excitation (see also Sec. II C.3); the $B(E2)$ values are determined so as to give the best fit to the experimental points. The measured angular dependence of the cross sections agrees rather well with the classical theory (the value of η in the present experiment is about 5) and also the absolute values of the cross sections are in approximate agreement with those expected on the basis of the γ -ray yield measurements (see the $B(E2)$ values in Table IV.2). The angular dependence of the cross sections is rather sensitive to the multipole order of the excitation process. This is illustrated by the broken curves which give the theoretical $E1$ differential cross sections, normalized to the same total cross section as the $E2$ curves.

IV.2. The reduced transition probability also determines the lifetime for the inverse radiative transition of order $E\lambda$ [see (II A.56) and (II A.57)]. One thus obtains for the transition probability for γ emission from the excited state I_f to the ground state I_i

$$T_\gamma(E1; I_f \rightarrow I_i) = 1.59 \times 10^8 (\Delta E)^3 \times B(E1; I_i \rightarrow I_f) \frac{2I_i + 1}{2I_f + 1} \text{ sec}^{-1}, \quad (\text{IV.2})$$

and

$$T_\gamma(E2; I_f \rightarrow I_i) = 1.23 \times 10^{-2} (\Delta E)^5 \times B(E2; I_i \rightarrow I_f) \frac{2I_i + 1}{2I_f + 1} \text{ sec}^{-1}, \quad (\text{IV.3})$$

where ΔE is measured in kev and $B(E\lambda)$ in units of $e^2 (10^{-24} \text{ cm}^2)^\lambda$.

In a number of cases, measurements are available of both the cross section for Coulomb excitation and the corresponding radiative lifetime, thus providing two independent measurements of $B(E\lambda)$. The comparison of these determinations is contained in Table IV.1; the agreement appears in all cases to be within the experimental error.

In many cases, Coulomb excited states may decay in several modes, either to the ground state with a mixed multipole transition or by a cascade to some other nuclear level. In these cases, measurements of multipole mixtures and branching ratios together with the absolute cross section for Coulomb excitation provide a determination of the absolute transition probabilities for the alternative modes. In this way, a number of $M1$ decay probabilities have been determined (see Table

V.5). In a similar manner, it has been possible to determine the transition probabilities for certain $E1$ transitions representing alternative modes of decay for levels in Se and Ag populated by $E2$ Coulomb excitation (see Table IV.2 and the references given there).

IV A.5. Coulomb Excitation at Higher Bombarding Energies

The above analysis refers to experimental arrangements in which the bombarding energy is sufficiently low that penetration into the nucleus can be neglected. The electromagnetic interaction is then the only mechanism for exciting the nucleus.

Already for energies appreciably below the Coulomb barrier, however, the projectile may penetrate to the

TABLE IV.1. Comparison of lifetime determinations with Coulomb excitation yield measurements. The table lists, in columns two and three, the spins of the nuclear ground state, I_0 , and of the excited state, I . The measured half-lives, $\tau_{1/2}$, listed in column five, are taken from the review by A. W. Sunyar, Phys. Rev. **98**, 653 (1955) and the additional references listed below. The number in parentheses in column five gives the power of ten for the observed lifetime measured in seconds. The half-lives yield the reduced transition probabilities $B(E2; I_0 \rightarrow I)$ by means of (IV.3) and the relation $(\tau_{1/2})^{-1} = 1.4 T_\gamma(E2) (1 + \delta - 2) (1 + \alpha)$ where $T_\gamma(E2)$ is the transition probability per second for $E2$ γ radiation, while δ^2 is the ratio of $E2$ to $M1$ γ -ray intensity, and α is the total conversion coefficient. The values of δ and α are taken from column six of Table IV.2. The $B(E2)$ values obtained from lifetime determinations are given in column six in units of $e^2 \times 10^{-48} \text{ cm}^4$, and are compared with the corresponding quantities obtained from the Coulomb excitation cross sections (see column seven of Table IV.2).

A similar comparison as for the $E2$ transitions in the table can be made for the 110-kev $E1$ transition in F^{19} ($I_0 = 1/2, I = 1/2$). The measured half-life of 7×10^{-10} sec yields by means of (IV.2) the value $4.8 \times 10^{-30} e^2 \text{ cm}^2$, while the Coulomb excitation cross section gives $B(E1) = 2.3 \times 10^{-30} e^2 \text{ cm}^2$.

Additional references for $\tau_{1/2}$: Thirion, Barnes, and Lauritsen, Phys. Rev. **94**, 1076 (1954) (F^{19} ; 110-kev transition); Fiehrer, Lehmann, Leveque, and Pick, Compt. rend. **241**, 1746 (1955) (F^{19} ; 197-kev transition); H. Schopper, Z. Physik **144**, 476 (1956) (V^{53}); F. R. Metzger, Phys. Rev. **101**, 286 (1956) (Ge^{72} and Ge^{74}); F. R. Metzger, Phys. Rev. **98**, 200 (1955) (Hg^{202}); H. deWaard, Phys. Rev. **99**, 1045 (1955), and R. E. Azuma and G. M. Lewis, Phil. Mag. **46**, 1034 (1955) (Tl^{203}); T. R. Gerholm (private communication) (Pb^{207}).

Nucleus	I_0	I	ΔE (kev)	$\tau_{1/2}$ (sec)	Lifetime excitation $B(E2)$	Coulomb excitation $B(E2)$
$^9\text{F}^{19}$	1/2	5/2	197	6(-8)	0.01	0.003
$^{23}\text{V}^{51}$	7/2	5/2	325	1.0(-10)	0.008	0.006
$^{32}\text{Ge}^{72}$	0	2	835	3.2(-12)	0.19	0.26
$^{32}\text{Ge}^{74}$	0	2	595	1.3(-11)	0.28	0.30
$^{62}\text{Sm}^{152}$	0	2	122	1.4(-9)	3.3	3.1
$^{64}\text{Gd}^{154}$	0	2	123	1.2(-9)	3.6	4.5
$^{68}\text{Er}^{166}$	0	2	81	1.7(-9)	5.7	6.8 ^b
$^{72}\text{Hf}^{176}$	0	2	89	1.35(-9)	5.3	6.0
$^{74}\text{Hf}^{180}$	0	2	93	1.4(-9)	4.9	5.0
$^{74}\text{W}^{182}$	0	2	100	1.27(-9)	4.3	5.6
$^{80}\text{Hg}^{198}$	0	2	411	2.1(-11)	1.1	0.8
$^{80}\text{Hg}^{199}$	1/2	5/2	159	2.4(-9)	0.35	0.26
$^{80}\text{Hg}^{202}$	0	2	439	2.2(-11)	0.8	0.5
$^{81}\text{Tl}^{203}$	1/2	3/2	280	1.4(-10) ^a	0.28	0.12
$^{82}\text{Pb}^{207}$	1/2	5/2	569	9(-11)	0.031	0.028

^a This value, obtained from a direct measurement of the delay, differs considerably from the value deduced from the resonance scattering cross section [F. R. Metzger and W. B. Todd, Phys. Rev. **95**, 627(A) (1954)].

^b The unresolved transitions from all the even erbium isotopes are assumed to have the same $B(E2)$ value.

nuclear surface and thus initiate proper nuclear reactions. Estimates of the expected reaction cross sections are given in Fig. III.1. In light elements, the radiation resulting from such nuclear reactions is characterized by a resonant structure which is superimposed on the more slowly varying yield of the Coulomb excitation. In heavier elements, the level spacing of the compound nucleus is usually below the energy resolution of the incident beam, and in addition the levels may overlap due to the effect of neutron emission.

Even when the average cross section for compound nucleus formation exceeds the Coulomb excitation cross section, it may still be possible to observe the latter, since the compound nucleus will usually decay preferentially through other channels, such as (p,n) , (α,n) , (α,p) , and also the elastic channel (see Fig. IV.8).

Moreover, for light elements where the resonance structure can be resolved, the cross section between resonances may result mainly from Coulomb excitation, and a quantitative determination of the Coulomb excitation yield may then be possible (see Fig. IV.7). In this connection it is significant that the interference between Coulomb excitation and the contribution of a particular resonance is confined to a few angular momenta of the projectile, while the total Coulomb excitation yield results from many angular momenta.

For bombarding energies equal to, or greater than, the Coulomb barrier, the compound nucleus formation takes place with a large probability. Still, the observed inelastic scattering leading to the low-lying states of the target, appears to result from a direct interaction, since the yields greatly exceed those expected from the decay

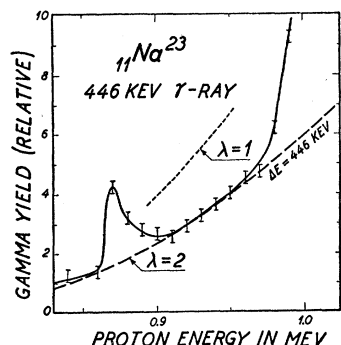


FIG. IV.7. Coulomb excitation of sodium by protons. The figure shows the yield of the 446-kev γ ray from a thin target of NaCl bombarded with protons. [G. M. Temmer and N. P. Heydenburg, Phys. Rev. **98**, 1198(A) (1955) and private communication]. Between the resonances due to compound nucleus formation one observes a smoothly rising background yield which may be ascribed to Coulomb excitation. It is possible to determine the multipole order of the Coulomb excitation by comparing with the yield observed in the excitation with α particles (loc. cit.). The dashed curves correspond to the cross sections expected for $\lambda=1$ and 2 on the basis of the observed cross section for excitation with α particles (see II C.15). The close agreement of the measured cross section with the theoretical curve for $E2$ excitation also confirms that the yield away from resonances is primarily due to Coulomb excitation.

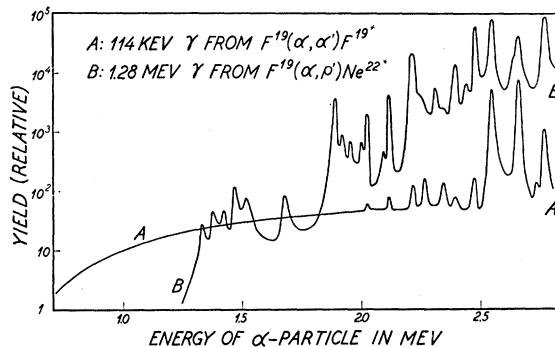


FIG. IV.8. Gamma rays from Coulomb excitation and compound nucleus formation in F^{19} bombarded with α particles. The figure shows the thin target yields of the 114-kev γ ray from the first excited state in F^{19} and the 1.28-Mev γ ray from the first excited state of Ne^{22} formed by an (α, β') process on F^{19} [Sherr, Li, and Christy, Phys. Rev. **96**, 1258 (1954)]. For bombarding energies below 1.2 Mev, the penetration of the α particle through the Coulomb barrier is very small (see Fig. III.1) and the cross section for compound nucleus formation is small compared to that for Coulomb excitation. With increasing bombarding energy, σ_{comp} increases rapidly and soon becomes larger than σ_{coul} . However, even for $E_\alpha \sim 2$ Mev, at which energy the average value of σ_{comp} is an order of magnitude larger than σ_{coul} , the yield of the 114-kev γ ray is only very little affected by the compound nucleus formation, since the probability that the compound nucleus decays by inelastic α -emission is small. Finally, for $E_\alpha \gtrsim 2.5$ Mev, the Coulomb excitation yield of the 114-kev γ ray is overshadowed by the resonance yield from compound nucleus formation.

of the compound nucleus.¹¹⁸ In these reactions one expects, however, besides the Coulomb interaction, an important contribution to the direct excitation from the interaction with the nuclear field. Moreover, the change of the projectile orbit and of the electric multipole fields when the projectile is inside the nucleus imply an essential modification of the calculations given in Chapter II (see, e.g., Sec. II E.3).

In some cases, it may be possible to separate the simple Coulomb excitation effect resulting from the particles which have not passed through the nucleus, by observing the inelastically scattered particles in the forward directions. Thus, if $\eta \gg 1$, so that the projectile orbits can be described in the classical approximation, the particles passing outside the nucleus will be scattered into angles less than a critical value ϑ_c . This angle depends on the ratio

$$x = \frac{E}{E_B}, \quad (IV.4)$$

between the projectile energy E and the Coulomb barrier E_B [see (III.1)] and is given by [see (II A.22) and (II A.23)]

$$\begin{aligned} \vartheta_c &= 2 \sin^{-1} \left(\frac{1}{2x-1} \right) \\ &\approx \frac{115^\circ}{2x-1} \quad (\text{for } x \gtrsim 2). \end{aligned} \quad (IV.5)$$

¹¹⁸ See, e.g., P. C. Gugelot, Phys. Rev. **93**, 425 (1954); Schrank, Gugelot, and Dayton, Phys. Rev. **96**, 1156 (1954), and also the review by H. McManus, Brookhaven report On the Statistical Aspects of the Nucleus, 1955.

If the Coulomb excitation populates several levels in the same nucleus, the radiation from the lower levels may partly result from a cascade decay of a higher level. In the determination of $\epsilon B(E2)$, it is then necessary to establish what part of the measured radiation is due to the direct excitation of the radiating level. In most cases, however, the correction for cascade is small compared with the accuracy of the yield determinations, and we have not attempted to include it except when it has already been taken into account by the original experimenters.

When the isotope responsible for the observed radiation has not been assigned, $\epsilon B(E2)$ has been calculated assuming 100% abundance for the responsible isotope. Where no yield determination is available, only the detected radiation is listed in this column.

Column V. Comments

This column contains a brief summary of other information on the observed levels, which has been obtained from Coulomb excitation. The abbreviations employed are

ex.func. $\Delta E=127$ The measured yield as a function of energy has been found to be consistent with Coulomb excitation with an excitation energy ΔE equal to the listed value, assuming multipole order $E2$. If the yield function also determines the multipole order of the excitation process, the notation $\lambda=2$ is added. While the excitation function is rather sensitive to the excitation energy, it often does not distinguish between $E1$ and $E2$ transitions (see Sec. IV A.1).

sep.iso. The isotope assignment has been established by Coulomb excitation experiments, employing enriched isotopes.

$\gamma(\theta)$ The angular distribution of the γ radiation has been measured. The spins and multipolarity of the transitions which have been deduced from the observed angular distribution are indicated by $I_i(E\lambda)I_f(L)I_{ff}$, where I_i , I_f , and I_{ff} are the spins of the initial state, Coulomb excited state, and final state, respectively, while $E\lambda$ and L are the multipolarity of the Coulomb excitation process and of the subsequent γ radiation, respectively.

δ The ratio of the amplitudes of $E2$ and $M1$ γ radiation in a mixed transition. For the definition of the sign of δ , see Sec. II A.4 and Table II.11.

$\sigma(p):\sigma(\alpha)$ gives $\lambda=2$. The measured ratio of the Coulomb excitation cross sections for protons and α particles implies $E2$ excitation.

$\alpha_K, K/L$ The K conversion coefficient α_K and K/L ratio measured in Coulomb excitation experiments. $\gamma(100)-\gamma(200)$ coinc. The two indicated γ rays are found to be in coincidence.

$\gamma(100):\gamma(200)$ The value listed is the measured intensity ratio of two γ rays assumed to originate from the same excited level.

Column VI. Multipole Order and Conversion Coefficients of the Decay Radiation

For even-even nuclei, the excited states are assumed to be of $(2+)$ character and to decay by pure $E2$ radiation. For odd- A nuclei, the decays are often of mixed $M1$ and $E2$ type, and the column lists the percentage of the γ decays which are of $E2$ type; the information is obtained from the angular correlation measurements or K/L ratios. In a number of cases, the transitions can be classified as $\Delta I=2$, and thus as pure $E2$ decays, on the basis of the rotational interpretation of the levels involved (see column VIII). For some of the rotational transitions with $\Delta I=1$, where no other evidence is available, the multipole mixture has been calculated from observed branching ratios [(V.10 and V.17); see also Fig. V.7]. In these cases the $E2$ percentage is listed in parenthesis.

In addition, the column gives the conversion coefficients employed in the derivation of the $B(E2)$ values in column VII. The listed values for the K shell conversion coefficients α_K for $Z<50$ are taken from the calculations appropriate to a point nucleus.¹¹⁹ The theoretical values for $Z>50$ include the effect of the finite nuclear size.¹²⁰ The L -shell conversion coefficients α_L have been obtained from the α_K values by assuming a K/L ratio equal to that for a point nucleus.¹¹⁹ The total conversion coefficients, α , are obtained by assuming $\alpha=\alpha_K+1.3\alpha_L$, in order to approximately take into account the conversion in the higher shells.

Column VII. Reduced Nuclear Transition Probability $B(E2)$

In cases where sufficient data are available, a total $B(E2)$ for the excitation process may be computed from the $\epsilon B(E2)$ values listed in column IV and the assumed conversion coefficients (column VI). The $B(E2)$ value is listed opposite the radiation which represents the ground-state decay mode of the level in question. The value given is a weighted average of the various experimental yield determinations.¹²¹

Column VIII. Level Scheme

The suggested level schemes are based on the Coulomb excitation measurements as well as the evidence from other sources indicated in column IX. Only levels which have been observed in Coulomb excitation experiments are included. The spin assignments listed in parenthesis are based on the assumed rotational char-

¹¹⁹ Rose, Goertzel, Spinrad, Harr, and Strong, Phys. Rev. **83**, 79 (1951) and Rose, Goertzel, and Swift, privately circulated tables.

¹²⁰ L. A. Sliv, privately circulated tables; see also L. A. Sliv, J. Exptl. Theoret. Phys. U.S.S.R. **21**, 770 (1951) and L. A. Sliv and M. A. Listengarten, *ibid.* **22**, 29 (1952).

¹²¹ There appears to be an unresolved discrepancy between the γ -ray yield measurements in the series of experiments reported in (M1, M3, M4, and M6) and those of other experimenters (see column IV). Rather than attempt to average such conflicting determinations, we have arbitrarily omitted the former values from the averages listed in column VII.

TABLE IV.2. Results obtained from Coulomb excitation. The description of this table is given in (IV B) of the text.

I	II	III	IV	V	VI	VII	VIII	IX
Nucleus	Decay energy	Bombarding conditions	$\epsilon B(E2)$	Comments	Multipole order and conversion coefficients	$B(E2)$	Level schemes	Other processes
${}^9\text{F}^{19}$	109	0.6-2.8 α (S1)	(γ)	ex. func. $\Delta E=110$, $\lambda=1$ or 2 (S1; J1; H9)				110 $\text{Ne}^{21}(\alpha\alpha)$; F($p\beta$); F($np\gamma$); O $^{20}(\beta\gamma)$; and others
	112	0.7-1.2 α (J1)	(γ)					
	113	1-3 α (T2; H9)	(γ)	$\gamma(\theta): 1/2(E1)1/2(E1)1/2(S1)$				
	124	15N (A1)	(γ)	$B(E1)2.3 \times 10^{-20} e^2 \text{ cm}^2 (S1) = 1 \times 10^{-28} e^2 \text{ cm}^2 (J1)$				
${}^{19}\text{F}$	196	0.8-2.8 α (S1)	0.003 (γ)	ex. func. $\Delta E=196$ (S1; H9)		0.003		197 $\text{Ne}^{21}(\alpha\alpha)$; F($p\beta$); F($np\gamma$); O $^{20}(\beta\gamma)$; and others
	195	0.7-1.2 α (J1)	0.002 (γ)	$\sigma(\beta): \sigma(\alpha)$ gives $\lambda=2$ (T1; B9)				
	196	1-3 α (H9; T2)	(γ)	$\gamma(\theta): 1/2(E2)5/2(E2)1/2(S1)$				
	205	15N (A1)	(γ)	no cascade transition via 110-keV level observed				
${}^{11}\text{Na}^{23}$	446	1.5-3.6 α (T2)	0.013 (γ)	ex. func. $\Delta E=446$ (T2)		0.013		439 Na($nm\gamma$); Na($p\beta\gamma$); $\text{Ne}^{20}(\beta\gamma)$; and others
	435	15N (A1)	(γ)	$\sigma(\beta): \sigma(\alpha)$ gives $\lambda=2$ (T1)				
${}^{22}\text{Ti}^{46}$	890	6 α (H2)	0.15 (γ)			0.15		890 $\text{Sc}^{46}(\beta\gamma)$ 160 $\text{Sc}^{47}(\beta\gamma)$
	160	1.2-3.4 α (T2)	0.040 (γ)	ex. func. $\Delta E=160$ (T2)		0.040		
${}^{48}\text{Ti}$	990	6 α (H2)	0.083 (γ)	$\gamma(750)$ also observed from 6 α , but assigned to $\text{Ti}^{38}(\alpha n\gamma)\text{Cr}^{51}(\text{H2})$		0.083		990 $\text{Sc}^{48}(\beta\gamma)$ $\text{V}^{48}(\beta\gamma)$
	225	6.5 α (H10)	0.011 (γ)	sep. iso. (H10)		0.011		
${}^{51}\text{V}$	320	1.6-3.4 α (T2)	0.0056 (γ)	ex. func. $\Delta E=320$ (T2)		0.0056		323 $\text{Ti}^{51}(\beta\gamma)$ 320 $\text{Cr}^{51}(\alpha\gamma)$ 321 $\text{V}(p\beta)$; V($nm\gamma$)
	325	1.5 β (M4)	(γ)		7% E2			
	320	15N (A1)	(γ)					
	155(?)	1.3 β (M4)	0.015 (γ)	sep. iso. (M4)				
${}^{24}\text{Cr}^{52}$	128	1-3.4 α (T2)	0.075 (γ)	ex. func. $\Delta E=128$ (T2; M4)		0.07		130 Mn($p\beta$) 126 Mn($nm\gamma$)
	131	0.5-2.5 β (M4)	0.087 (γ)	$\sigma(\beta): \sigma(\alpha)$ gives $\lambda=2$ (T2)				
	~125	1.75 β (H3)	0.0009 ($e\alpha$)	$\alpha_K=0.0144$; $\gamma(\theta): 5/2(E2)$				
	128	3 α (B5)	($e\alpha\gamma$)	$7/2(M1)5/2(B5)$				
	127	15N (A1)	(γ)					
	590	15N (A1)	(γ)					

TABLE IV.2.—Continued.

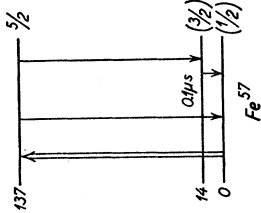
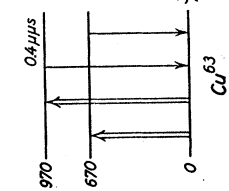
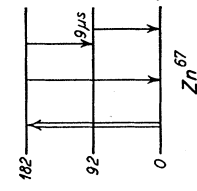
I	II	III	IV	V	VI	VII	VIII	IX
Nucleus	Decay energy	Bombarding conditions	$\epsilon B(E2)$	Comments	Multipole order and conversion coefficients	$B(E2)$	Level schemes	Other processes
$^{56}_{26}\text{Fe}$	854	6α (H2)	0.10 (γ)			0.10		845 $\text{Co}^{56}(\beta^+\gamma)$ 845 $\text{Mn}^{56}(\beta^-\gamma)$ 850 $\text{Fe}(mn, \gamma)$ 845 $\text{Fe}(pp)$
Fe^{57}	14	$1-3\alpha$ (T2)	(γ)	sep.iso. (T2); fed by 122-keV transition from 137-keV level				14 $\text{Co}^{57}(\beta^+\gamma)$
	123	$1-3\alpha$ (T2)	0.051 (γ)	sep.iso. (T2; H3)	$\alpha_K = 0.017$			123 $\text{Co}^{57}(\beta^+\gamma)$
	122	$1.75p$ (H3)	0.0007 (ex)	ex.func. $\Delta E = 137$ (T2)				117 $\text{Mn}^{57}(\beta^-\gamma)$
	123	$0.6p$ (L1)	~ 0.015 (γ)					
	137	$1-3\alpha$ (T2)	(γ)	sep.iso. (T2; H3); $\gamma(137)$	$\alpha_K = 0.19$	0.05		134 $\text{Co}^{57}(\beta^+\gamma)$
	137	$1.75p$ (H3)	0.0004 (ex)	weak compared to the cascade $\gamma(122)$				131 $\text{Mn}^{57}(\beta^-\gamma)$
$^{58}_{28}\text{Ni}$	1450	$3-4.5p$ (S2)	≤ 0.1 (γ)	nonresonant background observed between strong resonances (S2)		~ 0.1		1.47 $\text{Ni}^{58}(mn, \gamma)$ 1.453 $\text{Ni}^{58}(pp)$
$^{63}_{29}\text{Cu}$	990	7α (T7)	0.029 (γ)			0.029		960 $\text{Zn}^{63}(\beta^+\gamma)$ 960 $\text{Cu}(mn, \gamma)$ 968 $\text{Cu}^{63}(pp)$
	690	7α (T7)	0.010 (γ)			0.010		669 $\text{Cu}^{63}(pp)$ 660 $\text{Cu}(mn, \gamma)$
Cu^{65}	1150	7α (T7)	0.027 (γ)			0.027		1120 $\text{Ni}^{65}(\beta^-\gamma)$ 1112 $\text{Zn}^{65}(e\gamma)$ 1130 $\text{Cu}(mn, \gamma)$
$^{64}_{30}\text{Zn}$	815	7α (T7)	0.0087 (γ)			0.0087		
	1000	7α (T7)	0.11 (γ)			0.11		970 $\text{Ga}^{64}(\beta^+\gamma)$
Zn^{66}	1040	7α (T7)	0.087 (γ)			0.087		1044 $\text{Cu}^{66}(\beta^-\gamma)$ 1050 $\text{Ga}^{66}(e\gamma)$
Zn^{67}	90	3 and 6α (T2)		sep.iso. (T2); ex.func. $\Delta E = 182$ (T2)				92 $\text{Cu}^{67}(\beta^-\gamma)$ 90; 92 $\text{Ga}^{67}(e\gamma)$
	182	3 and 6α (T2)	0.032 (γ)	sep.iso. (T2)		0.04		182 $\text{Cu}^{67}(\beta^-\gamma)$ 182 $\text{Ga}^{67}(e\gamma)$
Zn^{68}	1170	7α (T7)						1100 $\text{Ga}^{68}(\beta^+\gamma)$
$^{70}_{32}\text{Ge}$	1020	6α (H2)	0.077 (γ)			0.077		1036 $\text{Ga}^{70}(\beta^-\gamma)$ 1070 $\text{As}^{70}(\beta^+\gamma)$ 1050 $\text{Ge}(mn, \gamma)$
Ge^{72}	830	6α (H2)	0.26 (γ)			0.26		834 $\text{Ga}^{72}(\beta^-\gamma)$ 835 $\text{As}^{72}(\beta^+\gamma)$ 820 $\text{Ge}(mn, \gamma)$

TABLE IV.2.—Continued.

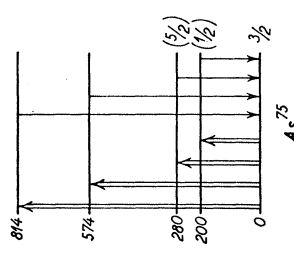
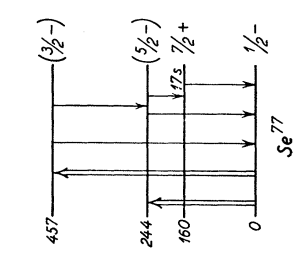
I	II	III	IV	V	VI	VII	VIII	IX
Nucleus	Decay energy	Bombarding conditions	$\epsilon B(E2)$	Comments	Multipole order and conversion coefficients	$B(E2)$	Level schemes	Other processes
Ge ⁷³	68.7 72	1-3 α (T2) 15N (A1)	0.085 (γ) (γ)	sep.iso.; ex.func. $\Delta E=69$ and $\lambda=2(T2)$		0.30		596 As ⁷⁴ ($\beta^+\gamma$) 610 Ge($n\pi^+\gamma$)
Ge ⁷⁴	593	6 α (H2)	0.30 (γ)			0.33		
Ge ⁷⁶	556	6 α (H2)	0.33 (γ)	isotope assigned on basis of systematics				
³² As ⁷⁵	68	3 α (T3)	(γ)					67 Se ⁷⁵ ($\epsilon\gamma$) 66 Ge ⁷⁵ ($\beta^-\gamma$)
	199	3 and 7 α (T3; T7)	0.025 (γ)			0.022		200 Se ⁷⁵ ($\epsilon\gamma$)
	200	2 β (P1)	0.016 (γ)					199 Ge ⁷⁵ ($\beta^-\gamma$)
	283	3 and 7 α (T3; T7)	0.071 (γ)			0.06		281 Se ⁷⁵ ($\epsilon\gamma$)
	280	2 β (P1)	0.05 (γ)					
	574	7 α (T7)	0.072 (γ)			0.072		
	814	7 α (T7)	0.066 (γ)			0.066		
³⁴ Se ⁷⁴	635	7 α (T7)	0.21 (γ)	sep.iso. (T7)		0.21		635 As ⁷⁴ ($\beta^-\gamma$)
Se ⁷⁶	567	7 α (T7)	0.43 (γ)	sep.iso. (T7)		0.43		560 As ⁷⁶ ($\beta^-\gamma$) 560 Br ⁷⁶ ($\beta^+\gamma$)
Se ⁷⁷	86	7 α (T7)	(γ)	sep.iso. (T7)				87 As ⁷⁷ ($\beta^-\gamma$)
	160	7 α (T7)	(γ)	sep.iso.; isomeric trans. $T_{1/2}=17$ sec. fed by 86 keV trans. from 244-keV level; $\gamma(160); \gamma(244)=0.02(T7)$				160 As ⁷⁷ ($\beta^-\gamma$) 160 Br ⁷⁷ ($\epsilon\gamma$)
	210	7 α (T7)	(γ)	sep.iso.; cascade trans. from 457-keV level; $\gamma(210); \gamma(244)$ coinc. $\gamma(210); \gamma(457)=0.28(T7)$				
	244	3 and 7 α (T3; T7)	0.12 (γ)	sep.iso. (T7)		0.12		246 As ⁷⁷ ($\beta^-\gamma$) 237 Br ⁷⁷ ($\epsilon\gamma$) Se($n\pi\gamma$)
	238	15N (A1)	(γ)					
	457	3 and 7 α (T3; T7)	0.68 (γ)	sep.iso. (T7)		0.9		
	452	15N (A1)	(γ)					
Se ⁷⁸	615	7 α (T7)	0.36 (γ)	sep.iso. (T7)		0.36		~ 600 Se($n\pi\gamma$)
Se ⁸⁰	654	7 α (T7)	0.23 (γ)	sep.iso. (T7)		0.23		
Se ⁸²	880	7 α (T7)	0.056 (γ)	sep.iso. (T7)		0.056		

TABLE IV.2.—Continued.

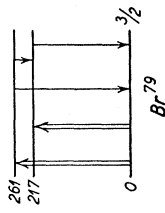
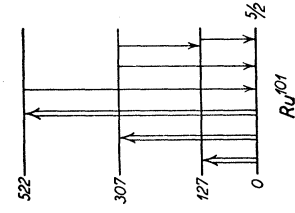
I	II	III	IV	V	VI	VII	VIII	IX
Nucleus	Decay energy	Bombarding conditions	$\epsilon B(E2)$	Comments	Multipole order and conversion coefficients	$B(E2)$	Level schemes	Other processes
$^{83}\text{Br}^{79}$	44	3α (H1)	(γ)					$44.5 \text{ Kr}^{79}(\beta^+\gamma)$
	219	p, α (W1)	0.025 (γ)	sep.iso. (W1)				$217.3 \text{ Kr}^{79}(\beta^+\gamma)$
	213	3α (H1)	(γ)					
	266	3α (H1)	(γ)					$261.3 \text{ Kr}^{79}(\beta^+\gamma)$
Br^{81}	278	p, α (W1)	0.031 (γ)	sep.iso. (W1)				
$^{87}\text{Rb}^{85}$	150	3α (T3)						$150 \text{ Kr}^{85m}(\beta^-\gamma)$ $150 \text{ Sr}^{85m}(\epsilon\gamma)$
$^{88}\text{Nb}^{88}$	850	(T8)	(γ)	ex.func. $\Delta E = 710$ (P2)				
	710	$2.75-4p$ (P2)	(γ)					
$^{88}\text{Mo}^{84}$	871	6α (H2)	0.29 (γ)			0.29		$874 \text{ Tc}^{84}(\beta^+\gamma)$ $\sim 900 \text{ Nb}^{84m}(\beta^-\gamma)$
Mo^{95}	204	3 and 6α (T3; H2)	0.070 (γ)	ex.func. $\Delta E = 200$ (S4)		0.055		$201 \text{ Tc}^{95}(\epsilon\gamma)$
	212	$2.1-2.9p$ (S4)	0.040 (γ)					
	199	$2.5p$ (M4)	0.057 (γ)					
	210	$15N$ (A1)	(γ)					
	778	6α (H2)	0.31 (γ)				0.4	$771 \text{ Tc}^{95}(\epsilon\gamma)$ $770 \text{ Nb}^{95}(\beta^-\gamma)$
Mo^{98}	786	6α (H2)	0.27 (γ)	sep.iso. (H2)		0.4		
$\text{Mo}^{96,98}$	770	$2.4-3p$ (S4)	0.59 (γ)	ex.func. $\Delta E = 770$ (S4)				
	528	6α (H2)	0.66 (γ)	sep.iso. (T7; H2)		0.64		
Mo^{100}	525	$2.3p$ (M4)		ex.func. $\Delta E = 540$ (S4)				
	540	$2.1-3p$ (S4)	0.61 (γ)					
	540	$15N$ (A1)	(γ)					
	89.5	3 and 7α (H1; T6)	0.054 (γ)					$89 \text{ Rh}^{98}(\beta^+\gamma)$ $535 \text{ Rh}^{100}(\beta^+\gamma)$ $550 \text{ Tc}^{100}(\beta^-\gamma)$
Ru^{100}	540	7α (T6)	0.30 (γ)			0.30		$307 \text{ Tc}^{101}(\beta^-\gamma)$ $307 \text{ Rh}^{101}(\epsilon\gamma)$
Ru^{101}	127	3 and 7α (H1; T7)	0.061 (γ)					
	307	7α (T7)	0.036 (γ)					
Ru^{102}	522	7α (T7)	0.041 (γ)					
	180	7α (T7)		cascade trans. from 307-keV level; $\gamma(180)\text{-}\gamma(127)$ coinc. (T7)				$475 \text{ Rh}^{102}(\beta^+\gamma)$
Ru^{102}	473	7α (T6)	0.63 (γ)			0.63		
Ru^{104}	362	7α (T6)	1.04 (γ)			1.0		

TABLE IV.2.—Continued.

I	II	III	IV	V	VI	VII	VIII	IX
Nucleus	Decay energy	Bombarding conditions	$\epsilon E(E2)$	Comments	Multipole order and conversion coefficients	$E(E2)$	Level schemes	Other processes
$^{46}\text{Rh}^{103}$	295	6α (H7)	0.18 (γ)	ex.func. $\Delta E = 305$ (S4);	0.21	0.21		300 $\text{Pd}^{103}(\epsilon\gamma)$
	305	$2.1-2.9p$ (S4)	0.23 (γ)	$\gamma(\theta): 1/2(E2)3/2(M1+E2)1/2$;				
	295	$15N$ (A1)	(γ)	$\delta = -0.18$ or -1.17 (M7)				
	357	6α (H7)	0.32 (γ)	ex.func. $\Delta E = 365$ (S4);				
$^{46}\text{Pd}^{108}$	365	$2.1-2.9p$ (S4)	0.32 (γ)	$\gamma(\theta): 1/2(E2)5/2(E2)1/2$	0.36	0.36		367 $\text{Pd}^{108}(\epsilon\gamma)$
	358	$15N$ (A1)	(γ)	(M7)				
$^{46}\text{Pd}^{108}$	65	$2.1-2.9p$ (S4)	0.020 (γ)	cascade trans. from 360-keV level (S4)	$\alpha = 1$	0.50		65 $\text{Pd}^{108}(\epsilon\gamma)$
	550	6α (T5)	0.46 (γ)	sep.iso. (T5)				
$^{46}\text{Pd}^{108}$	575	$2.1-2.9p$ (S4)	0.54 (γ)	ex.func. $\Delta E = 575$ (S4)	0.04	0.04		556 $\text{Ag}^{104}(\beta^+\gamma)$ 556 $\text{Rh}^{103}(\beta^+\gamma)$
	266	6α (T5)	0.04 (γ)	sep.iso. (T5; M4)				
$^{46}\text{Pd}^{108}$	270	$2.5p$ (M4)	0.0084 (γ)		0.17	0.17		512 $\text{Ag}^{106}(\beta^+\gamma)$ 513 $\text{Rh}^{106}(\beta^+\gamma)$
	433	6α (T5)	0.17 (γ)	sep.iso. (T5; M4)				
$^{46}\text{Pd}^{108}$	430	$2.5p$ (M4)	0.057 (γ)		0.66	0.66		430 $\text{Ag}^{108}(\epsilon\gamma)$
	510	6α (T5)	0.59 (γ)	sep.iso. (T5)				
$^{46}\text{Pd}^{108}$	500	$2.5p$ (M4)	0.18 (γ)	$\gamma(\theta): 0(E2)2(E2)0$ (M7)	0.89	0.89		
	520	$2.1-2.9p$ (S4)	0.72 (γ)	ex.func. $\Delta E = 520$ (S4)				
$^{46}\text{Pd}^{108}$	424	6α (T5)	0.78 (γ)	sep.iso. (T5)	1.0	1.0		
	425	$2.5p$ (M4)	0.21 (γ)	$\gamma(\theta): 0(E2)2(E2)0$ (M7)				
$^{46}\text{Pd}^{108}$	445	$2.1-2.9p$ (S4)	1.0 (γ)	ex.func. $\Delta E = 445$ (S4)	0.16	0.16		
	370	6α (T5)	1.04 (γ)	sep.iso. (T5)				
$^{46}\text{Pd}^{110}$	365	$2.5p$ (M4)	0.26 (γ)	ex.func. $\Delta E = 380$ (S4)	$\alpha_K = 0.014$	0.28		
	380	$2.1-2.9p$ (S4)	0.95 (γ)	$\gamma(\theta): 0(E2)2(E2)0$ (M7)				
$^{47}\text{Ag}^{107}$	318	6α (H7)	0.12 (γ)	sep.iso. (H7; F1)	0.17	0.17		94 $\text{Ag}^{107m}(\gamma)$ 88 $\text{Ag}^{107m}(\gamma)$
	319	4α (F1)	0.16 (γ)	ex.func. $\Delta E = 318$ (H7)				
$^{47}\text{Ag}^{107}$	323	$1.75p$ (H4; H3)	0.0022 (ϵ_K)		0.31	0.31		
	413	6α (H7)	0.21 (γ)	sep.iso. (H7; F1)				
$^{47}\text{Ag}^{107}$	419	$3p$ (F1)	0.23 (γ)		$\alpha_K = 0.019$	0.31		
	305	6α (H7)	0.13 (γ)	sep.iso. (H7; F1)				
$^{47}\text{Ag}^{109}$	306	4α (F1)	0.18 (γ)		0.16	0.16		
	308	$1.75p$ (H4; H3)	0.0026 (ϵ_K)					
$^{47}\text{Ag}^{109}$	400	6α (H7)	0.23 (γ)	sep.iso. (H7; F1)	0.16	0.16		
	412	$3p$ (F1)	0.31 (γ)					
$^{47}\text{Ag}^{109}$	90	$1.35-2p$ (H4)	(ϵ)	isomeric level fed by trans. from levels with $\Delta E \sim 400$ keV; branching ratio $e(90): \gamma(400) = 0.005:1$ (H4)	0.16	0.16		
	90	$1.35-2p$ (H4)	(ϵ)					

TABLE IV.2.—Continued.

I	II	III	IV	V	VI	VII	VIII	IX
Nucleus	Decay energy	Bombarding conditions	$\epsilon B(E2)$	Comments	Multipole order and conversion coefficients	$B(E2)$	Level schemes	Other processes
Ag	320	1.75p (H4)	0.1	composite line from both isotopes; ex.func. $\Delta E = 325(S4)$ $\gamma(\theta): 1/2(E2)3/2(M1+E2)1/2$ $\delta = -0.19$ or $-1.14(M7)$				
	315	2.8p (M4)	0.079					
	325	2.1-2.9p (S4)	0.22					
	320	p, α (B8)						
	310	15N (A1)						
	418	2.8p (M4)	0.086	composite line from both isotopes; ex.func. $\Delta E = 427(S4)$ $\gamma(\theta): 1/2(E2)5/2(E2)1/2(M7)$				
427	2.1-2.9p (S4)	0.34						
420	p, α (B8)			cascade trans. from 400-keV to 300-keV levels in both isotopes (S4)	$\alpha = 0.3$			
409	15N (A1)							
104	2.1-2.9p (S4)	0.016						
⁴⁸ Cd ¹¹⁰	654	6 α (T5)	0.41	sep.iso. (T5)		0.41		656 Ag ¹¹⁰ ($\beta^- \gamma$) 654 In ¹¹⁰ ($\beta^- \gamma$)
	340	6 α (T5)	0.19	sep.iso. (T5; M4)		0.19		340 Ag ¹¹¹ ($\beta^- \gamma$) 330 In ¹¹¹ ($\epsilon \gamma$)
		330	2.8p (M4)					
	620	6 α (T5)	0.46	sep.iso. (T5; M4)		0.46		620 Ag ¹¹² ($\beta^- \gamma$)
		610	2.8p (M4)					
	Cd ¹¹³	290	6 α (T5)	0.11	sep.iso. (T5; M4)		0.11	
		290	2.8p (M4)	0.058				
		297	15N (A1)					
	550	6 α (T5)	<0.2					
	Cd ¹¹⁴	550	6 α (T5)	0.55	sep.iso. (T5; M4)		0.55	
545		2.8p (M4)	0.14					
543		15N (A1)						
Cd ¹¹⁶	508	6 α (T5)	0.62	sep.iso. (T5)		0.62		
⁴⁹ In ¹¹⁵	500	3.8p (T3)	0.058	ex.func. indicates compound nucleus formation (D1)				500 Cd ¹¹⁵ ($\beta^- \gamma$)
	500	3p (M4)						
	562	15N (A1)						
⁵¹ Sb	~160	3 α (T3)		isotope uncertain				

TABLE IV.2.—Continued.

I	II	III	IV	V	VI	VII	VIII	IX
Nucleus	Decay energy	Bombarding conditions	$\alpha B(EZ)$	Comments	Multipole order and conversion coefficients	$B(EZ)$	Level schemes	Other processes
$^{120}_{52}\text{Te}$	560	6.5α (H10)	0.55 (γ)	sep.iso. (H10)		0.55		565 $\text{Sb}^{120}(\beta^- \gamma)$
Te^{122}	570	6.5α (H10)	0.47 (γ)	sep.iso. (H10)		0.47		159 $\text{I}^{123}(\epsilon \gamma)$
Te^{123}	159	$4\alpha, p$ (F1)	0.014 (γ)	sep.iso. ex.func. $\Delta E = 160$ (F1)	$\alpha = 0.2$	0.017		$\text{Te}^{123m}(\gamma \gamma)$
	274	$3.7p$ (F1)	(γ)	sep.iso., cascade trans. from 436-keV level; $\gamma(274) - \gamma(159)$ coinc. (F1)				
	342	$3.7p$ (F1)	(γ)	sep.iso., cascade trans. from 504-keV level; $\gamma(342) - \gamma(159)$ coinc. (F1)				
	436	$3.7p$ (F1)	(γ)	sep.iso. (F1)				
	504	$3.7p$ (F1)	(γ)	sep.iso. (F1)				
Te^{124}	608	6.5α (H10)	0.39 (γ)	sep.iso. (H10)		0.39		605 $\text{Sb}^{124}(\beta^- \gamma)$
Te^{125}	435	$3p$ (F1)	0.44 (γ)	sep.iso. (F1)		0.44		425 $\text{Sb}^{125}(\beta^- \gamma)$
	633	$3.5p$ (F1)	0.26 (γ)	sep.iso. (F1)		0.26		637 $\text{Sb}^{125}(\beta^- \gamma)$
Te^{126}	662	6.5α (H10)	0.32 (γ)	sep.iso. (H10)		0.32	650 $\text{I}^{126}(\epsilon \gamma)$	
Te^{128}	750	6.5α (H10)	0.28 (γ)	sep.iso. (H10)		0.28	750 $\text{I}^{128}(\epsilon \gamma)$	
Te^{130}	850	6.5α (H10)	0.26 (γ)	sep.iso. (H10)		0.26		
$^{127}_{53}\text{I}$	57	3α (H1)	(γ)					57 $\text{Xe}^{127}(\epsilon \gamma)$
	60	α (D1)	(γ)					62 $\text{I}(\text{mm}'\gamma)$
	60	$15N$ (A1)	(γ)					
	205	3α (H1)	0.039 (γ)			0.039		200 $\text{Xe}^{127}(\epsilon \gamma)$
	212	$2p$ (M4)	(γ)					208 $\text{I}(\text{mm}'\gamma)$
	203	$1.5-3.5p, \alpha$ (D1)	0.039 (γ)					
	205	$15N$ (A1)	(γ)					
	392	$2.0-3.5p$ (D1)	0.019 (γ)			0.019		390 $\text{I}(\text{mm}'\gamma)$
	438	$2-3.5p$ (D1)	0.0060 (γ)			0.006		435 $\text{I}(\text{mm}'\gamma)$
	631	$2-3.5p$ (D1)	0.10 (γ)			0.10		632 $\text{I}(\text{mm}'\gamma)$
	751	$2.5-3.5p$ (D1)	0.08 (γ)			0.08		750 $\text{I}(\text{mm}'\gamma)$
	941	$2.5-3.5p$ (D1)	0.36 (γ)			0.36		950 $\text{I}(\text{mm}'\gamma)$

TABLE IV.2.—Continued.

I	II	III	IV	V	VI	VII	VIII	IX
Nucleus	Decay energy	Bombarding conditions	$\epsilon B(E2)$	Comments	Multipole order and conversion coefficients	$B(E2)$	Level schemes	Other processes
$^{55}\text{Cs}^{133}$	85	3α (T3)	(γ)					$81 \text{ Xe}^{133}(\beta^- \gamma)$ $82 \text{ Ba}^{133}(\epsilon \gamma)$
^{56}Ba	60 118	3α (H1) 3α (H1)	(γ) (γ)	isotope uncertain isotope uncertain				
$^{57}\text{La}^{139}$				$\gamma(166)$ not observed with 6α $B(E2) < 10^{-2}(\text{H8})$				
$^{59}\text{Pr}^{141}$				$\gamma(145)$ not observed with 6α $B(E2) < 10^{-2}(\text{H8})$				
$^{60}\text{Nd}^{145}$	70 71	3 and 6α (H1; H8) $2.2p$ (S3)	~ 0.06 (γ) (γ)	sep.iso. (H8)	$\alpha=4$	~ 0.3		
Nd^{146}	455	6α (H8)	0.25 (γ)	sep.iso. (H8)		0.25		$455 \text{ Pr}^{146}(\beta^- \gamma)$
Nd^{148}	300 300	3 and 6α (T6; H8) $2.2-3.3p$ (S3)	0.68 (γ) 0.64 (γ)	sep.iso. (H8) ex.func. $\Delta E=300$ (S3)	$\alpha=0.04$	0.69		
Nd^{150}	128 131 132	3 and 6α (H1; H8) $1.5-3.3p$ (S3) $1.75p$ (H3)	1.32 (γ) 1.20 (γ) 0.31 (e_L)	sep.iso. (H8) ex.func. $\Delta E=131$ and $\lambda=2$; $\gamma(\theta):0(E2)2(E2)0(S3)$	$\alpha=0.90$ $\alpha_L=0.25$	2.3		
$^{62}\text{Sm}^{148}$	562 550 562	6α (H8) $2.9p$ (M6) p (S5)	0.50 (γ) 0.74 (γ) (γ)	sep.iso. (H8; M6; S5) $\gamma(\theta):0(E2)2(E2)0(S5)$		0.50		
Sm^{150}	337 337	6α (H8) $2.9p$ (M6) $2.6p$ (S5)	0.94 (γ) 0.51 (γ) (γ)	sep.iso. (H8; M6; S5) $\gamma(\theta):0(E2)2(E2)0$ ex.func. $\Delta E=337$ (S5)	$\alpha=0.04$	0.98		$337 \text{ Sm}^{149}(\beta \gamma)$ $340 \text{ Pm}^{150}(\beta^- \gamma)$
Sm^{152}	122 125 123 124 122	3 and 6α (H1; H8) $2.9p$ (M6) $1.75p$ (H3) $2.3p$ (S5) $6p$ (E2)	1.52 (γ) 0.43 (γ) 0.56 (e_L) 2.66 (p)	sep.iso. (H8; M6; S5) $\gamma(\theta):0(E2)2(E2)0$ ex.func. $\Delta E=124$ and $\lambda=2$ (S5)	$\alpha_L=0.36$ $\alpha=1.2$	3.1		$121.8 \text{ Eu}^{152}(\epsilon \gamma)$
Sm^{154}	82 84 83 85 84	3 and 6α (H1; H8) $2.9p$ (M6) $1.75p$ (H3) $2.1p$ (S5) $6p$ (E2)	0.80 (γ) 0.27 (γ) 2.55 (e_L) (γ) 3.60 (p)	sep.iso. (H8; M6; S5) $\gamma(\theta):0(E2)2(E2)0$ ex.func. $\Delta E=84$ and $\lambda=2$ (S5)	$\alpha_L=2.0$ $\alpha=4.4$	4.5		
$^{62}\text{Eu}^{151}$	195 193	6.5α (H10) $3.7p$ (C2)	0.067 (γ) (e)	sep.iso. (H10; C2)	$\alpha=0.3$	0.09		
	110	6.5α (H10)	0.024 (γ)	sep.iso. (H10) cascade trans. from 304-keV level	$\alpha=1.3$			

TABLE IV.2.—Continued.

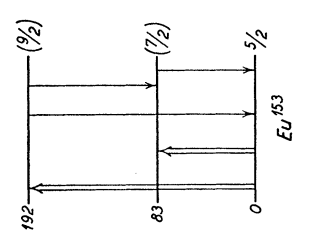
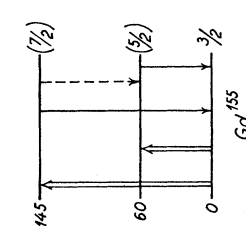
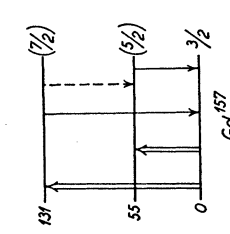
I	II	III	IV	V	VI	VII	VIII	IX
Nucleus	Decay energy	Bombarding conditions	$\epsilon B(E2)$	Comments	Multipole order and conversion coefficients	$B(E2)$	Level schemes	Other processes
Eu^{151}	304	6.5α (H8; H10)	0.22 (γ)	sep.iso. (H10; C2)	$\alpha=0.06$	0.29		
	300	$2.9p$ (M6)	(γ)					
	304	$3.7p$ (C2)	(e)					
	284	$3.7p$ (C2)	(e)	sep.iso. (C2) probably cascade trans. from 304-keV level				
Eu^{153}	82	3 and 6α (T6; H8)	0.60 (γ)	sep.iso. (H10; C2)	$\sim 50\% E2$	2.8		83.4 $\text{Sm}^{153}(\beta-\gamma)$
	85	$2.9p$ (M6)	0.20 (γ)	K/L ~ 1 (H3)	$\alpha_L=1.3$			
	84	$1.75p, d$ (H3)	0.65 (e_L)		$\alpha=4.0$			
	81	$6p$ (E2)	1.9 (p)					
	82.5	3.7α (C2)	(e)					
	105	6α (T6; H8)	0.18 (γ)	sep.iso. (H10; C2)	$\sim 50\% E2$			
	115	$2.9p$ (M6)	0.14 (γ)	cascade trans. from 195-keV level;	$\alpha_L=0.4$			
	~ 111 109	$1.75p$ (H3) 3.7α (C2)	~ 0.05 (e_L) (e)	$\gamma(108)-\gamma(84)$ coinc. (H8) $\gamma(110)-\gamma(195)=0.38$ (M6)	$\alpha=1.5$			
187	6α (T6; H8)	0.29 (γ)	sep.iso. (H10; C2)	100% E2	0.78			
200	$2.9p$ (M6)	0.14 (γ)		$\alpha_K=0.17$				
195	$1.75p$ (H3)	~ 0.051 (e_K)		$\alpha=0.25$				
192	3.7α (C2)	(e)						
${}_{64}\text{Gd}^{154}$	123	3 and 6α (H1; H8)	2.32 (γ)	sep.iso. (M6)	$\alpha_L=0.43$	4.5		123.4 $\text{Eu}^{154}(\beta-\gamma)$
	123	$1.9p$ (M6)	1.0 (γ)		$\alpha=1.2$			
	124	$1.75p$ (H3)	~ 0.73 (e_L)					
	60	$1.75p$ and α (B7)	0.48 (e_L)	sep.iso. (B7)	5% E2 $\alpha_L=1.6$ $\alpha=10$	3.3		59.8 $\text{Eu}^{155}(\beta-\gamma)$
Gd^{156}	145	6α (H8)	0.105 (γ)	sep.iso. (H8; B7)	100% E2			
	140	$2.9p$ (M6)	0.059 (e_K)					
	146	$1.75p$ (B7)						
	89	6α (H8)	1.90 (γ)	sep.iso. (M6)	$\alpha_L=1.8$ $\alpha=3.9$	7.7		88.8 $\text{Gd}^{156}(\beta\gamma)$ $\text{Eu}^{156}(\beta-\gamma)$
89	$1.9p$ (M6)	0.74 (γ)						
90	$1.75p$ (H3)	2.8 (e_L)						
91	$6p$ (E2)	5.0 (p)						
Gd^{157}	55	$1.75p$ and α (B7)	0.54 (e_L)	sep.iso. (B7)	4% E2 $\alpha_L=2.0$ $\alpha=13$	3.5		
	131	6α (H8)	0.086 (γ)	sep.iso. (H8; B7)	100% E2	1.3		
127	$2.9p$ (M6)							
131	$6p$ (E2)		1.2 (p)					
132	$1.75p$ (B7)		0.032 (e_L)					
Gd^{158}	79	6α (H8)	1.75 (γ)	sep.iso. (M6)	$\alpha_L=3.1$	10		79.1 $\text{Gd}^{157}(\beta\gamma)$
	80	$1.9p$ (M6)	0.63 (γ)		$\alpha=6.0$			

TABLE IV.2.—Continued.

I	II	III	IV	V	VI	VII	VIII	IX	
Nucleus	Decay energy	Bombarding conditions	$\epsilon B(E2)$	Comments	Multipole order and conversion coefficients	$B(E2)$	Level schemes	Other processes	
Gd ¹⁵⁸	79	6p (E2)	~4						
	80	1.75p (H3)	3.4						
Gd ¹⁶⁰	76	6 α (H8)	1.79	sep. iso. (M6)	$\alpha_L = 3.6$	11			
	76	1.9p (M6)	0.73		$\alpha = 7.0$				
	76	1.75p (H3)	3.4						
	75	6p (E2)	~4						
64Tb ¹⁶⁰	58	1.75d (H3)	0.45		(1.3% E2)	2.4		57.5 Gd ¹⁶⁰ ($\beta^- \gamma$)	
	58	6p (E2)	1.88		$\alpha_L = 1.5$ $\alpha = 11$				
	79	6 α (H8)	0.33	ex. func. $\Delta E = 136$	(1.3% E2)				
	77 81	2.9p (M6) 1.75d (H3)	(γ) (γ) (e_L)	$\gamma(79) \rightarrow \gamma(57)$ coinc. (T4)	$\alpha = 4.2$				
136	136	6 α (H8)	0.041		100% E2	1.4			
	135	6p (E2)	1.14		$\alpha = 0.8$				
167 (?)	2.9p (M6)	(γ)							
64Dy ¹⁶²	82	1.75p (H3)	3.2		$\alpha_L = 3.2$	6.7			
	82	6p (E2)	~6	isotope assignment on basis of systematics	$\alpha = 5.8$				
Dy ¹⁶⁴	75	1.75p (H3)	4.8		$\alpha_L = 4.7$	8.9		72.8 Ho ¹⁶⁴ ($\epsilon \gamma$)	
	72	6p (E2)	~6		$\alpha = 8.1$				
Dy ^{164, 165}	166	6 α (T6; H8)	0.24	isotope assignment on basis of systematics				170 Ho ¹⁶⁴ ($\epsilon \gamma$)	
Dy	76	3 and 6 α (T6; H8)	0.41	a composite line					
67Ho ¹⁶⁵	94	3 and 6 α (T6; H8)	0.78		4% E2	2.6		94 Dy ¹⁶⁵ ($\beta^- \gamma$)	
	96	1.75p, d (H3)	0.32	$K/L \sim 5$ (H3)	$\alpha_L = 0.45$ $\alpha = 3.1$				
	95	6p (E2)	1.7		(4% E2)				
116	116	1.75p (H3)	0.07	cascade from 211-kev level	$\alpha_L = 0.26$				
	112	6 α (T4)	0.15	$\gamma(116) \rightarrow \gamma(94)$ coinc. (T4)	$\alpha = 1.9$				
206	206	6 α (T7; H12)	0.024		100% E2	0.63			
	212	1.9p (H6)			$\alpha = 0.2$				

TABLE IV.2.—Continued.

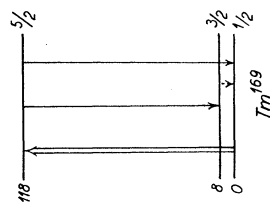
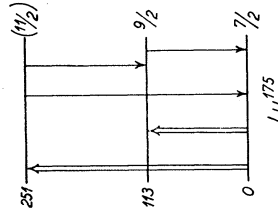
I	II	III	IV	V	VI	VII	VIII	IX
Nucleus	Decay energy	Bombarding conditions	$\epsilon B(E2)$	Comments	Multipole order and conversion coefficients	$B(E2)$	Level schemes	Other processes
$^{68}\text{Er}^{167}$	172	6α (T6; H8)	0.064 (γ)	isotope assignment on basis of systematics				
Er	79 81 79	3 and 6α (T6; H8) 1.75p (H3) 6p (E2)	0.83 (γ) 2.8 (e_L) 5.1 (p')	a composite line due to all isotopes	$\alpha_L=4.2$ $\alpha=7.1$	5.7		80 $\text{Ho}^{166}(\beta^- \gamma)$ 80 $\text{Ho}^{166m}(\beta^- \gamma)$ 80 $\text{Tm}^{166}(\epsilon \gamma)$
$^{69}\text{Tm}^{169}$	109 111	6α (H8) 1.75p (H3)	1.40 (γ) 0.32 (e_L)	cascade trans. from 119-keV level established by ex.func.; $K/L=7$ (H3)	(2% E2) $\alpha_L=0.32$ $\alpha=2.4$			109.9 $\text{Yb}^{169}(\epsilon \gamma)$
	119 119	1.75p (H3) 6p (E2)	0.11 (e_L) 3.47 (p')		100% E2 $\alpha_L=0.77$ $\alpha=1.7$	3.8		118.3 $\text{Yb}^{169}(\epsilon \gamma)$
$^{70}\text{Yb}^{170}$	180	6α (T6; H8)	0.065 (γ)	isotope assigned on basis of systematics				
Yb	78 77 76	3 and 6α (T3; H8) 1.75p (H3) 6p (E2)	0.42 (γ) 2.7 (e_L) 5.7 (p')	composite line from all isotopes	$\alpha_L=5.8$ $\alpha=9$	4.8		
	66(?) 110	1.75 α (H3) 6α (H8)	 0.037 (γ)					
$^{71}\text{Lu}^{175}$	114 112 114 116	3 and 6α (T6; H8) 2.6p (M1) 1.75p (H3) 6p (E2)	0.86 (γ) 0.35 (γ) 0.36 (e_L) 2.54 (p')	$K/L \sim 5.5$ (H3)	12% E2 $\alpha_L=0.44$ $\alpha=2.6$	2.9		113.4 $\text{Hf}^{175}(\epsilon \gamma)$ 114 $\text{Yb}^{175}(\beta^- \gamma)$
	136	6α (T4)	0.22 (γ)	$\gamma(136) \rightarrow \gamma(113)$ coinc. (T4)	(12% E2) $\alpha=1.4$			137.6 $\text{Yb}^{175}(\beta^- \gamma)$
	250 240	3 and 6α (T6; H8) 2.6p (M1)	0.11 (γ) (γ)		100% E2 $\alpha=0.14$	0.67		251.0 $\text{Yb}^{175}(\beta^- \gamma)$
Lu	180	3 and 6α (H1; T6; H8)	0.022 (γ)	isotope uncertain				

TABLE IV.2.—Continued.

I	II	III	IV	V	VI	VII	VIII	IX
Nucleus	Decay energy	Bombarding conditions	$\epsilon B(E2)$	Comments	Multipole order and conversion coefficients	$B(E2)$	Level schemes	Other processes
$^{72}\text{Hf}^{176}$	87	6α (H8)	0.88 (γ)	sep.iso. (M1; H8)	$\alpha=5.8$	6.0		$^{89}\text{Lu}^{176}(\beta^- \gamma)$ $^{89}\text{Lu}^{176m}(\beta^- \gamma)$
	87	$1.5p$ (M1)	1.7 (e_L)					
	90	1.75α (H3)						
Hf^{177}	112	6α (H8)	0.93 (γ)	sep.iso. (M1; H8)	(60% E2) $\alpha_L=0.87$	2.4		$^{112.97}\text{Lu}^{177}(\beta^- \gamma)$
	112	p (M1)	1.1 (γ)		$\alpha=2.5$			
	114	$1.75p$ (H3)	0.39 (e_L)		(60% E2) $\alpha=1.3$			
	136	6α (T4)	0.11 (γ)	$\gamma(138)-\gamma(113)$ coinc. (T4)	100% E2 $\alpha=0.15$	0.63		
Hf^{178}	250	6α (H8)	0.30 (γ)	sep.iso. (M1; H8)	$\alpha=5.4$	6.6		$^{249.69}\text{Lu}^{177}(\beta^- \gamma)$
	235	$2.6p$ (M1)						
Hf^{179}	90	6α (H8)	1.28 (γ)	sep.iso. (M1; H8)	(14% E2) $\alpha_L=0.40$	2.9		
	91	$1.5p$ (M1)	1.3 (γ)		$\alpha=2.3$			
Hf^{180}	119	6α (H8)	0.77 (γ)	sep.iso. (M1; H8)	(14% E2) $\alpha=1.5$	0.20		$^{93.3}\text{Ta}^{180}(\epsilon \gamma)$ $\text{Hf}^{180m}(\gamma)$
	122	p (M1)	0.49 (γ)					
	123	$1.75p$ (H3)	0.19 (e_L)					
	141	6α (T4)	0.066 (γ)	$\gamma(141)-\gamma(121)$ coinc. (T4)	100% E2 $\alpha=0.13$			
$\text{Hf}^{178,180}$	260	6α (H8)	0.029 (γ)					
	250	$2.6p$ (M1)						
$\text{Hf}^{177,179}$	112	$4p$ (S4)	0.59 (γ)					
	248	$4p$ (S4)						
Hf^{180}	93	6α (H8)	1.14 (γ)	sep.iso. (M1; H8)	$\alpha=4.8$	5.0		
	92	$1.5p$ (M1)	1.3 (γ)					
$\text{Hf}^{178,180}$	95	$1.75p$ (H3)	2.3 (e_L)		$\alpha_L=3.1$			
	90	$4p$ (S4)	0.88 (γ)	all even isotopes				
$^{73}\text{Ta}^{181}$	138	p (M1; M2)	0.58 (γ)	ex.func. $\Delta E=137$ (H5; T3; G1; B1; S8; D1)	16% E2 $\alpha_L=0.29$	1.9		$^{136.25}\text{Hf}^{181}(\beta^- \gamma)$ $^{136.5}\text{W}^{181}(\epsilon \gamma)$ $^{136}\text{Ta}^{181}(m\beta \gamma)$
	137	$1-2.2p$ (H5)	0.7 (γ)		$\alpha=1.7$			
	136	$2p$ (H3; H6)	0.21 (e_L)	$\gamma(\theta): 7/2(E2)9/2(E2+M1)7/2$				
	136	6α (H8)	0.70 (γ)	(G1; E1)				
	137	3α (T3)		$K/L=6.5$ (H3)				
	137	$2-4p$ (G1)		$=6.3$ (B4)				
	137	$1.2-4.5p$ (B1)						
	139	$3p$ (E1)						
	137	$1.4-5p, 4\alpha$ (S4)						
	137	$2-3p$ (D1)	0.83 (γ)					
	137	3.5α (B4)	0.60 (γ)					
	138	$15N$ (A1)						

TABLE IV.2.—Continued.

I	II	III	IV	V	VI	VII	VIII	IX
Nucleus	Decay energy	Bombarding conditions	$\epsilon E(E2)$	Comments	Multipole order and conversion coefficients	$B(E2)$	Level schemes	Other processes
Ta ¹⁸¹	165	2p (H3; H6)	0.22 (e _K)	cascade trans. from 303-kev level; $\gamma(165) \rightarrow \gamma(137)$ coinc. (G1; H8) $K/L \sim 7$ (H3) $\gamma(\theta): 7/2(E2)11/2(E2+M1)9/2$ $\delta = 0.51$ (M7) ex.func. $\Delta E = 303$ (S4)	20% E2 $\alpha_K = 0.78$ $\alpha = 1.0$			
	166	p (G1)	(γ)					
	167	6 α (H8)	0.13 (γ)					
	167	3p (E1)	(γ)					
	166	4p (B1)	(γ)					
	167	1.8-5p (S4)	0.22 (γ)					
	166	2-4p (B8)	(e)					
165	3p (D1)	0.18 (γ)						
Ta ¹⁸²	303	1.8-2.2p (H5)	0.1 (γ)	ex.func. $\Delta E = 300$ (B1; S4; D1) $\gamma(\theta): 7/2(E2)11/2(E2)7/2$ (G1; E1; M7) $\gamma(165): \gamma(303) = 1.7$ (G1) 1.25 (E1) 1.74 (S4) 1.7 (M5) 1.52 (D1)	100% E2 $\alpha = 0.08$	0.57		
	303	2-4p (G1)	(γ)					
	309	3p (E1)	(γ)					
	303	6 α (H8)	0.067 (γ)					
	303	2.2-4.5p (B1)	(γ)					
	300	p (M1)	0.07 (γ)					
	303	1.4-5p (S4)	0.13 (γ)					
	302	2-3p (D1)	(γ)					
	301	15N (A1)	0.12 (γ)					
γ -W ¹⁸²	100	1.75p (H3; H6)	2.7 (e _L)	sep.iso. (M3) $\sigma(\theta): \sigma(d): \sigma(\alpha)$ gives $\lambda = 2$ (B2)	$\alpha_L = 2.4$ $\alpha = 4.0$	5.6		100.09 Ta ¹⁸² ($\beta^- \gamma$)
	101	2.5p (M1; M3)	0.24 (γ)					
	102	p, α (B8)	(e)					
W ¹⁸³	46.5	1.45 α (H3)	0.5 (e _M)	sep.iso. (M3)				46.48 Ta ¹⁸³ ($\beta^- \gamma$)
	103	2.5p (M1; M3)	0.06 (γ)					
W ¹⁸⁴	295	4p (S4)	0.055 (γ)	see decay scheme established in Ta ¹⁸³ ($\beta^- \gamma$)		0.27		291.7 Ta ¹⁸³ ($\beta^- \gamma$)
	111	1.75p (H3; H6)	1.7 (e _L)					
	112	2.5p (M1; M3)	0.32 (γ)					
112	p, α (B8)	(e)						
W ¹⁸⁶	123	1.75p (H3; H6)	1.4 (e _L)	sep.iso. (M3)	$\alpha_L = 1.4$ $\alpha = 2.6$	4.2		110 Ta ¹⁸⁴ ($\beta^- \gamma$)
	124	2.5p (M1; M3)	0.39 (γ)					
	124	p, α (B8)	(e)					
W	115	2p (H5)	1.4 (γ)	composite line ex.func. $\Delta E = 114$ $\gamma(\theta): 0(E2)2(E2)0(G1)$		4.2		123 Re ¹⁸⁶ ($e^- \gamma$) 125 Ta ¹⁸⁶ ($\beta^- \gamma$)
	114	2-4p (G1)	(γ)					
	~120	3 α (T3)	(γ)					
	112	4p (S4)	(γ)					
	112	15N (A1)	1.3 (γ)					
			(γ)					

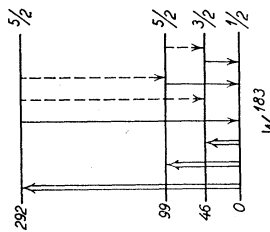


TABLE IV.2.—Continued.

I	II	III	IV	V	VI	VII	VIII	IX
Nucleus	Decay energy	Bombarding conditions	$\epsilon B(E2)$	Comments	Multipole order and conversion coefficients	$B(E2)$	Level schemes	Other processes
${}^{76}\text{Re}^{185}$	130	p (M1)	0.20 (γ)	sep.iso. (M1; W1; D1)	(3% E2) $\alpha_L = 0.40$	1.4		125 Os ¹⁸⁵ ($\epsilon\gamma$) 130 W ¹⁸⁵ ($\beta^-\gamma$)
	125	1.75p (H3)	0.30 (e_L)		$\alpha = 2.8$			
	126	p, α (W1)	0.30 (γ)		(3% E2) $\alpha = 1.5$			162 Os ¹⁸⁵ ($\epsilon\gamma$) 165 W ¹⁸⁵ ($\beta^-\gamma$)
	125	3.2p (D1)	0.22 (γ)		100% E2 $\alpha = 0.11$	0.37		
	160	p, α (W1)	0.16 (γ)	sep.iso. (W1; D1)				
${}^{187}\text{Re}$	158	3.2p (D1)	0.020 (γ)	γ (160)- γ (126) coinc. (W1)				
	290	p (M1)	0.19 (γ)	sep.iso. (M1; W1; D1)	(3% E2) $\alpha_L = 0.35$	1.2		134.25 W ¹⁸⁷ ($\beta^-\gamma$)
	286	p, α (W1)	0.18 (e_L)		$\alpha = 2.3$			
	280	3.2p (D1)	0.32 (γ)		(3% E2) $\alpha = 1.2$			
	135	3.2p (D1)	0.39 (γ)		100% E2 $\alpha = 0.1$	0.46		
Re	139	p (W1)	0.20 (γ)	sep.iso. (W1; D1)				
	163	3.2p (D1)	0.20 (γ)	γ (168)- γ (135) coinc. (W1)				
	320	p (M1)	0.038 (γ)	sep.iso. (M1; W1; D1)				
	303	p, α (W1)						
	300	3.2p (D1)						
${}^{188}\text{Os}$	130	3 α (H1)						
	305	6 α (T8)						
	158	3 α (H1)						155 Re ¹⁸⁸ ($\beta^-\gamma$)
	180	3 α (H1)						
	188	3 α (H1)						
${}^{191}\text{Ir}$	202	3 α (H1)						
	115	3.2p (D1)		sep.iso. (D1)				129.4 Pt ¹⁹¹ ($\epsilon\gamma$) 129 Os ¹⁹¹ ($\beta^-\gamma$)
	129	1.75p (H3)	0.12 (e_L)		$\sim 30\%$ E2 $\alpha = 2.5$	0.63		
	133	3.2p (D1)	0.15 (γ)		$\alpha_L = 0.0$			
	216	3.2p (D1)	0.33 (γ)	sep.iso. (D1)	$\alpha = 0.5$			
356	3.2p (D1)	0.28 (γ)	sep.iso. (D1)		0.8			

TABLE IV.2.—Continued.

I	II	III	IV	V	VI	VII	VIII	IX	
Nucleus	Decay energy	Bombarding conditions	$\epsilon B(E2)$	Comments	Multipole order and conversion coefficients	$B(E2)$	Level schemes	Other processes	
Ir^{193}	139	$1.75p$ (H3)	0.06 (e_L)	sep.iso. (D1)	$\sim 30\% E2$	0.47		$139 Os^{193}(\beta^- \gamma)$	
	143	$3.2p$ (D1)	0.18 (γ)		$\alpha = 2.0$ $\alpha_L = 0.4$				
	230	$3.2p$ (D1)	0.07 (γ)	sep.iso. (D1)	$\alpha = 0.4$				
Ir	368	$3.2p$ (D1)	0.21 (γ)	sep.iso. (D1)		0.3			
	133	3.4α (T9)	(γ)	composite line					
	219	3.4α (T9)	(γ)	composite line					
	360	3.4α (T9)	(γ)	composite line					
$78Pt^{194}$	328	3α and p (H1)	(γ)	sep.iso. (M1)	$\alpha = 0.07$	1.7		$326 Ir^{194}(\beta^- \gamma)$	
	330	$3p$ (M1)	0.51 (γ)	$\gamma(\theta): 0(E2)/2(E2)0(M7)$				$328 Au^{194}(\epsilon \gamma)$	
	330	$2.5-5p$ (S4)	1.62 (γ)	ex.func. $\Delta E = 330(S4)$					
	29	3α (H1)	(γ)	ex.func. $\Delta E = 29(B4)$				$31 Au^{195}(\epsilon \gamma)$	
	29	α (B4)	(γ)						
	98	3α (H1)	(γ)						
	100	4α (S4)	(γ)						
	97	$3-4\alpha$ (B4)	(e_L)						
	128	3α (H1)	(γ)						
	130	4α (S4)	(γ)						
Pt^{195}	212	3α and p (H1)	(γ)	sep.iso. (M1)	$\alpha \sim 0.7$	0.48		$129 Au^{195}(\epsilon \gamma)$	
	210	$3p$ (M1)	0.23 (γ)	$\gamma(\theta): 0(E2)/2(E2)0(M7)$	$\alpha_K \sim 0.55$				
	210	$1.75p$ (H3)	0.15 (e_K)	ex.func. $\Delta E = 126(B4)$					
	210	$5p$ (S4)	0.31 (γ)						
	210	$4p$ (B4)	(e_K)						
	240	$3-5p$ (S4)	(γ)						
Pt^{196}	360	$3p$ (M1)	0.26 (γ)	sep.iso. (M5)	$\alpha = 0.06$	1.3		$354 Au^{196}(\epsilon \gamma)$	
	358	$2.5-5p$ (S4)	1.2 (γ)	$\gamma(\theta): 0(E2)/2(E2)0(M7)$ ex.func. $\Delta E = 358(S4)$					
Pt^{198}	425	$3p$ (M1)	0.20 (γ)	ex.func. $\Delta E = 403(S4)$	$\alpha = 0.04$	1.4			
	403	$2.5-5p$ (S4)	1.3 (γ)						

TABLE IV.2.—Continued.

I	II	III	IV	V	VI	VII	VIII	IX		
Nucleus	Decay energy	Bombarding conditions	ϵE (E2)	Comments	Multipole order and conversion coefficients	$B(E2)$	Level schemes	Other processes		
⁷⁹ Au ¹⁹⁷	77	3 α and ρ (H1)	(γ)	ex.func. $\Delta E = 77$ (B4)				77 Pt ¹⁹⁷ ($\beta^- \gamma$) Hg ¹⁹⁷ ($\epsilon \gamma$)		
	77	3.25 α (B4)	(e)							
	190	3 α and ρ (H1)	(γ)	$\sigma(\alpha); \sigma(\rho)$ indicates a cascade transition from 268-keV level (S4)	$\alpha \sim 1$					191 Pt ¹⁹⁷ ($\beta^- \gamma$) Hg ¹⁹⁷ ($\epsilon \gamma$)
	195	3.9 ρ (G1)	(γ)							
	191	4 ρ , α (S4)	0.042							
	191	3.5 ρ (B4)	(e _L)							
	269	3.8 ρ (M8)	(e)			0.08				
	268	6 ρ (E3)	(ρ')							
	273	4 ρ (S4)	0.02	(γ)	cascade trans. from 550-keV level $\gamma(273) - \gamma(277)$ coinc. (S4)					
	277	3 α and ρ (H1)	(γ)		ex.func. $\Delta E = 277$ (C1; G1; S4)	30% E2				
279	2-5 ρ (C1)	0.14	(γ)	$\gamma(\theta); 3/2(E2) 5/2(E2) + M1) 3/2$	$\alpha = 0.32$					
277	2-4 ρ (T8)	0.25	(γ)	$\beta^0 = 0.6$ (C1)	$\alpha_K = 0.24$					
277	6 α (T8)	0.072	(e _K)	$\beta^0 = 0.07$ (G1)						
281	2 ρ (H3)	0.23	(ρ')	$\delta = -0.75$ (M7)						
277	1.6-5 ρ (S4)	0.23	(ρ')	$K/L = 5.5$ (B4)						
279	3.5 ρ (B4)	0.36	(e _K)	$K/L = 6.3$ (M8)						
279	6 ρ (E3)		(ρ')							
286	15N (A1)		(γ)							
555	3-5 ρ (C1)	0.26	(γ)	ex.func. $\Delta E = 550$ (C1; G1; S4)	100% E2	0.43				
545	3-4 ρ (G1)	0.56	(γ)	$\gamma(\theta); 3/2(E2) 7/2(E2) 3/2$						
550	6 α (T8)	0.42	(γ)	(C1; G1; M7)						
550	2.2-5 ρ (S4)	0.42	(ρ')	cascade trans. via 277-keV level						
550	6 ρ (E3)	0.42	(ρ')	$< 5\%$ (C1)						
580	15N (A1)		(γ)	$< 10\%$ (G1)						
				$= 4\%$ (S4)						
				$K/L = 3.6$ (M8)						
⁸⁰ Hg ¹⁹⁸	411	4 ρ (B6)	1.09	sep.iso. (B6)	$\alpha = 0.04$	0.8		411 Au ¹⁹⁸ ($\beta^- \gamma$)		
	411	3.2 ρ (D1)	0.4							
Hg ¹⁹⁹	163	3 α (H1)	(γ)	sep.iso. (D1; B6)	100% E2	0.26		159 Au ¹⁹⁹ ($\beta^- \gamma$) 158 Tl ¹⁹⁹ ($\epsilon \gamma$)		
	159	3.2 ρ (D1)	0.084		$\alpha = 0.9$					
	159	3 ρ (B6)	0.19	(γ)						
Hg ²⁰⁰	209	3.2 ρ (D1)	0.038	sep.iso. (D1; B6)	$\alpha = 0.9$	0.10		209 Au ¹⁹⁹ ($\beta^- \gamma$) 208 Tl ¹⁹⁹ ($\epsilon \gamma$)		
	209	3 ρ (B6)	0.071		$\alpha = 0.06$	0.7				
	375	3.2 ρ (D1)	0.47	(γ)	sep.iso. (D1; B6)					
Hg ²⁰²	368	4 ρ (B6)	0.80	sep.iso. (D1; B6)	$\alpha = 0.04$	0.5		368 Tl ²⁰⁰ ($\epsilon \gamma$) 370 Hg ($\pi \gamma$)		
	439	3.2 ρ (D1)	0.4	sep.iso. (D1; B6)						
439	4 ρ (B6)	0.57	(γ)							

TABLE IV.2.—Continued.

I	II	III	IV	V	VI	VII	VIII	IX
Nucleus	Decay energy	Bombarding conditions	$\epsilon B(E2)$	Comments	Multipole order and conversion coefficients	$B(E2)$	Level schemes	Other processes
$^{81}\text{Tl}^{205}$	279	3-4.5p (B3) 4p, α (S4)	0.09 (γ)	ex.func. $\Delta E = 279$ (B3)	73% E2 $\alpha = 0.20$	0.12		280 $\text{Pb}^{203}(\epsilon\gamma)$ 280 $\text{Hg}^{203}(\beta^-\gamma)$
	279		0.11 (γ)					
Tl^{205}	205	3-4.5p (B3) 4p, α (S4)	0.11 (γ)	ex.func. $\Delta E = 205$ (B3)	$\alpha \sim 0.5$	0.14		203 $\text{Hg}^{205}(\beta^-\gamma)$
	205		0.072 (γ)					
Tl	410	4-4.5p (B3) 4p (S4)	0.12 (γ)	probably from both isotopes; in coin. with both $\gamma(205)$ and $\gamma(280)$ (S4)	$\alpha \sim 0.1$	0.028		405 $\text{Pb}^{205}(\epsilon\gamma)$
	410		0.12 (γ)					
$^{82}\text{Pb}^{206}$	810	4.5p (S4)	0.14 (γ)	sep.iso. (S4)		0.14		803.3 $\text{Bi}^{206}(\epsilon\gamma)$
	570 580	4.5p (S4) 15N (A1)	0.028 (γ) (γ)			0.028		569 $\text{Bi}^{207}(\epsilon\gamma)$
$^{90}\text{Th}^{232}$	50	3 and 6α (T3; T8) 4α (S4) 2.5-3.3 α (D1)	0.057 (γ)		$\alpha = 290$	9		~ 50 $\text{U}^{238}(\alpha\gamma)$
	53		0.0096 (γ)					
	50		0.13 (γ)					
	760		($\epsilon\alpha$)					
	719	4.8p (M8)		$K/L = 3.5$ (M8)				

TABLE IV.2.—Continued.

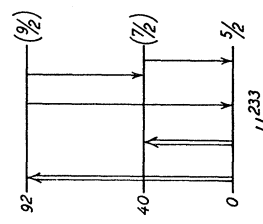
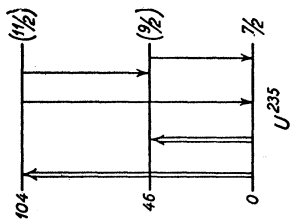
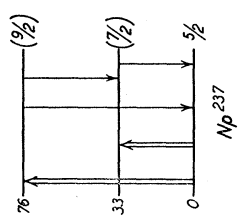
I	II	III	IV	V	VI	VII	VIII	IX
Nucleus	Decay energy	Bombarding conditions	$\epsilon B(E2)$	Comments	Multipole order and conversion coefficients	$B(E2)$	Level schemes	Other processes
$^{92}\text{U}^{233}$	40.4	2.8 α (N1)	0.015 (γ)		(80% $E2$) $\alpha=870$	13		40.5 $\text{Pu}^{233}(\beta-\gamma)$
	51.5	2.8 α (N1)	0.0070 (γ)	cascade trans. from 92-keV level	(80% $E2$) $\alpha=240$			
	92.3	2.8 α (N1)	0.032 (γ)		100% $E2$ $\alpha=21$	2.4		
U^{235}	46.2	2.8 α (N1)	0.057 (γ)		(6% $E2$) $\alpha=66$	3.8		
	56.7	2.8 α (N1)	0.017 (γ)	cascade trans. from 104-keV level	(6% $E2$) $\alpha=31$			
	103.2	2.8 α (N1)	0.0041 (γ)		100% $E2$ $\alpha=15$	0.60		44 $\text{Pu}^{242}(\alpha)$
U^{238}	44	3 α (H1; T8)	0.034 (γ)		$\alpha=680$	13		
	45	3.3 α (D1)	0.0070 (γ)					
	44.7	2.8 α (N1)	0.015 (γ)					
$^{93}\text{Np}^{237}$	33.2	2.8 α (N1)	0.026 (γ)		(2% $E2$) $\alpha=150$	4.0		33.20 $\text{Am}^{241}(\alpha\gamma)$ 33.2 $\text{U}^{237}(\beta-\gamma)$
	42.6	2.8 α (N1)	0.023 (γ)	cascade trans. from 76-keV level	(2% $E2$) $\alpha=68$			
	76	2.8 α (N1)	0.0026 (γ)		100% $E2$ $\alpha=60$	1.8		

TABLE IV.2.—Continued.

I	II	III	IV	V	VI	VII	VIII	IX
Nucleus	Decay energy	Bombarding conditions	$\epsilon B(E2)$	Comments	Multipole order and conversion coefficients	$B(E2)$	Level schemes	Other processes
$^{94}\text{Pu}^{239}$	49.6	2.8α (N1)	$0.0073(\gamma)$	probably cascade trans. from 57-keV level	$(22\%E2)$ $\alpha=150$	4.2		$49.40 \text{ Np}^{239}(\beta-\gamma)$ $57.25 \text{ Np}^{239}(\beta-\gamma)$

- A 1 Alkhozov, Andreyev, Greenberg, and Lemberg, *Nuclear Phys.* **2**, 65 (1956).
 B 1 K. Barfotaud and T. Gryebine, *Compt. rend.* **239**, 491 (1954).
 2 J. H. Bierregaard and T. Huus, *Phys. Rev.* **94**, 204 (1954) (1955).
 3 Barfotaud, Gryebine, and Ktor, *Compt. rend.* **240**, 1247 (1955).
 4 E. M. Bernstein and H. W. Lewis, *Phys. Rev.* **100**, 1345 (1955).
 5 E. M. Bernstein and H. W. Lewis, *Phys. Rev.* **101**, 1367 (1956).
 6 Barfotaud, Gryebine, and Ktor, *Compt. rend.* **242**, 1284 (1956).
 7 J. H. Bierregaard and U. Meyer-Bekhou, *Z. Naturforsch.* **11a**, 273 (1956).
 8 E. M. Bernstein and H. W. Lewis, *Phys. Rev.* **97**, 1226 (1955).
 9 C. A. Barnes, *Phys. Rev.* **97**, 1226 (1955).
 C 1 Cook, *Class. and Quant. Theory*, **96**, 658 (1954).
 D 1 C. M. Class and U. Meyer-Bekhou, *Phys. Rev.* (to be published).
 D 2 L. Davis, D. G. E. Smith, and G. M. Temmer, *Phys. Rev.* **103**, 1801 (1956).
 E 1 Elbeke, Cook, and Class, *Phys. Rev.* **94**, 735 (1954).
 2 B. Elbeke (to be published).
 3 B. Elbeke and C. K. Rockliffe, *Phys. Rev.* (to be published).
 F 1 Fagg, Wolicki, Rondelli, Dunning, and Snyder, *Phys. Rev.* **100**, 1299 (1955).
 G 1 W. P. Heydenburg and R. M. Williamson, *Phys. Rev.* **95**, 767 (1954).
 H 1 N. P. Heydenburg and G. M. Temmer, *Phys. Rev.* **93**, 906 (1954).
 2 N. P. Heydenburg and G. M. Temmer, *Phys. Rev.* **99**, 617(A) (1955) and private communication.
 3 Huus, Bierregaard, and Elbeke, *Kgl. Danske Vidensk. Selskab Mat. fys. Medd.* **30**, No. 17 (1956).
 4 T. Huus and A. Lundén, *Phil. Mag.* **45**, 966 (1954).
 5 T. Huus and C. Zupancic, *Kgl. Danske Vidensk. Selskab Mat. fys. Medd.* **28**, No. 1 (1953).
 6 T. Huus and J. Bierregaard, *Phys. Rev.* **92**, 1570 (1953).
 7 N. P. Heydenburg and G. M. Temmer, *Phys. Rev.* **95**, 861 (1954).
 8 N. P. Heydenburg and G. M. Temmer, *Phys. Rev.* **100**, 150 (1955) and privately circulated revisions of yield determinations.
 9 N. P. Heydenburg and G. M. Temmer, *Phys. Rev.* **94**, 1252 (1954).
 10 N. P. Heydenburg and G. M. Temmer, *Bull. Am. Phys. Soc. Ser. II*, **1**, 164 (1956) and private communication.
 J 1 G. A. Jones and D. H. Wilkinson, *Phil. Mag.* **45**, 230 (1954).
 L 1 Lemmer, Segert, and Grace, *Proc. Phys. Soc. (London)* **68A**, 701 (1955).
 M 1 McClelland, Mark, and C. Godman, *Phys. Rev.* **97**, 1191 (1955).
 2 McClelland, Mark, and C. Godman, *Phys. Rev.* **91**, 760 (1953).
 3 McClelland, Mark, and C. Godman, *Phys. Rev.* **93**, 904 (1954).
 4 Mark, McClelland, and Godman, *Phys. Rev.* **98**, 1245 (1955).
 5 H. Mark and G. T. Paulissen, *Phys. Rev.* **90**, 1654(A) (1955).
 6 H. Mark and G. T. Paulissen, *Phys. Rev.* **100**, 813 (1955).
 7 F. K. McGowan and P. H. Stelson, *Phys. Rev.* **99**, 127 (1955).
 8 Moore, Class, Prosser, and Schiffer, *Bull. Am. Phys. Soc. Ser. II*, **1**, 88 (1956).
 N 1 J. O. Newton (private communication).
 P 1 E. B. Paul and H. E. Gove (private communication, November 1953).
 2 van Patter, Rothman, Mandeville, and Swann, *J. Franklin Inst.* **259**, 261 (1955).
 S 1 Sherr, Li, and Christy, *Phys. Rev.* **94**, 1076 (1954) and **96**, 1258 (1955).
 2 Schiffer, Moore, and Class, *Phys. Rev.* (to be published).
 3 Simmons, van Patter, Famularo, and Stuart, *Phys. Rev.* **97**, 89 (1955).
 4 P. H. Stelson and F. K. McGowan, *Phys. Rev.* **99**, 112 (1955).
 5 Simmons, Famularo, and Freier, *Phys. Rev.* **100**, 1265(A) (1955).
 T 1 G. M. Temmer and N. P. Heydenburg, *Phys. Rev.* **98**, 1198(A) (1955).
 2 G. M. Temmer and N. P. Heydenburg, *Phys. Rev.* **96**, 426 (1954) and privately circulated revisions of yield determinations.
 3 G. M. Temmer and N. P. Heydenburg, *Phys. Rev.* **93**, 351 (1954).
 4 G. M. Temmer and N. P. Heydenburg, *Bull. Am. Phys. Soc. Ser. II*, **1**, 43 (1956) and privately circulated revisions of yield determinations.
 5 G. M. Temmer and N. P. Heydenburg, *Phys. Rev.* **98**, 1308 (1955) and privately circulated revisions of yield determinations.
 6 G. M. Temmer and N. P. Heydenburg, *Phys. Rev.* **99**, 617(A) (1955) and private communication.
 7 G. M. Temmer and N. P. Heydenburg, *Phys. Rev.* **100**, 961(A) (1955) and private communication.
 8 G. M. Temmer and N. P. Heydenburg (private communication).
 9 G. M. Temmer and N. P. Heydenburg, *Phys. Rev.* **94**, 1399 (1954).
 W 1 Wolicki, Fagg, and Geer, *Phys. Rev.* **100**, 1265(A) (1955) and private communication.

acter of the excited levels. Where directly measured lifetimes are available, the half-lives are listed, employing the following abbreviations: s (seconds), μs (10^{-6} sec), $m\mu s$ (10^{-9} sec).

The level populated in Coulomb excitation of an even-even nucleus appears in all cases to be the first excited, $2+$, state and no decay scheme is drawn.

Column IX. Other Processes

This column lists other reactions in which levels are observed that may tentatively be identified with those found in Coulomb excitation. The observed energies are given in kev, together with the reaction involved. References to the experimental work may be found in Hollander, Perlman, and Seaborg, *Revs. Modern Phys.* **25**, 469 (1953), and Nuclear Data Cards, edited by K. Way *et al.*, National Research Council, Washington D. C.

CHAPTER V. COLLECTIVE NUCLEAR EXCITATIONS

An outstanding feature of the nuclear spectra revealed by the Coulomb excitation studies is the systematic occurrence throughout the periodic system of low-energy electric quadrupole transitions of a strength greatly exceeding that which would be associated with the excitation of a single nucleon. The estimate (II A.58) of the reduced transition probability for a single proton transition of $E2$ type gives¹²²

$$B(E2)_{sp} = 3 \cdot 10^{-5} A^{4/3} e^2 10^{-48} \text{ cm}^4. \quad (\text{V.1})$$

Thus, from a comparison with the observed $B(E2)$ values in column VII of Table IV.2, it is seen that most elements exhibit $E2$ transitions of a strength more than 10 times the single particle unit, and that in certain regions transitions occur with a probability exceeding this unit by a factor of more than 100.

These enhanced transitions are clearly due to the cooperative effects of a large number of nucleons, and indeed most of the observed levels can be interpreted in terms of simple collective excitations of rotational or vibrational type. Where this interpretation can be made, the Coulomb excitation experiments yield valuable information on such collective nuclear properties as the equilibrium shape, the deformability, and the inertial parameters associated with the collective motion. In the present chapter, we shall outline the theory of collective nuclear excitations and discuss the evidence obtained from the Coulomb excitation experiments.

V A. Qualitative Considerations

In the analysis of nuclear excitation spectra it is possible to distinguish between two different modes of

¹²² As already noted in Chapter II, the statistical factor appearing in (II A.58) is somewhat arbitrary; it is the factor appropriate to a two proton excitation of the type $(j^2)_{J=0} \rightarrow (j^2)_{J=2}$ in the limit of large j .

excitation, the first associated with the motion of individual nucleons and the second with collective types of nuclear motion.^{123,124} One may think of the former degrees of freedom as representing the motion of the nucleons in a fixed nuclear potential (the intrinsic nuclear motion), while the latter are associated with variations in the shape and orientation of the nuclear field.

Such a separation of the motion becomes possible when the frequencies of the collective excitations are small compared with those characterizing the intrinsic nucleonic motion and is in many respects analogous to the separation between electronic and nuclear motion in molecules.

When this adiabatic condition is fulfilled, one may treat the equations of motion for the nucleus in two steps. First one considers the nucleonic motion for fixed values of the collective parameters α , specifying the nuclear field; the energy eigenvalues for this motion are denoted by $E_i(\alpha)$. The collective motion superposed on the intrinsic motion is then given by a Hamiltonian of the approximate form

$$H_{\text{coll}} = E_i(\alpha) + \frac{1}{2} B_i(\alpha) \dot{\alpha}^2. \quad (\text{V.2})$$

The functions $E_i(\alpha)$ are referred to as the potential energy surfaces of the nucleus and play a similar role as in the treatment of molecular vibrations and rotations. In the present discussion we are especially interested in the behavior of the potential energy surfaces near the equilibrium shape.¹²⁵

The second term in (2) gives the kinetic energy of the collective motion, which may be obtained by considering the nucleonic motion for slowly varying α . This kinetic energy can be written as a quadratic expression in the $\dot{\alpha}$, provided all the frequencies of the intrinsic motion are large compared to those of the collective motion, so that the intrinsic motion adjusts adiabatically to the variation in α .

If the intrinsic motion possesses degenerate or close lying energy levels, the adiabatic approximation may partially break down. The nucleus must then be described in terms of a coupled system of collective oscillations and the low energy intrinsic degrees of freedom in question.¹²⁴

¹²³ For a recent review of the nuclear independent particle model, see M. G. Mayer and J. H. D. Jensen, *Elementary Theory of Nuclear Shell Structure* (John Wiley and Sons, Inc., New York, 1955).

¹²⁴ Collective nuclear oscillations were first considered by N. Bohr and F. Kalckar, *Kgl. Danske Videnskab. Selskab Mat. fys. Medd.* **14**, No. 10 (1937). The interplay between collective and independent particle motion has been discussed by J. Rainwater, *Phys. Rev.* **79**, 432 (1950); A. Bohr, *Kgl. Danske Videnskab. Selskab Mat. fys. Medd.* **26**, No. 14 (1952); D. L. Hill and J. A. Wheeler, *Phys. Rev.* **89**, 1102 (1953); A. Bohr and B. R. Mottelson, *Kgl. Danske Videnskab. Selskab Mat. fys. Medd.* **27**, No. 16 (1953).

¹²⁵ The behavior of these surfaces for larger deformations has been discussed in connection with the nuclear fission process [N. Bohr and J. A. Wheeler, *Phys. Rev.* **56**, 426 (1939); D. L. Hill and J. A. Wheeler, reference 124; A. Bohr, *Proceedings of the International Conference on the Peaceful Uses of Atomic Energy* (Columbia University Press, New York, 1956), Vol. 2, p. 151 (Geneva, 1956)].

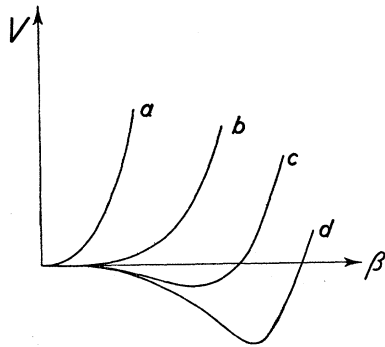


FIG. V.1. Potential energy surfaces for even-even nuclei. The nuclear potential energy V is plotted as a function of the deformation parameter β , which may, for instance, represent the quadrupole eccentricity of the nucleus [see (V.6)]. The various curves are intended to illustrate schematically the behavior of the potential energy surfaces for even-even nuclei as one moves away from closed shells.

The curve a represents a configuration with only relatively few particles outside of closed shells. As particles are added the restoring force decreases though the spherical shape ($\beta=0$) remains stable (curve b). Still further from the closed shell the spherical shape may become unstable (curve c) and the nucleus acquires a nonspherical equilibrium shape. With the addition of still more nucleons the equilibrium eccentricity increases and the minimum in the potential energy surface becomes sharper (curve d).

The curves all refer to the lowest intrinsic state. Additional sets of potential energy surfaces are associated with each excited intrinsic state.

Although the details of the figure have no quantitative significance, the qualitative trends are suggested by simple considerations (see the discussion in the text).

In the earliest treatments of collective nuclear oscillations, one attempted to estimate the potential and kinetic energy in (2) by comparing the nucleus with a liquid drop. It is found, however, that the shell structure in the nucleonic motion has a profound effect on the collective properties of the individual nuclei. Thus, the potential energy surfaces depend essentially on the nucleonic configuration and also the inertial parameters $B_i(\alpha)$ deviate from the hydrodynamical estimates.

The main features of the nuclear potential energy surfaces are determined by the competition between the particles in closed shells, which strongly prefer a spherical nuclear shape, and the particles in unfilled shells which tend to polarize the nucleus and bring about a nonspherical equilibrium shape.¹²⁶ The latter tendency is, however, counteracted by the residual interactions between the nucleons, which must be added to the interactions already included in the average field. The residual interactions imply correlations in the nucleonic motion which reduce the net polarizing effect. This reduction is a result of the attractive short-range character of the nuclear forces which favor states of maximum spherical symmetry.¹²³

The influence of the residual interactions is the greatest for small deformations of the nuclear shape, as a consequence of the degeneracy of the particle motion

in a spherical field. For large nuclear eccentricities, the strong coupling of the individual particles to the nuclear deformation removes the degeneracies, and the residual interactions are then of less importance.

The dependence of the potential energy surfaces on the number of nucleons in unfilled shells is illustrated schematically in Fig. V.1. The figure refers to even-even nuclei, for which the lowest intrinsic state for a spherical shape possesses zero total angular momentum. The spherical density distribution of such a state implies that the average polarizing effect of the particles vanishes. For an even-even nucleus, the spherical shape thus always represents an equilibrium, which may, however, be either stable or unstable. For configurations with only relatively few particles outside of closed shells, the deformation which would result in the absence of residual interactions is small; the coupling between the nucleons is then mainly determined by these interactions and the spherical nuclear shape remains a stable equilibrium. For sufficiently many particles in unfilled shells, however, the deformation caused by the nucleonic motion is large and thus only little affected by the residual interactions; the strongly deformed shape then gives the minimum in the potential energy surface, and the spherical shape is unstable.

On the basis of these qualitative considerations we consider briefly the general features of the collective nuclear excitation spectra for the different configurations.

For a closed shell nucleus, the special stability of the spherical equilibrium shape¹²⁷ implies that oscillations in shape would have high frequencies. Since these frequencies may be of the order of those involved in the single particle motion, there may be no sharp distinction between collective and single particle excitations of a closed shell nucleus.¹²⁸

If one or a few nucleons are added to (or subtracted from) a closed shell configuration, the low-energy nuclear states may be approximately described in terms of the motion of these added particles. There exists, however, a weak coupling between this nucleonic motion and the oscillations of the closed shell core, which implies a significant enhancement of the electric multipole transitions between the low-lying levels.

As more nucleons are added to the closed shell configuration, the description of the excitations in terms of the motion of the individual nucleons becomes highly complex, especially due to the effect of configuration mixing. Moreover, the coupling to the closed shell core increases.

Already for nuclei containing relatively few particles in unfilled shells, however, one observes states in the low-energy nuclear spectrum which can be approximately described in terms of simple collective oscillations. The collective behavior of the nucleons may be understood from the fact that the potential energy of

¹²⁷ S. Gallone and C. Salvetti, *Nuovo cimento* (9) **10**, 145 (1953). See also the references in footnote 124.

¹²⁸ D. Inglis, *Phys. Rev.* **97**, 701 (1955).

¹²⁶ J. Rainwater, reference 124.

deformation decreases as one moves away from closed shell configurations (see Fig. V.1); therefore, the frequency of collective oscillation soon becomes smaller than the main frequencies of the intrinsic motion.

In the vicinity of the closed shells, where the spherical shape represents a stable equilibrium, the collective excitations correspond to vibrations about this shape. The frequencies of these vibrations are expected to decrease fairly regularly with the addition of particles, corresponding to the decreasing restoring force. Eventually, this tendency may lead to instability of the spherical shape and a resulting nonspherical equilibrium shape (see Fig. V.1).

For such deformed nuclei the collective spectrum separates into excitations of vibrational and rotational type. The first corresponds to oscillations about the equilibrium shape for fixed orientation of the nucleus, while the second represents a collective motion which rotates the nuclear orientation while preserving the shape. Such a separation becomes possible since the nuclear deformation implies that a large mass transport is associated with the rotational motion. This motion can thus take place with small frequency and therefore without affecting the shape (or intrinsic structure) of the nucleus.

The simple character of the rotational motion gives rise to many regularities in the rotational excitation levels, which make them easily identifiable. The rotational states are also especially strongly excited in Coulomb excitation experiments, as a consequence of their low energy and large electric quadrupole transition probabilities. We therefore begin, in Sec. B, with a more detailed discussion of this special type of collective excitation.

The properties of the vibrational modes of excitation, in spherical and deformed nuclei, are at present less well established, but the Coulomb excitation process constitutes one of the most promising methods for a further exploration of these states. In Secs. C and D, we discuss the general characteristics expected for vibrational spectra and summarize the available evidence on these excitations. Finally, in Sec. E, we consider briefly some of the special features of the excitation spectra for nuclei in the closed shell regions.

V B. Rotational Excitations

The occurrence of rotational spectra is a general characteristic of nuclei possessing a nonspherical equilibrium shape. For such nuclei it is possible to separate between a collective rotational motion and the nucleonic motion for fixed nuclear orientation. This latter motion may again separate into vibrational and individual particle components, but will in the present section often be referred to simply as the intrinsic nuclear motion, since the main regularities in the rotational spectra are independent of the details of this intrinsic structure.

V B.1. Energy Spectrum

The rotational spectrum becomes especially simple if the nuclear shape possesses axial symmetry, as appears generally to be the case for the very strongly deformed nuclei.^{129,130} The angular momentum coupling scheme is then similar to that of a linear molecule¹³¹ and can be characterized by the three constants of the motion: the total angular momentum I , its projection M on a space-fixed axis, and its projection K on the nuclear symmetry axis (see Fig. V.2).

Since there can be no collective rotations about a symmetry axis (see footnote 147 later), the quantum number K is a constant for each rotational band and represents an intrinsic angular momentum. The rotational spectrum for the nucleus has the same general form as for a molecule and may be written¹³²

$$E_I = E_0 + \frac{\hbar^2}{2\mathfrak{I}} \{I(I+1) + a(-1)^{I+\frac{1}{2}}(I+\frac{1}{2})\delta_{K, \frac{1}{2}}\}, \quad (\text{V.3})$$

where E_0 is a constant depending only on the intrinsic structure, while \mathfrak{I} represents the effective moment of inertia about an axis perpendicular to the nuclear symmetry axis. The last term in the brackets, occurring only for states with $K = \frac{1}{2}$, is associated with a decoupling of the spin angular momentum from the rotational motion. The decoupling parameter a can be expressed as an expectation value for the intrinsic motion.^{132,133} A similar decoupling effect is well known from molecular spectra (see, e.g., the uncoupling of the electronic spin from the

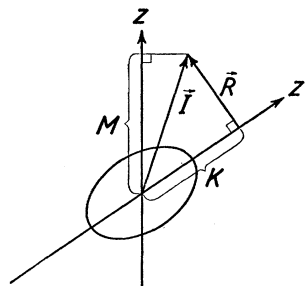


FIG. V.2. Coupling scheme for deformed nuclei. For strongly deformed nuclei possessing axial symmetry, the angular momentum properties may be characterized by the three constants of the motion I , M , and K . While I and M represent the total angular momentum and its component along the fixed z axis, the component of I along the nuclear symmetry axis, z' , is denoted by K . The collective rotational angular momentum R is perpendicular to the z' axis; thus K represents an intrinsic angular momentum.

¹²⁹ The principal empirical evidence for the axial symmetry is the observed $I(I+1)$ type of rotational spectra (see, e.g., Fig. V.4). The preference for axial symmetry is also consistent with theoretical estimates of the equilibrium shape for the nuclear shell structure.

¹³⁰ Rotational spectra for nuclei without axial symmetry have been considered by C. Marty [Nuclear Phys. I, 85 (1956)].

¹³¹ A. Bohr, Phys. Rev. 81, 134 (1951).

¹³² A. Bohr and B. R. Mottelson, reference 124.

¹³³ S. G. Nilsson, Kgl. Danske Videnskab. Selskab Mat. fys. Medd. 29, No. 16 (1955).

rotational motion for ${}^2\Sigma$ states, which leads to rotational spectra with $a=+1$ and $a=-1$.¹³⁴

The value of K for the nuclear ground state may be obtained from a consideration of the individual particle motion in the deformed nucleus. In such a nonspherical field, the angular momenta l_k and j_k of a nucleon are in general not constants of the motion, but for axially symmetric nuclei the nucleon orbitals may be labeled by the constant of the motion Ω_k , which represents the projection on the symmetry axis of the total angular momentum of the nucleon. States which differ only in the sign of Ω_k are degenerate, since they are the same except for the sense of the particle motion around the symmetry axis. This gives rise to an especially simple type of shell structure, in which the particles are filled pairwise in states of opposite Ω_k with no net contribution to K . Thus, for the lowest state of an even-even nucleus, all the particles are in paired orbits, and we have $K=0$. In an odd- A nucleus, the last nucleon occupies an unpaired orbit, and K equals the Ω_k of this orbit.¹³⁵

This coupling scheme, which would apply for independent particle motion, is somewhat modified by the residual interactions between the nucleons. However, there is evidence that these interactions can be considered as acting principally between paired nucleons, so that the above classification remains valid for the ground state of even-even nuclei and the intrinsic states of odd- A nuclei corresponding to the different orbits of the last odd nucleon.¹³⁶ On the other hand, the degrees of freedom associated with the excitation of paired nucleons may partly manifest themselves in collective vibrational motion (see Sec. V D).

For nuclear shapes possessing reflection symmetry with respect to a plane perpendicular to the nuclear axis, the possible rotational quantum states are governed by symmetry requirements similar to those applying to homonuclear diatomic molecules.^{137,138} Thus, for an intrinsic state with $K=0$, only even or odd values of I are allowed, according to the symmetry of the intrinsic state with respect to a rotation of 180° about an axis perpendicular to the symmetry axis. In particular, for the ground state of an even-even nucleus, only the even

values

$$I=0, 2, 4, 6, \dots \text{ (even parity)} \quad (\text{V.4})$$

occur in the rotational spectrum.¹³⁹

For intrinsic states with $K \neq 0$, the allowed values of the nuclear spin are

$$I=K, K+1, K+2, \dots \quad (\text{V.5})$$

The members of the band all have the same parity which equals the parity of the intrinsic motion. Thus, for an odd- A nucleus with a single unpaired nucleon, the orbit of this last particle determines the parity as well as the K -value of the rotational band.

Even-even nuclei.—The Coulomb excitation experiments have provided one of the most important sources of information on the rotational excitations. These are strongly populated by transitions of electric quadrupole type, and in an even-even nucleus, one should thus excite the first state ($I=2+$) of the lowest rotational band. It has also been found that the Coulomb excitation induces just one strong transition in each even-even nucleus far from closed shells. The excitation energy E_2 of this state is a rather smooth function of the atomic number and decreases as one moves away from closed shells. The energy systematics of the first excited states of even-even nuclei is shown in Fig. V.3.

The regions of large nuclear deformations are characterized by especially small values of the excitation energies E_2 , and, as will be discussed below, rotational spectra are only expected in nuclei for which E_2 is less than the critical value indicated by the dotted curve in Fig. V.3. Such small excitation energies are found in the light elements with $A \sim 8$ and 24, and in the heavier elements with $150 < A < 190$ and $A > 222$.

These regions include just the nuclei for which the number of particles in unfilled shells relative to those in closed shells is especially large. In the mass region $40 < A < 150$ the conditions for the occurrence of large deformations are less favorable, partly due to the effect of the spin orbit coupling which breaks the major shells, and partly due to the neutron excess which implies that the closings of neutron and proton shells occur for different nuclei.

The rotational interpretation of the states populated by Coulomb excitation in the mass regions $150 < A < 190$ and $A > 222$ is confirmed by the observation of higher excited states in the rotational band. These states which are populated in radioactive decay processes are found in even-even nuclei to have the spin sequence (4) with energies corresponding to (3). (See Fig. V.4)¹⁴⁰

The Coulomb excitation of these higher states would require either a transition of multipole order greater

¹³⁴ See G. Herzberg, *Spectra of Diatomic Molecules* (D. van Nostrand Company, Inc., New York, 1950), p. 222.

¹³⁵ For calculations of the single particle states in deformed axially symmetric potentials, see S. Moszkowski, *Phys. Rev.* **99**, 803 (1955); S. G. Nilsson, reference 133; K. Gottfried, *Phys. Rev.* **103**, 1017 (1956).

¹³⁶ Compare the classification of the spins and parities of the ground states and low-lying intrinsic excitations of odd- A nuclei with nonspherical shape in terms of the binding states of the last odd nucleon in an ellipsoidal potential (B. R. Mottelson and S. G. Nilsson, *Phys. Rev.* **99**, 1615 (1955); K. Gottfried, reference 135). Additional evidence is provided by the systematic occurrence of unhindered α decay in odd- A nuclei [Bohr, Fröman, and Mottelson, *Kgl. Danske Videnskab. Selskab Mat. fys. Medd.* **29**, No. 10 (1955)].

¹³⁷ A. Bohr, reference 124.

¹³⁸ K. W. Ford, *Phys. Rev.* **90**, 29 (1953).

¹³⁹ For the spin-parity values of rotational bands associated with vibrational excitations, see Sec. V D.1.

¹⁴⁰ Evidence for rotational bands in the nuclei with $A=24$ and 25 is discussed by Litherland, Paul, Bartholomew, and Gove, *Phys. Rev.* **102**, 208 (1956). For the nuclei around $A=8$, the consequences of the present description are similar to those which follow from the α -particle model [see the review by D. R. Inglis, *Revs. Modern Phys.* **25**, 390 (1953)].

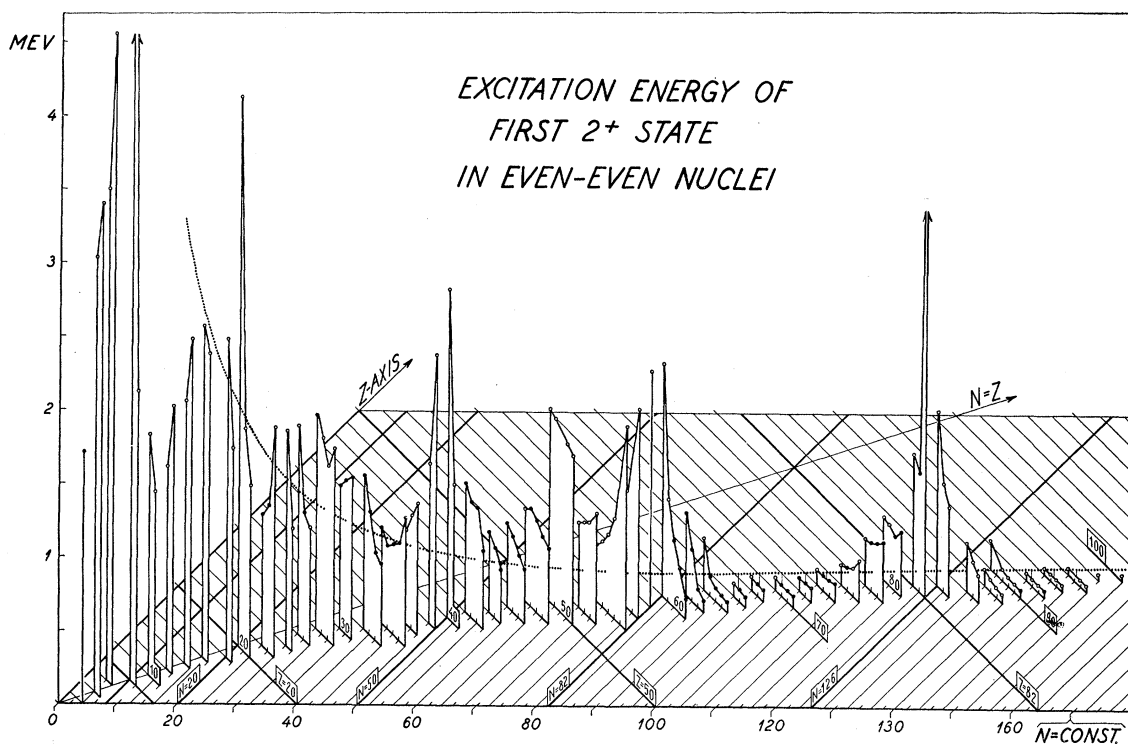


FIG. V.3. Energy systematics of first excited 2^+ states in even-even nuclei. The energies of the first excited 2^+ states of the even-even nuclei are plotted as a function of neutron number N and proton number Z . The black circles indicate levels that have been observed in Coulomb excitation, while the open circles represent levels which have so far only been observed in radioactivity or nuclear reaction studies.

The rotational spectra occur in the regions farthest from closed shells, where the excitation energies are lowest; in other regions, the excitations have the character of collective quadrupole vibrations (see Sec. V C). The separation between these two regions is approximately given by the criterion (9) which is illustrated by the dotted curve following the stable mass region. Thus, the rotational spectra are found in the regions where the observed first excited states have energies less than this separation line. For the value of \mathcal{S}_{rig} in (9), we have used the relation (7) with $R_0 = 1.2A^{1/3} \times 10^{-13}$ cm, and have estimated the higher order β -dependent corrections by assuming β to have the critical value $0.6v$ with the interaction parameter $v = 1.8A^{-1/3}$ (see reference 145).

The figure is a representation of the systematics first discussed by G. Scharff-Goldhaber, Phys. Rev. **90**, 587 (1953) and by P. Preiswerk and P. Stählerin, Nuovo cimento **10**, 1219 (1953). The experimental energies are taken from Table IV.2, and from the following compilations: F. Ajzenberg and T. Lauritsen, reference 187; P. M. Endt and J. C. Kluwyer, Revs. Modern Phys. **26**, 95 (1954); K. Way *et al.*, Nuclear Level Schemes, $40 \leq A \leq 92$, Washington (1955). Additional data are obtained from: Perlman, Bernstein, and Schwartz, Phys. Rev. **92**, 1236 (1953) Pd¹⁰⁸ and Cd¹⁰⁸; L. Grodzins and H. Motz, Phys. Rev. **100**, 1236(A) (1955) Sn¹¹⁴; C. L. McGinnis, Phys. Rev. **98**, 1172(A) (1955) Sn¹²⁰; Farrelly, Koerts, van Lieshout, Benczer, and Wu, Phys. Rev. **98**, 1172(A) (1955) Sn¹²²; M. J. Glaubman, Phys. Rev. **98**, 645, 1172(A) (1955) Sn¹²²; Benczer, Farrelly, Koerts, and Wu, Phys. Rev. **100**, 955(A) (1955) Te¹²⁸ and Xe¹²⁸; R. S. Caird and A. C. G. Mitchell, Phys. Rev. **94**, 412 (1954) Xe¹³⁰; H. N. Brown and R. A. Becker, Phys. Rev. **96**, 1372 (1954) Er¹⁶⁴; A. H. W. Aten, Jr., and G. D. de Feyfer, Physica **21**, 543 (1955) Os¹⁹⁰; Aten, de Feyfer, Sterk, and Wapstra, Physica **21**, 740 (1955) Os¹⁹⁰; M. W. Johns and S. V. Nablo, Phys. Rev. **96**, 1599 (1954) Os¹⁹² and Pt¹⁹²; V. E. Krohn and S. Raboy, Phys. Rev. **95**, 1354 (1954) Pb²⁰⁴; I. Bergström and A. H. Wapstra, Phil. Mag. **46**, 61 (1955) Pb²⁰⁴; Mihelich, Schardt, and Segrè, Phys. Rev. **95**, 1508 (1954) Po²¹⁰; I. Perlman (private communication of work by Asaro, Harvey, Hollander, Perlman, Smith, and Stephens) Em²¹⁸, Ra²²², Th²²², Th²²⁶, Pu²⁴⁰, Pu²⁴², Fm²⁵⁶; T. O. Passell, UCRL-2528 (1954), U²³⁸, Pu²³⁸; O. P. Hok and G. J. Sizoo, Physica **20**, 77 (1954) U²³²; Asaro, Stephens, Harvey, and Perlman, Phys. Rev. **100**, 137 (1955) Cm²⁴⁶, Cm²⁴⁸; Asaro, Stephens, Thompson, and Perlman, Phys. Rev. **98**, 19 (1955) Cf²⁵⁰.

than $E2$, or a multiple $E2$ transition, and has not yet been observed. For an estimate of the cross sections for these processes, see Sec. V B.2.

The moments of inertia derived from the observed rotational spectra of even-even nuclei in the region $150 \leq A \leq 188$ are plotted in Fig. V.5 as a function of the nuclear quadrupole deformation parameter β . If the nucleus is assumed to have spheroidal shape, β is given by

$$\beta = \frac{4}{3} \left(\frac{\pi}{5} \right)^{1/2} \frac{\Delta R}{R_0} = 1.06 \frac{\Delta R}{R_0}, \quad (\text{V.6})$$

where R_0 is the mean nuclear radius and ΔR the difference between the major and minor semiaxis of the spheroid. The values of β employed in Fig. V.5 are obtained from the observed $E2$ transition probabilities, which determine the quadrupole moment of the nuclear shape [see (10) and (12) and Table V.2]. The moments of inertia are plotted in units of the moment

$$\mathcal{S}_{\text{rig}} = \frac{2}{5} AMR_0^2 (1 + 0.31\beta + \dots), \quad (\text{V.7})$$

associated with a rigid rotation of a spheroid of mass AM about an axis perpendicular to the symmetry axis.

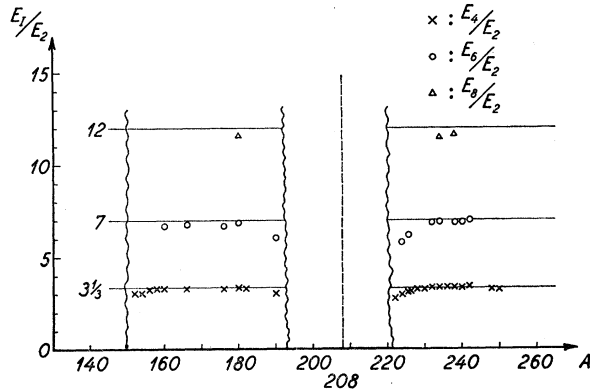


FIG. V.4. Energy ratios of rotational excitations in even-even nuclei. The figure shows the measured ratios of the energies of the higher rotational excitations to the energy of the first excited ($2+$) state in the regions $150 < A < 190$ and $A > 222$, where rotational spectra are expected (compare Fig. V.3). The horizontal lines are the limiting theoretical ratios obtained from (3), assuming the higher states to have the spins $4+$, $6+$, $8+$; while these spin values are experimentally established in only a few cases, they are in all cases consistent with available data on the decay scheme. The small systematic deviations from the limiting expression (3), which increase with the approach to closed shells and with I , can be interpreted in terms of the perturbation of the intrinsic structure produced by the rotational motion (compare Sec. V B.4).

The experimental data for the figure is taken from the compilation in Chapter XVII in *Beta- and Gamma-Spectroscopy*, edited by K. Siegbahn (North Holland Publishing Company, Amsterdam, 1955), and from: A. H. W. Aten, Jr., and G. D. de Feyfer, *Physica* **21**, 543 (1955) Os¹⁹⁰; Aten, de Feyfer, Sterk, and Wapstra, *Physica* **21**, 740 (1955) Os¹⁹⁰; I. Perlman (private communication of work by Asaro, Harvey, Hollander, Perlman, Smith, and Stephens) Ra²²², Th²²⁶, U²³⁴, Pu²³⁸, Pu²⁴⁰, Cm²⁴², Cm²⁴⁸; Asaro, Stephens, and Perlman (submitted for publication) Ra²²⁴, Ra²²⁶; Goldhaber, der Mateosian, Harbottle, and McKeown, *Phys. Rev.* **99**, 180 (1955) Th²²⁸; F. Asaro and I. Perlman, *Phys. Rev.* **99**, 37 (1955) Th²²⁸; O. P. Hok, *Phys. Rev.* **99**, 1613 (1955) Th²²⁸, Th²³⁰, U²³², U²³⁴; Asaro, Stephens, Thompson, and Perlman, *Phys. Rev.* **98**, 19 (1955) C²⁶⁰.

The empirical moments of inertia are seen from Fig. V.5 to be appreciably smaller than $\mathfrak{I}_{\text{rig}}$ and to increase strongly with increasing β . A simple classical model of a rotational motion with these properties is provided by a wave traveling on the surface of a liquid drop. Assuming irrotational flow, this model yields the moment of inertia¹⁴¹

$$\mathfrak{I}_{\text{irrot}} = \frac{2}{5} AMR_0^2 \beta^2 (0.89 + O(\beta^2)) \quad (\text{V.8})$$

for a nucleus of spheroidal shape. While the nuclear moments have some of the qualitative features of this irrotational flow model, it is seen from Fig. V.5 that the observed moments are considerably larger than $\mathfrak{I}_{\text{irrot}}$.¹⁴²

The nuclear moments of inertia can be interpreted in more detail in terms of the response of the nucleonic

motion to the slowly rotating nuclear field.^{143,144} It is found^{145,146} that, for independent particle motion, the effective moment of inertia would be approximately that corresponding to rigid rotation, but that the residual interactions between the nucleons reduce the moment, which then exhibits a dependence on β of the type observed.¹⁴⁷ Residual interactions so strong as to break down the shell structure would reduce the moment to values approaching $\mathfrak{I}_{\text{irrot}}$. The observed moments indicate interactions about three times smaller than this limit. The full drawn curve in Fig. V.5 corresponds to a rough estimate¹⁴⁸ of the moments of inertia for interactions of such a magnitude.

As one approaches the closed shell configurations, the value of β decreases and, eventually, as a consequence of the residual interactions, the nuclear deformation collapses and the equilibrium shape becomes spherical (see Fig. V.1). The nucleus then no longer possesses a rotational spectrum and the collective excitations correspond to vibrations about the spherical equilibrium (see Sec. V C.1).

A criterion for the transition from vibrational to rotational spectra may be obtained by noting that this transition is associated with a change of the nucleonic coupling scheme (see Sec. V A). For the nuclei with spherical equilibrium shape, the coupling of the particles in unfilled shells is determined mainly by the residual interactions, while the development of a stable equilibrium shape is associated with a tendency of the individual nucleonic orbits to align themselves in the deformed nuclear field. Since, for completely independent particle motion, the moment of inertia would have the value (7) corresponding to rigid rotation, the smallest moment compatible with the occurrence of rotational spectra is expected to be a certain fraction of $\mathfrak{I}_{\text{rig}}$. This fraction has been estimated on the basis of

¹⁴³ D. R. Inglis, *Phys. Rev.* **96**, 1059 (1954).

¹⁴⁴ The nuclear moment of inertia is also related to the dependence of the collective orientation angles on the nucleonic coordinates. The introduction of orientation angles associated with an irrotational collective flow has been considered by A. Bohr, *Rotational States in Atomic Nuclei* (Ejnar Munksgaard, Copenhagen, 1954); G. Süßmann, *Z. Physik* **139**, 543 (1954); H. A. Tolhoek, *Physica* **XXI**, 1 (1955); S. Tomonaga, *Progr. Theoret. Phys.* **13**, 467 (1955); F. Coester, *Phys. Rev.* **99**, 170 (1955); R. Nataf, *Compt. rend.* **240**, 2510 and **241**, 31 (1955); Marumori, Yukawa, and Tanaka, *Progr. Theoret. Phys.* **13**, 442 (1955); T. Marumori and E. Yamada, *ibid.* **13**, 557 (1955); T. Marumori, *ibid.* **14**, 608 (1955); Lipkin, de Shalit, and Talmi, *Nuovo cimento* (10) **2**, 773 (1955); T. Miyazima and T. Tamura, *Progr. Theoret. Phys.* (to be published); T. Tamura, *Nuovo cimento* (to be published); F. Villars (privately circulated manuscript); see also the discussion of this approach in reference 145).

¹⁴⁵ A. Bohr and B. R. Mottelson, *Kgl. Danske Videnskab. Selskab Mat. fys. Medd.* **30**, No. 1 (1955).

¹⁴⁶ S. Moszkowski, *Phys. Rev.* **103**, 1328 (1956).

¹⁴⁷ In the special case of a rotation about a symmetry axis, the moment of inertia vanishes, since a rotation of the field then has no effect on the nucleonic motion.

¹⁴⁸ This estimate (compare reference 145) is based on a "two nucleon model" in which the nucleons outside of closed shells are represented by two interacting nucleons in p states. Despite the schematic character of this model, it may provide a qualitative description of the competition between the residual interactions and the nuclear shell structure.

¹⁴¹ See, e.g., H. Lamb, *Hydrodynamics* (Cambridge University Press, New York, 1916), p. 82 ff (see also reference 137).

¹⁴² See A. Bohr and B. R. Mottelson, *Phys. Rev.* **89**, 316 (1953); reference 132; K. W. Ford, reference 138; **95**, 1250 (1954). For a more detailed comparison with the potential flow model, including the effect of higher multipoles in the nuclear shape, see T. Gustafson, *Kgl. Danske Videnskab. Selskab Mat. fys. Medd.* **30**, 5 (1955).

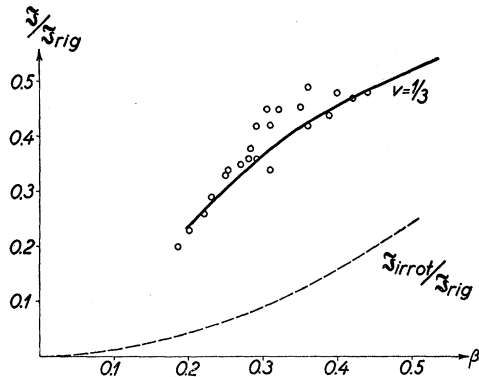


FIG. V.5. Dependence of moments of inertia on the nuclear deformation. The empirical moments of inertia of even-even nuclei in the region $150 < A < 188$ are plotted as a function of the nuclear deformation parameter β . The figure is taken from reference 145 which employed empirical data on \mathcal{I} and Q_0 which is substantially the same as that contained in Table V.2. The moments of inertia are plotted in units of the moment \mathcal{I}_{rig} associated with a rigid rotation [see (V.7)]. The full drawn curve represents a theoretical estimate based on a simplified model (reference 148). The parameter, ν , appearing in this estimate is a measure of the strength of the residual interactions and the value chosen has been adjusted to fit the experimental data.

For comparison the moment of inertia corresponding to irrotational flow (V.8) is shown by the dotted curve.

the simplified model¹⁴⁸ mentioned above, which yields a value of about one quarter of \mathcal{I}_{rig} . This would imply that the transition from vibrational to rotational spectra could be characterized approximately by a critical value

$$(E_2)_{crit} \approx 13\hbar^2/\mathcal{I}_{rig} \quad (V.9)$$

for the energy of the first excited state of an even-even nucleus. Stable equilibrium deformations and rotational spectra occur in this model only for even-even nuclei with E_2 values smaller than (9). However, the coefficient in (9) may have an A dependence which would lie outside the scope of this model. (See Fig. V.3.)

Odd- A nuclei.—For odd- A nuclei, the E_2 excitation process can populate both the first and second rotational excitations of the ground state [see (5)]. It is indeed found that, in the regions where rotational spectra are found in the even-even nuclei, the Coulomb excitation of odd- A nuclei strongly populates just two states. The energies of the states, identified in this manner as rotational excitations, are listed in Table V.1. It is seen that the ratios of the energies agree well with those calculated from (3). While the assumed spin sequence (5) appears in all cases to be consistent with Coulomb excitation data and with the evidence from the observed radioactive decay schemes, unambiguous spin determinations have been made in only a few cases (see Ta and W in Table IV.2).

For the nuclei with ground-state spin $I_0 = \frac{1}{2}$, the irregular sequence of the observed states reveals the effect of the second term in (3). The value of a obtained from the observed levels is listed in column seven of Table V.1. From the values of \mathcal{I} and a , the position of the higher members of the band can be calculated.

Although these levels are not populated by E_2 Coulomb excitation, they have been observed in a number of cases in radioactive decays with energies rather accurately given by (3).¹⁴⁹ The values of a can be approximately accounted for on the basis of the wave function for the last odd nucleon.^{133,150}

The rotational energy constants $3\hbar^2/\mathcal{I}$ determined from the odd- A spectra are listed in column five of Table V.1. The corresponding quantity for the related even-even nucleus, obtained by removing the last odd nucleon, is listed in column six of the table and is seen

TABLE V.1. Rotational states in odd- A nuclei populated by Coulomb excitation. The table lists the odd- A nuclei in the regions $152 < A < 190$ and $A > 222$ which have been studied by Coulomb excitation. The only nuclei omitted are the odd isotopes of Dy, Er, and Yb for which it appears that the radiation from the lowest excitations has not been resolved from that of the even isotopes.

The ground state spins I_0 , listed in column two, are taken from the compilation of Hollander, Perlman, and Seaborg, *Revs. Modern Phys.* **25**, 469 (1953) and the additional references listed below.

The energies of the first excited state, $E^{(1)}$, and of the second excited state, $E^{(2)}$, are listed in columns three and four. The $E^{(2)}$ value in parenthesis is that calculated from (V.3), assuming the spins I_0+1 , I_0+2 for the two excited states. The moment of inertia parameter employed is obtained from the experimental value of $E^{(1)}$ and is listed in column five. For comparison, the corresponding parameter for the neighboring even-even nucleus, obtained by removing the last odd nucleon, is listed in column six.

For nuclei with $I_0 = 1/2$, the rotational spectra involve an additional parameter, " a ." For these nuclei, the moment of inertia parameter and the value of " a " determined by means of (V.3) from the measured values of $E^{(1)}$ and $E^{(2)}$ are listed in column five.

Additional references for I_0 : D. R. Speck, *Phys. Rev.* **101**, 1725 (1956) ($Gd^{155,157}$); D. R. Speck and F. A. Jenkins, *Phys. Rev.* **101**, 1831 (1956) ($Hf^{177,179}$); K. L. van der Sluis and J. R. McNally, Jr., *J. Opt. Soc. Am.* **44**, 87 (1954) (U^{233}); Hutchinson *et al.*, *Phys. Rev.* **102**, 292 (1956) (U^{235}); van den Berg *et al.*, *Physica* **20**, 37 (1954), and Bleaney *et al.*, *Phil. Mag.* **45**, 991 (1954) (Pu^{239}).

Nucleus	I_0	$E^{(1)}$ (keV)	$E^{(2)}$ (keV)	$\frac{3\hbar^2}{\mathcal{I}}$ (keV)	$\left(\frac{3\hbar^2}{\mathcal{I}}\right)_{e-e}$ (keV)
⁶³ Eu ¹⁵³	5/2	83	192 (190)	71	122
⁶⁴ Gd ¹⁵⁵	3/2	60	145 (144)	72	123
⁶⁴ Gd ¹⁵⁷	3/2	55	131 (132)	66	89
⁶⁵ Tb ¹⁵⁹	3/2	58	138 (139)	70	79
⁶⁷ Ho ¹⁶⁵	7/2	95	211 (211)	63	73
⁶⁹ Tm ¹⁶⁹	1/2	8.4	118.3	74	80
				($a = -0.77$)	
⁷¹ Lu ¹⁷⁵	7/2	113.8	251.0 (252.9)	76	78
⁷² Hf ¹⁷⁷	7/2	113	250 (251)	75	89
⁷² Hf ¹⁷⁹	9/2	121	262 (264)	66	90
⁷³ Ta ¹⁸¹	7/2	136	303 (302)	91	93
⁷⁴ W ¹⁸³	1/2	46.5	99.1	78	100
				($a = 0.19$)	
⁷⁵ Re ¹⁸⁵	5/2	126	286 (288)	108	112
⁷⁵ Re ¹⁸⁷	5/2	135	303 (309)	116	123
⁹² U ²³³	5/2	40.4	92.1 (92.4)	35	45
⁹² U ²³⁵	7/2	46.2	103.0 (102.7)	31	45
⁹³ Np ²³⁷	5/2	33.2	75.8 (75.9)	28	44
⁹⁴ Pu ²³⁹	1/2	7.8	57.2	37	43
				($a = -0.58$)	

¹⁴⁹ Tm¹⁶⁹; S. E. Johannson, *Phys. Rev.* **100**, 835 (1955); J. M. Cork *et al.*, *Phys. Rev.* **101**, 1042 (1956); E. N. Hatch *et al.*, *Bull. Am. Phys. Soc. Ser. II* **1**, 170 (1956). W¹⁸³; see Fig. V.8. Pu²³⁹; Hollander, Smith, and Mihelich, *Phys. Rev.* **102**, 740 (1956).
¹⁵⁰ B. R. Mottelson and S. G. Nilsson, *Kgl. Danske Videnskab. Selskab Mat. fys. Medd.* (to be published); see also the analysis of the Tm¹⁶⁹ spectrum in *Z. Physik* **141**, 217 (1955).

to be systematically somewhat greater than the odd- A value. This difference appears to be associated, at least partly, with the difference in the intrinsic excitation spectra for even-even and odd- A nuclei. While the first intrinsic excitation of an even-even nucleus usually has an energy of the order of a Mev in heavy nuclei, the odd- A nuclei exhibit excitations with an average spacing of about two hundred kev, associated with the change of orbit of the last odd particle.¹⁵¹ The occurrence of low-lying intrinsic excitations in the odd- A nuclei implies that the intrinsic motion is less able to follow the rotational motion in an adiabatic manner, with a resultant increase in the effective moment of inertia (see Sec. V B.4).

V B.2. Excitation Cross Sections

An especially valuable feature of the Coulomb excitation process is the possibility of determining the absolute transition probability for the excitation by a measurement of the cross section. Since the rotational transitions leave the intrinsic structure unaltered, the transition matrix element can be expressed as an expectation value for the intrinsic structure, multiplied by a vector addition coefficient. Thus, one obtains¹³² for an $E2$ transition from a state I_i, K to another state I_f, K of the same rotational band, the reduced transition probability [see (II A.18)]¹⁵²

$$B(E2; I_i \rightarrow I_f) = \frac{5}{16\pi} e^2 Q_0^2 \langle I_i 2K0 | I_i 2I_f K \rangle^2, \quad (\text{V.10})$$

where Q_0 is the electric quadrupole moment of the nuclear shape, defined by

$$eQ_0 = \left\langle K \left| \int \rho r^2 (3 \cos^2 \theta' - 1) d\tau' \right| K \right\rangle. \quad (\text{V.11})$$

In (11), ρ is the nuclear charge density and the angle θ' is measured from the intrinsic nuclear axis (z' in Fig. V.2). The wave function for the intrinsic nuclear state is labeled by K .

For a uniformly charged nucleus of spheroidal shape, Q_0 can be expressed in terms of β , given by (6), and one obtains

$$Q_0 = \frac{3}{(5\pi)^{\frac{1}{2}}} Z R_0^2 \beta (1 + 0.16\beta + \dots), \quad (\text{V.12})$$

where Z is the nuclear charge number. Corresponding to the fact that, for the strongly deformed nuclei, the quadrupole moments are an order of magnitude larger than those associated with a single proton, the transition probabilities (10) are observed to be appreciably larger

¹⁵¹ See, e.g., the difference between the spectra of W^{182} and W^{183} (Murray *et al.*, Phys. Rev. **97**, 1007 (1955)) or between Pu^{238} (reference 176) and Pu^{239} (reference 149).

¹⁵² The relationship of the vector addition coefficients used in this chapter to the equivalent $3j$ symbols employed in Chapter II is given by (II A.17).

than the single particle unit (1), in some cases by more than a factor of a hundred.

The intrinsic quadrupole moments Q_0 deduced by means of (10) from the observed cross sections for Coulomb excitation of rotational levels are listed in Tables V.2 and V.3.

For odd- A nuclei, it is possible to compare the intrinsic quadrupole moments deduced from transition probabilities with the expectation values for the quadrupole moment Q in the nuclear ground state, as obtained from atomic hyperfine structure separations. The latter quantity is defined by

$$eQ = \left\langle I, M=I \left| \int \rho r^2 (3 \cos^2 \theta - 1) d\tau \right| I, M=I \right\rangle, \quad (\text{V.13})$$

where the angle θ is measured from the fixed z axis. For a state of a rotational band, the moment Q is related to Q_0 by

$$Q = Q_0 \frac{3K^2 - I(I+1)}{(I+1)(2I+3)}, \quad (\text{V.14})$$

TABLE V.2. Moments of inertia and quadrupole moments of even-even nuclei. The table lists the even-even nuclei which exhibit rotational spectra and for which there exists evidence on the transition probabilities. Column two gives the moment of inertia parameter obtained from the energy of the first excited state ($2+$). Column three gives the intrinsic quadrupole moments obtained from the measured transition probabilities by means of (V.10). The data come partly from Coulomb excitations, see Table IV.1, and the additional data given by A. W. Sunyar, Phys. Rev. **98**, 653 (1955). The deformation parameter, β , in the last column is obtained from the Q_0 values by means of (V.12), assuming $R_0 = 1.2A^{\frac{1}{3}} 10^{-13}$ cm.

Nucleus	$\frac{3\hbar^2}{2I}$ (kev)	$ Q_0 $ (10^{-24} cm ²)	β
⁶⁰ Nd ¹⁵⁰	130	4.8	0.25
⁶² Sm ¹⁵²	122	5.7	0.28
Sm ¹⁵⁴	83	6.7	0.33
⁶⁴ Gd ¹⁵⁴	123	6.3	0.30
Gd ¹⁵⁶	89	8.8	0.41
Gd ¹⁵⁸	79	10	0.46
Gd ¹⁶⁰	76	10	0.47
⁶⁶ Dy ¹⁶⁰	86	7.8	0.35
Dy ¹⁶²	82	8.2	0.36
Dy ¹⁶⁴	73	9.5	0.41
⁶⁸ Er ¹⁶⁴	90	7.8	0.33
Er ¹⁶⁶	80	7.8	0.33
Er ¹⁶⁸			
Er ¹⁷⁰			
⁷⁰ Yb ¹⁷⁰	84	7.5	0.30
Yb ¹⁷²	78	7.8	0.31
Yb ¹⁷⁴			
Yb ¹⁷⁶			
⁷² Hf ¹⁷⁶	89	7.5	0.29
Hf ¹⁷⁸	91	8.1	0.31
Hf ¹⁸⁰	93	7.1	0.27
⁷⁴ W ¹⁸²	100	7.1	0.26
W ¹⁸⁴	112	6.5	0.24
W ¹⁸⁶	124	6.5	0.24
⁷⁶ Os ¹⁸⁶	137	5.5	0.20
Os ¹⁸⁸	155	5.1	0.18
⁹⁰ Th ²³²	52	10	0.25
⁹² U ²³⁸	44	11	0.28

and, in the special case of the ground state ($I_0=K$), one obtains

$$Q=Q_0 \frac{I_0(2I_0-1)}{(I_0+1)(2I_0+3)}. \quad (V.15)$$

The smaller value of Q , as compared with Q_0 , reflects the fact that, even for the state $M=I$, the intrinsic nuclear axis is not completely aligned along the fixed z axis.

The intrinsic quadrupole moments obtained from the spectroscopic Q values by means of (15) are compared in Table V.3 with those derived from the Coulomb excitation cross sections by means of (10). The two determinations seem to be consistent, considering the rather large uncertainties involved, especially in the estimate of the nuclear quadrupole moments from the measured hyperfine structure intervals.

As is seen from expression (10), the ratio of the cross sections for the excitation of the first and the second rotational state in an odd- A nucleus is independent of

TABLE V.3. Intrinsic quadrupole moments of odd- A nuclei. The table lists the odd- A nuclei in the regions $152 < A < 190$ and $A > 222$ for which there is evidence on the nuclear deformation from Coulomb excitation cross sections or spectroscopic hyperfine structure measurements. The ground-state spins, I_0 , are taken from the references in Table V.1, and the intrinsic quadrupole moments (in column three) are obtained from the experimental transition probabilities in Table IV.2 by means of (V.10). The spectroscopic quadrupole moments, Q , in column four are taken from the compilation of N. F. Ramsey, *Nuclear Moments* (John Wiley and Sons, Inc., New York, 1953), and the additional references given below. From these moments, the intrinsic quadrupole moments in column five are obtained by means of (V.15).

Additional references for Q : D. R. Speck Phys. Rev. **101** 1725 (1956) (Gd^{155,157}); J. M. Baker and B. Bleaney Proc. Phys. Soc. (London) **68A** 1090 (1955) (Ho¹⁶⁵); Bogle *et al.*, Proc. Phys. Soc. (London) **65A**, 760 (1952) (Er¹⁶⁷); T. Kamei, Phys. Rev. **99**, 789 (1955) (Lu¹⁷⁵; Ta¹⁸¹); Fred *et al.*, Phys. Rev. **98**, 1514 (1955) (Ac²²⁷); K. L. van der Sluis and J. R. McNally, Jr., J. Opt. Soc. Am. **44**, 87 (1954) (U²³⁵); Korostyleva *et al.*, J. Exptl. Theoret. Phys. U.S.S.R. **28**, 471 (1955) and N. I. Kaliteevskij and M. P. Chaika, private communication (ratio between moments of U²³⁵ and U²³⁸).

Nucleus	I_0	$ Q_0 $ (Coul. exc.)	Q	Q_0 (hfs)
⁶³ Eu ¹⁵³	5/2	7.7	2.5	7.0
⁶⁴ Gd ¹⁵⁵	3/2	8.0	1.1	5.5
⁶⁴ Gd ¹⁵⁷	3/2	7.7	1.0	5.0
⁶⁵ Tb ¹⁵⁹	3/2	6.9		
⁶⁷ Ho ¹⁶⁵	7/2	7.8	~2	~4
⁶⁸ Er ¹⁶⁷	7/2		~10	~20
⁶⁹ Tm ¹⁶⁹	1/2	8.0	0	
⁷⁰ Yb ¹⁷³	5/2		3.9	11
⁷¹ Lu ¹⁷⁵	7/2	8.2	5.7	12
⁷² Hf ¹⁷⁷	7/2	7.5		
⁷² Hf ¹⁷⁹	9/2	~7		
⁷³ Ta ¹⁸¹	7/2	6.8	4.3	9.2
⁷⁵ Re ¹⁸⁵	5/2	5.4	2.8	7.8
⁷⁵ Re ¹⁸⁷	5/2	5.0	2.6	7.3
⁸⁹ Ac ²²⁷	3/2		-1.7	-8
⁹² U ²³³	5/2	14	~6	~17
⁹² U ²³⁵	7/2	9	~8	~17
⁹³ Np ²³⁷	5/2	9		
⁹⁴ Pu ²³⁹	1/2	8.3	0	

TABLE V.4. Relative intensities of rotational excitations. The table lists the odd- A nuclei for which the cross sections for the Coulomb excitation of the first two rotational states have been measured. The ratio of the experimental transition probabilities (compare Table IV.2) is listed in column three together with the theoretical value (in parenthesis) obtained from (V.10). The ground-state spins, I_0 , are taken from the references given in Table V.1.

Note added in proof.—A recent systematic study of the ratio of $B(E2)$ values obtained in Coulomb excitation of odd- A nuclei (G. Goldring and G. T. Paulissen, Phys. Rev. **103**, 1314 (1956)) has yielded values in approximate agreement with those listed in Table V.4. The one essential difference occurs for Hf¹⁷⁹, for which the new measurements give a ratio of 0.22.

Nucleus	I_0	$\frac{B(E2; I_0 \rightarrow I_0+2)}{B(E2; I_0 \rightarrow I_0+1)}$
⁶³ Eu ¹⁵³	5/2	0.28 (0.35)
⁶⁴ Gd ¹⁵⁷	3/2	0.38 (0.56)
⁶⁵ Tb ¹⁵⁹	3/2	0.56 (0.56)
⁶⁷ Ho ¹⁶⁵	7/2	0.24 (0.26)
⁷¹ Lu ¹⁷⁵	7/2	0.23 (0.26)
⁷² Hf ¹⁷⁷	7/2	0.26 (0.26)
⁷² Hf ¹⁷⁹	9/2	0.07 (0.20)
⁷³ Ta ¹⁸¹	7/2	0.29 (0.26)
⁷⁵ Re ¹⁸⁵	5/2	0.27 (0.35)
⁷⁵ Re ¹⁸⁷	5/2	0.39 (0.35)
⁹² U ²³³	5/2	0.18 (0.35)
⁹² U ²³⁵	7/2	0.16 (0.26)
⁹³ Np ²³⁷	5/2	0.44 (0.35)

Q_0 .¹⁵³ Thus, a measurement of this ratio provides a direct test of the nuclear coupling scheme. The available evidence is collected in Table V.4 and compared with the ratios calculated from (10).

The Q_0 values obtained from (10) are plotted in Fig. V.6, and show similar general trends as previously observed in the spectroscopic quadrupole moments.¹⁵⁴ Thus, the nuclear deformations increase strongly as one moves away from closed shell regions, reflecting the polarizing effect of particles outside of closed shells (see Sec. V A). A theoretical estimate of Q_0 may be obtained by calculating the binding energies of the individual nucleons as a function of the nuclear deformation and minimizing the total nuclear energy.¹⁵⁵ The deformations calculated in this manner are shown by the full drawn curve in Fig. V.6.

The excitation of higher members of the ground-state rotational band ($\Delta I \geq 3$) may be achieved by multiple $E2$ processes. (See Sec. II D.3.) The cross sections for such processes may become quite large for high bombarding energies, as may be employed especially with heavy ions as projectiles. Thus, for 20-Mev α particles incident on a target with $Z_2=90$, the cross section for a

¹⁵³ Such intensity relations apply quite generally to transitions leading to different members of a rotational band. For applications to β and γ transitions, see Alaga, Alder, Bohr, and Mottelson, Kgl. Danske Videnskab. Selskab Mat. fys. Medd. **29**, No. 9 (1955); for α transitions see Bohr, Fröman, and Mottelson, reference 136; for deuteron stripping reactions, see G. R. Satchler, Phys. Rev. **97**, 1416 (1955).

¹⁵⁴ W. Gordy, Phys. Rev. **76**, 139 (1949). Townes, Foley, and Low, Phys. Rev. **76**, 1415 (1949).

¹⁵⁵ D. Pfrisch, Z. Physik **132**, 409 (1952). S. Moszkowski, reference 135; B. R. Mottelson and S. G. Nilsson, reference 136; K. Gottfried, reference 135.

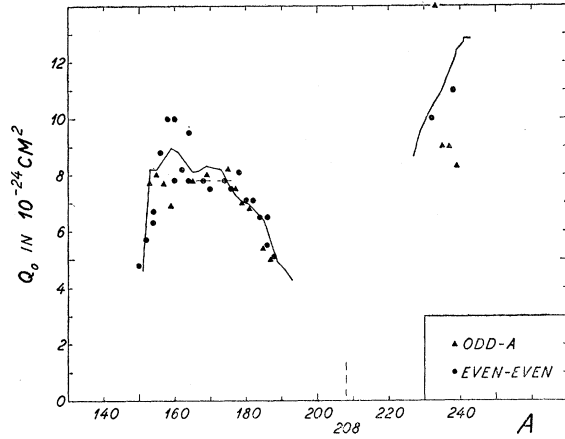


FIG. V.6. Intrinsic quadrupole moments of deformed nuclei. The experimental Q_0 values, determined from $E2$ transition probabilities (compare Tables V.2 and V.3), are plotted as a function of the nuclear mass number. The experimental uncertainties are usually of the order of 10–20%, but may be somewhat greater in the very heavy elements region. The full drawn curve gives a theoretical estimate of Q_0 based upon an independent particle description of the intrinsic structure (B. R. Mottelson and S. G. Nilsson, reference 136 and Kgl. Danske Vidensk. Selskab Mat. fys. Medd. (to be published)).

second order $E2$ excitation of the $4+$ state of an even-even nucleus is found from (II D.18) and (10) to be about 50 millibarns, assuming $Q_0=10$ barns.

While the cross sections for single or multiple $E2$ excitations of rotational states depend on the nuclear quadrupole moment, the possible occurrence of higher multipole moments in the nuclear shape can in principle be studied by means of the Coulomb excitation of corresponding multipole order populating higher members of the ground-state rotational band. Thus, an $E\lambda$ transition from the ground-state $I_i K$ to the rotational states $I_f K$ would be characterized by the reduced transition probabilities

$$B(E\lambda; I_i \rightarrow I_f) = \langle K | \mathfrak{N}'(E\lambda, 0) | K \rangle^2 \times \langle I_i \lambda K 0 | I_f \lambda I_f K \rangle^2, \quad (\text{V.16})$$

where $\mathfrak{N}'(E\lambda, 0)$ is the intrinsic $E\lambda$ moment defined by (II A.11) with the coordinates referring to the intrinsic nuclear system. The cross sections for higher multipole excitation will usually be appreciably smaller than those for multiple $E2$ transitions. Thus, if one assumes¹⁵⁶ a value for $B(E4; 0 \rightarrow 4)$ of $0.2e^2(10^{-24} \text{ cm}^2)^4$ in a nucleus with $Z_2=90$, one obtains from (II C.15) a cross section of about 0.2 millibarn for $E4$ excitation of a $4+$ state with 20-Mev α particles.

V B.3. Magnetic Dipole Decay of Rotational Excitations

Since the successive rotational states in an odd- A nucleus have $\Delta I=1$ [see (5)], the γ radiation emitted

¹⁵⁶ A recent analysis of the fine structure intensities in the α decay of the heavy nuclei [P. O. Fröman, Kgl. Danske Videnskab. Selskab Mat. fys. Medd. (to be published)] indicates $E4$ moments in the nuclear shape corresponding in some cases to values as large as $B(E4; 0 \rightarrow 4) = 0.2e^2(10^{-24} \text{ cm}^2)^4$; the single particle unit (II A.58) for $Z_2=90$ corresponds to $B(E4) = 0.01e^2(10^{-24} \text{ cm}^2)^4$.

in the decay of these states will in general be a mixture of $M1$ and $E2$, although the excitation is of almost pure $E2$ type (see Sec. II A.3). The absolute $E2$ transition probability can be determined from the cross section for Coulomb excitation. Thus, a determination of the relative strength of the $M1$ as compared with the $E2$ radiation in the decay of the first excited state will also yield the absolute $M1$ transition probability. This information can be obtained from angular distributions or internal conversion measurements on the emitted radiation (or from the lifetime of the excited state). The $M1$ transition probability in the cascade transition ($I_0+2 \rightarrow I_0+1$) can be determined from the relative strength of $M1$ and $E2$ in this transition together with the branching ratio between the mixed $M1+E2$ cascade radiation and the pure $E2$ cross-over ($I_0+2 \rightarrow I_0$) decay of the second excited state. If only one of these data is available one may employ the rotational formula (10) to provide the additional relation necessary for the estimate of the absolute $M1$ transition probability in the cascade radiation.

The magnitude of the $M1$ transition probabilities between rotational states can be related to the gyromagnetic ratios, g_K and g_R , of the intrinsic and collective motion. The reduced $M1$ transition probability from a state $I_i K$ to another state $I_f K$ of the same rotational band (with $K \neq \frac{1}{2}$) is given by¹³²

$$B(M1; I_i \rightarrow I_f) = \frac{3}{4\pi} \left(\frac{e\hbar}{2Mc} \right)^2 (g_K - g_R)^2 K^2 \times \langle I_i 1 K 0 | I_f 1 I_f K \rangle^2. \quad (\text{V.17})$$

The relative sign of $M1$ and $E2$ transition amplitudes may also be determined from angular distribution measurements (see Sec. II C.4). This phase is related to the sign of Q_0 and of $g_K - g_R$ and is given by

$$\text{sign } \delta = \text{sign} \frac{g_K - g_R}{Q_0}, \quad (\text{V.18})$$

where δ is the ratio between the reduced $E2$ and $M1$ matrix elements for the transition (see Sec. II A).

The static magnetic moment μ of a state in the rotational band may also be expressed in terms of the gyromagnetic ratios g_K and g_R . Thus, for $K \neq \frac{1}{2}$, one obtains

$$\mu = \frac{K^2}{I+1} (g_K - g_R) + I g_R. \quad (\text{V.19})$$

For a band with $K = \frac{1}{2}$, the magnetic properties involve an additional parameter b_0 similar to the decoupling parameter, a , in the energy spectrum.¹³³ For this case, the $M1$ transition probability and the magnetic moment may be written in the form

$$B(M1; I+1 \rightarrow I) = \frac{3}{64\pi} \left(\frac{e\hbar}{2Mc} \right)^2 \frac{2I+1}{I+1} (g_K - g_R)^2 \times (1 + (-1)^{I-\frac{1}{2}} b_0)^2, \quad (\text{V.20})$$

with

$$\text{sign } \delta = \text{sign} \frac{g_K - g_R}{Q_0} (1 + (-1)^{I-\frac{1}{2}} b_0), \quad (\text{V.21})$$

and

$$\mu = \frac{1}{4(I+1)} (g_K - g_R) \times [1 - (2I+1)(-1)^{I-\frac{1}{2}} b_0] + I g_R. \quad (\text{V.22})$$

A measurement of both the $M1$ transition probability and the ground state magnetic moment can thus yield g_K and g_R separately (and the value of b_0 for $K = \frac{1}{2}$ bands if an additional transition probability or moment is measured). The quantities g_K and b_0 can be related to the intrinsic nucleonic configuration, while g_R provides information on the rotational motion, and may be compared with the value

$$(g_R)_u = \frac{Z}{A}, \quad (\text{V.23})$$

corresponding to a flow of uniformly charged nuclear matter.

The g_R values obtained from Coulomb excitation studies and ground state moments of nuclei with $I_0 \neq \frac{1}{2}$ are listed in Table V.5. The uncertainties in these values

TABLE V.5. Magnetic properties of rotational levels in odd- A nuclei. The table lists the odd- A nuclei with $I_0 \neq 1/2$ for which there is evidence on both the ground state magnetic moment, μ , and the $M1$ rotational transition probability. The ground-state spins and magnetic moments in columns two and three are taken from the references given in Tables V.1 and V.3 and the additional references given below. The reduced $M1$ transition probabilities $B(M1)$ are obtained from the measured $B(E2)$ values and the $M1/E2$ ratios given in Table IV.2 by means of the relations (II A.52) and (II A.53). From the values of μ and $B(M1)$ the gyromagnetic ratios, g_R and g_K , are determined from (17) and (19). Since (17) is a quadratic expression, there exist two sets of possible g_K and g_R values, except in the case of Ta^{181} where angular correlation measurements have established the sign of $(g_K - g_R)$ by comparison with the sign of the quadrupole moment [compare (18)]. The g factors in columns four and five are listed in such a manner that the first value of g_R belongs together with the first value of g_K .

The table does not include nuclei with $I_0 = 1/2$, since the magnetic properties of these nuclei involve an additional parameter b_0 [compare (20), (21), and (22), and the analysis of the W^{183} spectrum in Fig. V.8].

Additional references for μ : J. M. Baker and B. Bleaney, Proc. Phys. Soc. (London) **68A**, 257 (1955) (Tb^{159}); D. R. Speck, Bull. Am. Phys. Soc. Ser. II, **1**, 282 (1956) (Hf^{177} and Hf^{179}).

Nucleus	I_0	μ	g_R		g_K	
$^{63}\text{Eu}^{153}$	5/2	1.5	0.5,	0.7	0.6,	0.5
$^{64}\text{Gd}^{155}$	3/2	-0.30	0.3,	-0.7	-0.5,	0.1
$^{64}\text{Gd}^{157}$	3/2	-0.37	0.3,	-0.7	-0.6,	0.1
$^{65}\text{Tb}^{159}$	3/2	1.5	0.1,	1.9	1.6,	0.4
$^{67}\text{Ho}^{165}$	7/2	3.3	0.3,	1.6	1.1,	0.8
$^{71}\text{Lu}^{175}$	7/2	2.6	0.3,	1.2	0.9,	0.6
$^{72}\text{Hf}^{177}$	7/2	0.61	0.3,	0.1	0.1,	0.2
$^{72}\text{Hf}^{179}$	9/2	-0.47	0.2,	-0.4	-0.2,	0.0
$^{73}\text{Ta}^{181}$	7/2	2.1	0.2		0.7	
$^{75}\text{Re}^{185}$	5/2	3.14	0.5,	2.1	1.6,	0.9
$^{75}\text{Re}^{187}$	5/2	3.18	0.5,	2.0	1.6,	1.0
$^{92}\text{U}^{233}$	5/2	0.8	0.4,	0.3	0.3,	0.3
$^{92}\text{U}^{235}$	7/2	-0.5	0.1,	-0.4	-0.2,	-0.1

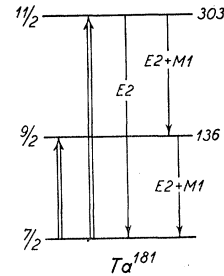


FIG. V.7. Rotational spectrum for Ta^{181} . The Coulomb excitation experiments have determined the energies and spins (from the angular distribution of the γ rays and measured conversion coefficients) of the first two rotational excitations in Ta^{181} . In addition the absolute magnitudes of all the $M1$ and $E2$ transition probabilities have been obtained by combining the Coulomb excitation cross sections with the measured branching ratio between the 167- and 303-keV γ rays, and the $M1$ to $E2$ ratios determined from the γ -ray angular distribution and the conversion coefficients (compare the data in Table IV.2). In addition, the relative phases of the $M1$ and $E2$ radiation have been determined for the 167-keV transition from the angular distribution in Coulomb excitation and for the 136-keV transition from the γ - γ angular correlation following the β decay of Hf^{181} [F. K. McGowan, Phys. Rev. **93**, 471 (1954); Heer *et al.* Helv. Phys. Acta **28**, 336(A) (1955); F. Boehm and P. Marmier, Phys. Rev. **103**, 342 (1956)]. These results test the rotational interpretation of the observed levels in the following ways.

(a) The spin sequence is that given by (V.5) in which we assume $K = 7/2$ as determined from the ground state spin, and the parity is the same for all the states.

(b) The observed energy ratio of the $I = 11/2$ and $I = 9/2$ states is 2.23 ± 0.02 which agrees with the ratio $20/9$ obtained from (V.3).

(c) The reduced $E2$ transition probabilities $B(E2; 7/2 \rightarrow 9/2)$, $B(E2; 7/2 \rightarrow 11/2)$, and $B(E2; 11/2 \rightarrow 9/2)$ are found to have the relative values $1:0.29 \sim 1.3$ which may be compared with relative values $1:0.26:0.81$ obtained from (V.10).

(d) The reduced $M1$ transition probabilities $B(M1; 11/2 \rightarrow 9/2)$ and $B(M1; 9/2 \rightarrow 7/2)$ have a ratio of ~ 2 while the theoretical value obtained from (V.17) is 1.53. Moreover the relative phases of $M1$ and $E2$ radiation are the same in the 136- and 167-keV transition as expected from theory (see V.18).

From the experimental data one determines a number of nuclear parameters characterizing the ground state configuration in Ta^{181} .

(a) The moment of inertia obtained from the rotational energies is given by $3\hbar^2/g = 91$ kev. For a discussion of the interpretation of this value compare Fig. V.5, Table V.1, and the comments in the text.

(b) The intrinsic quadrupole moment determined from the $E2$ transition probabilities by means of (V.10) has the value $Q_0 = 6.8$. This quantity determines the quadrupole eccentricity parameter which is found from (V.12) to be $\beta = 0.25$; see also the discussion of Q_0 in Fig. V.6 and Table V.3.

(c) The $M1$ transition probability and its phase relative to that of the $E2$ transition [together with the assumption of a positive Q_0 as indicated by spectroscopic evidence, (compare Table V.3)] yields by means of (V.17) and (V.18) the value $g_K - g_R = 0.5$ for the difference between the intrinsic and collective gyromagnetic ratios. This value, when combined with the measured magnetic moment, yields by means of (V.19) the separate g factors listed in Table V.5.

are considerable, but the data may indicate deviations from (23). In fact, one expects such deviations in odd- A nuclei as a consequence of the especially large contribution of the last odd nucleon to the rotational moment of inertia, and thus also to the rotational angular momentum.

The analysis of rotational spectra in odd- A elements

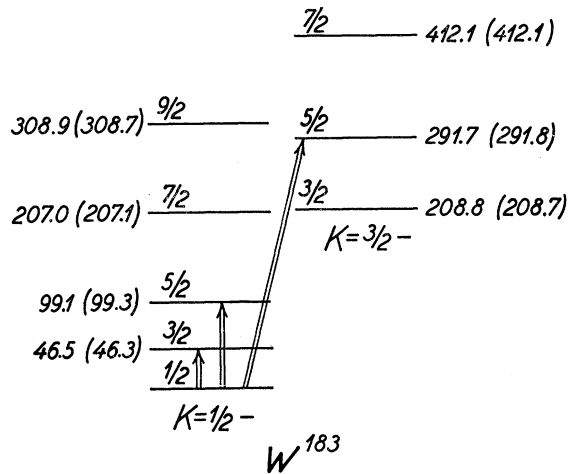


FIG. V.8. Low-lying energy levels in W^{183} . The figure shows the energies, spins, and parities of the low-lying states in W^{183} , populated in the β decay of Ta^{183} [Murray, Boehm, Marmier, and DuMond, Phys. Rev. **97**, 1007 (1955)].

The Coulomb excitation strongly populates the first two excited states of the ground state rotational band (compare Table IV.2). The energies in this band reveal the effect of the decoupling term in (V.3) characteristic of configurations with $K=1/2$. From the energies of the ($I=3/2$) and ($I=5/2$) states in this band, one can calculate the parameters \mathcal{J} and α . Using these parameters, the position of the ($I=7/2$) level calculated from (V.3) agrees well with the observed level, while the calculated energy for the $I=9/2$ state is a few percent below the observed value. Similarly, the relative energies in the ($K=3/2$) band are found to deviate somewhat from those obtained from (V.3). These perturbations have been interpreted in terms of a coupling between the two bands resulting from the Coriolis effect of the nuclear rotation. By suitably adjusting the matrix element associated with this coupling, the observed energies have been accounted for with great precision (A. K. Kerman, reference 157). The calculated energies are shown in parenthesis.

To a first approximation, the electric quadrupole transition probabilities for the rotational excitations can be discussed in a similar manner as for Ta^{181} (see Fig. V.7), although for W^{183} the data is less complete. However, the coupling to the ($K=3/2$) band implies small deviations from (V.10), and leads especially to enhanced $E2$ transition probabilities for the excitation of the states in this higher band. The magnitude of the $B(E2)$ values for these transitions provide a direct measure of the admixed amplitudes and can be calculated from the parameters involved in the analysis of the observed energies. The observed $B(E2)$ for the population of the 292-keV level (compare Table IV.2) is in good agreement with the analysis in reference 157, which, in addition, predicts $B(E2) \approx 0.1$ for the excitation of the 209-keV level.

The magnetic parameters, g_K , g_R , and b_0 for the ground-state rotational band may be obtained from the observed relative intensities in the decay of the 207-keV and 99-keV levels together with the estimated Q_0 value of 6.5 and the measured ground state magnetic moment $\mu = 0.115$ [P. P. Sogo and C. D. Jeffries, Phys. Rev. **98**, 1316 (1955)]. By means of (V.20) and (V.22) one finds $b_0 = 0.28$, $g_K = 0.30$, and $g_R = 0.49$, by a suitable choice of the phases (A. K. Kerman, private communication). The coupling between the bands has an appreciable effect on the magnetic transition probabilities, which have been analyzed in detail in reference 157.

As discussed in Sec. V B.4, the moment of inertia and the magnetic parameters determined directly from the ground state rotational band contain contributions from the coupling between this band and the $K=3/2$ band. In the present case where this coupling has been determined from the analysis of the energy perturbations, it is possible to derive the various parameters which would characterize the ground state band in the absence of this coupling. These "unrenormalized" values are found to be $(3\mathcal{J}^2/\mathcal{J})_0 = 95$ keV, $(\alpha)_0 = 0.17$, $(b_0)_0 = 0.46$, $(g_K)_0 = 0.16$, and $(g_R)_0 = 0.28$ (A. K. Kerman, reference 157 and private communication).

is summarized in the captions to Figs. V.7 and V.8, which discuss the spectra of Ta^{181} and W^{183} .

V B.4. Coupling Between Rotational and Intrinsic Motion

Rotational spectra of the simple form (3) are obtained when the rotation is so slow that the intrinsic motion can adjust adiabatically to the changing orientation of the nuclear field. The finite rotational frequency gives rise to small nonadiabatic excitations resulting from the Coriolis and centrifugal forces acting on the nucleons in the body fixed coordinate system. To lowest order in the rotational frequency, these virtual excitations imply an increase in the energy of the nucleus proportional to $I(I+1)$ and thus provide the moment of inertia associated with the rotational motion.^{143,145} To higher order, the nonadiabatic effects give rise to a coupling between the rotational and intrinsic motion, which implies deviations from the rotational spectrum (3) and the geometrical relations for the nuclear moments, e.g., (10), (14), (17), and (19).

In odd- A nuclei the nonadiabatic excitations of the last odd nucleon will play a special role, since these do not involve the breaking of any pairs. As noted above, in connection with the discussion of Table V.1, the inertial effect arising from these excitations may be largely responsible for the observed differences in the moments of inertia of even-even and odd- A nuclei. Small deviations from the energy ratios (3) may arise primarily from the higher order effects of the near lying bands associated with the lowest states of the last odd particle. Such effects have been detected (see, e.g., Table V.1 and reference 149) and a detailed analysis¹⁵⁷ has been made for the spectrum of W^{183} (see Fig. V.8). Even when the deviations from (3) are small, the electromagnetic transition probabilities may be appreciably affected. In particular the $E2$ transition probabilities between the coupled bands may be strongly enhanced. In the Coulomb excitation of W^{183} , an enhancement of this type has been observed and has been related quantitatively to the observed energy perturbations¹⁵⁷ (see Fig. V.8). Further studies of this phenomenon would provide valuable information on the relationship between the rotational motion and that of the individual nucleons.

In addition to the specific effects of the coupling between close lying bands, rotational perturbations also arise from the nonadiabatic excitation of higher lying intrinsic states. An important part of such perturbations may be described as rotation-vibration interac-

¹⁵⁷ A. K. Kerman, Kgl. Danske Videnskab. Selskab Mat. fys. Medd. **30**, No. 15 (1956).

It is of interest that the moment of inertia \mathcal{J}_0 is much closer to the moments of neighboring even-even nuclei than the effective moment (compare Table V.1). The coupling between the bands is seen in the present case to increase the effective value of g_K ; this is opposite to the general trend for odd neutron nuclei suggested in reference 146.

tions of a similar kind as in molecules. These interactions imply an energy depression which in first approximation is proportional to $I^2(I+1)^2$.¹⁵² In even-even nuclei, the small deviations of the observed rotational energies from the $I(I+1)$ ratios (see Fig. V.4) are indeed always negative and increase systematically with increasing rotational frequency; there is also some evidence that these perturbations to first order are proportional to $I^2(I+1)^2$.¹⁵³

V C. Vibrations of Spherical Nuclei

V C.1. Classification of Vibrations

The shape oscillations of a spherical nucleus¹⁵⁹ may be classified according to their multipole order λ . The excitation quanta, called phonons, have total angular momentum λ , parity $(-1)^\lambda$, and may be further characterized by their component of angular momentum μ along a space fixed axis.

The vibrational motion is associated with an oscillating electric multipole moment, and it is convenient to normalize the vibrational amplitudes $\alpha_{\lambda\mu}$ with respect to the multipole moments (II A.11) by the relation¹⁶⁰

$$\mathfrak{M}(E\lambda, \mu) = \frac{3}{4\pi} ZeR_0^\lambda \alpha_{\lambda\mu}^* \quad (V.24)$$

This normalization is chosen in such a manner that, in the idealized case of a nucleus with constant density and a sharp surface, the coordinates $\alpha_{\lambda\mu}$ would define the nuclear surface by

$$R(\theta, \varphi) = R_0 \left(1 + \sum_{\lambda\mu} \alpha_{\lambda\mu} Y_{\lambda\mu}(\theta, \varphi) \right) \quad (V.25)$$

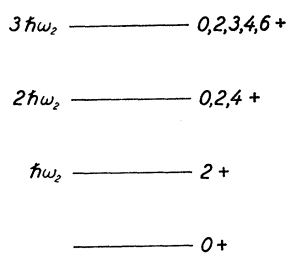


FIG. V.9. Quadrupole vibrational spectrum for even-even nuclei with spherical equilibrium shape. The quadrupole vibrational quanta each have an energy $\hbar\omega_2$ and carry two units of angular momentum. The resulting spectrum is indicated in the figure, in which the total angular momentum values are indicated on the right. The equality of the energy spacings and the degeneracy of the different spin values are a consequence of the harmonic oscillator approximation and will be removed by higher order terms in the nuclear energy.

¹⁵² See, e.g., the accurately measured spectrum of Hf^{180} (Mihelich *et al.*, Phys. Rev. **94**, 794 (A) (1954) discussed in *Beta- and Gamma-Ray Spectroscopy*, edited by K. Siegbahn (North Holland Publishing Company, Amsterdam, 1955), Chapter XVII, p. 487.

¹⁵⁹ See, e.g., reference 137.

¹⁶⁰ Equation (24) is meant to apply only to the matrix elements between the vibrational levels, and thus merely to give the normalization of the vibrational amplitude. Taken as a definition for $\alpha_{\lambda\mu}$ in terms of the nucleonic coordinates [see (II A.13)], the relation (24) would imply the assumption of irrotational flow for the collective motion, an assumption which is not in general expected to be valid (see reference 145 and Table V.7).

For small amplitudes of oscillation, the energy may be expanded in powers of $\alpha_{\lambda\mu}$ and of the time derivatives $\dot{\alpha}_{\lambda\mu}$, and one obtains to a first approximation

$$H_{\text{vib}} = \sum_{\lambda\mu} \left(\frac{1}{2} B_\lambda |\dot{\alpha}_{\lambda\mu}|^2 + \frac{1}{2} C_\lambda |\alpha_{\lambda\mu}|^2 \right), \quad (V.26)$$

corresponding to a set of independent harmonic oscillators, with energy quanta

$$\hbar\omega_\lambda = \hbar \left(\frac{C_\lambda}{B_\lambda} \right)^{\frac{1}{2}} \quad (V.27)$$

While the classification of the nuclear vibrations in multipole orders and the expression (26) are general consequences of the spherical equilibrium shape and small amplitudes of oscillation, the parameters B_λ and C_λ depend on the more detailed structure of the nucleus. The former represents the mass transport associated with the vibration, and it is of interest to compare the observed B_λ in nuclear vibrations with the value

$$(B_\lambda)_{\text{irrot}} = \frac{1}{\lambda} \frac{3}{4\pi} AMR_0^2, \quad (V.28)$$

corresponding to the surface oscillations of an irrotational and incompressible liquid drop. The parameter C_λ represents an effective surface tension which, within the scope of the liquid drop model, may be obtained from the surface energy appearing in the semiempirical mass formula (see, e.g., reference 124).

The lowest frequencies of collective vibration are in most cases expected to be of quadrupole type ($\lambda=2$), since a surface deformation with $\lambda=1$ simply represents a center-of-mass displacement.¹⁶¹

V C.2. Quadrupole Vibrations of Even-Even Nuclei

The vibrational excitation spectra have the simplest character for the ground-state configuration of even-even nuclei, for which the intrinsic structure does not contribute to the nuclear angular momentum. The quadrupole vibrational spectrum for an even-even nucleus is illustrated schematically in Fig. V.9. The exact equality of the energy separations as well as the degeneracies which result from the harmonic oscillator approximation (26) will be modified by higher order terms in the nuclear energy (see, e.g., references 163 and 166).

The vibrational excitations are characterized by enhanced electric transition probabilities. These can be expressed directly in terms of the parameters B_λ and C_λ , since the vibrational amplitudes have been normalized with respect to the electric multipole moments [see

¹⁶¹ Collective dipole oscillations ($\lambda=1$) of the neutrons with respect to the protons have been discussed in connection with the nuclear photoeffect. Such oscillations have been estimated to have energies of the order of 10–20 Mev [M. Goldhaber and E. Teller, Phys. Rev. **74**, 1046 (1948); H. Steinwedel and J. H. D. Jensen, Z. Naturforsch. **5a**, 413 (1950)].

TABLE V.6. Vibrational spectra in even-even nuclei. The table lists the even-even nuclei, for which the empirical data on the second excited state is compatible with a $2+$ assignment. The energies of the first and second excited states are listed in columns two and three, and their ratio in column four. The $E2$ transition probability from the ground state to the first excited state (compare Table V.7) is given in column five, in units of the single particle estimate (V.1). The cascade transition from the second to the first excited state may proceed by $M1$ or $E2$ radiation, and the ratio of the components, as determined by angular correlations, or conversion coefficients, is shown in column six. Finally, column seven gives the ratio of the reduced $E2$ transition probability of the cross-over and cascade radiation from the second excited state. In the cases where the $M1$ admixture in the cascade radiation is unknown, the value for the ratio in column seven corresponds to the assumption of pure $E2$ radiation for the cascade transition, and is then given in parenthesis. The table is based on the empirical data in Table V.7 and on the references listed below.

Nucleus	E_2 (MeV)	E_2' (MeV)	E_2'/E_2	$\frac{B(E2; 0 \rightarrow 2)}{B_{sp}(E2)}$	$(M1/E2)_{2' \rightarrow 2}$	$\frac{B(E2; 2' \rightarrow 0)}{B(E2; 2' \rightarrow 2)}$	Reference
$^{26}\text{Fe}^{58}$	0.81	1.62	2.00		0.2	0.01	s
$^{28}\text{Ni}^{60}$	1.33	2.18	1.64	17		$(3 \cdot 10^{-3})$	a
$^{30}\text{Zn}^{64}$	1.00	2.27	2.27	15		(0.1)	a
$^{32}\text{Zn}^{66}$	1.05	2.40	2.29	11		(0.04)	a
$^{34}\text{Se}^{76}$	0.55	1.19	2.17	45	~ 1	0.1	a
$^{36}\text{Kr}^{82}$	0.77	1.45	1.88			(0.01)	a
$^{38}\text{Kr}^{84}$	0.9	1.9	2.1			> 0.1	a
$^{40}\text{Zr}^{92}$	0.93	1.83	1.97			(0.06)	a
$^{44}\text{Ru}^{100}$	0.54	1.36	2.52	22		(0.02)	b
$^{46}\text{Ru}^{102}$	0.47	1.10	2.34	45		(0.15)	c
$^{52}\text{Te}^{122}$	0.57	1.26	2.21	26	0.1	0.01	d, e, f
$^{54}\text{Te}^{126}$	0.65	1.40	2.16	17		(0.004)	g, h
$^{64}\text{Xe}^{126}$	0.39	0.86	2.20			(0.01)	g, h
$^{66}\text{Xe}^{128}$	0.46	0.98	2.13			(0.01)	i
$^{78}\text{Pt}^{192}$	0.32	0.61	1.90		0.025	0.008	j, k
$^{80}\text{Pt}^{194}$	0.33	0.62	1.88	50	small	0.01	j, l
$^{82}\text{Pt}^{196}$	0.35	0.69	1.97	38	0.05	$< 4 \cdot 10^{-4}$	d, m
$^{80}\text{Hg}^{198}$	0.41	1.09	2.66	29	0.7	0.03	d, n, o-q
$^{84}\text{Po}^{214}$	0.61	1.38	2.26	15	≥ 1		r

^a Nuclear Level Schemes ($40 \leq A \leq 92$), edited by Way, King, McGinnis, and van Lieshout, U. S. Atomic Energy Commission, Washington, 1955.

^b L. Marquez, Phys. Rev. **92**, 1511 (1953).

^c P. Avignon, Compt. rend. **240**, 176 (1955).

^d R. M. Steffen, *Proceedings of the 1954 Glasgow Conference* (Pergamon Press, London and New York, 1955), p. 206.

^e M. J. Glaubman, Phys. Rev. **98**, 645 (1955).

^f B. Farelly *et al.*, Phys. Rev. **99**, 1440 (1955).

^g M. L. Perlman and J. P. Welker, Phys. Rev. **95**, 133 (1954).

^h L. Koerts *et al.*, Phys. Rev. **98**, 1230 (1955).

ⁱ N. Benczer *et al.*, Phys. Rev. **100**, 955(A) (1955).

^j M. W. Johns and S. V. Nablo, Phys. Rev. **96**, 1599 (1954).

^k H. W. Taylor and R. W. Pringle, Phys. Rev. **99**, 1345 (1955).

^l Mandeville, Varma, and Saraf, Phys. Rev. **98**, 94 (1955).

^m M. T. Thieme and E. Bleuler, Phys. Rev. **99**, 1646(A) (1955).

ⁿ D. Schiff and F. R. Metzger, Phys. Rev. **90**, 849 (1953).

^o C. D. Schrader, Phys. Rev. **92**, 928 (1953).

^p L. G. Elliot *et al.*, Can. J. Phys. **32**, 153 (1954).

^q D. Maeder *et al.*, Helv. Phys. Acta **27**, 3 (1954).

^r O. B. Nielsen, private communication.

^s Frauenfelder, Levine, Rossi, and Singer, Phys. Rev. **103**, 352 (1956).

(24)]. Thus, for the one phonon excitation, one obtains [see (II A.18)]

$$B(E\lambda; I=0 \rightarrow I=\lambda) = (2\lambda+1) \left(\frac{3}{4\pi} Z e R_0^\lambda \right)^2 \frac{\hbar}{2(B_\lambda C_\lambda)^{\frac{1}{2}}}. \quad (\text{V.29})$$

In the harmonic oscillator approximation, the transitions to higher states in the vibrational spectrum are forbidden.

The static electric moments of the vibrational excitations vanish to lowest order and are thus expected to be small in spite of the large transition moments. The smallness of the static $E2$ moments for the excited states of an even-even nucleus is a characteristic feature of vibrational as distinct from rotational excitations.

In the decay of vibrational states, $M1$ radiation is forbidden even when ΔI equals 0 or 1, such as in the transition from the second to the first $2+$ state in the quadrupole vibrational spectrum. In fact, the magnetic moment associated with the collective motion is propor-

tional to the angular momentum and is thus a constant of the motion which possesses no matrix elements between different energy levels.

The static magnetic moment of a vibrational excitation is given by

$$\mu = g_R \cdot I, \quad (\text{V.30})$$

where the collective g factor is expected to be similar to that associated with the rotational motion of the deformed nuclei (see Sec. V B.3).

The transitions between vibrational states with $\Delta I=0$ may also take place by emission of conversion electrons corresponding to a nuclear electric monopole transition. The matrix elements for these $E0$ transitions may be related to the vibrational parameters and the nuclear compressibility.¹⁶²

V C.3. Discussion of Empirical Data

Collective excitation spectra corresponding to vibrations about a spherical equilibrium shape are expected

¹⁶² E. L. Church and J. Weneser, Phys. Rev. **100**, 943 (1955).

in the extensive intermediate regions between the closed shell nuclei and the nuclei with especially many particles in unfilled shells and a resulting nonspherical equilibrium shape (see Sec. V A). In these intermediate regions, the low-lying excited states of even-even nuclei are indeed found to exhibit a pattern which resembles that of quadrupole vibrations about a spherical equilibrium.¹⁶³

The first excited states are always of 2+ type and the energies vary regularly with neutron and proton number, decreasing as one moves away from closed-shell regions (see Fig. V.3). Moreover, the cross sections for Coulomb excitation of these states are found to be an order of magnitude larger than for single particle transitions, exhibiting the collective character of the transitions [see (1) and Table IV.2].

In many cases, a second vibrational excitation with spin 0+, 2+, or 4+ has been observed in radioactive decay processes. The energy of this second state is found to be in almost all cases between 2 and 2.5 times that of the first excited state, and the vibrational character is especially indicated by the observed γ decay. Thus, when the second excited state is of 2+ type, it is found to decay to the first excited 2+ state mainly by E2 radiation, although M1 radiation would be strongly preferred, assuming single particle matrix elements. In addition, the reduced E2 transition probability to the ground state, which would be forbidden for harmonic vibrations, is found to be in most cases several orders of magnitude smaller than that to the first excited state.¹⁶⁴ These features are exhibited in Table V.6 which lists the evidence on the vibrational spectra in those cases where the second excited state has the 2+ character.

The observed deviations of the energy ratios from those obtained in the harmonic oscillator approximation may possibly be accounted for by higher order terms in the collective nuclear Hamiltonian.¹⁶⁵ However, the striking selection rule observed in the E2 decay of the second 2+ state suggests that the higher order terms in the potential energy depend only on the parameter $\beta^2 = \sum_{\mu} |\alpha_{2\mu}|^2$, since otherwise this selection rule would no longer hold.¹⁶⁶ The inclusion of such higher order terms in β would leave the two phonon states with spins 2+ and 4+ degenerate, while in most cases the 0+ state would lie higher.

From the energy and $B(E2)$ value for the excitation of the first 2+ state, one can determine the parameters B_2 and C_2 by means of (27) and (29). The values obtained, which are listed in Table V.7, exhibit the im-

TABLE V.7. Vibrational parameters for even-even nuclei. The table lists the even-even nuclei in the regions $A \leq 150$ and $190 < A < 220$ for which there exists evidence on the transition probability to the first excited (2+) state. The energies, E_2 , of these states and the reduced transition probabilities, $B(E2; 0 \rightarrow 2)$, are listed in columns two and three. The data are obtained from the Coulomb excitation results in Table IV.2, from the lifetime data in Table IV.1 and from the additional references given below. From the values of $E_2 = \hbar\omega$ and of $B(E2)$, the effective surface tension C_2 and mass parameter B_2 for quadrupole vibrations are obtained from (V.27) and (V.29). The B_2 values are given in units of $(B_2)_{\text{irrot}}$ [compare (V.28)]. In the immediate neighborhood of closed shells, the observed excitations may be described in more detail in terms of the excitations of the few particles outside of closed shells (see Sec. V.E).

Additional references: Devons *et al.*, Proc. Phys. Soc. (London) **69A**, 173 (1955) (C^{12} and Ne^{20}); F. R. Metzger, Bull. Am. Phys. Soc. Ser. II, **1**, 40 (1956) (Ni^{60}). The lifetime determinations for Po^{212} and Po^{214} from the α - γ branching are discussed in reference 132.

Nucleus	E_2 (keV)	$B(E2; 0 \rightarrow 2)$ ($e^2 \cdot 10^{-48} \text{ cm}^4$)	C_2 (MeV)	$B_2 / (B_2)_{\text{irrot}}$
$^6C^{12}$	4400	0.009	14	2.9
$^{10}Ne^{20}$	1630	0.045	5.8	3.6
$^{22}Ti^{46}$	890	0.15	14	7.3
$^{48}Ti^{90}$	990	0.083	29	12
$^{26}Fe^{56}$	854	0.10	36	15
$^{28}Ni^{58}$	1450	~ 0.1	77	10
$^{60}Ni^{130}$	1330	0.12	59	9.0
$^{30}Zn^{64}$	1000	0.11	61	15
$^{66}Zn^{140}$	1040	0.087	86	18
$^{32}Ge^{70}$	1020	0.077	120	23
$^{72}Ge^{150}$	830	0.23	32	9.2
$^{74}Ge^{154}$	593	0.29	19	10
$^{76}Ge^{158}$	556	0.33	17	9.3
$^{34}Se^{74}$	635	0.21	32	15
$^{76}Se^{150}$	567	0.43	14	8.1
$^{78}Se^{154}$	615	0.36	20	8.7
$^{80}Se^{156}$	654	0.23	34	13
$^{82}Se^{158}$	880	0.056	190	39
$^{42}Mo^{94}$	871	0.29	67	11
$^{96}Mo^{192}$	778	0.4	44	8.9
$^{98}Mo^{194}$	786	0.4	47	8.7
$^{100}Mo^{196}$	528	0.64	20	8.0
$^{44}Ru^{100}$	540	0.30	48	18
$^{102}Ru^{194}$	473	0.63	20	10
$^{104}Ru^{196}$	362	1.0	10	8.2
$^{46}Pd^{104}$	556	0.50	34	12
$^{106}Pd^{190}$	512	0.66	24	9.5
$^{108}Pd^{192}$	430	0.89	15	8.3
$^{110}Pd^{194}$	375	1.0	12	8.5
$^{48}Cd^{110}$	654	0.41	58	13
$^{112}Cd^{198}$	620	0.46	49	12
$^{114}Cd^{199}$	550	0.55	37	11
$^{116}Cd^{199}$	508	0.62	32	11
$^{52}Te^{120}$	560	0.55	48	13
$^{122}Te^{194}$	570	0.47	58	14
$^{124}Te^{196}$	608	0.39	77	16
$^{126}Te^{198}$	662	0.32	105	18
$^{128}Te^{199}$	750	0.28	140	18
$^{130}Te^{200}$	850	0.26	170	18
$^{60}Nd^{146}$	455	0.25	150	44
$^{148}Nd^{192}$	300	0.69	36	23
$^{62}Sm^{148}$	562	0.50	100	18
$^{160}Sm^{199}$	337	0.98	31	16
$^{78}Pt^{194}$	330	1.7	39	13
$^{196}Pt^{196}$	358	1.3	55	17
$^{198}Pt^{198}$	403	1.4	60	13
$^{80}Hg^{198}$	411	1.0	88	19
$^{200}Hg^{199}$	370	0.7	120	30
$^{202}Hg^{200}$	439	0.6	170	29
$^{82}Pb^{206}$	803	0.14	1400	72
$^{84}Po^{212}$	719	0.3	640	39
$^{214}Po^{214}$	606	0.6	270	23

¹⁶³ G. Scharff-Goldhaber and J. Weneser, Phys. Rev. **98**, 212 (1955).

¹⁶⁴ J. J. Kraushaar and M. Goldhaber, Phys. Rev. **89**, 1081 (1953); R. M. Steffen, *Proceedings of the 1954 Glasgow Conference* (Pergamon Press, London and New York, 1955), p. 206.

¹⁶⁵ The deviations from the harmonic oscillator spectrum have also been discussed in terms of the coupling of the collective vibrations to high-frequency nucleonic excitations (reference 163).

¹⁶⁶ M. Jean and L. Wilets, Compt. rend. **241**, 1108 (1955) and Phys. Rev. **102**, 788 (1956).

portant influence of the shell structure on the nuclear vibrational properties. The effective surface tension C_2 varies strongly with respect to the liquid drop value, which is of the order of 50 Mev throughout the mass region considered, and the inertial parameter B_2 deviates considerably from the value (28).

While no quantitative analysis of the nuclear vibrational parameters has been given, some of the qualitative trends of the data in Table V.7 can be understood as consequences of the nuclear shell structure and the residual interactions (see Sec. V A). Thus, the effective nuclear surface tension decreases as one moves away from the closed shell regions, as a result of the polarizing effect of the nucleons in unfilled shells. While in the regions of closed shell configurations the C_2 values considerably exceed the liquid drop estimate, the C_2 values are appreciably smaller than this estimate for nuclei with many particles in unfilled shells, corresponding to the approach to instability of the spherical shape (see Fig. V.1). The inertial parameters B_2 systematically exceed those corresponding to irrotational flow. In regions away from closed shells, the increase of the inertia over that for irrotational flow is comparable to, although somewhat larger than, that observed in the rotational motion (see Sec. V B.2, and especially Fig. V.5).

In the more detailed interpretation of the data in Table V.7, it is necessary to take into account that the nucleus does not oscillate as a homogeneous system because of the different behavior of the particles in the unfilled shells from those in the closed shell core. This distinction is of special significance when the number of particles outside of closed shells is small. For such nuclei the vibrational energy is mainly associated with the motion of these few particles; on the other hand, an important and sometimes dominating part of the electric quadrupole moment of the vibration arises from the polarization of the closed shell core by the outside particles. This accounts for the large values of the vibrational parameters in Table V.7 for nuclei in the vicinity of the closed shell regions; in fact, the amplitudes α , normalized by (24), measure essentially the small core deformation, and the kinetic and potential energies per unit of α thus become very large.

With the approach to closed shell configurations the collective description of the low-lying excited states becomes less appropriate, and a more detailed analysis may be given by considering the motion of the individual particles outside of closed shells under the influence of their mutual interactions (see Sec. V E).

V C.4. Octupole Vibrations of Even-Even Nuclei

The odd parity collective vibrations of lowest energy are expected to be of octupole character ($\lambda=3$). In even-even nuclei the one phonon excitation of this type has $I=3$ and negative parity, while the two phonon octupole excitations give rise to states with $I=0+, 2+$,

and $6+$. The levels with one quadrupole and one octupole phonon have $I=1-, 2-, \dots, 5-$.

A rather low-lying ($3-$) state has been observed¹⁶⁷ in the spectrum of Gd^{152} , and may possibly represent a $\lambda=3$ vibrational excitation. Such an interpretation would imply a transition probability for $E3$ Coulomb excitation appreciably in excess of the single particle estimate (II A.58). It is of interest that odd parity states of similar energy have also been observed in neighboring deformed nuclei; in these, the coupling between the quadrupole deformation and the octupole mode may give rise to a lowest odd-parity excitation of $I=1-$ (see Sec. V D.4).

V C.5. Spectra of Odd-A Nuclei

In the regions where the even-even nuclei exhibit collective excitations corresponding to vibrations about a spherical equilibrium, the spectra of the odd- A nuclei are somewhat more complex and in most cases less well understood.

For the description of the low-energy spectrum of an odd- A nucleus, one must consider intrinsic degrees of freedom in addition to the collective motion. The intrinsic motion possesses a nonvanishing angular momentum which must be combined with the collective angular momentum; moreover, low-lying intrinsic excitations may arise from the change of orbital of the last odd nucleon, such as in the case of the nuclear isomers.¹⁶⁸

The intrinsic nucleonic degrees of freedom are coupled to the collective oscillations, since the latter involve variations in the nuclear field. The effect of the coupling to the quadrupole vibrations depends essentially on the parameter¹⁶⁹

$$q = \left(\frac{5}{16\pi} \right)^{\frac{1}{2}} \frac{k}{(\hbar\omega_2 C_2)^{\frac{1}{2}}}, \quad (\text{V.31})$$

where the coupling constant k is of the order of magnitude of the average potential energy of a nucleon. Thus, as one moves away from closed shell regions, the coupling is expected to increase as a consequence of the decrease of the effective surface tension and of the vibrational frequencies.¹⁷⁰

If the coupling could be neglected, one would obtain, for each intrinsic state, a collective spectrum corresponding to the phonon excitations. The states most strongly excited in the Coulomb excitation are the one

¹⁶⁷ H. Kendall and L. Grodzins, *Bull. Am. Phys. Soc. Ser. II*, **1**, 164 (1956) and O. Nathan and M. Waggoner (private communication).

¹⁶⁸ See, e.g., M. Goldhaber and R. D. Hill, *Revs. Modern Phys.* **24**, 179 (1952).

¹⁶⁹ See reference 132. In this reference the strength of the coupling has been discussed in terms of the parameter $x=qj^{-4}$.

¹⁷⁰ In reference 132 the increase of the coupling as one moves away from closed shells has been described in terms of the coherence of the individual particles in the unfilled shells in polarizing the nuclear shape. In the present discussion the paired particles are included in the collective degrees of freedom and their polarizing effect is thus reflected in the variation of the vibrational parameters.

phonon quadrupole excitations of the ground state configuration. If the ground state has spin I_0 , these excited states have spins $I_0+2, I_0+1, \dots, |I_0-2|$ and energies of the same order of magnitude as the first excited state in the neighboring even-even nuclei. The reduced transition probability for the excitation of these states is given by

$$B(E2; I_0 \rightarrow I_f) = \frac{1}{5} \frac{2I_f+1}{2I_0+1} B(E2)_{\text{ph}}, \quad (\text{V.32})$$

where $B(E2)_{\text{ph}}$ is the quadrupole phonon excitation probability (29).

When the coupling between the intrinsic and collective motion is weak ($q < 1$), the effect on the energy spectrum and transition probabilities may be obtained from a perturbation treatment.¹⁷¹

If one estimates the coupling strength q employing the empirical vibrational parameters in Table V.7, one finds for most nuclei $1 < q < 3$ indicating an intermediate coupling situation. With such values of the coupling the stationary states represent a rather complicated superposition of individual particle and collective motions.¹⁷²

In a few regions ($A \sim 20, 75, 105, 150, \text{ and } 192$), one obtains $q \gtrsim 4$. For such strong couplings, the last odd particle may appreciably polarize the nuclear shape with a resulting approach to the coupling scheme characteristic of the deformed nuclei^{173,174} (see Sec. V B). The strongest transitions observed in Coulomb excitation may then be approximately described as rotational excitations.¹⁷⁴

In the limits of very weak or very strong coupling, the dominant quadrupole transitions are associated with a few simple excitations. For an intermediate coupling situation the pattern is more complex, but there exists an approximate sum rule which may be of use in the analysis of such spectra. Thus, the summed quadrupole strength $\sum_f B(E2; I_0 \rightarrow I_f)$ obtained by adding all the low-energy transitions (i.e., with energies less than a few times $\hbar\omega_2$) is proportional to the average value of β^2 in the nuclear ground state, aside from a small contribution due to the quadrupole transitions of the last odd particle. The sum is, therefore, expected to be approxi-

mately the same in odd- A nuclei as in neighboring even-even nuclei, except insofar as the last particle polarizes the nucleus and thereby increases the sum. If the nucleus possesses a ground-state spin $I_0 > \frac{1}{2}$, the sum over the final states I_f should include also the ground state quadrupole strength $B(E2; I_0 \rightarrow I_0)$. The latter quantity is related to the static electric quadrupole moment Q of the ground state by [see (13) and (II A.18)]

$$B(E2; I_0 \rightarrow I_0) = \frac{5}{16\pi} e^2 Q^2 \frac{(I_0+1)(2I_0+3)}{I_0(2I_0-1)}, \quad (\text{V.32a})$$

a relation which is independent of the structure of the nuclear state.

When the total strength observed in an odd- A nucleus is appreciably smaller than $B(E2; 0 \rightarrow 2)$ for the transition to the first excited state in the neighboring even-even nucleus, one may conclude that there exist strong quadrupole transitions as yet undetected. A total strength greatly exceeding this value implies an appreciable polarization produced by the last particle and may thus indicate that the coupling scheme is approaching that of a deformed nucleus. In this limit the ground-state strength contributes the fraction $\langle I_0 2 I_0 0 | I_0 2 I_0 I_0 \rangle^2 = I_0(2I_0-1)(I_0+1)^{-1}(2I_0+3)^{-1}$ of the total quadrupole strength [see (10)]. For weak or intermediate coupling, the relative contribution of the ground-state strength to the total sum is expected to be smaller than this fraction.

V D. Vibrations of Spheroidal Nuclei

V D.1. Classification of Vibrations

While the lowest collective excitations of the strongly deformed nuclei correspond to rotations with preservation of shape, one may also expect these nuclei to exhibit collective excitations which correspond to vibrations about the equilibrium shape. Only scanty evidence is at present available on such vibrational excitations, but since the Coulomb excitation is well suited for the exploration of these levels we shall briefly outline the expected patterns.

For a nonspherical nucleus, the angular momentum of a vibrational quantum is not a constant of the motion due to the coupling to the nuclear rotation. Still, one may characterize the symmetry of the vibrations by a quantum number λ which represents the number of nodal surfaces and which, in the limit of small nuclear eccentricities, corresponds to the multiple order. The parity of the vibrations is $(-1)^\lambda$. For axially symmetric nuclei, the vibrations may in addition be characterized by the quantum number ν , representing the component of vibrational angular momentum about the symmetry axis. For given λ , the component ν may take the values $0, \pm 1, \dots, \pm \lambda$ but, in contrast to the vibrations of spherical nuclei, the vibrational parameters B and C [see (26)], and thus also the frequency, depend on $|\nu|$

¹⁷¹ L. L. Foldy and F. J. Milford, Phys. Rev. **80**, 751 (1950); A. Reifman, Z. Naturforsch. **8a**, 505 (1953); M. Trocheris, J. phys. radium **14**, 635 (1953); reference 132; A. K. Kerman, Phys. Rev. **92**, 1176 (1953); F. J. Milford, Phys. Rev. **93**, 1297 (1953); K. W. Ford and C. Levinson, Phys. Rev. **100**, 1 (1955); B. J. Raz, thesis, University of Rochester, 1955; W. W. True, Phys. Rev. **101**, 1342 (1956).

¹⁷² Intermediate coupling calculations have been given by K. Ford, reference 138; reference 132; D. C. Choudhury, Kgl. Danske Videnskab. Selskab Mat. fys. Medd. **28**, No. 4 (1954); reference 163; B. J. Raz, reference 171.

¹⁷³ The near instability of the spherical shape for the even-even nuclei in these regions is also indicated by the comparison of the energies of the first excited states with the critical value drawn in Fig. V.3.

¹⁷⁴ See, e.g., the discussion of the spectra of Ag^{107,109} (F1, H4, H7), Ir^{191,193} (D1), and Au¹⁹⁷ (C1, G1, S4); the reference code refers to Table IV.2.

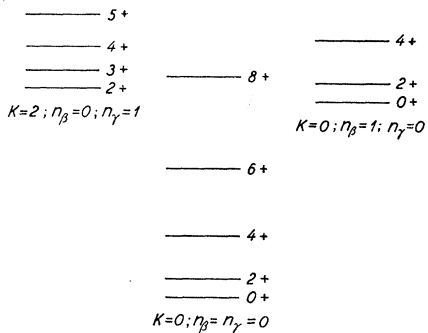


FIG. V.10. Quadrupole vibrations of an even-even nucleus with spheroidal shape. The quadrupole vibrations of the nucleus about a spheroidal equilibrium shape separate into two modes, of which the one has $\nu=0$ (β vibration) and the other $|\nu|=2$ (γ vibration). The figure illustrates the ground-state rotational band as well as the rotational bands associated with the first vibrational excitation of these two modes ($n_\beta=1$ and $n_\gamma=1$, respectively). The figure is meant for illustrative purposes only and no significance should be attached to the relative magnitude of the two vibrational frequencies.

It is expected that Coulomb excitation will strongly excite the two states ($n_\beta=1; I=2+$) and ($n_\gamma=1; I=2+$). These states decay by means of $E2$ radiation to the $I=0, 2$ and 4 members of the ground-state band with relative reduced transition probabilities $1:10/7:18/7$ for the β vibration and $1:10/7:1/14$ for the γ vibration [compare (V.33)]. $M1$ radiation is expected to be weak in these transitions, even when $\Delta I=0$ or 1 .

In an odd- A nucleus, the $n_\beta=1$ vibrational excitation gives rise to a rotational band with $K=K_0$, where K_0 is the ground-state K value. The $n_\gamma=1$ excitation gives rise to two bands with $K=|K_0\pm 2|$.

as well as on λ . In the special case of $\nu=0$, the vibrations preserve the axial symmetry of the nuclear shape.

The rotational band associated with a one-phonon excitation has $K=|K_0+\nu|$, where K_0 is the intrinsic angular momentum of the ground state. The band contains the members $I=K, K+1, K+2, \dots$ except for a $\nu=0$ vibration in a nucleus with a paired nucleonic configuration (ground-state configuration of even-even nuclei), in which case the band contains the states $I=0+, 2+, 4+, \dots$ (for λ even) or $I=1-, 3-, 5-, \dots$ (for λ odd).

V D.2. Transition Probabilities

The reduced transition probability of multipole order EL for the excitation of a vibration with angular momentum component ν may be written¹⁷⁵

$$B(EL; I_i K_i \rightarrow I_f K_f) = \langle K_f | \mathfrak{M}'(EL, \nu) | K_i \rangle^2 \times \langle I_i L K_i K_f - K_i | I_i L I_f K_f \rangle^2, \quad (\text{V.33})$$

where the first factor contains the vibrational matrix element of the electric multipole moment (II A.11) expressed in the intrinsic coordinate system. The second factor in (33) gives the relative probabilities for the excitation of the different members of the rotational band associated with the vibration. The formula (33)

¹⁷⁵ In the special case of $K_i=0$ and $K_f \neq 0$ (excitation of $\nu \neq 0$ modes in even-even nuclei), the value of $B(EL)$ is twice that given by (33).

also applies to the radiative decay of a vibrational excitation, and thus gives the branching ratios to the members of the ground-state band.

If the electric multipole order, L , of the excitation equals that of the vibration, λ , the transition probability (33) can be expressed in terms of the vibrational parameters $B_{\lambda\nu}$ and $C_{\lambda\nu}$ by means of the relation [compare (29)]

$$\langle K_f | \mathfrak{M}'(EL, \nu) | K_i \rangle^2 = \left(\frac{3}{4\pi} Z e R_0^\lambda \right)^2 \frac{\hbar}{2(B_{\lambda\nu} C_{\lambda\nu})^{\frac{1}{2}}}. \quad (\text{V.34})$$

We here assume a normalization of the vibrational amplitudes in analogy to (24).

V D.3. Quadrupole Vibrations

The lowest order shape vibrations have $\lambda=2$ and are of approximately quadrupole type. A deformation of order $\lambda=2$ and $\nu=\pm 1$ is equivalent to a rotation and the only occurring quadrupole vibrations thus have $\nu=0$ (β vibrations) or $\nu=\pm 2$ (γ vibrations). The quadrupole vibrational pattern expected for an even-even nucleus is illustrated in Fig. V.10.

While theoretical estimates of the vibrational frequencies are rather uncertain, due to the influence of the shell structure, the empirical data on the spectra of the even-even nuclei appears to indicate that the quadrupole vibrational energies for the very strongly deformed nuclei may be of the order of a Mev in the heavy nuclei. States with some of the expected properties have been found in a number of even-even nuclei.^{176, 176a} The determination of the $E2$ transition matrix elements would be of great value for the classification of these levels, since vibrational excitations should be appreciably stronger than single particle transitions. As in the case of spherical nuclei, $M1$ radiation is forbidden in the decay of vibrational excitations, even when $\Delta I=0$ or 1 . With decreasing deformation and gradual approach to the transition region, where the nuclear shape becomes spherical, the $(2+)$ rotational excitation increases in frequency and goes over into the one phonon quadrupole vibration. The lowest vibrational excitation goes over into a two phonon state and

¹⁷⁶ See, e.g., Er^{166} (1.46 Mev) J. S. Fraser and J. C. D. Milton, Phys. Rev. **98**, 1173(A) (1955). W^{182} (1.22 Mev) Murray *et al.*, reference 151; Alaga *et al.*, Kgl. Danske Videnskab. Selskab Mat. fys. Medd. **29**, No. 9 (1955). Pu^{238} (1.03 Mev) Rasmussen *et al.*, Phys. Rev. **99**, 42 and 47 (1955).

^{176a} Note added in proof.—Recent studies of the levels in the one-Mev region in heavy nuclei of the even-even type have revealed the systematic occurrence of states having many of the expected properties associated with both γ - and β -vibrational excitations (private communication from Asaro, Hollander, Perlman, Rasmussen, and Stephens; see also the review article on α radioactivity by I. Perlman and J. Rasmussen, to appear in *Handbook of Physics*, edited by S. Flügge). In this connection, it seems likely that the 760-keV level excited in Th^{232} (see Table IV.2) is a $2+$ level corresponding to a β vibration. Its excitation cross section would then indicate a $B(E2)$ value several times greater than the single particle unit (1).

its frequency may thus decrease somewhat with the approach to the transition region.¹⁷⁷

V D.4. Octupole Vibrations

The lowest odd parity modes ($\lambda=3$) should resemble octupole vibrations, and have $\nu=0, \pm 1, \pm 2$, and ± 3 .

Recently, relatively low lying $1-$ states, and in some cases also $3-$ and $5-$ states, have been observed in a number of even-even nuclei in the heavy elements region^{178,179} (see Fig. V.11 and Table V.8). Their systematic occurrence suggests an interpretation in terms of odd parity vibrations,¹⁸⁰ and the branching ratios in the $E1$ decays to the ground-state rotational band [see (33)] characterize the states as $K=0$ (and thus $\nu=0$) in all cases (see Table V.8). The lower energy of the $\nu=0$ mode as compared with the vibrations having $|\nu|=1, 2$, and 3 may be associated with a prolate nuclear shape.

The frequencies of these vibrations estimated on the basis of the liquid drop model would be a few Mev in heavy nuclei. However, as in the case of quadrupole vibrations, the shell structure is expected to have an important influence. Thus, the restoring force for odd parity vibrations will be strongly reduced by the occurrence of near lying single particle levels of opposite parity, which might even lead to stable odd parity deformations.

In an even-even nucleus, the odd parity vibrational levels of $1-$ type can be excited by an $E1$ transition from the ground state; there are two such levels having $|\nu|=0$ and 1 , respectively. The transition probability (33) depends on the displacement of the center of charge

TABLE V.8. States of $1-$ type in even-even nuclei. The excitation energies of the observed $1-$ states in the heavy elements are listed in column three, while the energies of the first excited $2+$ states are given in column two. The $1-$ states decay by $E1$ radiation to the $0+$ and $2+$ members of the ground state rotational band, and the ratios of the reduced transition probabilities are shown in column four. These may be compared with the theoretical ratios obtained from (V.33) for the assignments $K=0$ and $K=1$ for the $1-$ states. The table is taken from Stephens, Asaro, and Perlman, Phys. Rev. **100**, 1543 (1955).

Nucleus	$E(2+)$ (keV)	$E(1-)$ (keV)	$B(E1; 1- \rightarrow 0+)/B(E1; 1- \rightarrow 2+)$		
			exp.	theor. ($K=0$)	theor. ($K=1$)
⁸⁸ Ra ²²²	112	242	0.48±0.15	0.50	2.00
Ra ²²⁴	84	217	0.36±0.15		
Ra ²²⁶	68	253	0.49±0.08		
⁹⁰ Th ²²⁶	73	232	0.51±0.15		
Th ²²⁸	58	326	0.43±0.08		
⁹⁴ Pu ²³⁸	43	605	0.60±0.15		

¹⁷⁷ Thus the 633-Mev level in Os¹⁸⁸ with $I=2+$ may represent a γ vibration in the transition region (Johns *et al.*, Can. J. Phys. **34**, 69 (1956) and Potnis *et al.*, Phys. Rev. **102**, 459 (1956)).

¹⁷⁸ See especially Stephens, Asaro, and Perlman, Phys. Rev. **96**, 1568 (1954); **100**, 1543 (1955), and to be published.

¹⁷⁹ See also the 960-keV level in Sm¹⁵² which appears to have $I=1-$ and $K=0$ [O. Nathan and M. Waggoner, Nuclear Phys. (to be published)].

¹⁸⁰ R. F. Christy (private communication).

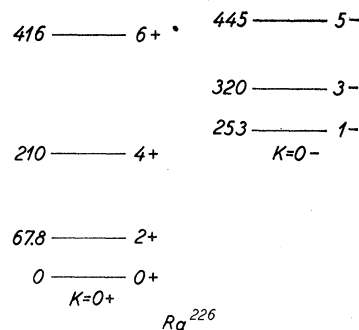


Fig. V.11. Level spectrum of Ra²²⁶. The figure shows the levels in Ra²²⁶ populated in the α decay of Th²³⁰ [Stephens, Asaro, and Perlman, Phys. Rev. (to be published)]. The observed levels appear to form two rotational bands, of which the first is the usual ground-state band of even-even nuclei with $K=0+$ (compare Fig. V.4). The negative parity levels form a rotational band with $K=0$ as determined by means of (V.33) from the observed relative intensities in the γ decay of these states (compare Table V.8).

As discussed in the text, the observed odd parity states may be associated with a collective vibration of approximately octupole type and with component $\nu=0$. The appreciably larger moment of inertia observed in this band as compared with that in the ground-state band may result from the coupling to the expected octupole vibrational mode with $|\nu|=1$ ($K=1-$).

with respect to the center of mass. Since this vanishes for a uniformly charged nucleus, the cross section is expected to be relatively small. A contribution to the nuclear dipole moment arises from the polarization of the nuclear charge resulting from the Coulomb forces. Estimates indicate that this effect would lead to $B(E1)$ values several orders of magnitude smaller than the single particle unit (II A.58).

The excitation of the $3-$ states would involve the $E3$ moment [see (34)], which is expected to be appreciably larger than that of a single particle. The determination of the cross section for $E3$ excitation would thus provide crucial information on the interpretation of these states. If $B(E3)$ for such an excitation were 10 times the value (II A.58) for a nucleus with $Z=90$ [i.e., assuming $B(E3; 0 \rightarrow 3) = 0.2e^2(10^{-24} \text{ cm}^2)^3$], the excitation cross section for 20-Mev α particles would be about one millibarn.

V E. Regions of Closed Shells

For nuclei with only a few particles outside of closed shells, a rather detailed analysis of the low-energy excitations may be obtained by considering these particles as moving, under the influence of their mutual interactions, in a fixed central binding field produced by the closed shell core.¹⁸¹ The weak coupling between the par-

¹⁸¹ Detailed analyses of this type have been discussed, e.g., by D. R. Inglis, reference 140 ($A \leq 16$); D. Kurath, Phys. Rev. **101**, 216 (1956) ($A < 16$); A. M. Lane, Proc. Phys. Soc. (London) **66A**, 977 (1954) ($A=13$); J. P. Elliot and B. H. Flowers, Proc. Roy. Soc. (London) **A229**, 536 (1955) ($A=18, 19$); M. G. Redlich, Phys. Rev. **99**, 1427 (1955) ($A=18, 19$); S. Goldstein and I. Talmi, Phys. Rev. **102**, 589 (1956) ($A=38, 40$); C. Levinson and K. W. Ford, Phys. Rev. **100**, 13 (1955) ($A=42, 43$); W. W. True, Phys. Rev. **101**, 1342 (1956) ($A=204$); D. E. Alburger and M. H. L. Pryce, Phys. Rev. **95**, 1482 (1954) ($A=206$).

ticles and the excitations of the core may be added as a perturbation and principally contributes to the electric moments associated with the particle motion. The dynamical effects of the core also imply a coupling between the outside particles¹⁸² which may contribute an appreciable part of the apparent interaction between the nucleons.

To the extent that the dynamics of the core can be described in terms of collective oscillations, an approximate expression for the resultant nuclear transition moment may be simply obtained from (II A.13) by including in the sum over k only the extra nucleons, and replacing their charges e_k by the effective radiating charges e_k' given by¹⁸²

$$e_k' = e_k + \frac{3Z'e}{4\pi} \frac{k}{C_\lambda'} \left(\frac{R_0}{r_k} \right)_{Av}^\lambda, \quad (\text{V.35})$$

where Z' and C_λ' are the charge number and effective surface tension of the closed shell core. The coupling constant k in (35) is the same as that employed in (31).

¹⁸² Reference 132, p. 27.

Estimates of C_λ' for a closed shell indicate that the induced charge is of the order of one unit.

Especially clear-cut examples of this effect are provided by the $E2$ Coulomb excitation cross section for the first excited states in Pb^{206} and Pb^{207} (see Table IV.2) and the measured $E2$ decay rate¹⁸³ of the first excited state in O^{17} . In these configurations consisting entirely of neutrons outside of closed shells, the observed transition rates imply an effective polarization charge of about one unit.^{184,185} A similar enhancement of the electric transition probability is observed for the 196-keV $E2$ excitation of F^{19} ,¹⁸⁶ and in the $E3$ decay of the 3- states in O^{16} ,¹⁸⁷ and Pb^{208} .¹⁸⁸

¹⁸³ J. Thirion and V. L. Telegdi, Phys. Rev. **92**, 1253 (1953).

¹⁸⁴ W. W. True, reference 171; J. Raz, reference 171.

¹⁸⁵ The polarization charge (35) contributes not only to the transition rate, but also to the static electric moments. Thus, the very small electric quadrupole moment reported for O^{17} [G. R. Bird and C. H. Townes, Phys. Rev. **94**, 1203 (1954)] seems surprising (see the detailed discussion by J. Raz, reference 171).

¹⁸⁶ J. Elliot and B. H. Flowers, reference 181.

¹⁸⁷ See F. Ajzenberg and T. Lauritsen, Revs. Modern Phys. **27**, 77 (1955).

¹⁸⁸ Elliot *et al.*, Phys. Rev. **93**, 356 (1954).